



TECHNICAL UNIVERSITY OF CRETE
SCHOOL OF PRODUCTION ENGINEERING AND MANAGEMENT
PRODUCTION SYSTEMS DIVISION

**CAD-based simulation of spiral bevel gear manufacturing
processes and investigation of optimal process parameters**

Thesis submitted in partial fulfillment of the requirements for the degree of
Doctor of Philosophy

by

Charikleia Efstathiou

Chania, Greece

December 2022



ΠΟΛΥΤΕΧΝΕΙΟ ΚΡΗΤΗΣ
ΣΧΟΛΗ ΜΗΧΑΝΙΚΩΝ ΠΑΡΑΓΩΓΗΣ ΚΑΙ ΔΙΟΙΚΗΣΗΣ
ΤΟΜΕΑΣ ΣΥΣΤΗΜΑΤΩΝ ΠΑΡΑΓΩΓΗΣ

**Προσομοίωση των κατεργασιών κοπής κωνικών ελικοειδών
οδοντώσεων μέσω συστήματος CAD και διερεύνηση των
βέλτιστων παραμέτρων κατεργασίας**

Διατριβή που υπεβλήθη για τη μερική ικανοποίηση των απαιτήσεων για την
απόκτηση Διδακτορικού Διπλώματος

υπό
Χαρίκλεια Ευσταθίου

Χανιά
Δεκέμβριος 2022

**Copyright © Χαρίκλεια Ευσταθίου
Χανιά, Δεκέμβριος 2022**

Απαγορεύεται η αντιγραφή, αποθήκευση και διανομή της παρούσας εργασίας, εξ' ολοκλήρου ή τμήματος αυτής, για εμπορικό σκοπό. Επιτρέπεται η ανατύπωση, αποθήκευση και διανομή για σκοπό μη κερδοσκοπικό, εκπαιδευτικής ή ερευνητικής φύσης, υπό την προϋπόθεση να αναφέρεται η πηγή προέλευσης και να διατηρείται το παρόν μήνυμα. Ερωτήματα που αφορούν στη χρήση της εργασίας για κερδοσκοπικό σκοπό πρέπει να απευθύνονται προς το συγγραφέα και μόνο. Οι απόψεις και τα συμπεράσματα που περιέχονται σε αυτήν τη διατριβή εκφράζουν το συγγραφέα και δεν πρέπει να ερμηνευθεί ότι αντιπροσωπεύουν τις επίσημες θέσεις του Πολυτεχνείου Κρήτης.

**Copyright © Charikleia Efstathiou
Chania, Greece, December 2022**

It is prohibited to copy, store and distribute this work, in whole or in part, for commercial purposes. Reproduction, storage and distribution for a non-profit, educational or research purpose is permitted, provided the source is acknowledged and this message is preserved. Questions regarding the use of the work for commercial purposes should be directed to the author only. The opinions and conclusions contained in this thesis are those of the author and should not be interpreted as representing the official positions of the Technical University of Crete.

**Επιχειρησιακό Πρόγραμμα
Ανάπτυξη Ανθρώπινου Δυναμικού,
Εκπαίδευση και Διά Βίου Μάθηση**
Με τη συγχρηματοδότηση της Ελλάδας και της Ευρωπαϊκής Ένωσης



Η παρούσα έρευνα έχει χρηματοδοτηθεί από την Ευρωπαϊκή Ένωση στα πλαίσια του επιχειρησιακού προγράμματος «Ανάπτυξη ανθρώπινου δυναμικού, εκπαίδευση και δια βίου μάθηση» (ΕΣΠΑ 2014-2020). ΠΡΑΞΗ «Ενίσχυση του ανθρώπινου ερευνητικού δυναμικού μέσω της υλοποίησης διδακτορικής έρευνας» - MIS 5000432

The present research is funded by the European Union within the framework of the operational programme “Human resources development, education and lifelong learning” (NSRF 2014-2020). Action: “Strengthening human research potential through doctoral research.” - MIS 5000432

The present thesis contains text and figures from two journal publications in which C. Efstathiou is the main and corresponding author. The paper titled "*Simulation of spiral bevel gear manufacturing by face hobbing and prediction of the cutting forces using a novel CAD-based model*" is first published in "*The International Journal of Advanced Manufacturing Technology, Vol. 122, p. 3789-3813, 2022*" by Springer Nature. The paper titled "*A Novel CAD-based Simulation Model for Manufacturing of Spiral Bevel Gears by Face Milling*" is first published in the "*CIRP Journal of Manufacturing Science and Technology, Vol.33, p. 277-292, May 2021*" by Elsevier. The content from the above articles has been used in the context of the present thesis exclusively for academic purposes.

Η διατριβή της Χαρίκλειας Ευσταθίου εγκρίνεται από τους:

Αριστομένης Αντωνιάδης (Επιβλέπων).....
Καθηγητής της Σχολής Μηχανικών Παραγωγής και Διοίκησης
Πολυτεχνείο Κρήτης

Νικόλαος Μπιλάλης (Μέλος Τριμελούς Συμβουλευτικής Επιτροπής).....
Καθηγητής της Σχολής Μηχανικών Παραγωγής και Διοίκησης
Πολυτεχνείο Κρήτης

Γεώργιος Σταυρουλάκης (Μέλος Τριμελούς Συμβουλευτικής Επιτροπής).....
Καθηγητής της Σχολής Μηχανικών Παραγωγής και Διοίκησης
Πολυτεχνείο Κρήτης

Παναγιώτης Αλευράς.....
Επίκουρος Καθηγητής της Σχολής Μηχανικών Παραγωγής και Διοίκησης
Πολυτεχνείο Κρήτης

Μιχαήλ Ζερβάκης.....
Καθηγητής του Τμήματος Ηλεκτρολόγων Μηχανικών και Μηχανικών Η/Υ
Πολυτεχνείο Κρήτης

Νικόλαος Ταπόγλου.....
Επίκουρος Καθηγητής του Τμήματος Μηχανικών Παραγωγής και Διοίκησης
Διεθνές Πανεπιστήμιο της Ελλάδος

Παναγιώτης Κυράτσης.....
Καθηγητής του Τμήματος Μηχανικών Σχεδίασης Προϊόντων και Συστημάτων
Πανεπιστήμιο Δυτικής Μακεδονίας

ACKNOWLEDGEMENTS

The present doctoral research was carried out in the Micromachining and Manufacturing Modeling Laboratory, School of Production Engineering and Management of the Technical University of Crete, Greece. The thesis achieved the kinematic simulation of two popular spiral bevel gear cutting methods and the calculation of the developed cutting forces. Within the framework of this research, the kinematic simulation algorithm *Ithaca BevelSim3D* and the cutting force prediction algorithm *Ithaca BevelForce3D* were developed. The algorithms were named after *Ithaca*, the Greek island and mythical home-island of *Odysseus* in Homer's epic poem *Odyssey* and also *C.P. Kavafy's poem "Ithaca"*. Additionally, the validation algorithm *Hermes BevelCurve3D* was developed and named after the messenger of the Olympian gods.

As the name of the developed algorithms suggests, this study has been a journey full of exciting experiences but also great challenges. As I tried to accomplish my mission, I felt like a little *Odysseus*, struggling to reach my *Ithaca* while facing many unexpected challenges. But as Homer taught us in the *Odyssey*, although I was tempted on many occasions, I always refused to give up. With the completion of this journey, I would like to thank everyone who have stood by my side during the past few years and offered me great support, memorable moments, and their invaluable love.

First and foremost, I would like to thank my supervisor, *Professor Aristomenis Antoniadis*, for his guidance and for giving me the excellent opportunity to become a member of the *m3 TUC laboratory* family and freely develop my skills through my participation in the laboratory's activities. My deepest thanks go to all *m3 TUC* members, partners, diploma- and master-thesis students, and PhD candidates for the experiences and the great moments we shared in our everyday collaboration. Especially *Dr. Dimitrios Vakondios*, *Dr. Maria Pappa*, *Dr. Anastasia Katsamaki*, *Kostas Sofiakis*, *Antonis Lyronis*, *Antonis Christodoulopoulos*, *Dr. Michel Mansour*, *Erasmia Tsiafi*, are some of the people that made the lab days, and after-lab evenings unique.

My friends and family have always played a major role in my life, and I am so thankful that I had them by my side throughout these challenging times. *Nikos*, *Michalis*, *Mina*, *Nikos and Magda*, *Semina*, *Michaela*, *Nikoleta-Maria*, *Giannis*, *Nantia*, *Marirena*, *Lefteris*, *Eleni*, *Konstantina and Pavlos*, *Nikoleta*, *Claire*, *Aris*, thank you for your love, your patience and for the kind support. My "Cretan" friends, especially, thank you for all the laughs, all the almost-drunk-nights, all the flavours, all the sunsets, all the sunburns and the music that we shared and enjoyed on this paradise-on-earth, that is Crete.

This thesis started and concluded on the island of Crete, at the city of Chania, a place I first visited for my post-graduate studies and where I ended up staying for over five years, exactly as I dreamt of as a child. A place that will always feel like a second home to me. There are no words to describe the magical atmosphere of Chania, a city full of colours, flavours and music, the breath-taking beauty of Crete, and the hospitality of most Cretans. Throughout my postgraduate studies, I created some of my loveliest memories there and I met wonderful people who will always be my friends.

Chara Efstathiou,
November 2022

Στον πιο ευγενή και όμορφο άνθρωπο που έχω γνωρίσει. Στη nonika μου, *Aigli*.

To the kindest and most beautiful human being I have ever known. To my nonika, *Aigli*.

SHORT CURRICULUM VITAE

Chara Efstathiou was born in Thessaloniki, Greece in 1986. In 2010 she graduated from the Department of Mechanical Engineering and Aeronautics of the University of Patras, majoring in design and manufacturing. In 2015 she obtained the MSc Degree in Production Systems from the Technical University of Crete (TUC). Following her Master studies, in 2016 she enrolled as a PhD student at the School of Production Engineering and Management, TUC.

After obtaining the Mechanical Engineering Diploma in 2010 she became a member of the Technical Chamber of Greece and started working as a freelance Mechanical Engineer in the building construction sector where she still works today. C. Efstathiou also formerly worked as a Teaching Assistant and a Research Associate in the Micromachining and Manufacturing Modeling Laboratory of TUC, where she lectured for the “Mechanical Drawing” and “Microscale Manufacturing Technologies” degree courses and carried out several laboratory and research projects between 2014-2018. From 2019 to 2020 she worked as a Manufacturing Engineer at AML Sheffield, UK. From 2020 to 2021 she worked as a Mechanical R&D Engineer at Doppler SA, Greece. Currently she works as a freelance Mechanical Engineer and a Research Associate. Her research interests focus on machining technologies, machining simulation, gear manufacturing and emerging manufacturing technologies.

During her post-graduate studies, C. Efstathiou has published the following journal publications, book chapters, conference proceedings articles and conference technical presentations as the main or co-author:

Journal publications

- **Efstathiou C**, Tapoglou N. Simulation of spiral bevel gear manufacturing by face hobbing and prediction of the cutting forces using a novel CAD-based model. *Int J Adv Manuf Tech* 122, 3789–3813 (2022). DOI: 10.1007/s00170-022-10065-x (SJR:Q1 IF: 3.47)
- **Efstathiou C**, Tapoglou N. A novel CAD-based simulation model for manufacturing of spiral bevel gears by face milling. *CIRP J Manuf Sci Technol* (2021); 33: 277–292. DOI: 10.1016/j.cirpj.2021.04.004 (SJR:Q1 IF: 4.19)
- Vlachou M, **Efstathiou C**, Antoniadis A, Karapantsios T. Micro-grooved surfaces to enhance flow boiling in a macro-channel. *Experimental Thermal and Fluid Science* (2019), 108, May 2019. DOI:10.1016/j.expthermflusci.2019.05.015 (SJR:Q1 IF: 3.37)

Book chapters

- Tapoglou N, **Efstathiou C**, Tzotzis A, Kyratsis P. Study of the Topography of Face Milled Surfaces Using CAD-Based Simulation. *Computational Design and Digital Manufacturing*. Springer. ISBN 978-3-031-21166-9.

Articles in conference proceedings

- **Efstathiou C**, Vakondios D, Lyronis A, Sofiakakis K, Antoniadis A. Finite element modeling and experimental study of burr formation in drilling processes. Proceedings of the *ASME International Mechanical Engineering Congress and Exposition*, November 2016, Phoenix, AZ, USA. DOI: 10.1115/IMECE2016-66026
- **Efstathiou C**, Vakondios D, Chatzikokolaki A, Antoniadis A. Optimal cutting conditions in ball-end milling of complex surfaces taking into account the desired surface roughness. Proceedings of the *International Conference on Advances in Mechanical and Automation Engineering*, June 2014, Rome. DOI: 10.15224/978-1-63248-022-4-48

- Vakondios D, **Efstathiou C**, Pappa M, Antoniadis A. Cad based simulation and surface topomorphy prediction in ball end milling. Proceedings of the *International Conference on Advances in Mechanical & Automation Engineering*, Rome, June 2014. DOI: 10.15224/978-1-63248-022-4-47

Conference technical presentations

- **Efstathiou C**, Tapoglou N. A novel approach for the simulation of spiral bevel gear manufacturing processes. *ASME International Mechanical Engineering Congress and Exposition*, November 2019, Salt Lake City, UT, USA.
- Tapoglou N, **Efstathiou C**. Simulation of manufacturing gears through power skiving using a CAD based approach. *ASME International Mechanical Engineering Congress and Exposition*, November 2019, Salt Lake City, UT, USA.
- Pappa M, **Efstathiou C**, Livanos G, Xidas P, Vakondios D, Katsamaki A, Maravelakis E, Zervakis M, Antoniadis A. Active Deformable Micro Cutters with Nano Abrasives. *9th International Conference "New Horizons in Industry, Business and Education"*, NHIBE 2015, Skiathos, Greece.

SUMMARY

The present doctoral dissertation focuses on the simulation of spiral bevel gear manufacturing processes. The ultimate goal of the study is to build the necessary simulation models for the optimization of the spiral bevel gear machining methods so that costly machining experiments can be avoided. The kinematics of the two most important spiral bevel gear machining processes, face milling and face hobbing, are simulated using *BevelSim3D*, an algorithm developed as part of this thesis. The algorithm models the blank gear, either pinion or crown, and cutting tool geometries, and creates the tool trajectory achieving the simulation of the process kinematics. As a result, the tooth flank generation and chip formation processes are revealed and the solid work gear and undeformed chip geometries are generated. The generated tooth flank topography can be used for further analysis to determine the effect of process parameters on tooth surface quality.

To validate the simulation results, the *BevelCurve3D* algorithm is developed to compare the simulated tooth surface to the theoretical one. The validation process is carried out using a simple geometric approach by comparing the simulated with the theoretical 3D tooth surface coordinates and calculating the deviation between them. In addition to evaluating the surface topography, kinematic simulation can also be used to calculate the cutting forces that occur during the process.

Utilizing the simulation results, the *BevelForce3D* algorithm calculates the cutting forces by analyzing the undeformed chip geometry. This is realized by dividing the solid chip geometry into elementary chips. Local cutting forces calculated on the revolving tip of the cutting blade can be used to predict tool wear, whereas global forces calculated at a fixed point on the work gear can be used to predict work gear deformation and specify the fixture type and clamping force that must be applied prior to machining.

Finally, after the simulation and cutting forces algorithms are developed, several simulations are executed to investigate the effect of crucial cutting parameters on the quality of the simulated surface and the developed cutting forces. More specifically, the study revealed that generation feedrate has a major effect on the quality of both tooth flanks and finishing stock allowance, plunge feedrate and generation feedrate greatly impact the developed cutting forces.

Σύνοψη

Η παρούσα διδακτορική διατριβή εστιάζει στην προσομοίωση της κατασκευής ελικοειδών κωνικών οδοντώσεων. Στα πλαίσια της διατριβής αναπτύχθηκε το προσομοιωτικό μοντέλο *BevelSim3D* το οποίο βασίζεται σε ένα αναγνωρισμένο σύστημα CAD. Το προσομοιωτικό μοντέλο επιτυγχάνει την κινηματική προσομοίωση των δύο σημαντικότερων κατεργασιών κοπής ελικοειδών κωνικών οδοντώσεων, του μετωπικού φραιζαρίσματος (FM - face milling) και του μετωπικού φραιζαρίσματος με κύλιση (FH - face hobbing). Αποτέλεσμα της κινηματικής προσομοίωσης των κατεργασιών είναι η μοντελοποίηση της προσομοιωμένης γεωμετρίας του εκάστοτε κωνικού οδοντωτού τροχού και η παραγωγή των απαραμόρφωτων στερεών αποβλίπτων που προκύπτουν ως αποτέλεσμα της κατεργασίας. Οι γεωμετρίες που προκύπτουν από την προσομοίωση μπορούν να χρησιμοποιηθούν για την περαιτέρω ανάλυση και διερεύνηση της κατεργασίας. Πιο συγκεκριμένα, η τρισδιάστατη γεωμετρία του οδοντωτού τροχού μπορεί να χρησιμοποιηθεί για διερεύνηση της επίδρασης των παραμέτρων κοπής στην ποιότητα της κατεργασμένης επιφάνειας. Αντίστοιχα, τα τρισδιάστατα απαραμόρφωτα απόβλιπτα μπορούν να χρησιμοποιηθούν για την ανάλυση της διαδικασίας δημιουργίας του αποβλίπτου της κατεργασίας καθώς και τον υπολογισμό των δυνάμεων κοπής.

Αναγκαιότητα και αντικείμενο έρευνας, ερευνητικός στόχος

Η ζήτηση της παγκόσμιας αγοράς σε οδοντώσεις εκτιμάται ότι αγγίζει τα 160 δισεκατομμύρια δολάρια, καθώς οι οδοντωτοί τροχοί αποτελούν τα σημαντικότερα στοιχεία σε συστήματα μετάδοσης ισχύος. Ως αποτέλεσμα αυτού, τις τελευταίες δεκαετίες έχουν ενταθεί οι προσπάθειες βελτιστοποίησης των σύγχρονων τεχνολογιών παραγωγής οδοντώσεων, συγκεντρώνοντας μεγάλο ερευνητικό ενδιαφέρον παγκοσμίως. Συγκεκριμένα οι κωνικές οδοντώσεις είναι από τα πλέον πολύπλοκα στοιχεία μετάδοσης ισχύος και οι τεχνολογίες παραγωγής τους είναι επίσης εξαιρετικά σύνθετες. **Αντικείμενο** της παρούσας διατριβής είναι η εις βάθος μελέτη και ανάλυση των κατεργασιών κοπής ελικοειδών κωνικών οδοντώσεων και **απώτερος στόχος** είναι η βελτιστοποίησή τους. Η προσομοίωση των κατεργασιών κοπής εν γένει συμβάλει στη δημιουργία μοντέλων τα οποία επιτρέπουν την εύρεση των βέλτιστων παραμέτρων κοπής με στόχο την αύξηση της ποιότητας της επιφάνειας των κατεργασμένων οδοντωτών τροχών, τη μείωση της φθοράς των κοπτικών εργαλείων -που συνεπάγεται αύξηση του χρόνου ζωής των-, και τη μείωση του χρόνου κατεργασίας. Χωρίς την ύπαρξη αυτών των μοντέλων η παραπάνω διερεύνηση θα προϋπέθετε τη διεξαγωγή χρονοβόρων πειραμάτων υψηλού κόστους, τα οποία με την προσομοίωση μπορούν να αποφευχθούν.

Θεωρία κωνικών οδοντώσεων και τεχνολογιών παραγωγής αυτών

Οι κωνικοί οδοντωτοί τροχοί χρησιμοποιούνται σε **εφαρμογές** στις οποίες απαιτείται μετάδοση κίνησης και ισχύος μεταξύ μη παράλληλων αξόνων. Οι άξονες μπορεί να τέμνονται ή και όχι και η συνηθέστερη γωνία που σχηματίζουν είναι οι 90°. Οι ευρύτερα γνωστές εφαρμογές των κωνικών οδοντωτών τροχών εντοπίζονται στην αυτοκινητοβιομηχανία, όπου συνηθέστερα χρησιμοποιούνται σε διαφορεικά οχημάτων. Στην αεροπορική βιομηχανία, στα ελικόπτερα, για τη μετάδοση ισχύος από τον κινητήρα του ελικοπτέρου στο κύριο και το ουραίο στροφέιο, σε μηχανισμούς ελέγχου και μεταβολής του σχήματος των πτερύγων των αεροσκαφών καθώς και σε jet κινητήρες αεροσκαφών για τη μετάδοση κίνησης από έναν κύριο άξονα του κινητήρα (π.χ. του συμπιεστή) σε παρελκόμενα μέρη όπως υδραυλικές αντλίες, γεννήτριες, εκκινητήρες κ.ά. Κωνικοί οδοντωτοί τροχοί χρησιμοποιούνται και σε μηχανές χειρισμού σκαφών, πλοίων, πλατφορμών εξόρυξης για τη μετάδοση ισχύος από τον κινητήρα στο άξονα της προπέλας. Άλλες αξιοσημείωτες εφαρμογές των κωνικών οδοντώσεων είναι σε εκσκαφείς, πύργους

ψύξης, μονάδες παραγωγής ηλεκτρικής ενέργειας, μηχανές εκτύπωσης, στη βιομηχανία τροφίμων καθώς και σε μηχανήματα εξόρυξης πετρελαίου.

Σχετικά με τη **γεωμετρία** των υπό μελέτη τροχών, οι κωνικοί οδοντωτοί τροχοί χαρακτηρίζονται από το βασικό τους σχήμα το οποίο είναι ένας κόλινος κώνος. Η γωνία του κώνου, δηλαδή η γωνία που σχηματίζει η κεφαλή του δοντιού με τον άξονα του τροχού, μπορεί να διαφέρει από τροχό σε τροχό. Οι κωνικοί οδοντωτοί τροχοί έχουν ποικίλα σχήματα και μπορούν να διακριθούν με βάση κάποια κριτήρια. Η βασική **κατηγοριοποίηση** στηρίζεται στην εφαρμογή του τροχού μέσα στο σύστημα μετάδοσης κίνησης στο οποίο χρησιμοποιείται. Έτσι, οι κωνικοί οδοντωτοί τροχοί διακρίνονται σε κινητήριους (driving) και κινούμενους (driven) τροχούς. Ο κινητήριος τροχός ονομάζεται και 'πινιόν' και ο κινούμενος 'κορώνα'. Μια ακόμη κατηγοριοποίηση των κωνικών τροχών αφορά την γεωμετρία του δοντιού. Πιο συγκεκριμένα, ανάλογα με τη μορφή του δοντιού, οι τροχοί διακρίνονται σε ευθείς / λοξούς / ελικοειδείς / zero / υποειδείς κωνικούς οδοντωτούς τροχούς. Τέλος, όλοι οι τροχοί εκτός από τους ευθείς, διαχωρίζονται σε τροχούς με δεξιόστροφα ή αριστερόστροφα δόντια ανάλογα με την κλίση της ευθείας ή της καμπύλης του δοντιού σε σχέση με τον άξονα του τροχού.

Η **παραγωγή** κωνικών οδοντωτών τροχών αναπτύχθηκε ιδιαίτερα στις αρχές του 20^{ου} αιώνα όταν εκτινάχθηκε η χρήση των διαφορικών στην αυτοκινητοβιομηχανία. Τις τελευταίες δεκαετίες οι κατασκευαστικές μέθοδοι των κωνικών οδοντωτών τροχών και ιδιαίτερα των ελικοειδών κωνικών τροχών έχουν αποτελέσει αντικείμενο έρευνας αρκετών ομάδων παγκοσμίως. Η μελέτη των μεθόδων παραγωγής ελικοειδών τροχών και κυρίως των δύο βασικότερων FM και FH, παρουσιάζει ιδιαίτερο ενδιαφέρον αλλά ταυτόχρονα αποτελεί και πρόκληση για τους ερευνητές λόγω της πολυπλοκότητας της κινηματικής των μεθόδων, της ιδιαίτερης γεωμετρίας των οδοντωτών τροχών και των κοπτικών εργαλείων. Επιπροσθέτως, από τη στιγμή που αναπτύχθηκαν οι δύο δημοφιλείς μέθοδοι FM και FH από δύο κυρίαρχες εταιρείες παραγωγής εργαλειομηχανών κοπής οδοντώσεων, η γνώση γύρω από τα ιδιαίτερα χαρακτηριστικά της κάθε μεθόδου και των αντίστοιχων κοπτικών εργαλείων περιορίστηκε σε μεγάλο βαθμό σε βιομηχανικό πλαίσιο ανάμεσα στις ερευνητικές ομάδες των συγκεκριμένων εταιρειών. Αυτό αναγκαστικά οδήγησε σε μεγάλα κενά στην ακαδημαϊκή έρευνα στο συγκεκριμένο πεδίο, τουλάχιστον για την πλειοψηφία των ερευνητών.

Οι δύο **μέθοδοι κατεργασίας κοπής** FM και FH αναπτύχθηκαν από τις εταιρείες Gleason και Klingelberg αντίστοιχα και για πολλά χρόνια η κάθε εταιρεία εστίαζε αποκλειστικά στην ανάπτυξη της μίας μόνο μεθόδου. Πλέον, οι εργαλειομηχανές των δύο εταιρειών έχουν τη δυνατότητα παραγωγής οδοντωτών τροχών εφαρμόζοντας και τις δύο μεθόδους, αν και η καθεμία από τις μεθόδους συνεχίζει να αποτελεί σήμα κατατεθέν της εταιρείας που την ανέπτυξε. Οι δύο μέθοδοι χρησιμοποιούνται εξίσου ευρέως από την παγκόσμια βιομηχανία παραγωγής κωνικών οδοντώσεων ανάλογα με τις ανάγκες του κάθε συστήματος παραγωγής και την εφαρμογή για την οποία προορίζεται το ζεύγος των οδοντωτών τροχών. Η βασικότερη διαφορά των δύο μεθόδων εντοπίζεται στην κινηματική τους. Πιο συγκεκριμένα, με την εφαρμογή της μεθόδου FM το κοπτικό εργαλείο κατεργάζεται ένα αυλάκι κάθε φορά, μέχρι να ολοκληρωθεί η κοπή του, ενώ κατά τη διάρκεια της κατεργασίας κοπής ο οδοντωτός τροχός παραμένει σταθερός. Στη συνέχεια ο κατεργαζόμενος τροχός περιστρέφεται κατά μία θέση, ώστε το κοπτικό εργαλείο να κατεργαστεί το επόμενο αυλάκι. Η διαδικασία αυτή επαναλαμβάνεται μέχρι να ολοκληρωθεί η κατεργασία όλων των αυλακιών. Αντίθετα, στη μέθοδο FH, τα αυλάκια κατεργάζονται όλα ταυτόχρονα, αφού κατά τη διάρκεια της κοπής ο οδοντωτός τροχός περιστρέφεται γύρω από τον άξονά του. Έτσι, ο οδοντωτός τροχός και το κοπτικό εργαλείο συνεργάζονται σαν δύο τροχοί σε εμπλοκή με συγκεκριμένη σχέση μετάδοσης η οποία προκύπτει από τον αριθμό των δοντιών του τροχού και τον αριθμό των κοπτικών ακμών της κεφαλής. Αποτέλεσμα αυτής της μεγάλης διαφοροποίησης στην

κινηματική των δύο κατεργασιών είναι η παραγωγή οδοντώσεων διαφορετικής γεωμετρίας. Συγκεκριμένα, η μορφή του δοντιού κατά το πλάτος του ή αλλιώς η χαρακτηριστική καμπύλη του δοντιού προσεγγίζει ένα τόξο κύκλου στην περίπτωση της κατεργασίας FM ενώ στην κατεργασία FH η μορφή του δοντιού που προκύπτει από την υπέρθεση της περιστροφής του τροχού στην κύρια κίνηση κοπής του κοπτικού εργαλείου χαρακτηρίζεται από μία εκτεταμένη επικυκλοειδή καμπύλη. Η ιδιαιτερότητα αυτή στη γεωμετρία που προκύπτει από τις δύο μεθόδους αποτελεί εμμέσως ένα από τα καθοριστικά κριτήρια για την επιλογή μιας εκ των δύο. Ο λόγος ξεκινά από το ότι όλοι οι οδοντωτοί τροχοί μετά την κατεργασία κοπής, υποβάλλονται σε θερμική κατεργασία για τη βελτίωση των ιδιοτήτων τους. Η θερμική κατεργασία έχει ως αποτέλεσμα τη μείωση της διαστατικής ακρίβειας των οδοντώσεων. Για το λόγο αυτό, όλοι οι οδοντωτοί τροχοί μετά την θερμική κατεργασία υποβάλλονται και σε κατεργασία αποπεράτωσης. Η επιλογή της κατεργασίας αποπεράτωσης διαφέρει ανάλογα με την κατεργασία κοπής που έχει προηγηθεί. Πιο συγκεκριμένα, οι οδοντωτοί τροχοί που έχουν προκύψει από τη μέθοδο κατεργασίας FM αποπερατώνονται συνηθέστερα με λειαντικό τροχό (grinding), επειδή ο λειαντικός τροχός έχει τη δυνατότητα να ακολουθήσει την τοξοειδή γεωμετρία της οδόντωσης. Από την άλλη μεριά, οι οδοντώσεις που έχουν προκύψει από FH, μπορούν να αποπερατωθούν μόνο με λάπινγκ (λείανση με τη χρήση ειδικής λειαντικής πάστας) και όχι με τη χρήση λειαντικού τροχού διότι ο λειαντικός τροχός δεν μπορεί να ακολουθήσει την γεωμετρία της εκτεταμένης επικυκλοειδούς που έχει προκύψει από την κατεργασία κοπής χωρίς να τη μεταβάλλει. Άλλες διαφορές των δύο βασικών μεθόδων κατεργασίας FM και FH είναι η καθ' ύψος γεωμετρία του δοντιού. Οι οδοντωτοί τροχοί που προκύπτουν από την FM κατεργασία έχουν δόντια με μεταβαλλόμενο, κατά το πλάτος τους, ύψος ενώ αντίθετά στους FH τροχούς το ύψος του δοντιού είναι σταθερό. Ως προς την παραγωγικότητα, η FH μέθοδος εισήχθη ως μία επαναστατική μέθοδος που προσφέρει πολύ υψηλούς ρυθμούς παραγωγής λόγω της ταυτόχρονης κατεργασίας όλων των δοντιών του τροχού. Παρ' όλα αυτά, τις τελευταίες δεκαετίες η FM μέθοδος έχει εξελιχθεί σημαντικά προσφέροντας πολύ χαμηλούς χρόνους κατεργασίας και ανταγωνίζεται την FH ως προς την παραγωγικότητά της. Μία άλλη παράμετρος που καθορίζει την κινηματική των συγκεκριμένων κατεργασιών κοπής, είναι η διαμόρφωση της γεωμετρίας της οδόντωσης με κύλιση ή χωρίς. Έτσι, και στις δύο μεθόδους υπάρχει η δυνατότητα υλοποίησής τους χωρίς τη χρήση πρόσθετης κύλισης, όπου πλέον η FM κατεργασία απλοποιείται σε κατεργασία με εργαλείο μορφής ενώ η FH κατεργασία συμπεριλαμβάνει μόνο την κύλιση που προκύπτει φυσικά από την εμπλοκή και τη συνεργασία του κοπτικού εργαλείου με τον οδοντωτό τροχό. Η κατεργασία κοπής χωρίς την πρόσθετη κύλιση (non-generating ή Formate™) χρησιμοποιείται συνήθως ως κατεργασία ξεχονδρίσματος του ακατέργαστου τροχού. Εναλλακτικά οι δύο μέθοδοι FM και FH μπορούν να υλοποιηθούν ενσωματώνοντας και την πρόσθετη κίνηση κύλισης (generating) η οποία χρησιμοποιείται συνηθέστερα στην κατεργασία αποπεράτωσης. Σε κάθε περίπτωση το ένα μέλος του ζεύγους των οδοντωτών τροχών πρέπει να έχει προκύψει από κατεργασία κοπής με πρόσθετη κύλιση (generated) ώστε να μπορούν οι δύο οδοντωτοί τροχοί να συνεργαστούν σωστά. Επιπλέον, οι δύο μέθοδοι μπορούν να υλοποιηθούν είτε σε ένα στάδιο είτε σε δύο. Στη δεύτερη περίπτωση, στο πρώτο στάδιο ολοκληρώνεται το ξεχόνδρισμα του τροχού μέχρι ένα συγκεκριμένο βάθος και στο δεύτερο στάδιο πραγματοποιείται η αποπεράτωσή του.

Προσομοιωτικό μοντέλο και αλγόριθμος επαλήθευσης

Κατά την ανάπτυξη του μοντέλου προσομοίωσης *BevelSim3D* αναλύθηκε η γεωμετρία του αρχικού ακατέργαστου κομματιού καθώς και η βασική γεωμετρία της κωνικής οδόντωσης με βάση το πρότυπο ISO 23509:2016. Επίσης προσδιορίστηκε το προφίλ του κοπτικού εργαλείου με βάση το πρότυπο DIN 3792 και η βασική γεωμετρία της κεφαλής κοπής. Έπειτα αναλύθηκε πλήρως η κινηματική των δύο κατεργασιών κοπής FM και FH και προσδιορίστηκαν όλες οι σχετικές περιστροφικές και γραμμικές κινήσεις του κοπτικού εργαλείου και του οδοντωτού

τροχού και στις δύο περιπτώσεις. Τέλος, όλα τα παραπάνω δεδομένα εισόδου ενσωματώθηκαν στον αλγόριθμο *BevelSim3D* ο οποίος υλοποιεί την κινηματική της κάθε κατεργασίας με χρήση λογικών πράξεων (Boolean) μεταξύ των δύο στερεών του κοπτικού εργαλείου και του τροχού. Προκειμένου να αυξηθεί η ακρίβεια των αποτελεσμάτων, ο αλγόριθμος διακριτοποιεί την ολική σχετική κίνηση του κοπτικού εργαλείου σε βήματα με βάση την ανάλυση που έχει ορίσει ο χρήστης. Αποτελέσματα της κινηματικής προσομοίωσης είναι οι γεωμετρίες του κατεργασμένου τροχού και του απαραμόρφωτου αποβλίπτου σε κάθε βήμα της προσομοίωσης αλλά και η τελική προσομοιωμένη τοπομορφία του οδοντωτού τροχού. Η προσομοιωμένη γεωμετρία περιλαμβάνει ένα αυλάκι του τροχού, άρα μία κυρτή παρειά του δοντιού, το πόδι του δοντιού και την κοίλη παρειά του απέναντι δοντιού. Οι γεωμετρίες του απαραμόρφωτου αποβλίπτου περιλαμβάνουν ένα απόβλιπτο που έχει προκύψει από την κοπή της κυρτής παρειάς καθώς και ένα απόβλιπτο από την κοίλη παρειά. Οι διαδοχικές γεωμετρίες των απαραμόρφωτων αποβλίπτων επιτρέπουν τη μελέτη της διαδικασίας δημιουργίας του αποβλίπτου από την αρχή έως το τέλος της κατεργασίας. Οι διαδοχικές τοπομορφίες του προσομοιωμένου αυλακιού, δίνουν πληροφορίες για την θέση του εργαλείου σε σχέση με το κατεργαζόμενο τεμάχιο κάθε χρονική στιγμή της κατεργασίας. Η τελική προσομοιωμένη γεωμετρία του αυλακιού μπορεί να χρησιμοποιηθεί για τη μελέτη της επίδρασης των διαφόρων παραμέτρων της κοπής στην ποιότητα της επιφάνειας της οδόντωσης. Για την επαλήθευση των αποτελεσμάτων του μοντέλου προσομοίωσης *BevelSim3D*, αναπτύχθηκε ο αλγόριθμος επαλήθευσης *BevelCurve3D*. Ο αλγόριθμος επαλήθευσης συγκρίνει την τελική προσομοιωμένη επιφάνεια της οδόντωσης με τη θεωρητική επιφάνεια η οποία εξάγεται από ένα καθιερωμένο πρόγραμμα υπολογισμού και σχεδιασμού οδοντωτών τροχών, το KISSsoft. Η μέθοδος επαλήθευσης που χρησιμοποιήθηκε χωρίζει τις δύο παρειές του αυλακιού σε καμπύλες και διακριτοποιεί αυτές τις καμπύλες σε σημεία ώστε να προκύψει ένα σύνολο 3D σημείων. Στη συνέχεια εντοπίζει την απόκλιση της προσομοιωμένης από τη θεωρητική επιφάνεια υπολογίζοντας την ελάχιστη απόσταση των 3D σημείων των προσομοιωμένων καμπυλών από τις θεωρητικές καμπύλες.

Μοντέλο υπολογισμού δυνάμεων κοπής

Ένας από τους βασικούς στόχους της προσομοίωσης των κατεργασιών με αφαίρεση υλικού είναι η μείωση της φθοράς των εργαλείων κοπής η οποία συνεπάγεται μείωση του κόστους παραγωγής. Χρησιμοποιώντας τα αποτελέσματα του μοντέλου *BevelSim3D*, το μοντέλο *BevelForce3D* υπολογίζει τις δυνάμεις κοπής που αναπτύσσονται κατά την κατεργασία. Ο αλγόριθμος *BevelForce3D* δέχεται ως είσοδο τις στερεές γεωμετρίες των απαραμόρφωτων αποβλίπτων που έχουν προκύψει από την κατεργασία, διακριτοποιεί τις γεωμετρίες αυτές σε στοιχειώδη απόβλιπτα και χρησιμοποιώντας το εμπειρικό μοντέλο Kienzle-Victor υπολογίζει τις συνιστώσες των δυνάμεων κοπής και πιο συγκεκριμένα τη δύναμη κοπής, τη δύναμη πρόωσης και τη δύναμη απώθησης. Οι συνιστώσες αυτές έπειτα μετασχηματίζονται στο τοπικό σύστημα συντεταγμένων κοπτικής ακμής το οποίο δεν είναι σταθερό αλλά περιστρέφεται κατά τη διάρκεια της κατεργασίας ακολουθώντας το κοπτικό εργαλείο. Οι τοπικές δυνάμεις μπορούν να χρησιμοποιηθούν για τη διερεύνηση των παραμέτρων κοπής με στόχο τη μείωση της φθοράς του κοπτικού εργαλείου. Ταυτόχρονα, ο αλγόριθμος μετασχηματίζει τις τοπικές συνιστώσες των δυνάμεων κοπής σε ένα καθολικό σύστημα συντεταγμένων το οποίο προσαρμόζεται σε ένα σταθερό σημείο. Οι καθολικές συνιστώσες των δυνάμεων κοπής ισοδυναμούν με τις δυνάμεις που θα μετρούνταν πειραματικά με ένα δυναμόμετρο σταθερά προσαρμοσμένο στον οδοντωτό τροχό. Οι καθολικές δυνάμεις μπορούν να χρησιμοποιηθούν στην εκτίμηση της απαραίτητης δύναμης συγκράτησης αλλά και της κατάλληλης διάταξης συγκράτησης του ακατέργαστου τροχού πριν ξεκινήσει η κατεργασία αλλά και στην εκτίμηση της παραμόρφωσης του οδοντωτού τροχού και των παραμενουσών τάσεων μετά το πέρας της κατεργασίας.

Διερεύνηση των παραμέτρων της κατεργασίας

Μετά την υλοποίηση και την παρουσίαση των αλγορίθμων προσομοίωσης και υπολογισμού *BevelSim3D* και *BevelForce3D*, τα δύο μοντέλα χρησιμοποιήθηκαν για τη διερεύνηση της επίδρασης σημαντικών παραμέτρων της κατεργασίας αφενός μεν στην ποιότητα της προσομοιωμένης επιφάνειας και αφετέρου στις δυνάμεις κοπής. Πιο συγκεκριμένα, μελετήθηκε η επίδραση της πρόωσης κύλισης στην τοπομορφία της επιφάνειας χρησιμοποιώντας τις τελικές προσομοιωμένες γεωμετρίες του αυλακιού για την περίπτωση προσομοίωσης μιας κορώνας που έχει κατεργασθεί με τη μέθοδο FH. Με βάση τα αποτελέσματα της διερεύνησης, με την αύξηση της πρόωσης κύλισης παρατηρήθηκε αύξηση της απόκλισης της προσομοιωμένης επιφάνειας από τη θεωρητική αλλά και μείωση της ποιότητας της επιφάνειας, αφού το μέγιστο ύψος της τραχύτητας αυξήθηκε. Το ίδιο συμπέρασμα προέκυψε και στην περίπτωση προσομοίωσης της κατεργασίας ενός πινιόν με τη μέθοδο FM. Στη συνέχεια, μελετήθηκε η επίδραση σημαντικών παραμέτρων της κατεργασίας στις δυνάμεις κοπής για την προσομοίωση κατεργασίας μιας κορώνας με τη μέθοδο FH. Συγκεκριμένα μελετήθηκε η επίδραση του βάθους κοπής για την κατεργασία ξεχονδρίσματος/μορφής FH πριν την τελική κατεργασία αποπεράτωσης, η επίδραση της πρόωσης κύλισης σε μία κατεργασία FH μονού σταδίου και τέλος η επίδραση του βάθους του εναπομείναντος υλικού προς αποπεράτωση FH. Και στις τρεις περιπτώσεις παρατηρήθηκε σημαντική επίδραση των παραμέτρων της κατεργασίας στις αναπτυσσόμενες δυνάμεις κοπής.

CONTENTS

ACKNOWLEDGEMENTS.....	vii
SHORT CURRICULUM VITAE.....	ix
SUMMARY.....	xi
ΕΚΤΕΝΗΣ ΠΕΡΙΛΗΨΗ.....	xii
CONTENTS.....	xvii
LIST OF FIGURES.....	xx
LIST OF TABLES.....	xxiii
NOMECLATURE.....	xxiv
1. INTRODUCTION.....	1
2. STATE OF THE ART.....	5
2.1 Bevel gears and fields of application.....	5
2.1.1 Bevel Gears in the automotive industry.....	5
2.1.2 Bevel gears in aviation and aerospace industry.....	5
2.1.3 Marine engine applications.....	6
2.1.4 Cooling towers gearboxes.....	7
2.2 Bevel Gear Fundamentals.....	7
2.2.1 Classification of Bevel Gears.....	7
2.2.2 Unique features and advantages of bevel gears.....	9
2.3 Bevel Gear Geometry Standards.....	10
2.3.1 Main areas of bevel gear geometry.....	10
2.3.2 Basic geometry of Bevel Gear pairs.....	11
2.3.3 Tooth profile - Spherical involute.....	16
2.3.4 Transmission ratio.....	17
2.3.5 Bevel gear tooth widths and depths.....	18
2.4 Bevel gear materials.....	22
2.5 Bevel gear manufacturing.....	22
2.5.1 History of Bevel Gear Manufacturing.....	23
2.5.2 Modern machining methods for spiral bevel gears.....	25
2.5.3 Face milling and face hobbing processes.....	26
2.5.4 Machine tools for Spiral Bevel Gear Manufacturing.....	27
2.5.5 Cutter heads.....	29
2.5.6 Cutting blades.....	30
2.5.7 Cutting tool material and cutting speeds.....	31
2.6 Hard Finishing of Spiral Bevel Gears.....	31
2.6.1 Lapping.....	32
2.6.2 Grinding.....	32
2.6.3 Hard Skiving.....	33

2.7	Academic state of the art in spiral bevel gear manufacturing	33
2.7.1	State of the art in face milling process	33
2.7.2	State of the art in face hobbing process.....	35
2.7.3	State of the art in 5-axis universal machines.....	36
2.7.4	Previous simulation models in bevel gear manufacturing.....	37
2.8	Present research necessity and contribution	39
3.	KINEMATICS OF SPIRAL BEVEL GEAR CUTTING	41
3.1	Spiral Bevel Gear Machining Theory	41
3.1.1	Generation Principle	41
3.1.2	Plunging and generating roll motions.....	42
3.1.3	Single or continuous Indexing processes.....	45
3.2	Face milling	46
3.2.1	Indexing method	46
3.2.2	Kinematics.....	46
3.2.3	Gear and tooth geometry.....	48
3.2.4	Five-cut double flank vs Completing processes	49
3.2.5	The advantage of grinding	49
3.3	Face hobbing.....	50
3.3.1	Indexing Method	50
3.3.2	Kinematics.....	50
3.3.3	Gear and Tooth Geometry.....	52
4.	SPIRAL BEVEL GEAR CUTTING SIMULATION MODEL	55
4.1	Simulation model structure.....	55
4.1.1	Simulation process input parameters.....	56
4.1.2	Simulation process algorithm.....	60
4.2	Kinematic Analysis	62
4.2.1	Revolving Positions	62
4.2.2	Generation Positions	64
4.3	Simulation Results: Simulated work gear geometry and simulated undeformed chip geometry	66
4.3.1	Simulated work gear geometry	66
4.3.2	Simulated undeformed chip geometry	72
4.4	Ithaca Bevel Gear Suite - Graphical User Interface.....	77
4.4.1	<i>Ithaca BevelSim3D</i> – Graphical User Interface	78
5.	VALIDATION OF THE SIMULATION MODEL	81
5.1	Hermes BevelCurve3D validation software.....	81
5.1.1	Application GUI.....	81
5.1.2	Validation procedure.....	82

5.2	Simulation Model Validation.....	85
5.2.1	Face milling validation case study.....	85
5.2.2	Face hobbing validation case study.....	87
5.3	Tool trajectory validation.....	89
6.	CUTTING FORCES CALCULATION	91
6.1	Forces in machining operations	91
6.2	Cutting forces calculation algorithm	93
6.3	Ithaca BevelForce3D - Cutting forces calculation software	95
6.4	Cutting Forces presentation.....	99
6.4.1	Introduction.....	99
6.4.2	Cutting forces graphs.....	100
7.	SIMULATION RESULTS ANALYSIS AND PROCESS PARAMETERS INVESTIGATION	103
7.1	Chip thickness and cross-sectional area analysis	103
7.2	Investigation of the effect of process parameters on simulated gear topography	105
7.2.1	Investigation of process parameters in face hobbing	105
7.2.2	Investigation of process parameters in face milling.....	108
7.3	Investigation of the effect of process parameters on the developed cutting forces	109
7.3.1	The effect of finishing stock allowance on cutting forces.....	109
7.3.2	The effect of plunge feedrate in the roughing stage of the process.....	111
7.3.3	The effect of generation feedrate in a single stage finishing process	112
8.	CONCLUSIONS	115
	REFERENCES	117

LIST OF FIGURES

Figure 2.1:	Open differential mechanism. [3].....	5
Figure 2.2:	Internal (left) and external (right) gearbox in a jet engine. [4].....	6
Figure 2.3:	Bevel Gears in Helicopters. [1].....	6
Figure 2.4:	Flap drive mechanism. [1].....	6
Figure 2.5:	Bevel gear set in a) bow thruster unit (left) and b) external thrust drive (right). [1].....	7
Figure 2.6:	Cooling tower gearbox.....	7
Figure 2.7:	Straight bevel gears. [1].....	8
Figure 2.8:	Spiral (left) and Zerol (right) bevel gears. [1].....	8
Figure 2.9:	Hypoid gears. [1].....	8
Figure 2.10:	Drive and coast flanks of spiral bevel gears.	11
Figure 2.11:	Generation principle of straight bevel gears. [10].....	11
Figure 2.12:	Bevel gear pair geometry according to ISO 23509:2016 – Axial plane. [9]....	13
Figure 2.13:	Bevel gear pair geometry according to ISO 23509:2016 – Mean transverse section. [9].....	14
Figure 2.14:	Representation of an octoid gear. [1].....	16
Figure 2.15:	Schematic representation of the spherical involute. [11].....	17
Figure 2.16:	Transmission ratio of bevel gear train.....	18
Figure 2.17:	Bevel gear tooth depth, thickness and slot width. [9].....	19
Figure 2.18:	Tooth depth variants in bevel gears according to ISO 23509:2016. 1: mean whole depth, 2: mean addendum, 3: mean dedendum. [9].....	20
Figure 2.19:	Tooth width and depth according to ISO 23509:2016. [9].....	20
Figure 2.20:	Process flow chart of bevel gear manufacturing. [13].....	23
Figure 2.21:	Gear planning and Gear Shaping.....	24
Figure 2.22:	Klingelberg's first spiral bevel gear face hobbing machine. (1923).....	25
Figure 2.23:	Input and output parameters of spiral bevel gear cutting process. [13].....	26
Figure 2.24:	Mechanical spiral bevel and hypoid gear generator (top). [17] Gleason Phoenix II CNC spiral bevel hypoid generator basic structure (bottom left & right). [10, 16].....	28
Figure 2.25:	Gleason Phoenix series for spiral bevel and hypoid gear cutting.....	28
Figure 2.26:	Gleason Heller CP series for bevel and cylindrical gear 5-axis machining.....	29
Figure 2.27:	C27 and C100U Klingelberg-Oerlikon machines.	29
Figure 2.28:	Gleason cutters for straight and spiral bevel gears for face milling, face hobbing and 5-axis machining (top left to right: Coniflex straight, Pentac Plus FM-FH, Tri-AC FH. bottom left to right: RSR FM, Solid FM Pentac slim line 5-Axis....	30
Figure 2.29:	Klingelberg cutters for face milling (left-Arcoflex) and face hobbing (right-Zyklo Palloid) operations.	30
Figure 2.30:	Common types of cutting blades (Top, left to right: Hardac, RSR, Pentac, finished with PVD coating, roughed, blank geometry. Bottom: ETC carbide and HSS stick blades).....	30
Figure 2.31:	Cutting stick blades geometry.	31
Figure 2.32:	Lapping of spiral bevel gears.	32
Figure 2.33:	Grinding of spiral bevel gears.....	32
Figure 2.34:	5-axis machining kinematics for spiral bevel gears.....	36
Figure 3.1:	Generation principle in spiral bevel gears. [56].....	41
Figure 3.2:	a. Generated pinion - formate ring gear (left), b. Generated pinion - generated ring gear (right).	43
Figure 3.3:	Generating roll in bevel gear manufacturing. [10].....	43
Figure 3.4:	Plunge motion in gear manufacturing. [10].....	44
Figure 3.5:	Single indexing in face milling. [59].....	46

Figure 3.6:	Cutter position and reference plane in face milling. [10]	47
Figure 3.7:	Cutting and contact lines are almost parallel in face milling. [12]	48
Figure 3.8:	Conical tooth thickness after adjusting the tooth depth in face milling. [10] ...	49
Figure 3.9:	Continuous indexing in Face Hobbing. [55]	51
Figure 3.10:	Velocity vector of cutting blades in face hobbing. [10, 55]	52
Figure 3.11:	Flank line geometry and relative motions in face hobbing. [12]	53
Figure 3.12:	Tooth depth, tooth thickness and slot width in face hobbing process.[10].....	53
Figure 3.13:	Cutting lines in face hobbing. [12]	53
Figure 4.1:	Structure of the <i>Ithaca BevelSim3D</i> model. [59]	55
Figure 4.2:	Modelling the blank work gear 3D-geometry.	56
Figure 4.3:	Cutting blade profile according to DIN3972.	57
Figure 4.4:	Inner and outer blades arrangement in single and continuous cutting processes.	57
Figure 4.5:	Generating Method A. [10]	58
Figure 4.6:	Generating Method F. [10]	59
Figure 4.7:	Calculation of Simulation steps.	61
Figure 4.8:	Roughing and finishing generation positions.	61
Figure 4.9:	Cutting tool 3D geometry creation. [59]	61
Figure 4.10:	Boolean operations in machining simulation. [55, 59].....	62
Figure 4.11:	Cutting tool to work gear relative revolutions. [55]	63
Figure 4.12:	Face milling and face hobbing UCS revolutions. [55, 59]	64
Figure 4.13:	Generation trajectory – Inner blade. [59]	65
Figure 4.14:	Generation trajectory – Outer blade. [59]	66
Figure 4.15:	Simulated tooth flank surfaces of a face-milled pinion gear. [59]	67
Figure 4.16:	Simulated tooth flank surfaces of a face-milled ring gear. [59].....	68
Figure 4.17:	Assembly of a simulated face-milled gear pair. [59].....	69
Figure 4.18:	Simulated tooth flank surfaces of a face-hobbed pinion gear. [55].....	70
Figure 4.19:	Simulated tooth flank surfaces of a face-hobbed ring gear. [55]	71
Figure 4.20:	Assembly of a simulated face-hobbed gear pair. [55]	72
Figure 4.21:	Undeformed solid chip geometries of a pinion gear for various simulation steps of face milling method. [59]	73
Figure 4.22:	Undeformed solid chip geometries of a ring gear for various simulation steps of face milling method. [59]	74
Figure 4.23:	Undeformed chip geometries of a pinion gear for various simulation steps in face hobbing method. [55].....	75
Figure 4.24:	Undeformed solid chip geometries of a ring gear for various simulation steps of face hobbing method.....	76
Figure 4.25:	<i>Ithaca Bevel Gear Suite</i> GUI.	77
Figure 4.26:	Configuration tab.....	78
Figure 4.27:	Geometry setup tab.....	78
Figure 4.28:	Cutting tool setup tab.	79
Figure 4.29:	Manufacturing setup tab.....	79
Figure 5.1:	<i>BevelCurve3D</i> graphical user interface.	81
Figure 5.2:	Calculation of the simulated flank profile curves and extraction of points in <i>BevelCurve3D</i> . [59]	83
Figure 5.3:	Calculation of the theoretical flank profile curves in <i>BevelCurve3D</i>	84
Figure 5.4:	Validation graphs in <i>BevelCurve3D</i> interface.	84
Figure 5.5:	Simulated and theoretical profile curves for pinion (left) and ring gear (right). [59]	85
Figure 5.6:	Simulated surface deviation for face-milled pinion (left) and ring gear (right). 87	

Figure 5.7:	Simulated and theoretical profile curves for pinion (left) and ring gear (right). [55]	88
Figure 5.8:	Simulated surface deviation for face-hobbed pinion (left) and ring gear (right). [55].	88
Figure 5.9:	Tool trajectory deviation. [59]	89
Figure 6.1:	Cutting force components in orthogonal and oblique cutting. [62].	91
Figure 6.2:	Cutting force analysis. [55]	92
Figure 6.3:	Calculation of the cutting force components on each cutting plane, for every generation position. [55].	93
Figure 6.4:	Transformation of cutting force components to XYZ CSYS of each cutting plane. [55].	95
Figure 6.5:	Initiation of the Bevel Force 3D application.	95
Figure 6.6:	<i>BevelForce3D</i> .	96
Figure 6.7:	Main window of <i>BevelForce3D</i> application for the calculation of the cutting forces.	96
Figure 6.8:	Inner and outer blade 3D chip analysis sample.	97
Figure 6.9:	Cutting forces presentation and data input GUI.	99
Figure 6.10:	Local XYZ CSYS for both inner and outer blades.	99
Figure 6.11:	Local and Global Coordinate Systems.	100
Figure 6.12:	Discretized forces on inner and outer blades relative to the local blade coordinate system. [55]	101
Figure 6.13:	Total forces from inner and outer blades for all generation positions relative to the global gear coordinate system. [55]	101
Figure 7.1:	Maximum chip thickness and cross-sectional area analysis. [59]	103
Figure 7.2:	Effect of generation feedrate on the quality of the produced concave surface. [55].	106
Figure 7.3:	Effect of generation feedrate on the quality of the produced convex surface. [55]	107
Figure 7.4:	Effect of the generation feedrate on the quality of the produced work gear surface – face-hobbed ring gear. [55].	108
Figure 7.5:	Effect of generation feedrate on the quality of the produced work gear surface – face-milled pinion. [55]	109
Figure 7.6:	Effect of finishing allowance on the developed cutting forces. [55]	110
Figure 7.7:	Effect of plunge (forming) feedrate on the developed cutting forces. [55]	111
Figure 7.8:	Effect of generation feedrate on the developed cutting forces in a single stage process. [55]	112

LIST OF TABLES

Table 2.1:	Drive and coast flanks of spiral bevel gears.	11
Table 2.2:	Basic geometric parameters of bevel gears according to ISO 23509:2016. [9]	12
Table 2.3:	Basic geometric parameters of bevel gears according to ISO 23509:2016....	14
Table 3.1:	Generating and Non-Generating Processes.....	45
Table 4.1:	Work gear input parameters.....	56
Table 4.2:	Cutting blade and cutter head input parameters.....	57
Table 4.3:	Process-related input data.	60
Table 4.4:	Maximum chip thickness values in the finishing generation stage of the face- milled pinion gear.....	73
Table 4.5:	Maximum chip thickness values in the finishing generation stage of the face- milled ring gear.	74
Table 4.6:	Maximum chip thickness values in the finishing generation stage of the face- hobbed pinion and ring gears.....	77
Table 5.1:	Minimum and maximum values of tooth surface deviation between theoretical and simulated geometries.....	86
Table 6.1:	Forces calculation text output sample file.....	98
Table 7.1:	Geometric and cutting parameters in the investigation of the effect of process parameters on cutting forces. [55].....	109

NOMECLATURE

Symbol	Description	Units
Σ	shaft angle	°
δ_1, δ_2	pitch angle	°
R_i	indexing ratio	-
R_{e1}, R_{e1}	outer cone distance	mm
R_{m1}, R_{m2}	mean cone distance	mm
d_{m1}, d_{m2}	mean pitch diameter	mm
d_{e1}, d_{e2}	outer pitch diameter	mm
d_{a1}, d_{a2}	outside diameter	mm
δ_a	face angle	°
δ_f	root angle	°
c_b	cone angle	°
Z_1, Z_2	number of gear teeth	-
d_{01}, d_{02}	pitch circle diameter	mm
m_{mn}	mean normal module	mm
h_{m1}, h_{m2}	mean tooth depth	mm
h_{am1}, h_{am2}	mean addendum	mm
h_{fm1}, h_{fm2}	mean dedendum	mm
c	clearance	mm
t_0	pitch	mm
b_1, b_2	face width	mm
a_n	normal pressure angle	°
β_{m1}, β_{m2}	mean spiral angle	°
ζ_m	offset angle on the pinion axial plane	°
γ_b	base cone angle	°
θ	involute polar angle	°
ψ	Involute roll angle	°
v_i	linear velocity of gear i on the pitch circle	m/s
ω_i	angular velocity of gear i	rad/s
r_i	radius of the pitch circle of gear i	mm
n_i	rotational speed of gear i	rpm
b_{e1}, b_{e2}	outer face width	mm
b_{i1}, b_{i2}	inner face width	mm
h_{ae1}, h_{ae2}	outer addendum	mm
h_{ai1}, h_{ai2}	inner addendum	mm
h_{fe1}, h_{fe2}	outer dedendum	mm
h_{fi1}, h_{fi2}	inner dedendum	mm
h_{e1}, h_{e2}	outer whole depth	mm
h_{i1}, h_{i2}	inner whole depth	mm
θ_{a1}, θ_{a2}	addendum angle	°
θ_{f1}, θ_{f2}	dedendum angle	°
R_g	generating ratio of roll	-
ω_g	angular velocity of the cradle	rad/s
ω_w	angular velocity of the gear around its axis	rad/s
δ_g	pitch angle imaginary generating gear	°
δ_w	pitch angle work gear	°
Z_g	imaginary generating gear number of teeth	-

Symbol	Description	Units
ω_c	angular velocity of the cutter around its axis	rad/s
Z_w	work gear number of teeth	-
r_{c0}	cutter head radius	mm
r_1	cutting blade edge radius	mm
f_g	generation feedrate	$^\circ/\text{rev}$
f_p	plunge feedrate	mm/rev
t_f	finishing stock allowance	mm
φ	revolution discretisation	$^\circ$
θ_c	cutter rotation angle	$^\circ$
θ_w	work gear rotation angle	$^\circ$
θ_g	generating gear rotation angle	$^\circ$
g.p.	generating position	-
p.p.	plunge position	-
F_s	tangential cutting force	N
F_r	Passive (radial) force	N
F_v	feed force	N
F_a	active force	N
F_d	thrust force	N
F_z	resultant force	N
v_c	cutting speed	m/min
v_f	feed velocity	mm/min
K_s, K_r, K_v	material specific cutting force	N/mm^2
s, r, v	material specific constant value	-
h_{eq}	elementary chip equivalent thickness	mm
h_1, h_2	elementary chip thickness	mm
b_{eq}	elementary chip equivalent width	mm
b_1, b_2	elementary chip width	mm
h_{av1}, h_{av2}	chip thickness on the upper and lower part of the elementary segment	mm
b_{av1}, b_{av2}	chip width on the upper and lower part of the elementary segment	mm
$F_{x,loc}$	x-axis component of the local force developed on the tool tip	N
$F_{y,loc}$	y-axis component of the local force developed on the tool tip	N
$F_{z,loc}$	z-axis component of the local force developed on the tool tip	N
k	the angle between the cutting edge on the specific elementary chip and the y-axis	$^\circ$

*1 & 2 indexes refer to pinion (1) and ring gear (2) respectively.

1. INTRODUCTION

Gears are among the most important machine elements which have been employed in the transmission of motion and power between shafts for several centuries. Spiral bevel and hypoid gears are widely used as transmission elements in automotive vehicles, helicopters, naval and industrial applications. Bevel gears are angular transmission mechanisms with straight or curved teeth and are employed in applications that require transmission of torque between non-parallel axles. Spiral bevel gears with a helical tooth form surpass straight bevel gears in terms of efficiency, strength, vibration, and noise, as a result of the higher tooth contact ratio.

Although tooth curvature in spiral bevel gears offers higher efficiency compared to straight bevel gears, it inevitably makes them harder to manufacture. This is mainly caused by the geometric and kinematic complexity of the manufacturing processes employed to generate the curved tooth geometry. The kinematic complexity is the very reason why it is still quite difficult to fully comprehend and analyse these manufacturing processes, whilst there have been many research efforts on the subject. Increasing demand for efficient transmissions, demonstrating low noise and high strength, imposes higher quality requirements in spiral bevel gear manufacturing. Furthermore, excessive tool wear can occur during the manufacturing process, forcing the production to stop and imposing additional tool changes and intervention down time, which consequently raise the manufacturing cost. Due to the constant rise in global competition, production costs need to be reduced at the earliest stages of production, specifically during the development of a manufacturing process. Those are the core reasons why there is a need for an in-depth analysis on the subject and the creation of simulation models that will embody all the main process characteristics and parameters, to provide the manufacturers with useful results and an insight into the manufacturing process.

Spiral bevel gears can be manufactured in either specialized bevel gear cutting machines and hypoid generators or universal 5-axes milling machines. Manufacturing in specialized bevel gear cutting machines is up to now the most common practice for the production of this type of gears due to the increased productivity that it offers in comparison with 5-axis machining. Face milling and Face hobbing are the two major methods carried out on these dedicated machines. As implied by its name, face milling is similar to the common process of milling with face cutters. On the other hand, face hobbing resembles the process of gear hobbing applied for the production of cylindrical gears, but the two processes greatly differ as to the process kinematics and the geometry of the cutter which in the case of bevel gears is a disc face cutter. A fundamental difference between face milling and face hobbing methods lies in the way the cutter indexes relative to the workpiece. In face milling, the cutter machines one slot at a time, thus face milling is described as a single indexing process, whereas in face hobbing all slots of the bevel gear are machined simultaneously reducing the total production time and the manufacturing cost.

The present study introduces the ***Ithaca Bevel Gear Suite*** which integrates three separate algorithms developed for the kinematic simulation of the process, the validation of the results and the prediction of cutting forces. ***Ithaca BevelSim3D*** is a novel simulation model developed for the simulation of face milling and face hobbing processes. Simulation is integrated in a commercial CAD platform, exploiting the benefit of high precision of the results, which are obtained via Boolean operations between solid models. The simulation algorithm receives the gear type and main geometric characteristics, the tool profile geometry and the type of manufacturing process as inputs. Following, the model calculates the undeformed chip geometry, the gear tooth flanks in every simulation step and the final results after the completion of the process. The ***Ithaca BevelForce3D*** algorithm allows for the calculation of

cutting forces through the analysis of the undeformed chip geometry. In order to validate the simulation results and specifically the calculated tooth flank geometry, a novel validation model, **Hermes BevelCurve3D**, was also developed and is presented in this study. The validation algorithm receives the theoretical spherical involute curves and the simulated octoid curves along the width of the tooth, creates the theoretical and simulated flank surface approximations and also calculates their deviation along the tooth length. The results of the validation are presented to the user both numerically and with 3D-figures as well.

The **1st chapter** of the present study briefly introduces the reader to the main topic and scope of the research, while the structure of the thesis is also outlined.

The current state of the art is summarized in the **2nd chapter**, providing a detailed description of the most important issues in spiral bevel gear theory and the respective manufacturing methods. Bevel gear geometry, the major aspects of the manufacturing processes as well as a review of the research conducted so far in face milling and face hobbing, are presented. Furthermore, previous research efforts for the simulation of bevel gear manufacturing, are also reported.

The **3rd chapter** provides a thorough review of the spiral bevel gear cutting kinematics, for both face milling and face hobbing processes, the analysis of which is the main objective of the study.

The **4th chapter** focuses on a full description of the **Ithaca BevelSim3D** simulation model developed within the framework of this study. The programming environment used is presented and the structure of the model is described through model flow charts and figures. Following, the kinematic analysis, which is essentially the most important part of the model and the core of the simulation, is described. After the model is fully described, simulation results concerning 3D tooth flank surfaces and 3D undeformed chip geometries are reported and thoroughly discussed. Finally, the Graphical User Interface of the model and the procedure followed by the user, starting from the data input until the extraction of the simulation outcomes, are presented.

Hermes BevelCurve3D, presented in the **5th chapter** of the study, is a novel validation model developed to verify the simulation results. The graphical user interface of the validation model as well as an outline of the validation procedure is provided. Finally, two validation case studies are covered in the chapter including a face milling along with a face hobbing simulation example.

Ithaca BevelForce3D cutting forces calculation model is presented in the **6th chapter**. Firstly, a brief introduction to the theory of cutting forces, as it has been described in various research studies in the past, is provided. Following, the process of chip geometry analysis for the calculation of cutting forces in spiral bevel gear cutting, employed in this study, is presented. Finally, the graphical user interface of the software is presented.

The **7th Chapter** presents the investigation of the influence of process parameters on the simulation results. More specifically, the effect of generation feedrate on the simulated gear tooth surface for both face milling and face hobbing process is investigated, along with the effect of plunge feedrate, finishing stock allowance and generation feedrate on the developed cutting forces.

The **8th Chapter** reviews the methodology, summarizes the research results and conclusions and sets the grounds for further work on the improvement of the model and the experimental validation of the simulation results.

Finally, all the sources consulted throughout the preparation of this thesis, which were used to improve the general knowledge and understanding of the topic, are cited in the thesis and included in the **References** section.

[This page intentionally left blank]

2. STATE OF THE ART

Bevel gears are important motion transmission elements which are used in various fields and applications. This chapter firstly provides a brief introduction of bevel gears as a motion transmission element, then a brief description of spiral bevel gear geometry is presented and finally, the current state of research in spiral bevel gear cutting is summarized.

2.1 Bevel gears and fields of application

Bevel gears are used in applications where rotational motion must be transmitted between non-parallel shafts. The range of their application includes several fields, though their use in the automotive industry is the first significant and still most common application.[1] Other common applications of bevel gears are in aerospace industry, marine engines, cooling towers, power plants, printing presses, mining machines, food machinery etc. In non-parallel shaft drives, where transmission ratios between 1:1 and 10:1 are required, bevel gears are generally preferred over worm gears. When it comes to speed reducers $i_{\max} \approx 10$ is the maximum gear ratio that is commonly used, while the maximum gear ratio for single stage speed increasers is approximately $i_{\max} \approx 5$. [2]

2.1.1 Bevel Gears in the automotive industry

Bevel gears became important transmission elements with the development of automotive industry in the early 20th century. They were mainly used in differential mechanisms on rear axle transmissions. Bevel gears are still widely employed in differentials, changing the direction of motion from the engine output shaft to the wheel shafts and also allowing the two wheels to rotate at different speeds when a vehicle is going around a corner.[1] A typical open differential mechanism is shown in [Figure 2.1](#). The small bevel gear, driven by the pinion shaft, is called “pinion”, while the larger bevel gear, driven by the pinion, is called “wheel” or “ring gear” or sometimes just “gear”.

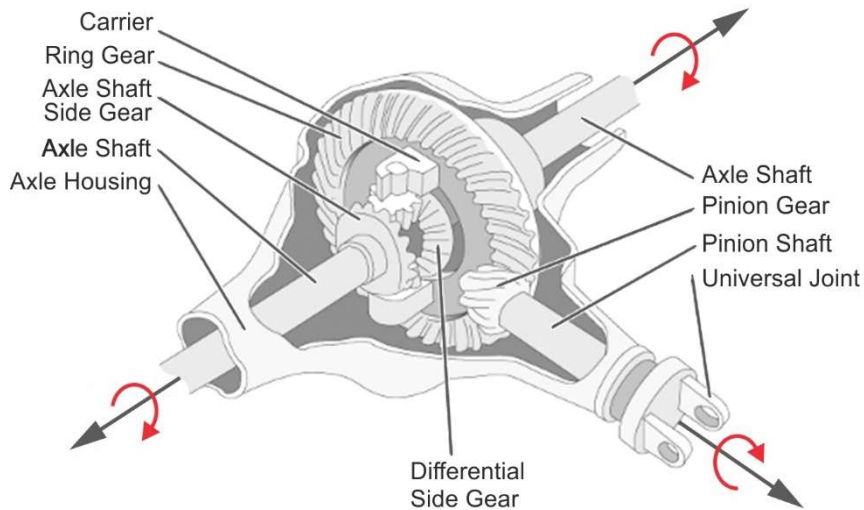


Figure 2.1: Open differential mechanism. [3]

2.1.2 Bevel gears in aviation and aerospace industry

Common applications of bevel gears in aviation include main rotor and tail rotor drives for helicopters, accessory drives for aircraft engines or flap actuators for aircraft wings. [1]

2.1.2.1 Bevel gears in aircraft engines

An accessory drive is a gearbox which is used to transmit power from a gas turbine to accessory parts of a jet engine, such as fuel pumps, hydraulic pumps, generators, starters etc. The gear train takes power from the shaft connecting the turbine with the compressor and transfers it to auxiliary parts of the engine. This layout normally consists of an internal, an

intermediate and an external gearbox. Bevel gears are used between non-parallel axes in all these stages.

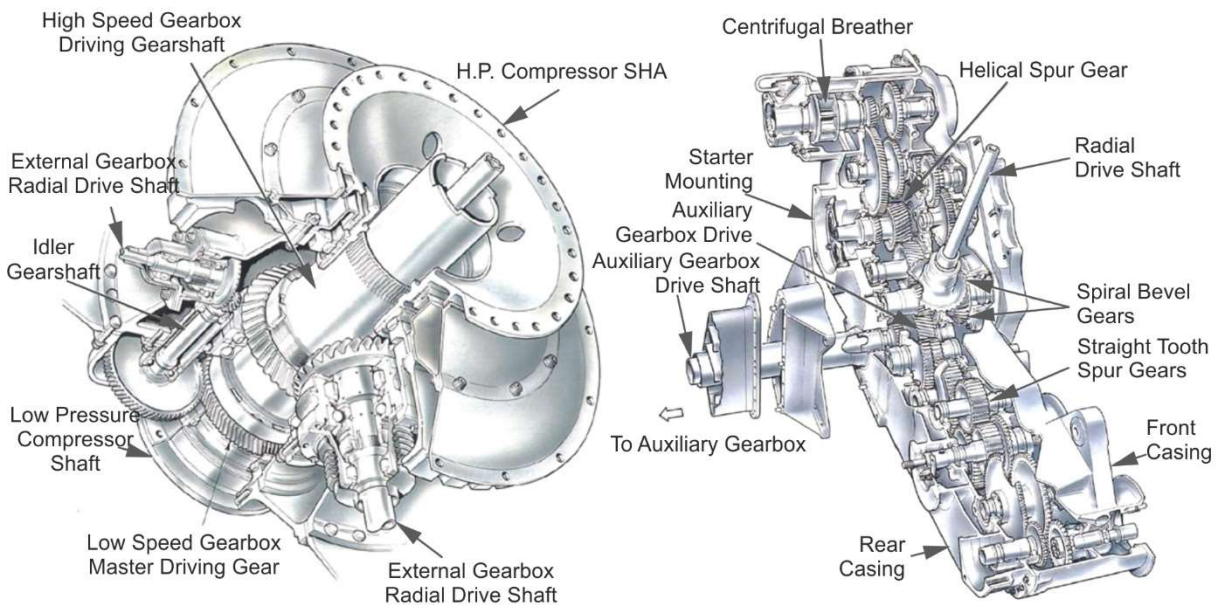


Figure 2.2: Internal (left) and external (right) gearbox in a jet engine. [4]

2.1.2.2 Bevel gears in helicopters

Main rotor: Similar to airplane engines, gas turbines are used in helicopter engines to provide the necessary power for the main and tail rotors. The shaft of the engine is placed parallel to the helicopter's body while the main rotor's shaft is perpendicular, so an angular gear pair is employed to transmit the power between the motor and the rotor. The bevel gear pair is placed before the input stage of the planetary gear train, **Tail rotor:** The tail rotor shaft is also mounted at an angle relative to the main shaft of the helicopter. As a consequence, a bevel gear train is used to allow the transmission of power between these two non-parallel shafts. Finally, secondary bevel gear sets are utilized to transmit motion to each of the tail rotor sections. [1] Figure 2.3 shows the location of above-described bevel gear drives in helicopters.

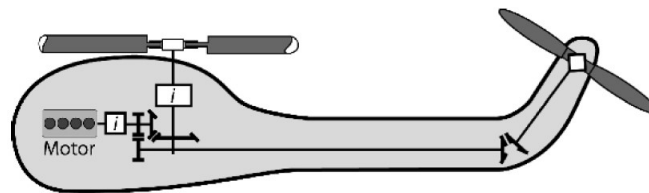


Figure 2.3: Bevel Gears in Helicopters. [1]

2.1.2.3 Flap drives on aircraft wings

Bevel gears are also included in actuators of aircraft wing flaps, which are used to alter the wing shape during take-off and landing. The motions of these flaps are performed via a crank mechanism. Bevel gears are used to transmit the rotational motion which moves the flap. Figure 2.4 shows the operating principle of flap drive mechanisms. [1]



Figure 2.4: Flap drive mechanism. [1]

2.1.3 Marine engine applications

Bevel gears are used in bow thruster units of ships to enable the transmission of power from the motor to the propeller shaft. The left picture in Figure 2.5 shows a bow thruster unit and

the bevel gear pair installed inside. Bevel gears are also used in external thrust drives. In this case, the bevel gear train consists of one or two ring gears driven by the same pinion, depending on the number of the propellers. However, the use of bevel gears in these engines limits the maximum transmitted power to 15MW. [1]

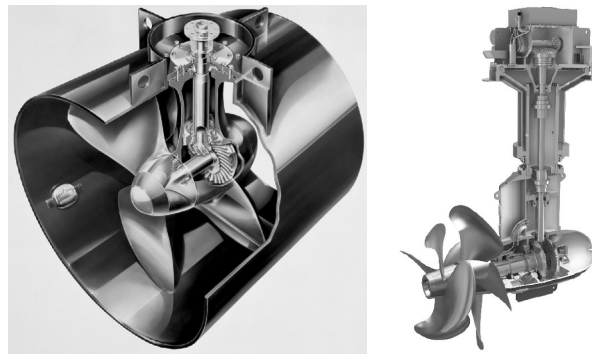


Figure 2.5: Bevel gear set in a) bow thruster unit (left) and b) external thrust drive (right). [1]

2.1.4 Cooling towers gearboxes

These are two-stage gearboxes with the first stage being a spiral bevel pair combined with a helical gear pair. Normally the output shaft is vertical, designed to receive the dynamic thrust of the fan.



Figure 2.6: Cooling tower gearbox

2.2 Bevel Gear Fundamentals

This section will provide a detailed presentation of the fundamentals of bevel gears, such as the various types of bevel gears and the benefits that they offer when employed to transmit motion and power.

2.2.1 Classification of Bevel Gears

Bevel gears can be classified in certain types according to their tooth form, the cutting method used to manufacture them, the tooth curve form and whether they are used as pinions (driving gears) or ring gears (driven gears). [Figure 2.7](#), [Figure 2.8](#) and [Figure 2.9](#) show the basic types of bevel gears when classified according to their tooth form.

Classification according to the tooth form

Based on the tooth form, bevel gears may be classified into:

- **Straight bevel gears**, which are the simplest of all bevel gears with straight teeth along the face-width pointing to the cone-apex. If their teeth were extended towards the centre of the gear, they would all intersect on the gear axis. The operation of two gears in mesh resembles two cones rolling onto each other. [5–7]

- **Spiral bevel gears**, the teeth of which are curved and oblique along their width (right or left). The curvature of the teeth leads to gradual engagement and continuous overlapping between the two mating gears. [5, 6]
- **Zerol bevel gears**, which have curved teeth with zero spiral angle at the middle of the face width. [6, 7]
- **Hypoid gears**, similar to spiral gears, their teeth are curved and oblique. They differ from spiral bevel gears in that the two shafts of a gear set are non-parallel and non-intersecting as well.

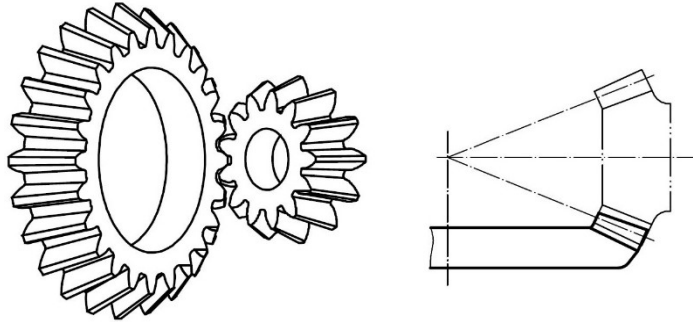


Figure 2.7: Straight bevel gears. [1]

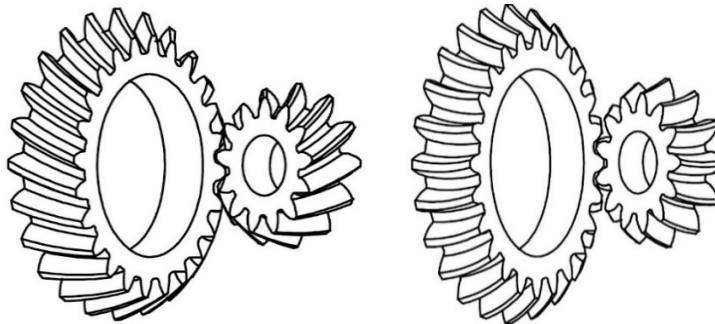


Figure 2.8: Spiral (left) and Zerol (right) bevel gears. [1]

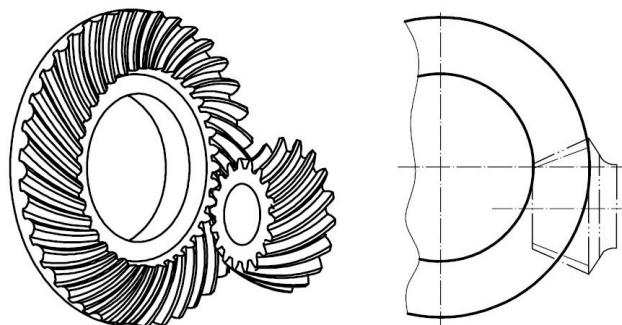


Figure 2.9: Hypoid gears. [1]

Classification according to the manufacturing method

Bevel gears can be machined either via a generating process or a simple plunge cutting. Based on the selection of manufacturing method, bevel gears are subdivided into **generated** or **non-generated** bevel gears.

Classification according to the tooth curve form

Spiral bevel gears vary according to the form of their tooth lengthwise curve. Spiral bevel gears produced by single-indexing processes have a **circular arc** tooth curve, while gears produced with continuous indexing processes have an **extended epicycloid** tooth curve.

Classification according to the application

A bevel gear can either act as the **driving gear**, that transmits rotational motion from the shaft that it is mounted on, to another shaft, or act as the **driven gear**, that meshes with the driving gear so that motion can be transmitted between the two shafts.

2.2.2 Unique features and advantages of bevel gears

Bevel gears in general, but each specific type as well, have special features and characteristics that differentiate them from other types of gears. The most obvious characteristic of all bevel gears is their conical shape which makes them suitable to transmit motion between non-parallel shafts. The most common shaft angle in angular transmissions is 90° but other angles can be applied as well.

Straight bevel gears are mostly used in applications where there is a need to transmit large forces and the drives operate at low rotational speeds, such as reduction gearboxes in lifting machines, where excess noise is also not of great importance. Straight bevel gears are also used in machine tools and differentials. The maximum allowed operation speed is about 5 m/sec unless the gear teeth are ground, then speeds up to 20 m/sec can be safely reached. Straight bevel gears are very sensitive to profile, pitch and assembly errors. These errors lead to uneven motion transmission, causing vibrations and noise. What is more, straight bevel gear teeth cannot be ground after heat treatment. On the plus side, straight bevel gears are easier than spiral bevel gears to manufacture and also do not produce inward thrust, simplifying the mounting design of the shaft. [5–7]

Spiral bevel gears are usually preferred because they offer smoother transmission of power compared to straight bevel gears, owing to the gradual teeth engagement and continuous overlapping, which is caused by the teeth curvature. In spiral bevel gear sets, multiple teeth are in contact at all times. The spiral angle allows more than one teeth to overlap if the face-width is adequately large. [2] Higher spiral angles offer higher face contact ratio leading to smoother and lower-noise operation, but also increase the axial loads on shafts and bearings. [2] Unlike straight bevel gears, spiral bevels can be ground after heat treatment, offering higher geometric precision. They are commonly employed in general use reduction boxes or as input stages in high-speed reduction boxes due to the low noise and low vibration offered, as a result of the higher tooth contact ratio. The most common applications include automotive speed reducers and machine tools. Spiral bevel gears are preferable to straight bevel gears in speeds greater than 5 m/sec and can operate up to 11 m/sec or even 60 m/sec if their teeth are hard-finished. However, spiral bevel gear manufacturing is far more complex than straight bevel gear cutting. [2, 5–7]

Zerol bevel gears tooth form resembles straight bevel gears. Zerol gears can replace straight bevel gears without mounting changes to achieve higher loads and faster speeds, similar to spiral bevel gears. In general, zerol bevel gears combine the advantages of both straight and spiral bevel gears. Due to the fact that the forces applied on the teeth of straight and zerol bevel gears are the same, the two types of gears can substitute each other without any changes on the mounting and the bearings of the shafts. Moreover, zerol bevel gears can be ground similar to spiral bevel gears, offering higher accuracy and lower-noise operation. Contrary to spiral bevel gears, zerol bevel gears can rotate in both directions due to the zero spiral angle at the middle of the face width. This type of bevel gear has high mechanical strength, as a result of the larger tooth thickness, and is widely used in the aircraft industry. [2, 6, 7]

Hypoid bevel gears are cone-shaped gears whose axes are non-parallel and non-intersecting. An offset between the two gear-axes is introduced allowing for the pinion spiral

angle to be larger than that of the ring gear, contrary to spiral bevel gears where the two angles are equal. Due to the greater pinion spiral angle, the pinion diameter is also increased offering a larger contact ratio, higher tooth strength and increased gear life. Therefore, the number of the gear teeth can be reduced and hypoid bevel gears can transmit more torque compared to spiral bevel gears, offering higher transmission ratios. Hypoid gears can handle rotating speeds over 1500 rpm. Moreover, the higher contact ratio of hypoid gears makes them run smoothly and reduces noise and vibration. On the downside, hypoid gears are more difficult to manufacture than spiral bevel gears. Hypoid gears are mostly used in differential mechanisms in the automotive industry. [1, 7]

In general, smooth operation and long service life of reduction gearboxes, operating with bevel gears, highly depend on precision and special attention during manufacturing, assembly and mounting. [5]

Miter gears are bevel gears with identical geometry and number of teeth. Therefore they cannot be used to increase or decrease speed but only to change the transmission direction. Their axes are non-parallel and intersecting. The teeth of miter gears can be either straight, spiral or zerol. When the two shafts are not perpendicular, the gears are called **angular miter gears** and the shaft angle Σ lies in the range of 45° to 120° . [7]

2.3 Bevel Gear Geometry Standards

The following sections deal with the macroscale geometry of bevel gears on the whole, but also with the specific geometric features of spiral bevel gears in particular. Bevel gears are elements with complex geometry and are more difficult to analyse and describe compared to cylindrical gears. This complexity comes as a result of the conical shape of bevel gears which leads to a constantly changing geometry along the width of the tooth. In the past few decades, there have been several approaches to the definition and description of bevel gear geometry. For many decades before the 2000s, information on bevel gear geometry has been developed and released only by gear machine manufacturers like Gleason and KlingelInberg. In 2003, the American Gear Manufacturers Association released a design standard for bevel gears which provides the standards for the design of all types of bevel gears, including also information for manufacturing and mounting of these gears. The standard was revised in ANSI/AGMA 2005-D03 [8]. In 2006, the International Standardization Organization created the ISO 23509 “Bevel and Hypoid Gear Geometry”, which attempts to provide a universal description of bevel gear geometry taking most of the previous approaches into consideration. Other standards, such as the AGMA 929-A06/2006 information sheet for the calculation of bevel gear top land and guidance on cutter edge radius, have been also released. The analysis carried out in the present study is solely based on ISO 23509 as it was revised in 2006 and 2016 editions and all calculations agree with and follow this standard. [9]

2.3.1 Main areas of bevel gear geometry

Bevel gear tooth geometry can be subdivided in some major areas, as shown in Figure 2.10. The top surface of the tooth is the gear's **top land** while the bottom area of the gear slot is called **root**. When observing the tooth in the lengthwise direction, the area closer to the centre is the **toe** and the area close to the outer part of the gear is called **heel**. When a pinion and a ring gear are assembled in a gear drive and motion is transmitted from one shaft to the other, the **concave tooth flank** of the pinion drives the **convex tooth flank** of the wheel. This flank is used as a **drive** when motion is transmitted from the pinion axle to the ring gear axle, for instance, when the engine is moving a vehicle forward. In the reverse direction, when the system is in coast mode, for example when the wheels drive the engine and the engine decelerates the vehicle, the convex flank of the pinion is loaded and this side is called the

coast side. [1] Based on the above principle, the tooth flanks of spiral bevel gears, are categorized as follows:

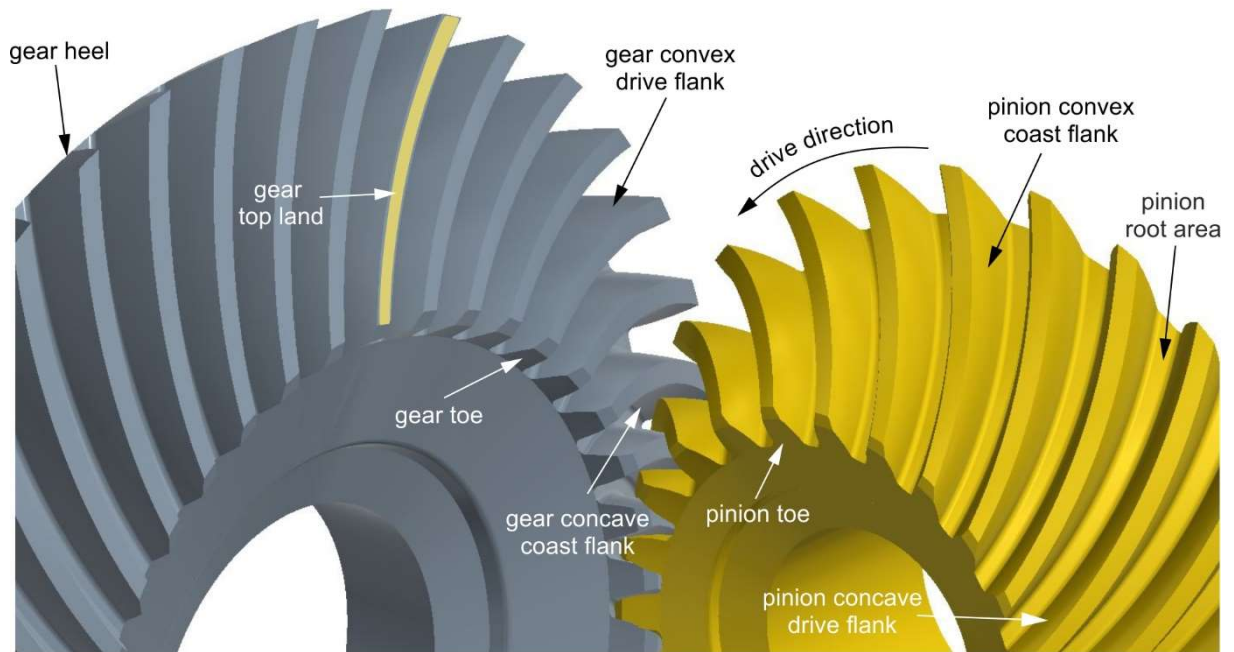


Figure 2.10: Drive and coast flanks of spiral bevel gears.

	Pinion	Ring Gear
Drive flank	Concave	Convex
Coast flank	Convex	Concave

Table 2.1: Drive and coast flanks of spiral bevel gears.

2.3.2 Basic geometry of Bevel Gear pairs

A bevel gear pair normally consists of two bevel gears meshed at an angle relative to each other. These two bevel gears are called “*pinion*”, which is the driving gear and “*ring gear*” or “*crown gear*” or just “*gear*”, which is the driven gear, with the pinion being the smallest of the two gears in mesh. The two gears are mounted on two shafts aligned to intersect at 90° . Angular bevel gears with shaft angles other than 90° do exist, but due to the complexity of such gearboxes, they are not so commonly used. In a cylindrical gear mesh, one of the two mating gears can be represented by a linear rack whose teeth are perfectly conjugate with the teeth of the other gear. This way, every pair of conjugate involute gears corresponds to a generating rack whose geometry can be used to specify the dimensions of the respective generating cutting tool for this gear.

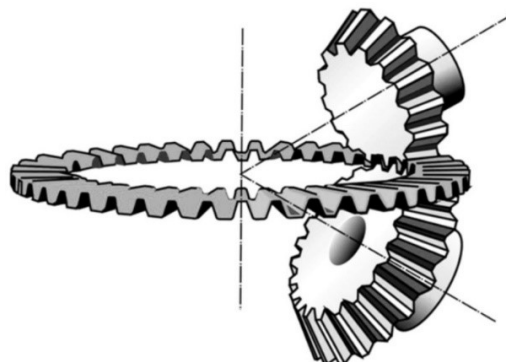


Figure 2.11: Generation principle of straight bevel gears. [10]

The same applies to bevel gears if this generating rack is rotated around an imaginary vertical axis. In a straight bevel gear assembly, the imaginary generating gear can be placed between the pinion and the ring gear, as shown in [Figure 2.11](#). If the thickness of this imaginary gear was close to zero, then all three gears could be in mesh at the same time. [10] Motion between two bevel gears in mesh is equivalent to rolling without sliding of the pitch cones which are in contact with each other along their generating curve, and both their apexes coincide on the intersection point of their shafts. Cutting bevel gears based on the generation principle results in a conjugate pair of gears in which the two gears have a line contact in each rotating position. As the rotation of the gears in mesh progresses, the contact line moves from the heel top of the gear to the toe root area. However, a perfectly conjugate bevel gear pair cannot operate under load because any possible misalignment would cause high-stress concentration on the tooth edges. This is the reason why crowning both in the lengthwise and in the profile direction is applied to almost all pinions. The extent to which a pinion flank is crowned is determined depending on the expected contact stress and deflections through tooth contact analysis (TCA). [10] In general, it is more beneficial to crown the pinion because it performs more revolutions per minute, thus it may generate more noise and vibrations.

[Figure 2.12](#) and [Figure 2.13](#) show the basic geometry of a bevel gear pair in mesh, as described by ISO 23509:2016. Three main cones are identified in bevel gears and these are the face cone (a), the pitch cone and the root cone (f). The pitch cone is the most characteristic geometric feature of the gear and is used to define important geometric parameters. The pitch, tooth heights and depths are all measured on the pitch cone as shown in [Figure 2.13](#). In order to make the visualization of the gear geometry easier, the surface of the pitch cone is “unwrapped” on a plane which is the pitch plane of the gear and all geometric parameters of the gear are shown on this plane. In some cases, the face line and the root line converge at one point (point O in [Figure 2.12](#)) which is the apex of the bevel gear and it's also the apex of the pitch cone. This geometry, though, can vary depending on the specific type of the bevel gear and the method used to manufacture it, so that the face line and root line can also be parallel to the pitch line.

The angles between the two gear shafts and the pitch lines of each gear are called **pitch angles** δ_1 and δ_2 , referring to the pinion and the ring gear respectively. The sum of the two pitch angles equals the shaft angle Σ .

$$\Sigma = \delta_1 + \delta_2 \quad (2.1)$$

For a given shaft angle Σ , the pitch angle of the pinion δ_1 can be calculated as follows:

$$\tan \delta_1 = \frac{\sin(\Sigma)}{i + \cos(\Sigma)} \quad (2.2)$$

where: i is the transmission ratio of the bevel gear pair.

Outer cone distance	R_e	[mm]	Face angle	δ_a	[°]
Mean cone distance	R_m	[mm]	Pitch angle	$\delta_{1,2}$	[°]
Mean pitch diameter	d_m	[mm]	Root angle	δ_f	[°]
Outer pitch diameter	d_e	[mm]	Cone angle	c_b	[°]
Outside diameter	d_a	[mm]	Face width	b	[mm]

Table 2.2: Basic geometric parameters of bevel gears according to ISO 23509:2016. [9]

In case the shaft angle equals 90° , the gears axes are perpendicular to each other, and the pitch angles of the pinion and ring gear can be calculated as follows:

$$\cotan(\delta_1) = \tan(\delta_2) \cdot i \quad (2.3)$$

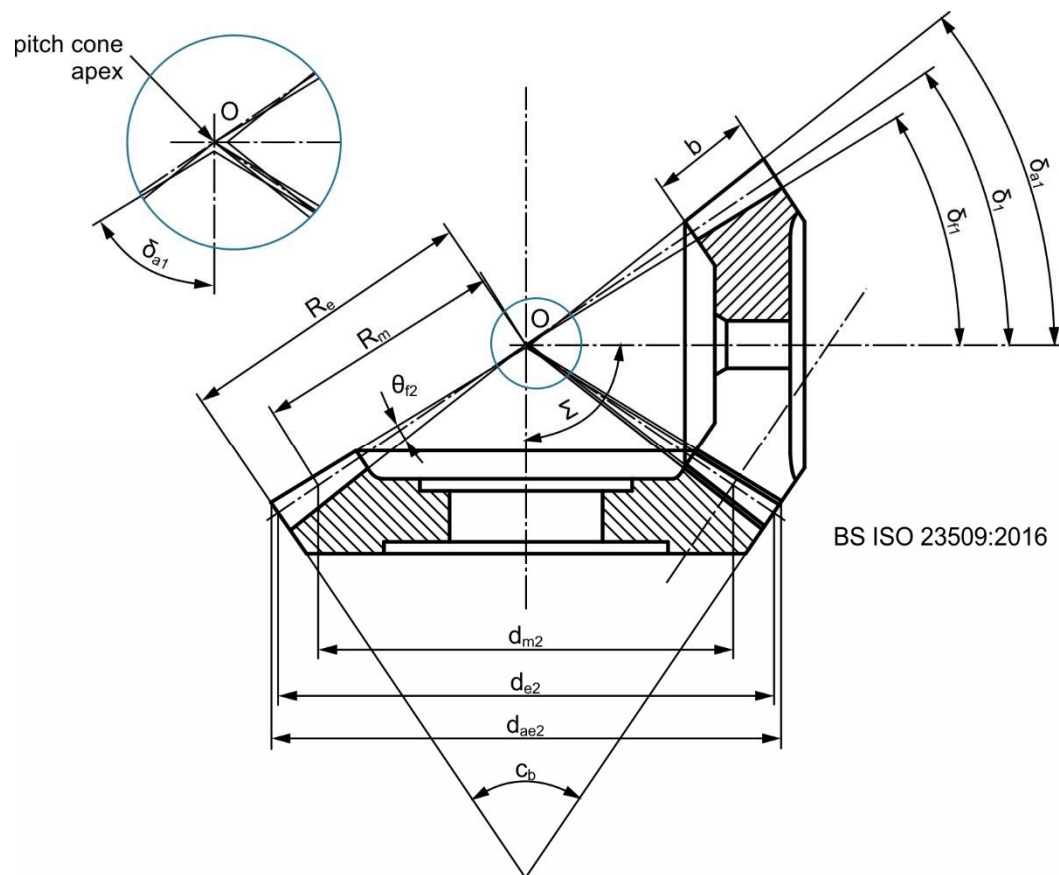


Figure 2.12: Bevel gear pair geometry according to ISO 23509:2016 – Axial plane. [9]

On a given plane perpendicular to the gear shaft, the intersection of the pitch cone with the plane produces the pitch circle. The diameter of the pitch circle is given by equation 2.4.

$$d_0 = z \cdot m \quad (2.4)$$

where:

- d_0 diameter of the pitch circle (mm)
- m module of the bevel gear (mm)
- z number of gear teeth

The diameter of the pitch circle, which varies along the width b of the tooth, has a characteristic value when measured in the middle of the tooth and it is given by equation 2.5.

$$d_m = z \cdot m_{mn} \quad (2.5)$$

where:

- d_m mean pitch diameter (mm)
- m_{mn} mean normal module of the bevel gear (mm)

z number of gear teeth

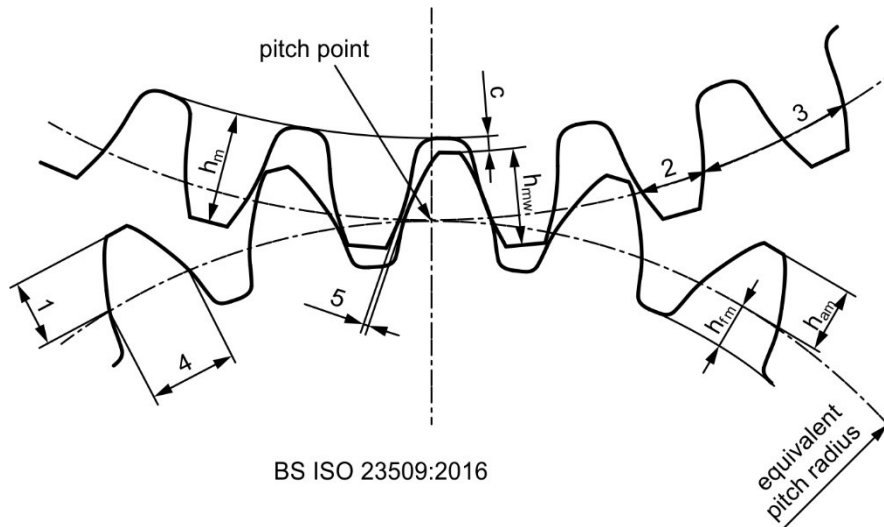


Figure 2.13: Bevel gear pair geometry according to ISO 23509:2016 – Mean transverse section. [9]

Chordal Addendum	1	[mm]	Backlash	5	[mm]
Clearance	c	[mm]	Working depth	h_m	[mm]
Circular Thickness	2	[mm]	Addendum	h_{am}	[mm]
Circular Pitch	3	[mm]	Dedendum	h_{fm}	[mm]
Chordal Thickness	4	[mm]			

Table 2.3: Basic geometric parameters of bevel gears according to ISO 23509:2016.

The pitch of the gear on the pitch circle is given by the following formula:

$$t_0 = m_{mn} \cdot \pi \quad (2.6)$$

All of the parameters included in Table 2.2 and presented in Figure 2.13 are calculated on the pitch cone and pitch circle. The following formulas provide the expressions for the most crucial geometric parameters in bevel gear design.

Pinion pitch angle,

$$\delta_1 = \arctan\left(\frac{\sin \Sigma}{\cos \Sigma + i}\right) \quad (2.7)$$

Gear pitch angle,

$$\delta_2 = \Sigma - \delta_1 \quad (2.8)$$

Outer pitch cone distance,

$$R_{e1,2} = \frac{d_{e2}}{2 \cdot \sin \delta_2} \quad (2.9)$$

Mean cone distance,

$$R_{m1,2} = R_{e1,2} - \frac{b_2}{2} \quad (2.10)$$

Normal pressure angle,

$$a_n \quad (2.11)$$

In the majority of bevel gear drives, the pressure angle is set to 20°. However, smaller pressure angles can be the best option when the gear has a large number of teeth, so a higher contact ratio can be achieved. On the other side, larger values of the pressure angle increase the strength of the tooth and allow fewer teeth without causing undercut.

Spiral angle,

$$\beta_{m1} = \beta_{m2} \quad (2.12)$$

Spiral angle is usually defined in the middle of the face width, even though in spiral bevel gears the spiral angle changes along the face width. This is not the case in skew bevel gears where the spiral angle remains constant along the width of the tooth, like helical cylindrical gears. The most common spiral angle is 35°, but spiral angles ranging from 20° to 45° may also be used. [2]

Mean pitch diameter,

$$d_{m1,2} = 2 \cdot R_{m1,2} \cdot \sin \delta_{1,2} \quad (2.13)$$

Shaft angle,

$$\Delta \Sigma = \Sigma - 90^\circ \quad (2.14)$$

Mean normal module,

$$m_{mn} = \frac{2 \cdot R_{m2} \cdot \sin \delta_2 \cdot \cos \beta_{m2}}{z_2} \quad (2.15)$$

Offset angle on the pinion axial plane,

$$\zeta_m = \arcsin \left(\frac{2a}{d_{m2} + d_{m1} \cdot \frac{\cos \delta_2}{\cos \delta_1}} \right) \quad (2.16)$$

Outer pitch diameter,

$$d_{e2} = 2 \cdot R_{e2} \cdot \sin \delta_2 \quad (2.17)$$

Outer transverse module,

$$m_{et2} = \frac{d_{e2}}{z_2} \quad (2.18)$$

2.3.3 Tooth profile - Spherical involute

If two mating bevel gears are rolling without sliding, one point of the tooth flank rotates over a spherical surface, the centre of which, is the crossing point of the two gear axes. The tooth profile corresponding to this motion is derived either from the intersection of the gear tooth and the spherical surface or from the unrolled complementary cone. [1] Similar to cylindrical gears, a trapezoidal profile is used as the reference profile for bevel gears (profile of the generating rack). The octoid gear has tooth flanks which are identical to the enveloping surfaces generated by the straight flank-generating gear (rotated rack) as the pitch cones of the generating gear and bevel gear roll on each other. Thus the methods used to generate octoid gear teeth and involute teeth on cylindrical gears are equivalent. However, contrary to rolling on a cylinder, when rolling on a cone, the line of action in the case of meshing octoid gear teeth deviates from a straight line. On the spherical surface, the projection of the line of action forms a figure eight curve, shown in [Figure 2.14](#). Although the line of action (E) deviates from a straight line, the two octoid gears are kinematically exact.

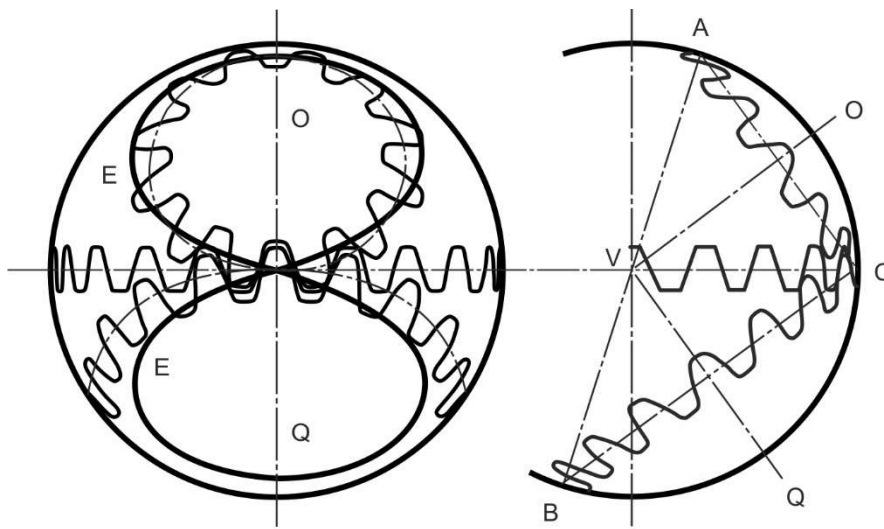


Figure 2.14: Representation of an octoid gear. [1]

Contrary to the straight generating profile of the octoid gears, the spherical involute tooth form requires a curved generating profile. [1] [Figure 2.15](#) shows the schematic representation of the spherical involute which is defined as “a 3D curve traced by a point P on a taut chord MP unwrapping from a base circle of radius r_b that lies on sphere S with origin at O_s and radius r_0 ”. [11] A spherical involute curve is traced on sphere S while P unwraps from the base circle r_b , which is a result of the intersection of the base cone and the sphere of radius r_0 . [11] Therefore, the arc length MP on the sphere periphery equals the arc length MQ on the base circle:

$$r_0 \cdot \omega = r_b \cdot (\phi + \theta) = r_0 \cdot \sin \gamma_b \cdot \psi \quad (2.19)$$

where:

γ_b	base cone angle	(°)
θ	involute polar angle	(°)
ψ	involute roll angle	(°)

$$\psi = \phi + \theta \quad (2.20)$$

Simplifying equation 2.19,

$$\omega = \psi \cdot \sin \gamma_b \quad (2.21)$$

The torque transmitted between the two cylindrical gears is associated with the transmission ratio as follows: The torque on the gear drive input shaft equals $T_1 = F \cdot r_1$ while the torque transmitted to the output shaft equals $T_2 = F \cdot r_2$. As a result, the torque transmitted via the gear drive is multiplied by r_2 / r_1 which equals the transmission ratio.

$$i_{12} = \frac{r_2}{r_1} = \frac{T_1}{T_2} \quad (2.25)$$

where:

T_i torque on shaft i (N·m)

The gear ratio i_{12} of a bevel gear pair is given by the following equations:

$$i_{12} = \frac{n_1}{n_2} = \frac{z_2}{z_1} = \frac{\sin \delta_2}{\sin \delta_1} = \frac{d_{m2}}{d_{m1}} \quad (2.26)$$

where:

z_i number of teeth for gear i (°)

δ_i pitch angle of gear i (°)

d_i mean pitch diameter of gear i (mm)

Figure 2.16 shows a simple bevel gear pair in mesh and the respective gear transmission ratio.

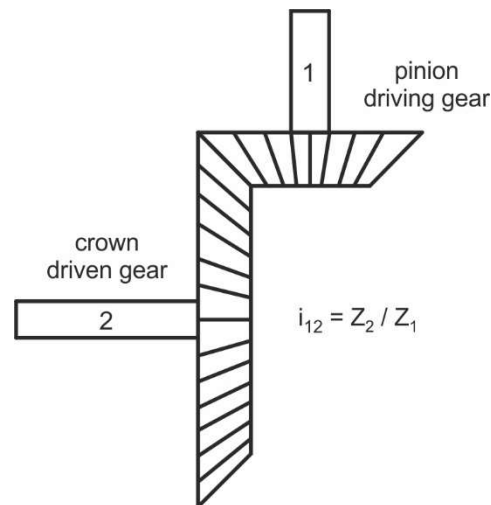


Figure 2.16: Transmission ratio of bevel gear train.

2.3.5 Bevel gear tooth widths and depths

Like most features in bevel gear geometry, tooth width and tooth depth highly depend on the manufacturing method. As a result, the **tooth depth** may be constant or uniform along the face width or increase gradually from toe to heel. Tooth depth is always measured perpendicular to the pitch cone. **Tooth thickness** always varies along the face width, in a way that also depends on the manufacturing method. For instance, tooth thickness in face milling processes can be extremely tapered due to the constant slot width, whereas in face hobbing processes thickness and width variation is split proportionally between the tooth and the slot. Tooth thickness is measured on the pitch cone. The **slot width** is usually tapered so that the width variance is uniformly distributed between the slot and the tooth.

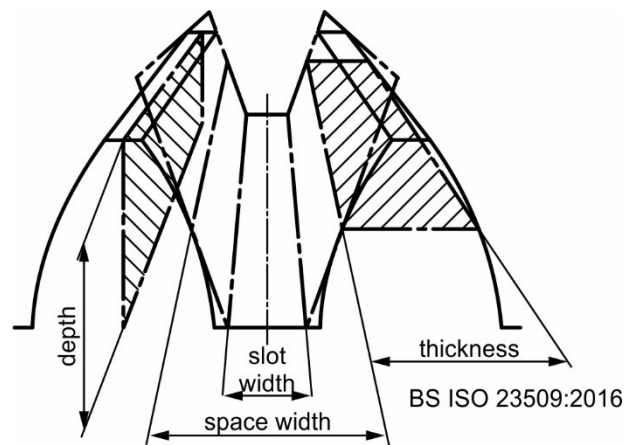


Figure 2.17: Bevel gear tooth depth, thickness and slot width. [9]

Slot width remains the same only in certain face milling processes (completing process) and in Palloid method. The **space width** on the normal section, measured on the pitch cone, is not usually constant. The root line is tilted in the completing face milling process, thus the slot width is constant whereas the space width is tapered along the pitch cone. [Figure 2.17](#) shows the above-mentioned features on a straight bevel gear reference geometry [9]. [Figure 2.18](#) shows the tooth depth variants according to ISO 23509:2016. [9]

Case a: When **the tooth depth is tapered**, the depth becomes bigger proportionally to the distance from the pitch cone apex (cone distance), therefore as the cone distance becomes bigger, the tooth gets deeper. The extension of the root line intersects the gear axis at the pitch cone apex, whereas the tip line intersection to the axis is at a different point, defined by the root line of the mating gear. **Standard depth taper** applies on most straight bevel gears. [9]

Case b: Tooth depth taper coupled with a **constant slot width and a tapered space width**, occurs when the root line is tilted (completing face milling). In this case, the tool radius (r_{c0}) affects significantly the tilt angle of the root line. Large radius tools can produce a very shallow tooth depth at the toe and a very deep tooth at the heel. This may result in very thin top lands and may also cause undesired undercut. Thus in such processes, it is recommended that a tool radius (r_{c0}) no larger than the mean cone distance (R_{m2}) should be used. On the other side, a very small tool radius may have the opposite effect on the root line, resulting in a deeper toe and a shallower heel, thus a lower limit to the value of the tool radius of $[1.1 \cdot R_{m2} \cdot \sin(\beta_{m2})]$ is also recommended. An alternative geometry may occur if the root line is tilted about the mean point. In this case, the ring gear is characterized by a constant tooth width while the pinion has a tapered tooth width along the face width. [9]

Case c: When the **depth is uniform** along the tooth length, the root and tip lines are parallel, therefore root (δ_f) and face (δ_a) angles are equal. Both root and tip lines intersect the gear axis at different points than the pitch cone apex. Constant tooth depth typically occurs as a result of the face hobbing processes. Values of $R_{m2} \cdot \sin(\beta_{m2}) \leq r_{c0} \leq 1.5 \cdot R_{m2} \cdot \sin(\beta_{m2})$ of the cutter radius are suitable for a constant tooth depth geometry. [9]

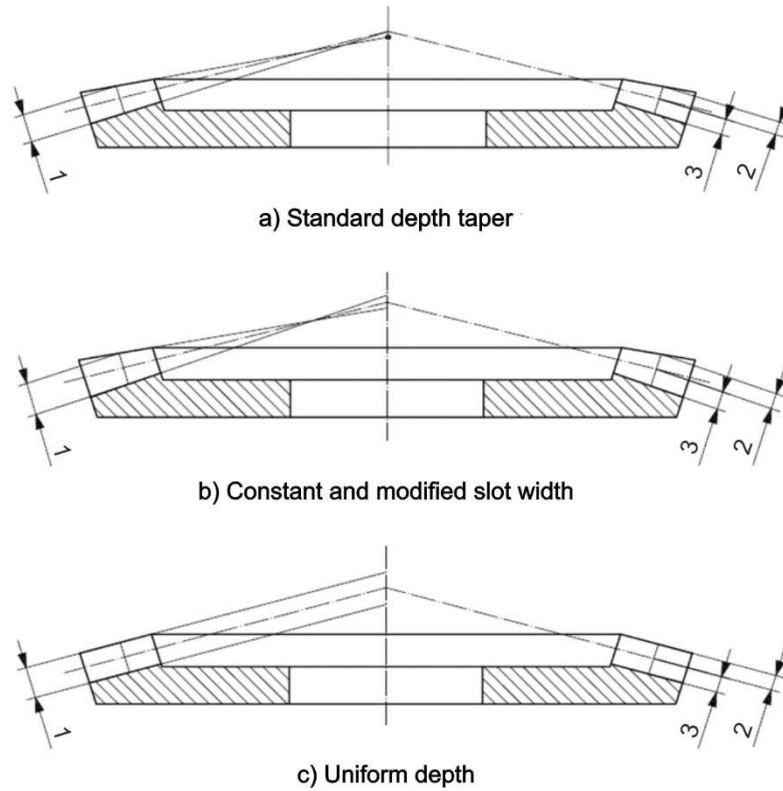


Figure 2.18: Tooth depth variants in bevel gears according to ISO 23509:2016. 1: mean whole depth, 2: mean addendum, 3: mean dedendum. [9]

All tooth depth and width values are specified in ISO 23509:2016. As mentioned above, tooth depth is always measured perpendicular to the pitch cone, while tooth width is measured on the pitch line. Figure 2.19 and the following formulas fully describe the tooth depth and width characteristics calculation process.

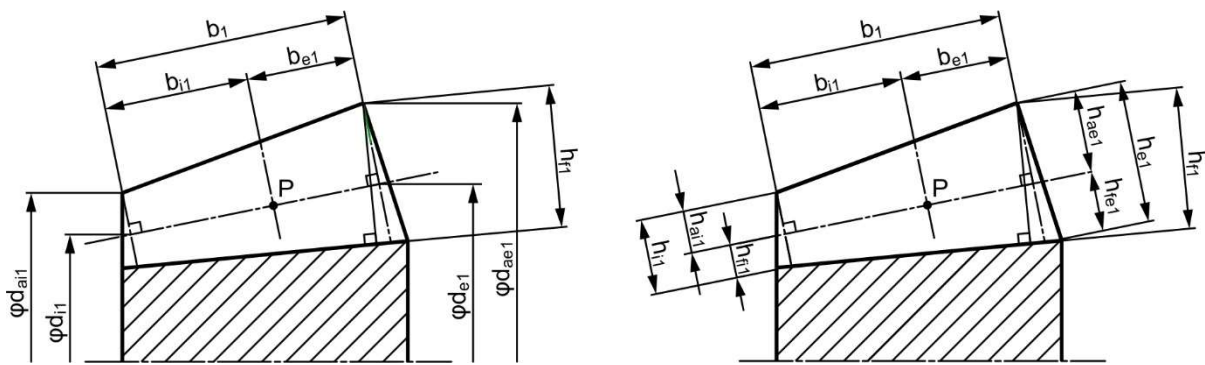


Figure 2.19: Tooth width and depth according to ISO 23509:2016. [9]

Tooth width

Ring gear face width from calculation point P to the outside diameter, b_{e2}

$$b_{e2} = R_{e2} - R_{m2} \tag{2.27}$$

Ring gear face width from calculation point P to the inside diameter, b_{i2}

$$b_{i2} = R_{m2} - R_{i2} \tag{2.28}$$

Ring gear face width, b_2

$$b_2 = b_{e2} + b_{i2} \quad (2.29)$$

Pinion face width, b_1

$$b_1 = b_2 \quad (2.30)$$

Pinion face width from calculation point to the outside diameter, b_{e1}

$$b_{e1} = c_{be2} \cdot b_1 \quad (2.31)$$

Pinion face width from calculation point to the inside diameter, b_{i1}

$$b_{i1} = b_1 - b_{e1} \quad (2.32)$$

Tooth depth

Mean addendum, $h_{am1,2}$

$$h_{am1,2} = m_{mn} \cdot (k_{hap} \pm X_{hm1}) \quad (2.33)$$

Mean dedendum, $h_{fm1,2}$

$$h_{fm1,2} = m_{mn} \cdot (k_{hfp} \pm X_{hm1}) \quad (2.34)$$

Mean whole depth, h_m

$$h_m = h_{am1,2} + h_{fm1,2} \quad (2.35)$$

Outer addendum, $h_{ae1,2}$

$$h_{ae1,2} = h_{am1,2} + b_{e1,2} \cdot \tan\theta_{a1,2} \quad (2.36)$$

Outer dedendum, $h_{fe1,2}$

$$h_{fe1,2} = h_{fm1,2} + b_{e1,2} \cdot \tan\theta_{f1,2} \quad (2.37)$$

Outer whole depth, $h_{e1,2}$

$$h_{e1,2} = h_{ae1,2} + h_{fe1,2} \quad (2.38)$$

Inner addendum, $h_{ai1,2}$

$$h_{ai1,2} = h_{am1,2} - b_{i1,2} \cdot \tan\theta_{a1,2} \quad (2.39)$$

Inner dedendum, $h_{fi1,2}$

$$h_{fi1,2} = h_{fm1,2} - b_{i1,2} \cdot \tan\theta_{f1,2} \quad (2.40)$$

Inner whole depth, $h_{i1,2}$

$$h_{i1,2} = h_{ai1,2} + h_{fi1,2} \quad (2.41)$$

2.4 Bevel gear materials

Steels, cast materials and plastics are commonly used as gear materials. The selection of the suitable material depends on multiple criteria such as gear application, the expected loading conditions, material and production cost etc. [1] More specifically, bevel gears are usually manufactured by one of the following material groups:

- **Plastic and injection molded materials**, such as Nylatron® MC901, Duracon® M90-44, Polyacetal-POM, Polyketone-PK, are used for cost reduction when the expected loads and stresses are low. Plastic gears also offer lower operating noise compared to metal gears. [1, 7]
- **Sintered metals**, made by powder metallurgy, such as SMF 5040, are employed when gears are expected to be subjected to higher loads. Sintered gears are classified between plastic and steel gears as to their load capacity-to-weight ratio. [1]
- **Grey cast iron, ductile iron and cast steels** have the advantage of very good machinability. However, they are considered weak materials, due to the low to medium load carrying capacity compared to steel gears. Cast materials are mostly employed in large-gears manufacturing. [1] High carbon cast steel or alloy steel with Cr, Ni and Mo are commonly used as cast materials for gears to provide high tensile strength. Grey cast iron is indeed a brittle and weaker material when compared to steel, whereas ductile iron has great mechanical properties and can effectively replace carbon steel for cost reduction and vibration damping.
- **Structural and tempering carbon or alloy steels**, such as C45, S45C, 20Cr, 40Cr, show high machinability, medium load capacity, high toughness and lower cost than higher quality steels. [1, 7]
- **Surface-hardened tempering carbon or alloy steels**, such as S45C, SCM440 are used when the requirements in contact strength are higher. The material is heat treated in order to improve the tooth load carrying capacity. Typical heat treatment processes for this group of materials are induction hardening and thermal refining through quenching and tempering. [1, 7]
- **Carbon or alloy steels for thermo-chemical heat treatment** such as nitriding, case hardening or carburizing steels, for example, SCM415, 20MnCr5, SACM645, S15CK. This group of materials offers high geometry and surface quality and also high load carrying capacity and wear resistance. Although thermochemical heat treatment processes are complex and the material subsequently requires hard finishing, high surface hardness and toughness can be achieved. [1, 7]
- **Through-hardened steels** the hardness of which is uniform through the material, thus surface hardness is high regardless of the material removed in hard finishing. [1]
- **Stainless steels**, such as SUS303 and SUS304 are highly resistant to corrosion and rust and are mostly used in applications where rust contamination must be prevented, for example in food processing machinery. Stainless steel, except martensitic stainless steel, does not go through heat treatment to improve mechanical properties such as hardness but only to improve other properties, like brittleness and corrosion resistance. [12]

2.5 Bevel gear manufacturing

Bevel gears can be manufactured either by cutting or casting/forging/forming processes. However, due to complications that may occur when the workpiece is extracted from the mould

or die, casting processes are not commonly applied in bevel gears and especially in spiral bevel gear manufacturing. Non-cutting processes include casting, sintering, extrusion, die forging and tumble forging while cutting processes include planning, milling, face milling, and face hobbing for the soft cutting of bevel gears. Grinding, lapping and honing are frequently used as hard finishing processes.

Figure 2.20 shows the typical process flow chart in a modern high-volume production system for bevel gears. Raw parts imported at the beginning of the bevel gear manufacturing process are forgings that can be used for the production of a variety of parts. Firstly the forgings are turned on a lathe to achieve the desired shape so that bevel gear blank geometry is produced. Following, the main and most crucial process of the production procedure takes place. The formation of gear tooth geometry, via soft cutting processes, lies in the core of the manufacturing procedure. This step can be performed by means of various machining processes that will be thoroughly discussed in this thesis. Further processes such as milling, drilling or tapping are typically performed after tooth formation. When gearing is formed and all additional soft-cutting processes are also completed, the bevel gear goes through the essential hardening through heat treatment. The final stage of gear manufacturing involves the hard finishing of the bevel gear via grinding, lapping or honing depending on the respective soft cutting process used in the previous step. [13]

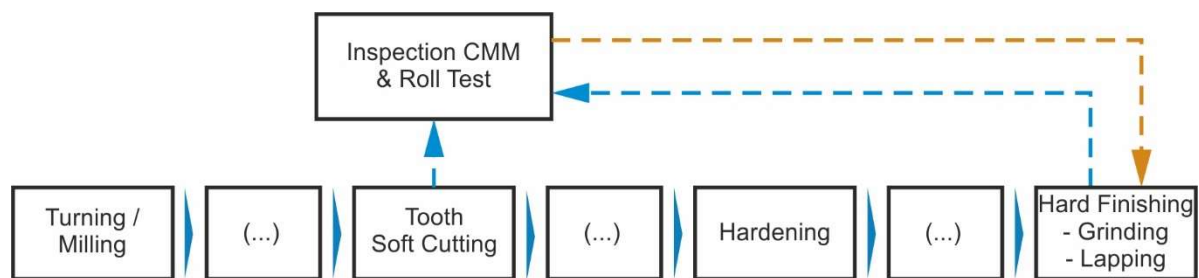


Figure 2.20: Process flow chart of bevel gear manufacturing. [13]

Following, the key historical points in spiral bevel gear manufacturing, with a focus in soft cutting processes, are outlined. Afterwards, the main machining processes for spiral bevel gears, utilized in the soft tooth cutting stage of the production procedure, are presented and their key features and variances are thoroughly discussed.

2.5.1 History of Bevel Gear Manufacturing

Until the early 19th-century gear manufacturing used to be an art and almost all gears were made by hand with the use of mechanisms custom-made for this purpose. The first motorized machines for gear manufacturing and specifically the first gear shapers and gear hobbing machines for cylindrical gears were manufactured in the 19th century. At the end of the 19th century, the first bevel gear cutting machines were also developed. Gear cutting technology evolved radically during the 20th century and various types of machinery and cutting tools were invented. In modern times, toothed wheels are produced in high volumes in numerical control (NC) machine tools which can vary from universal machining centres to specially designed machines produced to perform one or more gear manufacturing methods.

Straight Bevel Gears

As mentioned above, bevel gear cutters started evolving in the late 19th century. As the automotive industry grew rapidly in the 20th century, bevel gears were in high demand for use in differentials. The first bevel gear cutting machine was a gear planer invented by William Gleason in the U.S.A. in 1865 and was employed for the **gear planning** of straight bevel gears. An improved process for bevel gear machining was bevel **gear shaping (milling)** which was

realized in straight bevel gear generating machines, called gear shapers. A major difference between these two methods is found in their kinematics which, in the case of gear planning, is realized by a straight-edged cutting tool mounted on a reciprocating slide while in gear shaping two circular cutter heads (cutting discs), with a peripheral blade arrangement, rotate about their axes to generate the gear slots, as shown in [Figure 2.21](#).

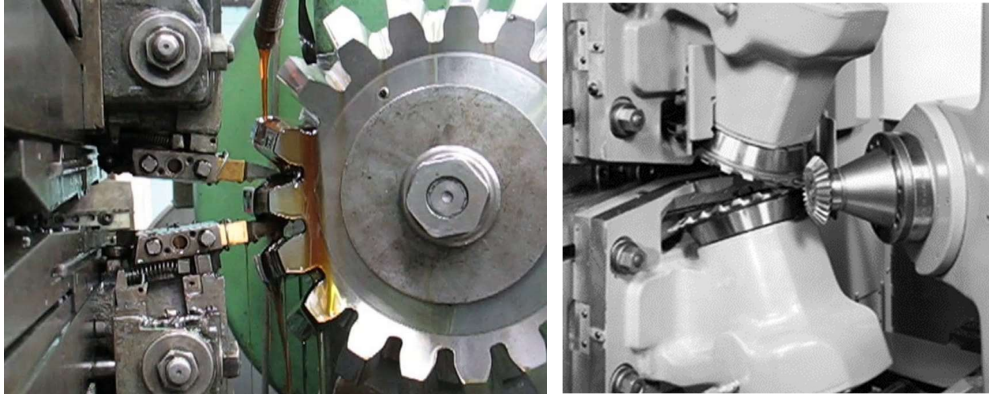


Figure 2.21: Gear planning and Gear Shaping.

Spiral Bevel Gears

During the early 20th century, car differentials were primarily made with straight bevel gears. Following straight bevel gear manufacturing, special generating machines for spiral bevel gear cutting were invented in the early 20th century. In **1913** *'The Gleason Works'* developed a single-indexing **face milling** cutter head method. At that point, the company founder James S. Gleason decided to focus on the single-indexing method only. Most automotive companies in America and Asia used this new method for car and truck axles. The Gleason method was also introduced to Europe where the market was split between Gleason and local European manufacturers. In **1921**, Germans Schicht and Preis applied for a patent for a new method of cutting spiral bevel gears with a conical hob. In **1923** a German manufacturer, *Klingelberg*, produced the first spiral bevel gear **continuous indexing** machine in Europe, using a conical hob based on the Palloid method. The application of this method required two conical hobs with opposing threads in order to produce a pinion and a wheel. This system was utilized by many automotive companies in Europe until the late **1940s**. Apart from the above two methods introduced by the two leading manufacturers (Gleason, Klingelberg), some automotive companies like Fiat and Renault developed their own bevel gear machining methods which were applied until the late 1940s, when the automotive industry stopped using them along with the Palloid method. In the next period, Gleason's single indexing method was the most commonly used for the mass production of bevel and hypoid gear transmissions in the automotive industry. The main reason behind the decision of Gleason to focus only on the single indexing method and the dominance of face milling in the global market for many decades was that, contrary to face-hobbed gears, face-milled gears can go through grinding after heat treatment. In **1946**, *Oerlikon* developed a continuous indexing **face hobbing** method. During this time, some European companies favoured the newly developed face hobbing processes introduced by Oerlikon, called the "N" and "G" methods. However, the first modern continuous indexing process using cutter head tilt and cutters with HSS stick blades for high volume production was introduced by *Oerlikon* in the **1970s**. This new process caught the attention of heavy truck manufacturing companies both in Europe and in America. Ten years later, the first face hobbing machines were installed in gear labs in the U.S for trials and research on this 'new method'. In the meantime, Gleason had also adopted the continuous indexing principle and developed their own face hobbing method. The new method was provided by Gleason with the first CNC bevel gear cutting machines (G-MAXX). Face hobbing gained popularity in the U.S. offering many advantages, for example the reduced machining

time of the completing process, the good tooth spacing and the easy-to-lap tooth surface. At the same time, the completing Gleason face milling process replaced the five-cut method in the European market. The completing method, coupled with the rapid motions provided by CNC technology, offered a reduced overall machining time and high productivity almost comparable with face hobbing. [1, 10, 14]

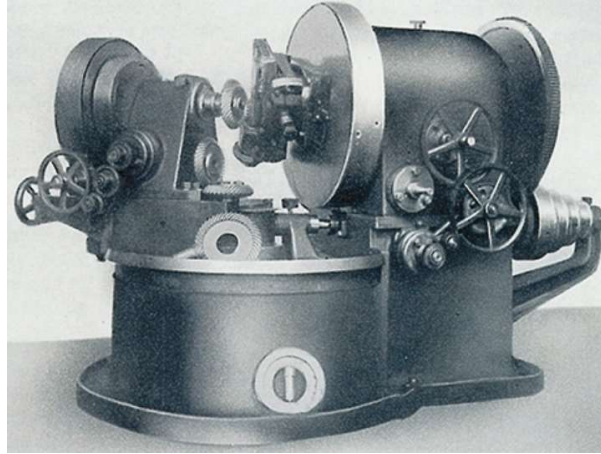


Figure 2.22: Klingelnberg's first spiral bevel gear face hobbing machine. (1923)

For several decades, all these cutting machines had extremely complex mechanics and mechanical drive chains. These high-precision drive chains were replaced by numerically controlled drives in the early **1980s**. Later, the -up to ten- axes of these complex mechanical systems were converted into the kinematics of a six-axes CNC machine, via coordinate transformation. In general, the machining of spiral bevel gear requires all six axes to move simultaneously. The first machine that enabled the production of both face-milled and face-hobbed gears was introduced in **1988**. Nowadays, six-axes generating machines perform almost all machining methods for spiral bevel gears. Since the early **21st century**, there is a growing trend in dry cutting of spiral bevel gears, replacing wet cutting with cooling lubricants. This tendency towards dry cutting leads to further development of the generating machines and cutters to ensure the necessary removal of the hot metal chips produced by the process. Cemented carbide tools in the form of coated stick blades are dominating the field of cutting blades and allow higher cutting speeds, reducing tool wear and production time to a great extent.

2.5.2 Modern machining methods for spiral bevel gears

Various manufacturing processes can be applied to produce spiral bevel gears. Unlike cylindrical gears, the lengthwise geometry and the tooth profile of spiral bevel gears vary according to the employed manufacturing method. Nowadays, there are three dominant types of processes for the soft cutting of spiral bevel gears. Face milling and face hobbing are two completing processes applied in modern CNC spiral bevel gear generators. Alternatively, 5-axis machining on universal milling machines is also used by some manufacturers. The main reason why face milling and face hobbing prevail in the field of soft cutting of spiral bevel gears is their high productivity compared to 5-axis machining. Although face hobbing is superior to five-cut face milling with regards to productivity and machining time, the evolution of face milling to a completing process raised the process productivity up to the level of face hobbing. As a result, these two processes are now mostly used to produce spiral bevel gears, and the selection among them is based on the benefits of each process as per the specific gear-application demands.

Although the CNC evolution simplified the machining of spiral bevel gears to a certain extent, the manufacturing method is still remarkably complex with numerous input parameters. [Figure 2.23](#) provides a diagram of the process input and output parameters.

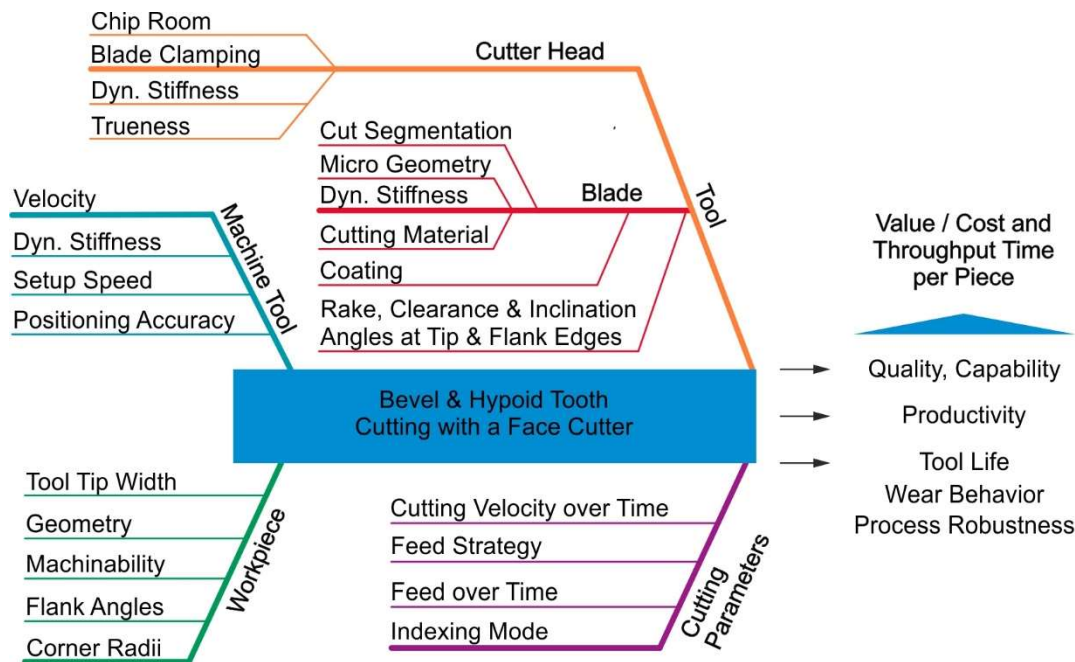


Figure 2.23: Input and output parameters of spiral bevel gear cutting process. [13]

2.5.3 Face milling and face hobbing processes

Face milling is the first manufacturing method of spiral bevel gears by means of a bevel gear generator and a circular cutter head. Face milling is one of the two most popular and productive processes for spiral bevel gear manufacturing. A significant feature that differentiates it from face hobbing is the single indexing technique of machining and that is the reason why face milling processes are also referred to as single indexing processes.

Face hobbing was firstly introduced in Germany by Klingelnberg as a new revolutionary completing process for the machining of spiral bevel gears, aiming to minimize manufacturing time. Face hobbing earned popularity in a short time drawing the attention of constantly more manufacturers and was soon established as one of the two dominant methods for spiral bevel gear manufacturing. A unique attribute of the process and one of its major benefits is the fact that all gear slots are cut simultaneously, therefore face hobbing processes are often mentioned as continuous indexing processes. Face hobbing kinematics is more complex than the kinematics of face milling, making it harder to analyse. Face hobbing cutter heads carry a number of blade groups positioned radially on the cutter. Each group normally has an outer finishing followed by an inner finishing blade, though some cutters also carry a middle roughing blade. In the next few sections, there will be an effort to summarize some of the previous research studies on these processes and a brief presentation of some sample cutting machines and tools, before proceeding to the detailed analysis of each one of them.

Although Gleason, Klingenberg and Oerlikon produce machines that perform both methods successfully, they are still and probably always will be linked with the process that each of them first developed, i.e. face milling (Gleason) and face hobbing (Klingelnberg and Oerlikon) respectively. [15]

In his book [10], Stadtfeld H. documented the major subjects in modern bevel gear technology. In this great contribution to the field, Stadtfeld presented the basics of gear theory including

the transition from cylindrical to bevel gear geometry. An analysis of the two major bevel gear cutting processes providing useful details on the general geometry and kinematic aspects of each process was provided. Pinion and gear tooth geometry produced by both face milling and face hobbing, including width and depth characteristics, surface topology, ease-off and root fillet were described in detail. The effect of specific machine settings, cutter head geometry and cutting blade profile on the produced gear, was also revealed. Application of angular transmissions and useful suggestions for the optimal design of bevel gears based on the optimization of strength, noise and efficiency were included in the textbook. Finally, all major manufacturing methods, machines, and cutting tools were reviewed, with a particular emphasis on Gleason technology.

In his work [1], Klingelnberg J. provided a very useful textbook about bevel gear technology and covered the most important aspects of the subject. Topics such as fields of application, the complicated 3D geometry of bevel gears, and also bevel gear cutting methods and equipment, were all discussed in detail. The textbook also included an analysis on tooth flank development, load capacity and efficiency as well as noise behaviour of bevel gears.

2.5.4 Machine tools for Spiral Bevel Gear Manufacturing

Section 2.5.2 highlighted the complexity of a spiral bevel gear manufacturing system. The core of this system is the machine tool as well as the cutter employed for the machining process. In the following paragraphs, the most common machine tools and cutter heads employed in face milling and face hobbing operations will be briefly presented.

Machine tools used in spiral bevel gear manufacturing are considered to be among the most complex modern cutting machines. The generation of the respective tooth geometry requires the linear motion and/or rotation of six axes in both face milling and face hobbing. As presented in section 2.5.1, spiral bevel gear machine tools progressed significantly during the 20th century with a major milestone being the transition to CNC machining from the conventional machine tools, resulting in more accurate geometries and increased flexibility with respect to the available cutting strategies. Nowadays, there are two major and pioneer machine tool manufacturers for spiral bevel gears based in the U.S.A. and Europe. Following, the general type of modern spiral bevel gear cutting machines but also some of the most characteristic machine tool types of the two dominant manufacturers will be presented, so that the reader can have a full picture of the technological aspects of spiral bevel gear machining. [Figure 2.24](#) shows two generic 3D models of a traditional mechanical (top) and a modern CNC (bottom) spiral bevel and hypoid gear generator. The tooth surface generation model may be derived from the traditional cradle-style machine as the one presented at the top of [Figure 2.24](#). With the use of CNC technology, the motions once performed by the traditional machines have been translated into the motions of the six-axes hypoid gear generators. The six axes move linearly or rotate simultaneously in order to produce the correct tooth geometry. [16] In modern bevel gear generators, such as the Phoenix II generator, the six axes that provide the necessary degrees of freedom for the correct position and orientation of the cutting tool relative to the workpiece are the following:

- A-axis: work gear spindle axis
- C-axis: cutter head spindle axis
- B-axis: swing axis
- 1-axis: Z-axis linear
- 2-axis: X-axis linear
- 3-axis: Y-axis linear

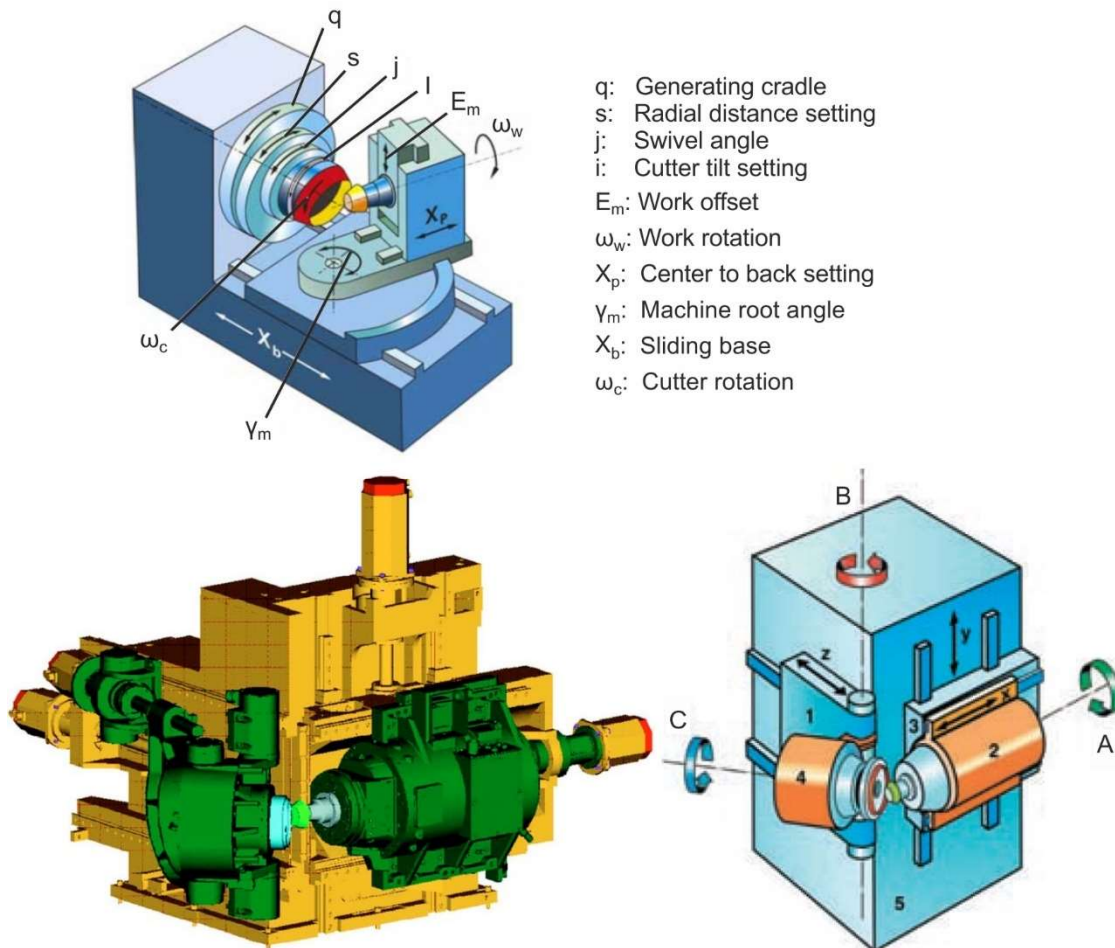


Figure 2.24: Mechanical spiral bevel and hypoid gear generator (top). [17] Gleason Phoenix II CNC spiral bevel hypoid generator basic structure (bottom left & right). [10, 16]

Gleason machine tools

Gleason machine tools are divided into gear generators for spiral bevel gear cutting and universal machining centres for the 5-axis milling of the gears. Hypoid generators such as the Phoenix series generators shown in [Figure 2.25](#), are employed to implement the face milling and face hobbing processes. On the other hand, 5-axis centres like the Heller series presented in [Figure 2.26](#), have gained ground providing more freedom and flexibility, especially in cases of low-volume spiral bevel gear production systems.



Figure 2.25: Gleason Phoenix series for spiral bevel and hypoid gear cutting.



Figure 2.26: Gleason Heller CP series for bevel and cylindrical gear 5-axis machining.

Klingelberg machine tools

Nowadays, all Klingelberg machine tools for spiral bevel gear cutting are Oerlikon-type 6-axis CNC machines. [Figure 2.27](#) shows two typical machine tools included in the Klingelberg C-series.



Figure 2.27: C27 and C100U Klingelberg-Oerlikon machines.

2.5.5 Cutter heads

Bevel gears tooth flank geometry highly depends on the type and geometry of the cutting tool selected for the machining of the gear. Normally, each tool type is used in different machining processes although some tools are designed in such a way that they can be utilized in more than one method. Disc cutter heads with blades that protrude radially on the circumference of the tool are used in the machining of straight bevel gears. In spiral bevel gears, a disc face cutter with the blades protruding axially from the face of the cutter at a particular diameter is used in single indexing processes and produces spiral bevel gears with a circular lead function (face milling). In the case where the blades are axially oriented but positioned in groups of two (or in some cases three) blades, then the cutter is used in continuous indexing processes, producing gear teeth with an extended epicycloid lead function (face hobbing). Another feature that differentiates the existing cutter systems is the way the blades are adjusted on the cutter head. The blades can be either integrated into the cutter head as one solid body (Figure 2.28 bottom centre) or adjusted on the cutter either in groups (Figure 2.29 right) or individually (Figure 2.29 left). Another characteristic that differentiates the type of cutter heads is the way the blades are adjusted on the cutter. There are two different systems: the 1st system where the blades are bolted radially on the circumference of the cutter head (Hardac and Zyklo Palloid), and the 2nd system where the stick blades are housed in cutter head slots and are positioned with clamp screws (Figure 2.28 top centre and right, bottom left).



Figure 2.28: Gleason cutters for straight and spiral bevel gears for face milling, face hobbing and 5-axis machining (top left to right: Coniflex straight, Pentac Plus FM-FH, Tri-AC FH. bottom left to right: RSR FM, Solid FM Pentac slim line 5-Axis).



Figure 2.29: Klingelnberg cutters for face milling (left-Arcoflex) and face hobbing (right-Zyklo Palloid) operations.

2.5.6 Cutting blades

All modern disc cutter heads for spiral bevel gear cutting in generating machines are equipped with blades that protrude from the face of the cutter, as presented above. The shape, material, and arrangement of the blades on the cutter have been the subject of research and development, as bevel gear technology advances. [Figure 2.30](#) shows some characteristic types of blades and stick blades and [Figure 2.31](#) presents their most significant geometric features.



Figure 2.30: Common types of cutting blades (Top, left to right: Hardac, RSR, Pentac, finished with PVD coating, roughed, blank geometry. Bottom: ETC carbide and HSS stick blades).

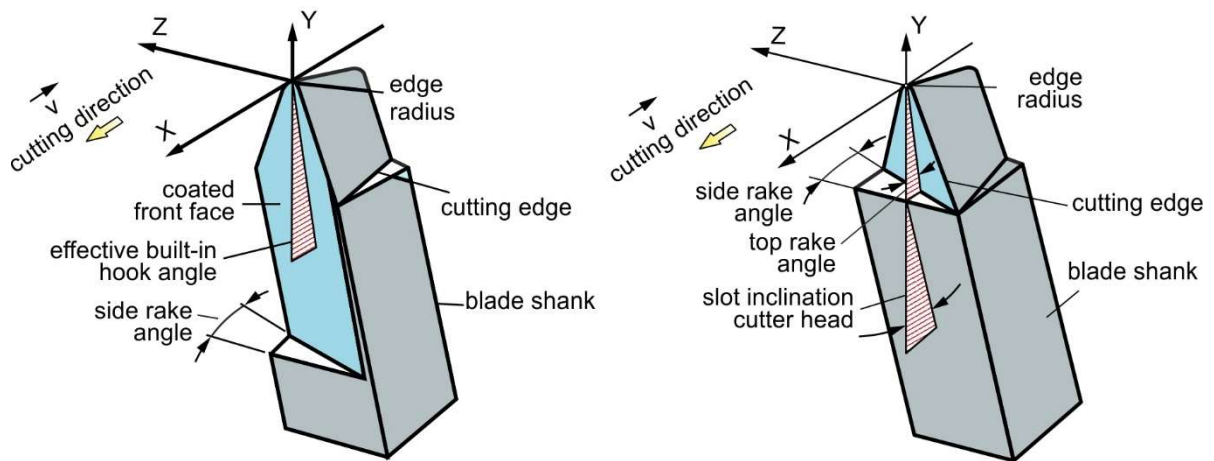


Figure 2.31: Cutting stick blades geometry.

2.5.7 Cutting tool material and cutting speeds

2.5.7.1 Main or substrate materials

The first cutting tools used in spiral bevel gear machining were mostly made of **HSS** which consisted of 18% tungsten carbide, 4% chromium, and 1% vanadium. Nowadays, there is a variety of materials that can be used in cutting blades such as various types of HSS and carbide materials. Due to the complexity of their manufacturing, profile blades are still made with HSS materials. When it comes to stick blades which are much easier to manufacture though, cemented carbide cutting tools have greatly progressed due to the direction of the current technology towards high-speed dry cutting, which has been constantly gaining ground against the old wet cutting processes. Carbide is heavier than steel, and much harder but not as tough. **Cemented carbides** which consist of 70-95% tungsten carbide, **ISO K** grade carbides of up to 90% tungsten carbide and up to 6-10% cobalt are commonly used and have proven to be very suitable for machining of bevel gears. It is worth mentioning that the high cobalt content increases not only toughness but brittleness as well, compromising the wear resistance properties of the material. One thing is certain when it comes to selecting a substrate material, the specific machining task and the material of the work gear should be taken into account. For instance, cemented carbide substrates are prone to diffusion wear in case of hardened steel cutting, whereas tungsten carbide dissolves. Finally, coating the stick blades is necessary in most cases and considerably prolongs tool life. [1, 18]

2.5.7.2 Coatings

The first tool coatings for bevel gear cutting tools were introduced in the 1980s, with the most prevalent choice being Titanium Nitride (TiN) which worked well with HSS tools in wet cutting processes. Titanium Aluminum Nitride (TiAlN) was developed in the next decade and was established as a coating for carbide cutting blades in dry cutting processes of hard materials. Some of the most popular coatings used nowadays are AlNite, a single layer TiAlN coating with a 50:50 ratio of Titanium to Aluminum. It is suitable for wet or dry cutting of all steels including stainless and cast iron. AlNite-X, which is also a single layer TiAlN coating specialized for wet or dry cutting of hardened steel workpieces. AlCroNite, which is a high-performance, titanium-free coating with very good wear resistance. nACo, a nanocomposite coating consisting of AlTiN nano-sized particles included in an amorphous silicon nitride matrix. [18]

2.6 Hard Finishing of Spiral Bevel Gears

The final stage of spiral bevel gear manufacturing is the finishing process that all gears undergo regardless of which method has been used for the soft-cutting process. Finishing is necessary in order to improve surface quality after soft cutting and heat treatment, depending on the

quality requirements of the specific application. There are three commonly used hard finishing processes for spiral bevel gears: Lapping, Grinding and Hard Skiving.

2.6.1 Lapping

Spiral bevel gear lapping is applied mostly on face-hobbed bevel gears. During lapping, the pinion and the ring gear roll together as if they were assembled in a gearbox. The operation is applied on special machines manufactured for this purpose, the lapping machines. A compound which has both lubricating and abrasive properties is fed between the meshed teeth of the gear pair. This way, the contacting surfaces are finished, and any distortions caused by the heat treatment process are compensated. Following the lapping operation, the correct relative position of the two gears is verified in a testing machine so that transmission errors are minimized. [12] Lapping is mostly applied as a hard finishing process of face-hobbed spiral bevel gears. Generally, face-milled spiral bevel gears are difficult to lap due to the parallel generating flanks and contact lines, a feature that will be discussed in the following chapter. Hypoid gears are even more suitable for the lapping process. [10]

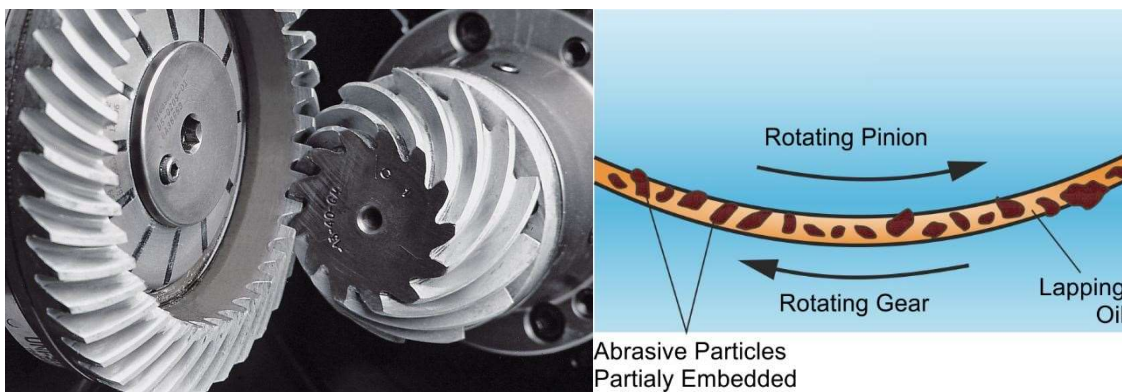


Figure 2.32: Lapping of spiral bevel gears.

2.6.2 Grinding

Hard finishing through grinding can only be applied for face-milled spiral bevel gears in a completing process. This is because face-milled spiral bevel gears have circular lengthwise tooth curves in contrast to face-hobbed gears which have teeth with an epicyclic lead function. This makes grinding of face-hobbed gears with a circular disc cutter impossible without modifying the tooth geometry.

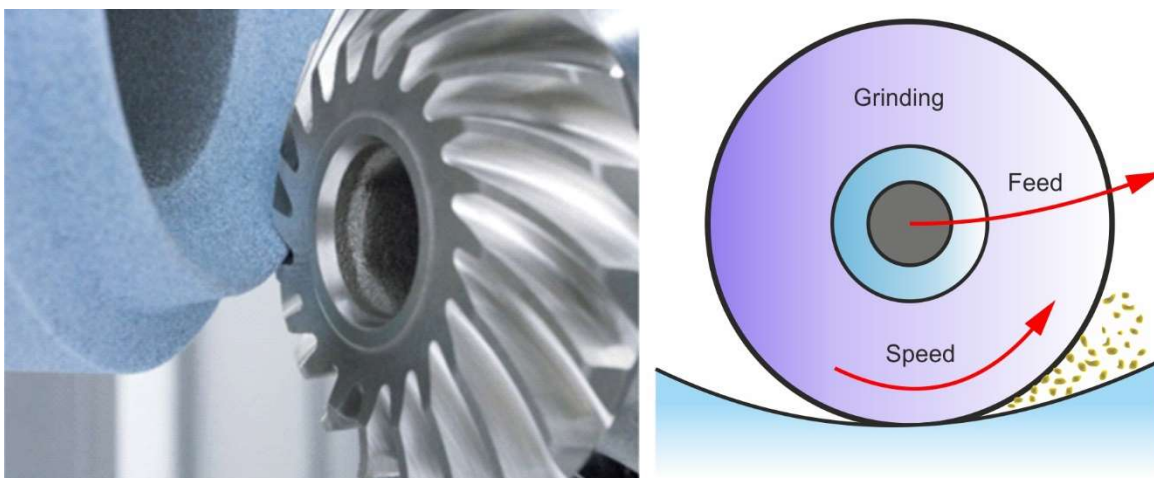


Figure 2.33: Grinding of spiral bevel gears.

For face-milled gears grinding, it is recommended that, due to strength reasons, the roots are not ground. However, a smooth transmission from the ground flank surfaces to the root through the fillet region is expected. Ground spiral bevel gear sets demonstrate quality conforming to AGMA class 12 and 13. Even so, the surface roughness after grinding is higher than after lapping operations. The strength of ground gear pairs equals the strength of the respective lapped gear pairs. [10]

2.6.3 Hard Skiving

Hard Skiving is a finishing process applied only on face-hobbed spiral bevel gears. In hard skiving, excess material of about 0.1 mm to 0.15 mm is removed with the use of either coated carbide blades (Gleason) or brazed CBN cutting strips (Klingelnberg). The tips of the cutting blades do not contact the workpiece; therefore, the depth of the hard finishing process is smaller than the respective soft cutting process. The quality achieved through hard skiving of spiral bevel gears is AGMA 12 to 13. The flank surfaces have a very good finish. [10]

2.7 Academic state of the art in spiral bevel gear manufacturing

2.7.1 State of the art in face milling process

Klocke F. and Klein A. [19] conducted experimental trials of dry high-speed bevel gear cutting, to determine the effect of cutting speed and feed on the tool life of the cutting blades, in a thorough cutting parameter investigation. Wear land width and chipping size were measured in order to monitor the blade wear through tool life. At the end of each trial, the cutting blades were examined with the use of a scanning electron microscope. Regarding the parameter investigation, the increase in cutting speed led to the increase of tool wear, while an optimum value of feedrate was determined. Fully coated tools showed a much better wear behavior than only-rake coated tools whose tool life was significantly lower. Finally, a new concept face milling cutting tool was presented.

Fan Q. et al. [17] presented a new method for the correction of tooth flank form error using the universal motions of face milling for spiral bevel and hypoid gears manufacturing. An investigation of the sensitivity of tooth flank form geometry to the variation of universal motion coefficients was carried out. The study proposed the corrective universal motion coefficients which were obtained via an optimization process aiming at the minimization of tooth flank form errors. Finally, a case study of a face milling completing process was presented by the authors, in order to prove the proposed method.

Zheng F. et al. [20] proposed a face milling method for the manufacturing of noncircular spiral bevel gears offering high productivity, using common CNC hypoid generators. The study presented the mathematical model of the new method, the tooth surfaces by position and normal vectors and also the kinematic model of free-form CNC machines. A real pair of noncircular spiral bevel gears, manufactured as an example of the proposed generation method, was showcased. A roll test of the new gear pair was conducted, and the obtained contact patterns showed good agreement with those modelled in a commercial CAE software.

Zhang Y. et al. [21] presented a study for the optimization of meshing performance of spiral bevel gears, machined with the duplex helical method, by modifying the straight cutting edges of the tool blades and using circular cutting edges instead. The mathematical model of the spiral bevel and hypoid gear tooth, generated by the circular cutting edges, was presented. A tooth contact analysis to investigate the effect of straight-lined and circular cutting edges on the tooth bearings and contact stresses in four design cases was conducted. The results revealed that the use of the appropriate circular blade profile, can increase the length of the

bearing contact, and reduce the contact stresses, while the areas of edge contact can be avoided.

Wang P.Y. et al. [22] proposed a method to improve the adjustability of face-milled spiral bevel gears by modifying the radial motion of the cutter. The conventional way to modify the lengthwise curve of the tooth requires a change of the cutter diameter or tilt. On the contrary, the modifications proposed by this study can be applied by the CNC controller without requiring any tool change or tool dismounting. The results showed an increase on the adjustability while the bearing contact ratio remained the same.

In his PhD thesis, Xie S. [23] presented an approach of modelling the genuine tooth surfaces for the face-milled bevel and hypoid gears. A geometric model of a cutter was created, and gear tooth surfaces were developed based on the non-generated gear and generated pinion kinematics. The tooth surfaces were represented as NURBS surfaces by optimizing the number of sampling and control points.

Usubamatov R. et al. [24] introduced a new method for face milling of spiral bevel gears with the use of two cutter heads to machine both concave and convex flanks simultaneously. The purpose of their work was to improve both the productivity and quality of the produced gears.

Zheng F. et al. [25] proposed an algorithm for the calculation of surface roughness in face milling taking the insert run-out errors into consideration. The effect of the design and process parameters on roughness distribution was presented through both a numerical study and experiments.

Zhou Y. et al. [26] proposed a novel method that recalculates the face-milled tooth surface points to generate approximately equidistant curves. The study included a mapping between the isoparametric surface curves and the new approximately equidistant curves, as well as an optimization algorithm, in order to obtain the tooth surface points of the new curves.

A method that replaced the straight cutting edge blades with arc-shaped blades in order to achieve a tooth surface modification on face-milled spiral bevel gears was proposed by Mu Y. et al. [27]. The modified tooth surfaces of pinion and gear were obtained based on the principle of gear mesh and differential geometry. Finite element analysis and tooth contact analysis were employed to verify the effectiveness of the proposed modifications, showing a reduction of the tooth edge contact and also a reduction of the maximum contact stress.

Zheng F. et al. [28] proposed an analytical model for the prediction of static cutting forces in face milling of spiral bevel gears, analyzing the elementary chip geometry in six cutter-workpiece relative positions. Then a dynamic chip calculation method was developed. The proposed method was validated through experimental trials for the dynamic cutting force, cutting vibration and chatter stability.

Mazak J. et al. [29] presented a simulation model for face milling of bevel gears based on discretised gear blank and tool geometries. The simulation model they developed was based on a series of intersecting planes, on which the tool profile was projected in order to calculate the penetration of the tool. In this way, the 3D simulation of the process was reduced in a 2D analysis. The authors presented an investigation of the process kinematics, the chip geometry and the effect of the chip thickness calculation method on the results of the model. The resulting gear geometry was compared with theoretical flank points.

Litvin F. et al. [30] proposed a method for conjugate spiral bevel gear generation with no kinematic errors. The method could be applied with the use of Gleason generators. As a result of their study, machine tool settings were determined and a tooth contact analysis (TCA) program was developed to simulate bearing contact and investigate the effect of assembly and manufacturing errors.

2.7.2 State of the art in face hobbing process

Vimercati M. [31] presented a method for the computerized design of face-hobbed hypoid gears. A mathematical model for the computation of gear tooth surface representation was developed. The obtained geometry was used as input for a tooth contact analysis conducted with a method that combines finite element analysis and semi-analytical solutions.

In his study, Fan Q. [16], gave a detailed insight into the theoretical framework of the face hobbing process developed by Gleason. The article presented a complete description of the process kinematics, a mathematical model of the tooth flank surface generation process for both non-generated and generated Gleason methods and a general description of the cutting blades' geometry. Additionally, the study introduced a new TCA algorithm for face-hobbed gearsets.

Fan Q. [32] in his paper presented the theory of the face hobbing process and provided useful mathematical models of the tooth lengthwise curve and tooth surface generation for Formate and generating methods.

Shih Y.P. et al. [33] proposed a universal mathematical model for the simulation of all face hobbing and face milling processes. The model calculates the transformation matrices that represent the relative positions of the cutter blade, the generating gear and the work gear. For the verification of the proposed approach, the model is applied to a Klingelnberg Cyclo-Paloid hypoid generation.

An optimization algorithm was developed by Simon V. [34] in order to detect the optimal cutter-head geometry and machine-tool settings, so to reduce the tooth contact pressure and angular displacement error, and also minimize the sensitivity of face-hobbed gears to misalignments.

Habibi M. and Chen Z.C. [35], conducted research focusing on the improvement of tool wear that occurs on the tool tip corner during face hobbing of bevel gears. After presenting a complete mathematical description of the cutting blade, the study proposes a new method to design blades with decreased gradients of working rake and relief angles along the cutting edge, in order to improve tool wear on the tool corner. The positive influence of this approach in tool life is verified by a FEA simulation that compares the effectiveness of the proposed blades and the conventional ones.

Habibi M. et al. [36] introduced a semi-analytical description of the projection of the undeformed chip geometry on the rake face of face hobbing cutting blades. The purpose of the study is to achieve the prediction of cutting forces utilizing the oblique cutting theory on the derived chip geometry, converting face hobbing into many small oblique cuts along the cutting edge. The proposed method was applied in two case studies.

Perez I. and Aznar A.F. [37] presented a comparative study of two popular face hobbing methods, ie *Cyclo-Paloid*TM and *Cyclo-Cut*TM. The study compared the two tooth surfaces produced by the respective computerized generation models. Through the implementation of tooth contact and backlash analysis, the similarities and differences of the two processes were

detected and the possibility of interchanging the two produced gear geometries in cyclo-palloid and cyclo-cut drives was examined.

In their study, Perez I. and Aznar A.F. [38] proposed a method for the analytical determination of the basic machine-tool settings to achieve conjugated action in face-hobbed and hypoid gear drives using the Spirac system. They also proposed a new method for longitudinal crowning of the pinion tooth surfaces.

Liu S. et al. [39] proposed a mathematical model, mesh models and a quasi-static loaded tooth contact analysis with FEA to investigate the effect of radial and angular eccentricity errors of the work holding equipment on both the gear flank geometry and the contact behavior of face-hobbed hypoid gears.

Zhang W. et al. [40] presented a method for grinding the teeth of formate face-hobbed hypoid gears with the use of a large-diameter conical grinding wheel. In this scope, a 5-axis tool location calculation model was established, to position the grinding wheel correctly, avoid interferences and achieve an accurately produced tooth profile in a CNC hypoid grinding machine.

In their study, Guo W. et al. [41] focused on a tool path active design method for tooth modification of face-hobbed spiral bevel gears. The method uses integrated cutter heads without tilting, along with simplified machine settings, achieving the correction the face-hobbed tooth surfaces by modifying the tool path and curvature radius of the circular profile blades, according to the meshing performance.

Habibi M. et al. [42] proposed a semi-analytical method for the optimization of Formate face hobbing of spiral bevel gears by minimizing the plunge time with respect to cutting forces and tool wear constraints.

2.7.3 State of the art in 5-axis universal machines

The most popular methods for spiral bevel gear manufacturing are the face milling and face hobbing processes. However, the main drawback of these methods lies in the fact that they can only be applied in specialized hypoid generators which are exclusively made for these processes. Although these machine tools are suitable for mass production of bevel gears, they are not suitable for limited production, small batches, or prototypes.

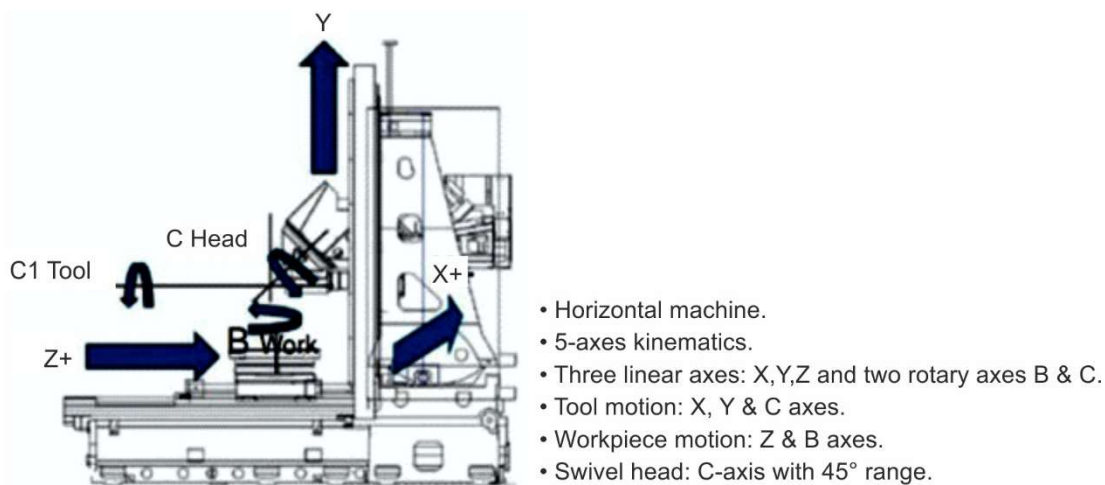


Figure 2.34: 5-axis machining kinematics for spiral bevel gears.

When this is the case, spiral bevel gears can be manufactured more efficiently in 5-axis universal milling centres, since these machine tools can be utilized for a wide range of machining processes. In recent years, many machine tool and cutting tool manufacturers have developed methods, tools and software for 5-axis bevel gear cutting. The 5-axis machining of spiral bevel gears can be applied with the use of either disc-shaped cutters with indexable inserts or solid carbide endmills.

Alvarez A. et al. [43] conducted experiments of 5-axis milling of spiral bevel gears applying different cutting strategies and tool paths in roughing and finishing operations. Solid endmills and tapered ball endmills were used for roughing and finishing respectively. The purpose of the study was to identify the optimal cutting strategy with respect to machining time and surface quality which was measured with the use of a profilometer and a surface roughness tester.

Zhou Y. et al. [44] studied the process of 5-axis milling of spiral bevel gears and presented a new method for the design of tooth flanks with ruled surfaces. As a result of this method, cutter position and orientation during the process can be calculated and the actual tooth flank surfaces can be accurately represented with the cutter envelope surface. The method is applied for both pinion and ring gear and the two gears are meshed so a tooth contact analysis can be performed. Results of the TCA indicate that the proposed method is valid and can be used for the 5-axis machining of spiral bevel gears.

Shih Y.P. et al. [45] proposed an alternative method for the machining of large spiral bevel gears with a disc-shaped tool in a 5-axis machine. The mathematical models of the tool and the machine's coordinate systems were presented, and a method that converts the tooth surface topography into machine and tool coordinates through inverse kinematics was developed. The coordinates were then used for the generation of the respective NC code which was simulated in Vericut.

2.7.4 Previous simulation models in bevel gear manufacturing

The simulation of manufacturing processes has been a field of significant research interest. In most cases, simulation is necessary for process optimization, as it contributes significantly to improving productivity, increasing of tool life, reducing machining time and cost, and increase of the machined part quality. Simulation models can substitute extensive experimental trials which are time-consuming and raise the total manufacturing cost. The goal of machining simulation is to increase the knowledge of the cutting process and improve it by optimizing the process parameters. Although many researchers have focused on this area and worked on building simulation approaches, there are many challenges in this effort, the most important of which are:

1. Complexity and variety of the phenomena that occur during machining.
2. Complexity of the kinematic aspect of the process.
3. High sensitivity of the process results in tool geometry and machine settings.
4. High computational power requirements.

Depending on each simulation method, some of these challenges can be overcome. For example, a purely kinematical simulation would not have to deal with issues concerning the thermomechanical phenomena of the process.

Gear cutting simulation has drawn the attention of many researchers due to the high productivity of these processes but also the excessive tool wear phenomena that occur during the material removal. Although many simulation approaches and models have been introduced for most gear cutting processes, research on simulation of bevel gear manufacturing is limited

to a few research studies. The reasons for this lack of research in this field are mainly the high complexity of the process kinematics, the specialized tool geometry, and the customized machine settings. All these challenges make these processes very difficult to analyse and therefore almost impossible to simulate in a universal model. In the following paragraphs, the most important simulation approaches are summarized and their strengths as well as their limitations are highlighted.

A study was carried out by Klocke et al. [46] to analyze the effect of cutting tool profile geometry on thermal and mechanical tool load in spiral bevel gear cutting. To this end, a finite element simulation model was developed to calculate chip formation in ring gear cutting. The simulation results showed high thermal and mechanical load on the tool corner. The investigation of tool profile geometry revealed a significant effect of both pressure angle and corner radius variation on the thermal and mechanical load on the tool corner and a minor effect on the respective load on the tip and flank edge.

Brecher et al. [47] developed a manufacturing simulation approach for the analysis and optimization of bevel gear cutting processes. The simulation included modelling of the tool, workpiece and kinematics, and also a 3D-geometrical penetration calculation which was realized by ray-tracing. The undeformed chip geometry was calculated from the penetrated volume and characteristic values, like the chip thickness, were derived. Since the material of the chip is compressed and squeezed on the corner radius of the tool tip, a simple analysis of the chip thickness in this area of the tool was considered not sufficient by the authors. A new characteristic value was proposed, which integrated the variation of the chip thickness, working rake angle and working relief angle into one value, and allowed a different approach to a tool wear prediction model.

Jiang C. et al. [48] presented a mathematical method for the calculation of cutting forces in form cutting (non-generating) of hypoid gears. The model considers the tooth line and corner radius of the cutting blade and calculates both cutting depth and cutting thickness. These values are used so that cutting forces can be calculated. In addition, a FEA simulation of the cutting process was conducted in *Deform* and the results were compared to the theoretical ones. Finally, an experimental procedure was carried out to further verify the results of the proposed calculation method.

Brecher C. et al. [49] conducted a finite element-based tooth contact analysis for the optimization of face-milled bevel gears in terms of load capacity, efficiency, and noise performance. For this purpose, the excitation behavior of face-milled gears was evaluated through the analysis of the gear set transmission error. The comparison of the simulated and experimentally measured transmission error showed good agreement between simulation results and testing measurements.

In their work [50], Litvin F.L. and Fuentes A., developed a FEA model of a spiral bevel gear drive to identify contact and bending stresses, investigate the formation of bearing contact and detect any hidden areas with increased contact stress. An example of a face milled generated spiral bevel gear drive was presented.

Figliolini G. and Angeles J. [51] presented formulations and algorithms, based on the envelope theory, for the mathematical generation of involute and octoidal bevel gear. The spherical involute tooth profile and the tooth-flank surface of octoidal gears were obtained.

Bijonowski B. [52] proposed a method for the calculation of a close approximation of the spiral bevel gear geometry, based on formulas described in AGMA 929-A06 [53]. The purpose of the

proposed method was to produce generalized equations for the calculation of the normal tooth thickness anywhere along the tooth lengthwise direction. The resulted 3D geometry was compared with data obtained from a Gleason software.

Shiraishi S. et al. [54] developed an analytical model for the prediction of cutting force in hypoid gear machining. A cutting experiment was conducted to validate the results of the model.

2.8 Present research necessity and contribution

The above research efforts are mainly based on mathematical, analytical or finite element analysis models for face-milled and face-hobbed bevel gears. Therefore, there is a lack of research in the field of 3D kinematic simulation of face milling and face hobbing process, the calculation of cutting forces using the undeformed solid chip geometry as well as the investigation of cutting parameters' effect on the process. The present study introduces the simulation methodology and simulation results of the first full 3D kinematic simulation model of the spiral bevel gear cutting processes, which is one of the key innovations of the proposed methodology. Face milling and face hobbing simulation has not yet been investigated in the context of 3D CAD-based simulation. The 3D CAD kinematic simulation approach offers higher accuracy compared to purely mathematical models. Furthermore, kinematic simulation requires much lower computational power and resources, compared to 3D finite element analysis approaches. Spiral bevel gear cutting forces calculation, by means of undeformed solid chip geometry analysis, is also first introduced in the present study along with indicative calculation results. Both *BevelSim3D* and *BevelForce3D* algorithms can assist academic research teams in performing in-depth analysis of face milling and face hobbing and also contribute to the complete optimization of the process from an academic perspective. In practical application, simulation models are powerful tools in modern machine shops and gear manufacturing companies, they support manufacturing process development and optimization while reducing the amount of experimentation required. [55]

The cutting simulation model *BevelSim3D* achieves the generation of the solid tooth flank and solid chip geometries that can be subsequently used in the selection of the correct cutting parameters for improved surface quality and also the calculation of cutting forces. The model performs the simulation of both face milling and face hobbing processes, and the results are validated through the comparison of the simulated and theoretical surface geometry by means of a novel validation algorithm. Furthermore, cutting forces calculation methodology is described for the first time and cutting forces results for sample face hobbing simulations are also included. This approach aims to enable the selection of optimal process parameters, such as cutting conditions and machining method, according to the desired tooth flank surface quality and minimization of the cutting forces. The implementation of multiple simulations using key cutting parameters can reveal the effect of each parameter on the obtained tooth surface quality. An investigation of the influence of generation feedrate on the quality of the simulated tooth surface geometry is presented in the study. In addition, finishing stock allowance, plunge feedrate, and generation feedrate are investigated for their effect on the developed cutting forces. Regarding the limitations of the present methodology, it must be mentioned that in a purely kinematic simulation model, thermomechanical phenomena that take place during the machining process are not taken into account and the participating tool and workpiece geometries are considered to be undeformed. [55]

[This page intentionally left blank]

3. KINEMATICS OF SPIRAL BEVEL GEAR CUTTING

The heart of a kinematic simulation model is the process kinematics together with the geometric characteristics of the workpiece and the tool involved in the process. This chapter aims to provide a detailed description of face milling and face hobbing kinematics, to ensure a complete understanding of the two processes before presenting the model created to simulate them. In the following sections, the kinematics of both processes will be analysed and all the advantages and drawbacks of each process will be highlighted.

3.1 Spiral Bevel Gear Machining Theory

3.1.1 Generation Principle

As described in section 2.3.2, the transition from cylindrical to bevel gear generation theory can be easily made if the generating rack of the cylindrical gears bends around an imaginary axis. In accordance with the generation of a cylindrical gear pair with the use of two complementary rack cutters, when it comes to a bevel gear pair generation, i.e. pinion – ring, two complementary crown gears are used. Obviously, in the case of spiral bevel or hypoid gears, the corresponding generating crown gear has spiral teeth as well. Taking it a step further, if the pinion gear engages perfectly with the generating crown gear and if the ring gear is also in an exact mesh with the generating crown, then it can be safely deduced that should the common generating gear be virtually removed from the system, the two mating gears, pinion and ring would perfectly mesh with each other. [Figure 3.1](#) presents the basic concept of bevel gear cutting and gives the generic set-up of all hypoid gear generators. [10, 17]

The above theory also leads to the identification of the necessary kinematic coupling conditions for a conjugate pair of bevel gears. First, the generating gears of the two mating bevel gears must have congruent flanks. Simply put, the pinion and the ring gear have one virtual common generating gear with mirror flank surfaces. Secondly, the two generating gears rotate around the same axis. Finally, the surfaces of engagement of the three virtual pairs, i.e. pinion-virtual generating gear, ring-virtual generating gear, pinion-ring gear must be identical. As it can be easily concluded by the three kinematic conditions, in order for the pinion to be conjugate to the ring in a bevel gear mesh, the two virtual generating crown gears must in fact be a common generating crown for both gears.

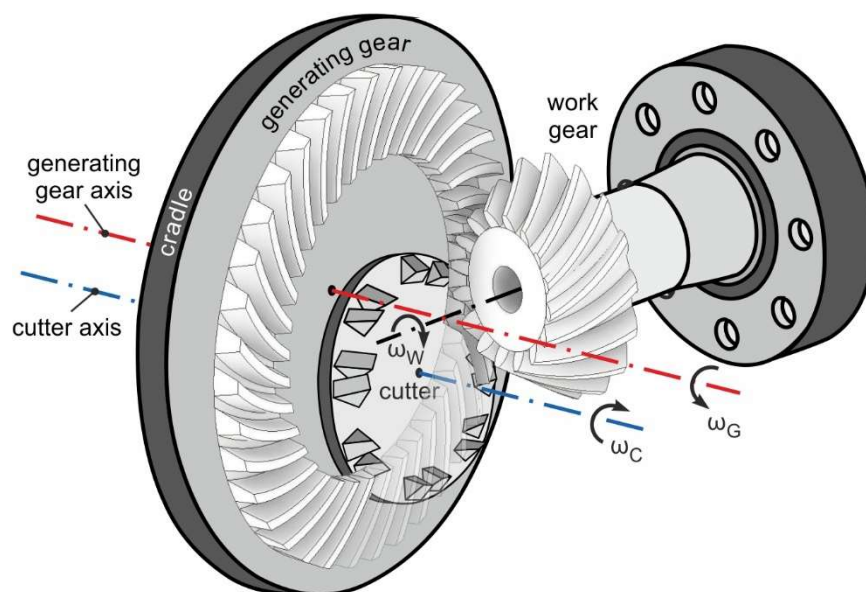


Figure 3.1: Generation principle in spiral bevel gears. [56]

A bevel gear set that not fulfils all the above kinematic conditions can still be generated, though the roll and transmission quality of the gearset may decrease significantly as the deviation from the coupling conditions increases. Given this, the extent to which two meshing bevel gears roll exactly onto each other depends on the level that these coupling conditions are satisfied. [10] According to the definition of a conjugate gear pair, based on Colbourne J.R. [57], "When two gears are in mesh, and the two profiles in the same transverse section are such as to produce constant transmission of motion, these profiles are said to be conjugate. Or else, a pair of transverse gear tooth profiles are said to be conjugate if a constant angular velocity of one profile produces a constant angular velocity in the meshing profile." As mentioned above, the arrangement presented in Figure 3.1 is used as a basis for all spiral bevel gear / hypoid generators. On the traditional mechanical hypoid generator, as the one presented in Figure 2.24, the generating crown is represented by a cradle mechanism. The cutter centre is placed at a certain offset from the cradle axis, and cutter's blades represent one tooth of the generating crown gear. The generating roll motion rotates the workpiece and the imaginary generating gear with a specific ratio, called the ratio of roll, while at the same time the two gears are engaged. [10, 16, 32, 58] This virtual motion is represented by the rotation of the cutter around the generating gear axis. The starting roll position is commonly on the heel of the tooth and the generation develops from heel to toe until it reaches the finishing roll position.

The generating ratio of roll is a crucial value in the generating process and can be calculated by the following equations [10, 16, 32, 58]:

$$R_g = \frac{\omega_g}{\omega_w} = \frac{z_w}{z_g} \quad (3.1)$$

$$\frac{z_w}{z_g} = \frac{\sin(\delta_w)}{\sin(\delta_g)} = \sin(\delta_w) \quad (3.2)$$

Combining equations 3.1 and 3.2 we get [10, 16, 32, 58]:

$$R_g = \sin(\delta_w) \quad (3.3)$$

where:

ω_g	angular velocity of the generating gear around its axis	(rad/sec)
ω_w	angular velocity of the work gear around its axis	(rad/sec)
R_g	generating ratio of roll	(-)
z_g	generating gear number of teeth	(-)
z_w	work gear number of teeth	(-)
δ_g	pitch angle imaginary generating gear = 90°	(°)
δ_w	pitch angle work gear	(°)

The produced work gear geometry is very sensitive to the value of the generating roll, so it is recommended that when it comes to either machine or simulation settings, at least six decimal places should be provided to accurately define the R_g value.

3.1.2 Plunging and generating roll motions

There are two different motions that can be either combined or performed separately for the machining of hypoid or spiral bevel gears. The first one is a simple plunge feed motion where the tool is fed to the final depth to form a gear slot and the second is the generating motion

where the tool profile rolls on one or both flank surfaces of a gear slot. The plunge only strategy can be applied only in non-generating processes. The ring gear of a bevel gear pair can be manufactured with a non-generating process. Based on bevel gear theory, at least one member of a gear pair must be manufactured via a generating roll motion and that is the pinion so that the necessary contact characteristics are satisfied. Both motions are presented and described graphically in [Figure 3.2](#).

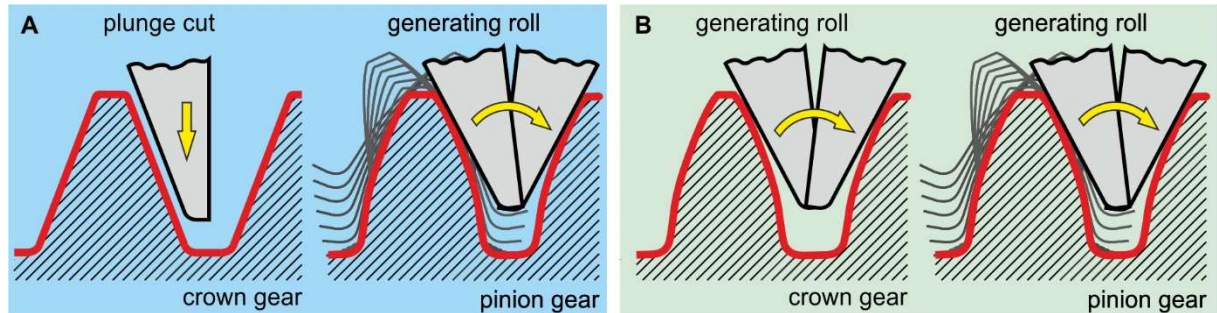


Figure 3.2: a. Generated pinion - formate ring gear (left), b. Generated pinion - generated ring gear (right).

[Figure 3.3](#) shows the basic steps of pure generating motion. At the first step of the **generating roll**, the cutter approaches the workpiece. As generation progresses, the gear blank rotates around its axis while the cutter rotates around the axis of the imaginary generating gear that has an offset relative to the cutter axis. The combination or superimposition of the two motions results in the contact between the cutting blade and the workpiece at the beginning of the material removal process (step two). During this cutting process, the tooth flank is formed as a result of the generating motion between the cutter and the workpiece. In the third step of the process, the cutter approaches the middle slot position where it begins to exit the workpiece until it reaches the last generating position, where the cutter and the newly formed gear slot are essentially disengaged (step four). After the fourth step of generation, the cutter is no longer in contact with the gear until their combined counter-rotations bring them back to the first step and the beginning of generating process. [10] Chip thickness is not constant along the cutting edge. Although generating roll can be applied by means of either climb or conventional cutting strategies, climb milling is mostly preferred, especially when a high-quality tooth flank surface is expected. Assuming that climb milling is selected, the cutting direction dictates the generating roll direction. For a ‘toe to heel’ cutting direction, generating roll is performed from heel to toe. If tooth flank surface quality is of high priority, the generating roll may be performed in two cycles, a roughing and a finishing one. [1, 10]

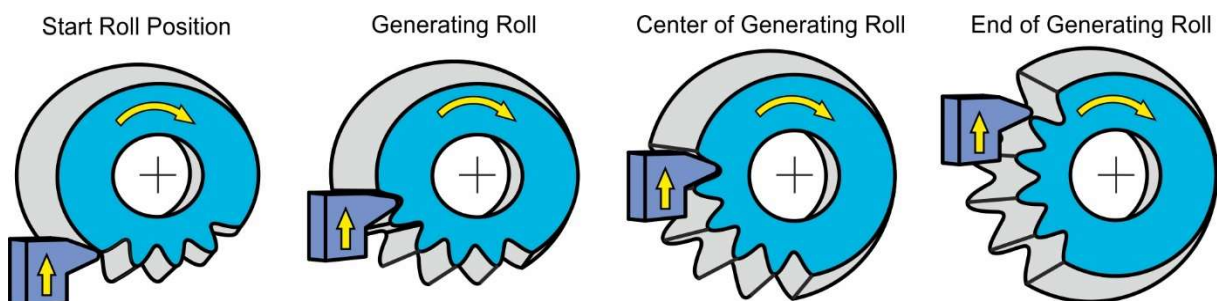


Figure 3.3: Generating roll in bevel gear manufacturing. [10]

Plunge cutting is far simpler, in terms of kinematics, compared to generating roll motion. Plunge feed in gear machining results in a form cutting process since the tool is fed towards the workpiece performing a linear motion. As shown in [Figure 3.4](#), the process starts with the

cutter and the workpiece not being in contact, but the workpiece is already placed in the correct position for the machining of the next gear slot. During the second step of the process, the cutting blade is fed to the final machining depth, material is removed, and an exact copy of the blade profile forms a gear slot. The profile of the blade is essentially reproduced in the gear slot and a negative profile of the blade is formed. Chip thickness varies along the cutting edge and chip width increases with the plunge depth. In the next step, the cutter withdraws from the part to the point that they are no longer engaged. The procedure is repeated starting from the first step after the workpiece is rotated around its axis so that the tool blade reaches the correct position for the next slot [10]. In face hobbing plunge cutting, the process shown in figure 3.4 is performed for all slots at the same time. When used as a finishing process, the process is frequently called “Formate” due to its forming nature, though this label is owned by the Gleason Company. Other methods in this category of plunge only-motion methods are Helixform and Cyclex. The gears produced by plunge-only cut are non-generated gears.

In most cases, a cutting direction from toe to heel is applied during plunge cutting in order to enable burr formation on the outside diameter of the gear so their removal is easier. Another reason that makes this strategy preferable is the direction of cutting forces towards the work fixture, which results in a steadier cutting. In plunge cutting, the cutting speed ranges from 45 to 70 m/min for HSS tools and from 160 to 280 m/min for carbide tools respectively. [1]

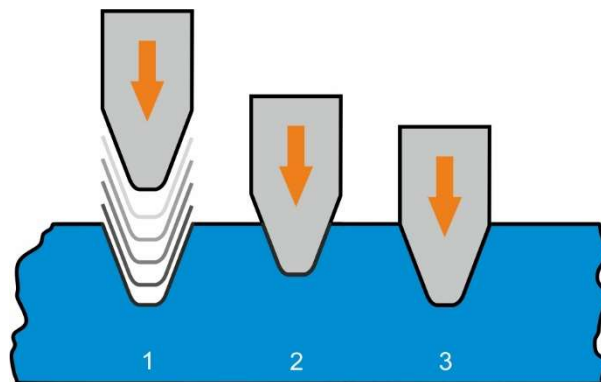


Figure 3.4: Plunge motion in gear manufacturing. [10]

Based on these two separate motions, many manufacturing variations, that utilize either only one of the above processes or a combination of both, are applied. [Table 3.1](#) shows the alternative machining processes depending on the employed method. As it can be observed, the two strategies can be used in both face milling and face hobbing processes. It should be noted that regardless of the chosen process, the pinion is always generated in order to satisfy the necessary contact characteristics, therefore plunging as a finishing method may only be used for the form-cutting of the ring gear. The two motions described above constitute the basic kinematics applied to every spiral bevel gear cutting process. Nevertheless, it must be mentioned that when the above methods, especially the generating roll, are applied in practice, they might include additional motions or modifications. Some of these possible modifications are the modified roll, i.e. a non-constant roll ratio throughout the cradle rotation, a helical motion between the cutter and the gear as well as linear horizontal or vertical slide motions. When a crown gear identical to the ring gear is used as a generating gear, the pinion is generated by rolling with the generating ring gear and the ring gear is cut by pure plunging without generation. [10, 13]

Plunge cutting can be used either as the finishing operation of a non-generated ring gear or as a roughing operation prior to the generating finishing. In the latter case, the cradle angle at

which the plunge cutting is carried out does not affect the final tooth flank geometry and it can be selected in order to cause minimum tool wear.

Process	Generation/Plunge
Face milling generated	Pinion and gear generated
Face milling formate	Pinion generated, gear plunge cut
Face hobbing generated	Pinion and gear generated
Face hobbing formate	Pinion generated, gear plunge cut

Table 3.1: Generating and Non-Generating Processes.

From the combination of the two processes the following three alternative strategies may occur:

- Plunge cutting process (Forming).
- Generation roll with prior plunge cutting.
- Generating only process.

Generating roll with or without prior plunge cutting

The generating roll motion can be performed either without a previous plunge roughing operation or as a finishing operation after plunge cutting. Regarding the second strategy, a common practice in spiral bevel gear machining, when both generating roll and plunge cutting are used, is the partition of the machining process into two cycles. During the first cycle, the workpiece is roughed out to the finishing allowance by means of the plunge-only feed motion. The reason behind this is the increased efficiency and productivity of plunge cutting method when it comes to removing as much material as possible, regardless of the machined surface quality. The most common practice for this cycle is to set the cradle angle so that the cutter is positioned in the middle of the gear slot. In the second cycle, the cutter moves to the first roll position, if it is not there already, and the tooth flanks are finished by applying the generating roll motion. In face milling, the gear slots are firstly roughed out one by one by plunge cutting and then generated also one by one, while in face hobbing all slots are roughed out and then generated simultaneously.

Regarding the cutting strategy, climb milling is always recommended for a higher flank surface quality. Rolling direction depends on the selection of cutting strategy and the cutting direction of the cutter. Provided that cutting from toe to heel is mostly preferred for the reasons mentioned above, climb cutting requires the generating roll to be performed from heel to toe.

3.1.3 Single or continuous Indexing processes

Face milling and face hobbing have fundamental differences in their kinematics, in the produced gear geometry, and in the philosophy behind the cutting tools. Each process has positive and negative aspects, so whether a gear manufacturer chooses one process over another for a particular application depends solely on their requirements. With regards to which one of the two methods offers higher quality gears with more strength and better rolling performance, one might find the answer in the selection of the hard finishing process that follows the soft cutting process. On the other hand, if productivity is the main objective, the selection between the two processes is determined by the overall manufacturing times that each of them offers. The main feature that distinguishes face milling from face hobbing is the indexing relation between the cutter and the workpiece. Face milling is a *single indexing* operation; hence gear slots are cut one at a time. On the contrary, all slots are cut

simultaneously in face hobbing, thus this process is defined as a *continuous indexing* process. It can be concluded that, due to this difference, face hobbing kinematics is more complex than the respective motions performed in face milling. The modification in kinematics that offers the feature of continuous indexing in face hobbing, changes the tool path significantly and consequently changes the produced gear geometry. The main difference identified between the two produced geometries is the lead function or the lengthwise curve of the tooth. In both processes, the methods described in section 3.1.2, namely plunge cut and generating roll, can be applied either in combination or independently. In the following sections, the two processes are thoroughly described and their major features regarding their kinematics, the produced tooth geometry and the productivity offered, will be presented and discussed.

3.2 Face milling

3.2.1 Indexing method

Face milling is a single indexing method which means that the gear slots are cut in a sequence, one slot after another and not simultaneously. During the cutting process, the workpiece is held still or, in the case of generating cutting, it performs a narrow rotation required for the generating roll. All cutting blades pass through the same slot consecutively as the cutter rotates. After each slot is machined to the desired depth, the cutter withdraws from the workpiece and the workpiece rotates around its axis and indexes to the next slot position. This process is repeated until all slots are machined. [Figure 3.5](#) shows how all cutter blades, inside and outside, pass through the same slot while the cutter plunges to the full depth or rolls until roughing or generation is completed. Following, the cutter retracts so that the work gear can rotate by one pitch for the next slot to be cut.

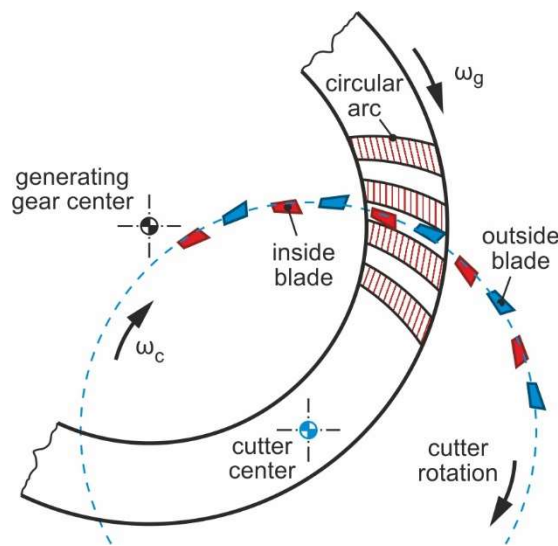


Figure 3.5: Single indexing in face milling. [59]

3.2.2 Kinematics

As face milling is the simpler of the two manufacturing processes, the kinematics of the process is not of very high complexity. In order to provide a full description of the kinematics, two cutting processes, i.e. plunge cutting and generating roll cutting must be considered separately.

Non-generating Plunge cutting: When only plunge cutting is performed, the cutter executes two separate motions. The first one is a rotation ω_c about its axis which is the primary cutting motion with the cutter's axis being in a fixed position relative to the generating axis and the second motion is a plunge feed to reach the full depth of the slot.

Generating roll: In the case of generating roll, the cutter performs the cutting rotation around its axis and the generating motion is executed due to the combined rotation of the generating gear and the work gear. The cutter starts rotating about its axis with the rotating speed ω_c , then it is fed to the final machining depth and rolled in the first generation position where the generating rotation about the cradle-generating axis ω_g begins. Meanwhile, the workpiece rotates around its axis ω_w , without of course exceeding the limits of the current indexing position. This relative rotation of the cradle and the workpiece is described by the following formula [10, 16, 32, 58]:

$$\frac{\omega_g}{\omega_w} = R_g \quad (3.4)$$

where:

ω_g	angular velocity of the generating gear around its axis	(rad/sec)
ω_w	angular velocity of the work gear around its axis	(rad/sec)
R_g	generating ratio of roll	(-)

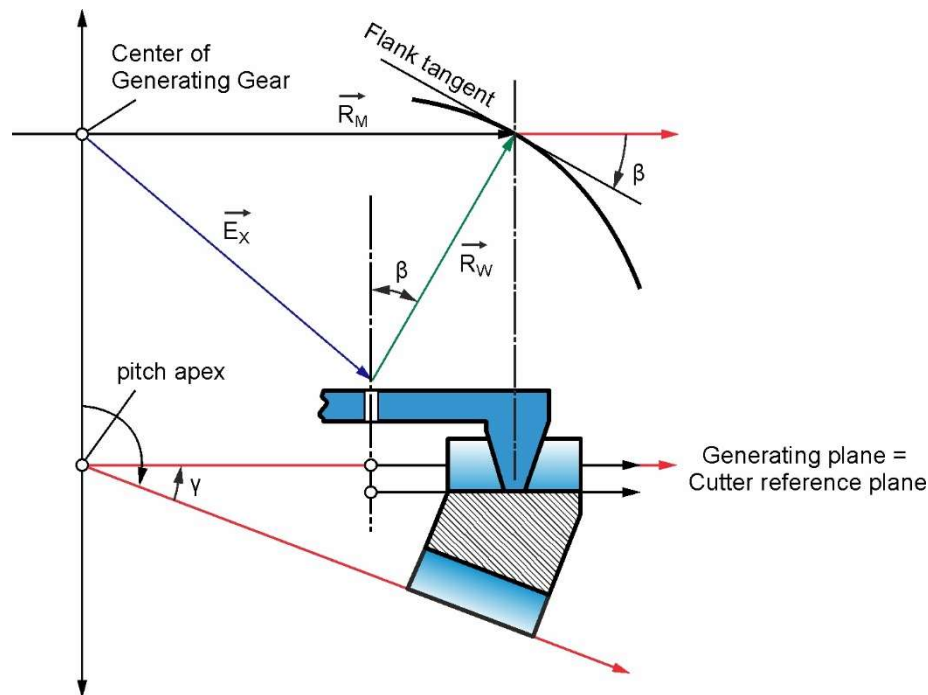


Figure 3.6: Cutter position and reference plane in face milling. [10]

The generating ratio of roll is essentially the ratio of generating gear number of teeth to work gear number of teeth and is calculated as follows: $R_g = Z_w / Z_g$. [10, 16, 32, 58]

The distance between the cutter axis and the generating gear axis as well as the exact position of the cutter centre is calculated with the use of the spiral angle β and the cutter radius R_w according to [Figure 3.6](#). As illustrated in [Figure 3.7](#), the traces that the cutter leaves on the flank of the tooth in case of face milling cutting, are almost parallel to the contact lines between pinion and ring gear when the two are in mesh. The distance between the cutting traces depends on the rolling feedrate and the angular distance of the blades on the cutter.

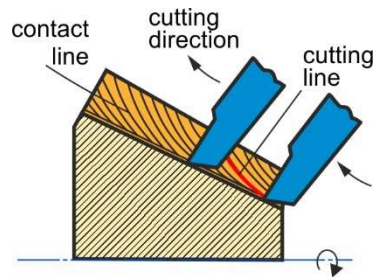


Figure 3.7: Cutting and contact lines are almost parallel in face milling. [12]

3.2.3 Gear and tooth geometry

The motions described in section 3.2.2 produce a specific gear tooth and slot geometry that characterizes the face milling process.

Flank line geometry along the face width

One of the most characteristic features of the face-milled gear geometry is the flank lead function, i.e. the lengthwise tooth curve, which is a circular arc. This geometry is produced by the cutter rotation around its axis and by the fact that the cutter rotations is not combined with a work gear rotation since the workpiece in face milling is held still. This circular flank line in spiral bevel gears is wrapped around a conical pitch element/surface. The curvature of the teeth is constant along the face width and equal to the cutter radius. Consequently, when both flanks are cut simultaneously in a completing process, the radius of the concave flank is approximately the sum of the radius of the convex flank plus the slot width.

Tooth depth, tooth thickness and slot width

The circular flank lines produced by the cutter rotation in face milling, form a gear slot with a constant slot width. In the case of completing processes when both flanks are cut simultaneously with one cutter head, this feature combined with the conical shape of the gear and more specifically the deviation between the inner and outer cone diameters results in an extreme tooth thickness variation (un-proportional tooth thickness taper). The produced tooth is thick close to the heel, while it is very thin close to the toe. This geometry may have the following disadvantages: The top land of the toe may degrade to a point, but more importantly, if both members of the gear-set are manufactured with this method, the tapered teeth of one gear would not fit in the parallel slots of the other gear and therefore the two gears could not mesh with each other. [10]

The need for a proportional tool thickness from heel to toe, makes the formation of a tooth depth taper necessary so that a space width taper can be also generated. The tooth depth taper is applied in such a way that the resulting space width taper splits the difference in tooth thickness between the heel and the toe, to form equal tooth thickness and space width taper. Generation of tooth depth taper may be accomplished by lifting the root towards the toe, introducing a dedendum angle which is usually combined with an addendum angle too. The root line is tilted around the mean point ensuring that the mean working depth of the tooth remains the same. [10] This keeps the root width of the slot parallel while at the same time a proportionally reduced space width from heel to toe is formed. It is worth mentioning that both tooth thickness and space width values are calculated on the generating gear pitch plane. This modification ensures that the teeth of one gear fit in the slots of the mating gear and provides a smooth roll.

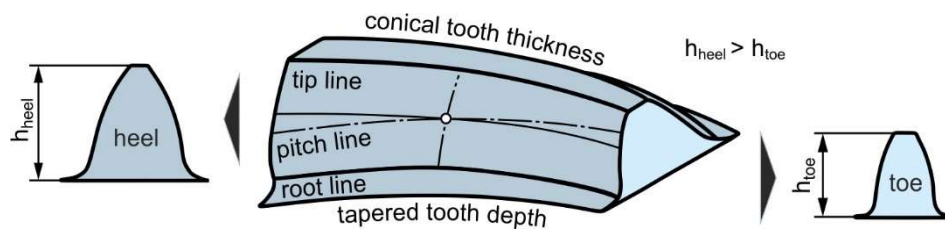


Figure 3.8: Conical tooth thickness after adjusting the tooth depth in face milling. [10]

3.2.4 Five-cut double flank vs Completing processes

Manufacturing of spiral bevel gears by means of face milling can be applied either in a completing or in a five-cut two-flank process. Five-cut processes were introduced in the U.S.A. in 1913 as the first face milling manufacturing process. Due to the competition that arose when face hobbing was developed as a revolutionary completing manufacturing process, the company that focused its research on face milling developed a competitive completing face milling method. The benefits of cutting in a two-flank process are obvious. Each flank is cut in a separate cycle, so the flank form can be adjusted or corrected according to the design requirements without affecting the geometry of the opposite flank. This is mostly achieved by changing the machine and the cutter head settings from one cycle to the other. The five main steps of the five-cut method are listed below. [10]

Steps of the five cut process

1. Ring gear roughing, cutter head has inside and outside roughing blades,
2. Ring gear finishing, cutter head has inside and outside finishing blades,
3. Pinion roughing, cutter head has inside and outside roughing blades,
4. Pinion finishing of convex flanks, cutter head has inside blades only,
5. Pinion finishing of concave flanks, cutter head has outside blades only.

Steps of the completing process

1. Ring gear roughing / finishing, with inside and outside roughing / finishing blades,
2. Pinion roughing, with inside and outside roughing blades,
3. Pinion finishing, with inside and outside finishing blades.

The five-cut method requires five different setups, one for each step. This further increases manufacturing time as gear parts must be moved from one machine to another. A typical cutter used in five-cut processes is the Hardac cutter. [10] This cutter is capable of roughing and finishing of pinions and ring gears. [10] In five-cut methods length crowning is possible with the variation of cutter radius, whereas profile crowning is achieved with the modification of machine settings. It must be mentioned that nowadays five-cut methods are rather outdated and mostly replaced by completing methods, because apart from raising the total manufacturing time and cost, they also require wet-cutting conditions. During completing processes, the process parameters change in order to be adjusted in either roughing or finishing conditions. Typical cutter heads employed in completing processes are the RSR cutter head which carries HSS stick blades with a rectangular cross-section and the Pentac cutter head which carries stick blades optimized with a pentagon-shaped cross-section. [10]

3.2.5 The advantage of grinding

After the soft cutting operations, all bevel gears undergo the necessary heat treatment in order to improve their mechanical properties. Following the heat-treating process, a hard finishing process is applied so that any deflections and dimensional changes resulting from heat

treatment are corrected and the quality of flank surfaces is enhanced. Hard finishing processes in spiral bevel gears were briefly presented in section 2.6. Regarding the finishing of face-milled spiral bevel gears, the circular arc flank curve produced by the soft cutting process offers a great advantage compared to face-hobbed gears. The geometry of the tooth allows the hard finishing of the gear using grinding, which is reported to improve important properties such as strength, noise, and efficiency more than the other hard-finishing processes. This advantage, coupled with the increased productivity offered by the modern completing processes, has made face milling more competitive and preferable to the manufacturers, compared to previous decades.

3.3 Face hobbing

Face hobbing was firstly introduced in Germany by Klingelnberg as a new revolutionary completing process for the machining of spiral bevel gears, aiming to minimize manufacturing time. Face hobbing earned popularity in a short time drawing the attention of more and more manufacturers and was soon established as one of the two dominant methods for spiral bevel gear manufacturing. A unique attribute of the process and one of its major benefits is the fact that all slots are cut simultaneously, thus face hobbing processes are often mentioned as continuous indexing processes. All face hobbing processes are completing methods; hence the two flanks are cut in the same cycle either by a roll only operation, a plunge cut or a combination of the two. Length crowning in face-hobbed gears can be achieved by tilting the cutter head, similar to the completing face milling process. Profile crowning can be generated by means of curved cutting edges. [10] Face hobbing kinematics and all the process-included motions are far more complex than the respective ones in face milling and thus, they are more difficult to be analysed. Face hobbing cutter heads carry a series of blade groups protruding axially from the face of the cutter at a certain diameter. Each group normally consists of an outer blade followed by an inner blade to machine the outer and inner tooth flank respectively. The next sections will attempt to analyse the process and highlight all features of great importance.

3.3.1 Indexing Method

Face hobbing is a continuous indexing method; hence all gear slots are cut at once, in contrast to face milling where slots are cut one by one. During machining, the workpiece rotates in timed relation with the cutter as if the two “gears” were meshed in a gearbox assembly. When an outer and inner blade cut a slot of the work gear, the gear rotates in the opposite direction so that the next blade group enters the next gear slot, and so on. The ratio of the two rotations is equivalent to the indexing ratio as if the cutter and workpiece were engaged in a gear set, hence the rotation of the cutter to the rotation of the work equals the number of work gear teeth divided by the number of blade groups, i.e. starts of the cutter.

3.3.2 Kinematics

The complexity of face hobbing kinematics processes lies mainly in their complicated relative motions. Three independent motions, indexing, generating roll, and feed are combined in face hobbing. As in the case of face milling, face hobbing may be performed either in a non-generating plunge cutting or in a generating roll motion.

Non-generating plunge cutting in face hobbing: Non-generating cutting in face hobbing offers high productivity so it is often used in order to machine the ring gear but also as a roughing process prior to finishing with a generating roll, when higher material removal rate is required. When non-generating cutting is used as a roughing process, the cutter is fed to the workpiece at the centre roll position until it reaches a certain cutting depth, when generating rolling motion begins.

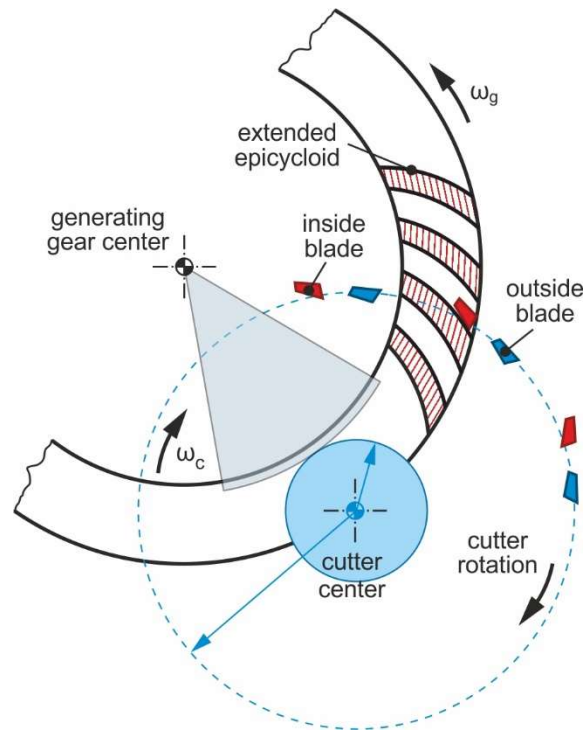


Figure 3.9: Continuous indexing in Face Hobbing. [55]

Two independent motions are involved in this non-generating process and that is the feeding motion until the cutter reaches the final depth and the indexing motion which consists of a combined rotation of the cutter and the workpiece and resembles the rotation of two gears in mesh. The indexing motion includes the cutting rotation of the tool which, as an independent motion, defines the primary cutting motion of the process. The feedrate of the cutter moving towards the work gear is slower than in face milling.

Generating roll cutting in face hobbing: In the case of generating roll, the cutter head executes two motions while the gear rotates around its axis. The first one is the cutting motion, which also contributes to the indexing procedure i.e., the timed rotation of the cutter around its axis. The second motion is the generating roll of the cutter around the generating-cradle axis. The motions involved in generating face hobbing cutting can be described by the following formulas [10, 16, 32, 58]:

Continuous indexing, as a result of the combined cutter and workpiece rotation:

$$\frac{\omega_w}{\omega_c} = \frac{Z_c}{Z_w} = R_i \quad (3.5)$$

or continuous indexing through the rotation of the tool and the generating gear:

$$\frac{\omega_c}{\omega_g} = \frac{Z_g}{Z_c} \quad (3.6)$$

Generating roll, as a result of the combined generating gear and workpiece rotation:

$$\frac{\omega_g}{\omega_w} = \frac{Z_w}{Z_g} = R_g \quad (3.7)$$

where:

ω_g	angular velocity of the generating gear around its axis	(rad/sec)
ω_w	angular velocity of the work gear around its axis	(rad/sec)
ω_c	angular velocity of the cutter around its axis	(rad/sec)
R_g	generating ratio of roll	(-)
R_i	indexing ratio	(-)
z_g	imaginary generating gear number of teeth	(-)
z_w	work gear number of number of teeth	(-)
z_c	number of cutter blade groups	(-)

In the non-generating cutting process, only the indexing motion takes part along with the feed of the cutter to the final depth. Unlike face milling, in face hobbing of spiral bevel gears, the cutter blade's velocity vector is not tangent to the circle formed by the rotation of the cutter around its axis. Instead, as presented in [Figure 3.10](#), while the cutter rotates around its axis, it simultaneously rolls on a base circle. Hence, the cutting blades move from point A to point C instead of B, as a result of the superimposed indexing and cutting motions as described above. This combination of motions results in the tooth lengthwise curve, the most representative geometric feature of face-hobbed spiral bevel gears.

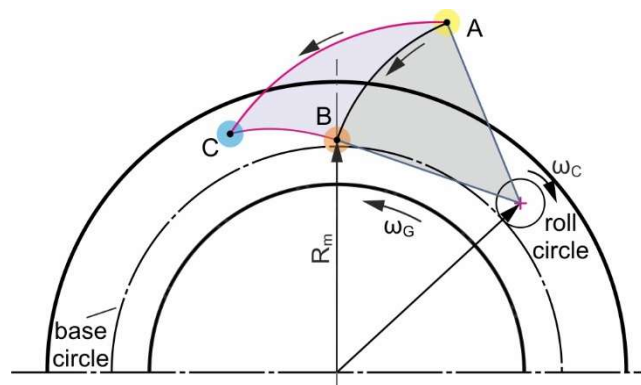


Figure 3.10: Velocity vector of cutting blades in face hobbing. [10, 55]

3.3.3 Gear and Tooth Geometry

The face-hobbed gears tooth geometry is uniquely defined by the process kinematics described in the previous section. These geometric features are detailed below.

Flank line geometry along the face width

The superimposition of the two primary motions in face hobbing, i.e., indexing and cutting, generates an extended epicycloid flank line function, in contrast to face milling where the lead function is a circular arc resulting simply from the cutter rotation. The curvature radius of the tooth flank in face-hobbed gears is not constant but increases from toe to heel. The mean curvature depends on the radius of the cutter and the number of blade groups. As presented in [Figure 3.10](#), the combined effect of the rotation of the cutter about its axis and the rolling on the base circle of the generating gear changes the direction of the blade velocity from being tangent on the cutter circle as in face milling. [Figure 3.11](#) shows the relative cutting and indexing motions and the resulting extended epicycloid flank line. When the epicycloid is formed, the ratio of the number of generating gear teeth to the number of blade groups is equal to the ratio of the base circle radius to the roll circle radius. An extended epicycloid occurs, when the radius on which the cutting edges are positioned is greater than the radius of the roll circle. [10]

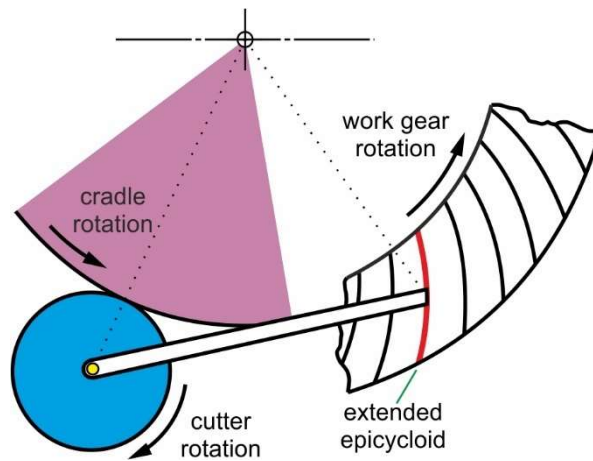


Figure 3.11: Flank line geometry and relative motions in face hobbing. [12]

Tooth depth, tooth thickness and slot width

The extended epicycloid flank lines produced by the continuous indexing motion between cutter and gear, result in a proportional space width and tooth thickness taper along the face width. If the tooth depth remains constant along the face width, then the pitch plane is parallel to the root plane which results in conjugate gear geometry between pinion and ring gear. [10]

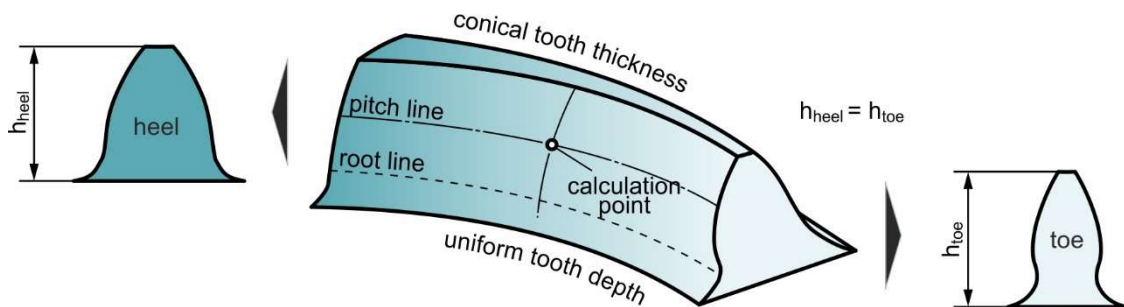


Figure 3.12: Tooth depth, tooth thickness and slot width in face hobbing process.[10]

Opposite to face milling, the traces of the tool on the tooth flank are not parallel to the contact lines, instead, they are extended and intersect the contact lines with a corner, as shown in [Figure 3.13](#). This feature makes face-hobbed gears suitable for lapping after heat treatment.

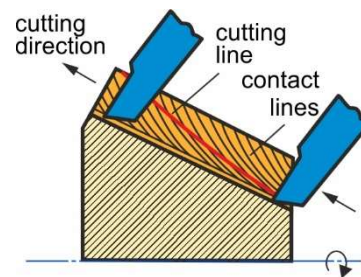


Figure 3.13: Cutting lines in face hobbing. [12]

[This page intentionally left blank]

4. SPIRAL BEVEL GEAR CUTTING SIMULATION MODEL

The objective of the present research is to fill the gap in understanding and simulating spiral bevel gear cutting. For this purpose, a novel simulation software called *Ithaca BevelSim3D* was developed, and is presented in this study. The model receives as input some necessary geometric characteristics of the cutting tool and the work gear, simulates the process kinematics and produces valuable output data. The outputs of the model include the 3D tooth flank surface topography and the 3D undeformed chip geometry at each simulation step. The outputs of the kinematic simulation, specifically the 3D undeformed chip geometry, can be then used for the calculation of cutting forces via *Ithaca BevelForce3D*, a subject which will be further discussed in Chapter 6.

4.1 Simulation model structure

The structure of the *Ithaca BevelSim3D* model follows the general structure of most simulation models which receive specific parameters as inputs, apply the simulation process by means of functions and calculation routines and provide the values of certain parameters as output. More specifically, the simulation is implemented in the following steps:

1. The user sets the input parameters.
2. The algorithm automatically models the work gear and tool geometries.
3. Face milling and face hobbing methods are simulated in steps, according to pre-defined resolution.
4. Tooth flank and gear slot topographies and undeformed chip geometries are calculated in each simulation step.
5. Cutting forces are calculated for each simulation step. (*BevelForce3D*)
6. Investigation of optimal cutting parameters based on the above results.

The simulation algorithm is completed in step 4 and the study continues with the calculation of cutting forces (step 5) and the investigation of optimal cutting conditions (step 6). A flow chart of the simulation procedure is presented in [Figure 4.1](#).

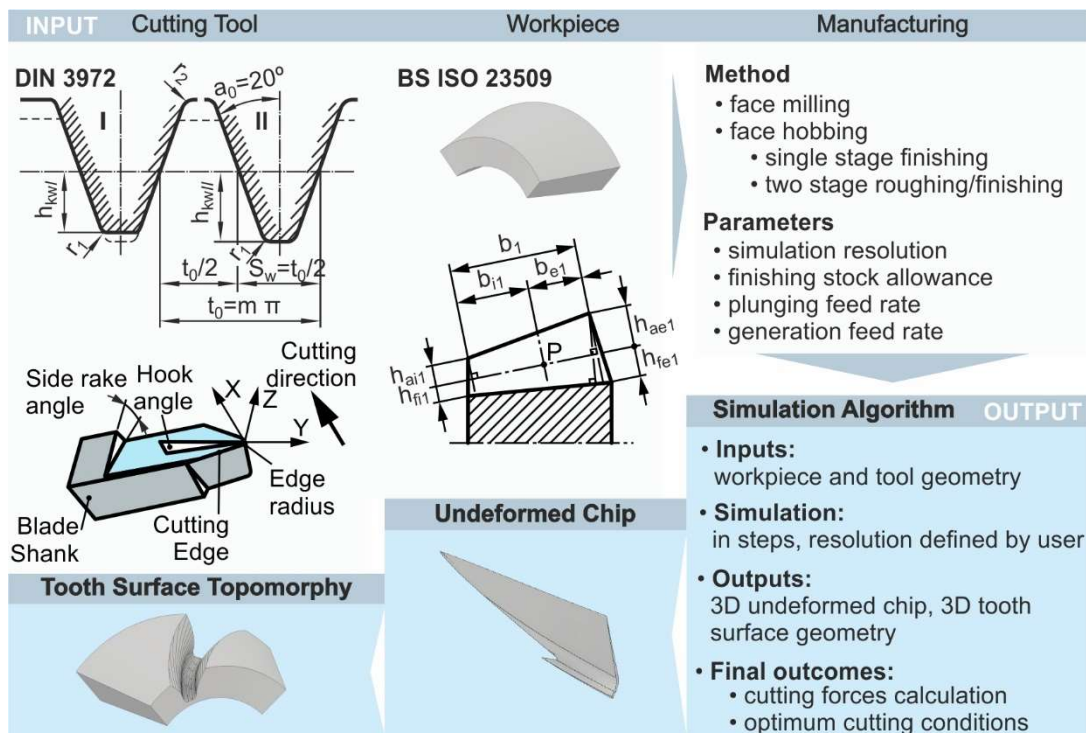


Figure 4.1: Structure of the *Ithaca BevelSim3D* model. [59]

4.1.1 Simulation process input parameters

The three major input parameter groups for the software are 1. work gear geometry, 2. tool geometry and 3. process-related parameters. Both work gear and tool geometries are modelled automatically by the algorithm, according to international standards and regulations.

4.1.1.1 Work gear blank 3D-Geometry

Work gear blank geometry is modelled according to ISO 23509:2016, which is the International Standard for bevel and hypoid gear geometry. This standard essentially defines the basic bevel gear cone and tooth geometry both in the lengthwise and in the transverse direction. According to this standard, there are four methods currently used for the calculation and design of spiral bevel and hypoid gear geometry. The developed model implements two of these methods, specifically *Method 0* for the face-milled spiral bevel gears and *Method 2* for the face-hobbed gears. Table 4.1 shows the necessary work gear input parameters which must be provided by the user so that an accurate solid model of the work gear blank geometry is built, and the rest of the parameters are used for the accurate positioning of the tool and the development of the correct tool path. After the parameters are imported by the user, the model automatically calculates all necessary values and geometric characteristics, using over 50 equations included in ISO 23509.

Parameter	Symbol	Units
Shaft angle	Σ	$^{\circ}$
Number of teeth (pinion, wheel)	z_1, z_2	-
Wheel face width	b_2	mm
Outer & mean pitch diameter, wheel	d_{e2}, d_{m2}	mm
Mean spiral angle	β_{m2}	$^{\circ}$
Addendum & dedendum angle, wheel	θ_{a2}, θ_{f2}	$^{\circ}$

Table 4.1: Work gear input parameters.

Additional to the tooth geometry, the above input parameters are also used for the specification of critical kinematic conditions, such as the position of the tool relative to the workpiece etc. When all necessary geometric parameters are calculated, the blank work gear geometry, which is essentially represented by a part of a cone (frustum), is modelled. Figure 4.2 shows the steps followed in this process.

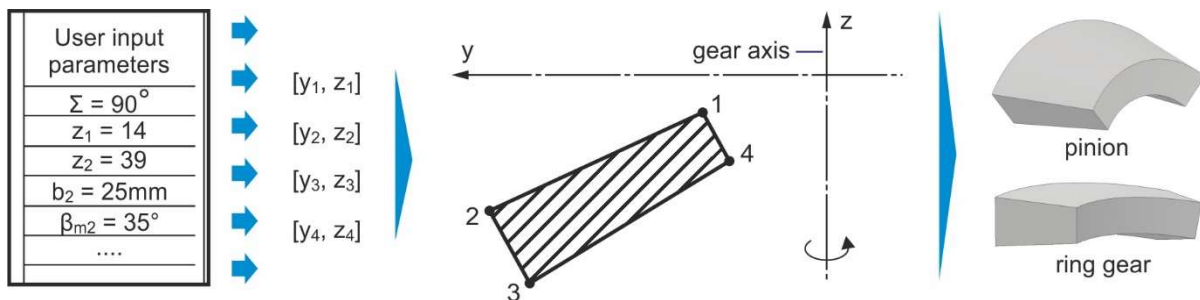


Figure 4.2: Modelling the blank work gear 3D-geometry.

4.1.1.2 Cutting tool geometry

Cutting tool geometry plays a crucial role in spiral bevel gear machining. Even minor changes in the geometry of the tool, have a dramatic effect on the produced gear geometry. Cutting blade profile, blades arrangement on the cutter head and cutter head orientation are the three factors that mostly affect the result of the process. The following paragraphs show the way

these elements are used as inputs in the simulation process depending on the manufacturing method.

Cutting Blade Profile

The cutting tool used in the simulation process is also automatically modelled by the software in two steps. Firstly, the user provides all the necessary parameters so that the profile 2D-geometry can be calculated according to DIN3972. [Figure 4.3](#) shows the basic profile specified in DIN3972 as well as the input parameters and equations involved. After the tooth profile is fully described and modelled, the 3D geometry of the tool which participates in the machining assembly is modelled for each calculation step as a loft feature. The solid geometry is defined by the tool profile and the kinematic curve, which is essentially the tool trajectory, and is used as a drive geometry. [Table 4.2](#) shows all the input geometrical data regarding the cutting blade and cutter head geometry.

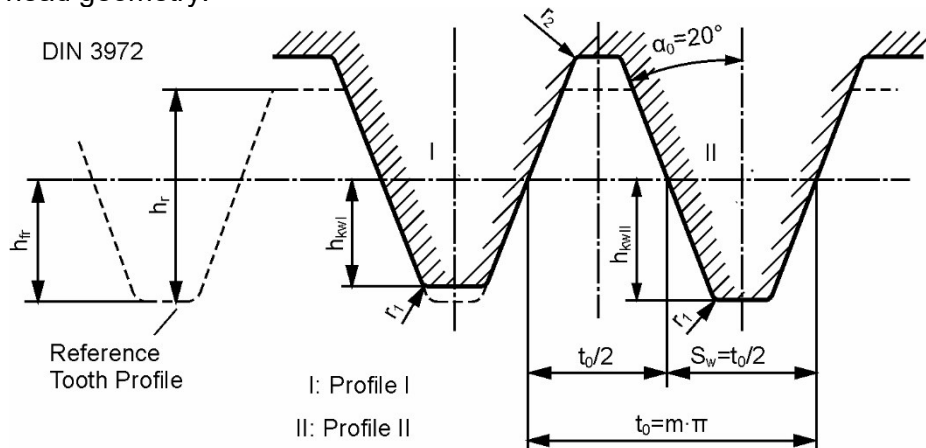


Figure 4.3: Cutting blade profile according to DIN3972.

Parameter	Symbol	Units
Number of blade groups	Z_0	-
Cutter radius	r_{c0}	mm
Normal pressure angle	α_0	°
Blade edge radius	r_1	mm

Table 4.2: Cutting blade and cutter head input parameters.

Cutting blades arrangement

Depending on the machining method employed for manufacturing a spiral bevel gear, the relative position of the cutting blades changes during machining according to the indexing method. [Figure 4.4](#) presents the two alternative blade arrangements implemented in the simulation model in the case of face milling and face hobbing simulation.

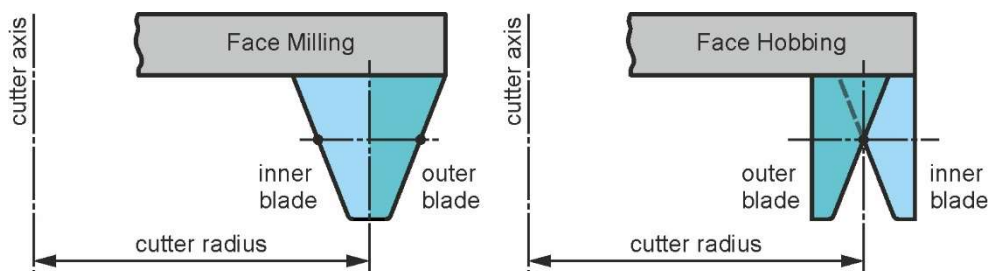


Figure 4.4: Inner and outer blades arrangement in single and continuous cutting processes.

In the face milling process, the inner and outer blades are modelled in such a way so that they form a gear slot, while in face hobbing, the two calculation points coincide and the two cutting edges cross each other and intersect on the common calculation point. The crossed blade arrangement combined with the continuous indexing rotation of the work gear place both blades in the correct positions with respect to the concave and convex tooth flanks. The intermediate angle between the inside and outside blade defines the tooth thickness which can be modified with an adjustment of the blades on the cutter head by changing the distance of the blades from the cutter centre.

4.1.1.3 Cutter head orientation

The geometry of the cutting tool plays an important role in spiral bevel gear machining, but so does the position of the cutter head relative to the workpiece. According to Stadtfeld [10], there are several methods for positioning the tool and selecting the appropriate generating plane, all of which lead to different results in terms of tooth and slot geometry. The orientation of the cutter and the generating plane is adjusted according to the kinematics of the applied process, e.g. single or continuous indexing. Depending on these settings, both pinion and ring gears are produced with different tooth depth and thickness, which ultimately affects the way the two gears mesh with one another and their ability to transmit motion smoothly. Two of these methods, *Method A* and *Method F*, are embedded in the simulation model.

Method A

As described by Stadtfeld [10], and presented in [Figure 4.5](#), this method is used for the generation of spiral bevel gears with a uniform tooth depth. The generating plane coincides with the pitch plane. The cutter is tilted so that the cutter axis is perpendicular to the generating plane for both pinion and ring gear. The cutter axis for the pinion is the same as the cutter axis for the ring gear and both of them are parallel to the generating gear axis. The tooth depth produced with this method is parallel along the face width. This method can be applied in both single and continuous indexing processes, however, in the case of face milling the selection of method A for the generation of the gear causes major compatibility issues. It is quite obvious that the gear produced with method A corresponds to the third gear defined by ISO 23509 in [Figure 2.18](#).

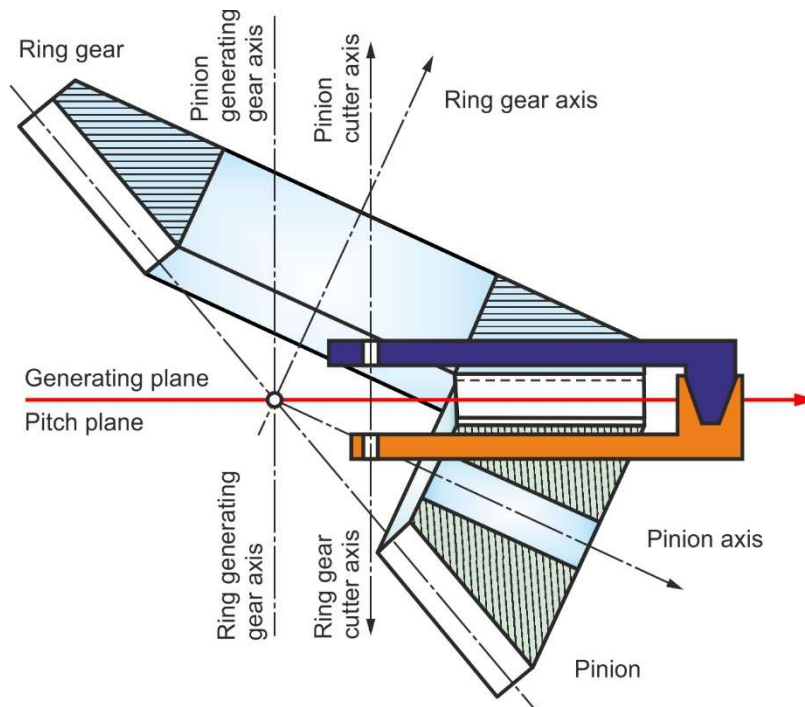


Figure 4.5: Generating Method A. [10]

The extended epicycloid form of the tooth requires spiral bevel gears manufactured with continuous indexing to have a parallel tooth depth along the face width in order to achieve even distribution between the tooth thickness and the space width. The proportional split between tooth thickness and space width is automatically produced by the process kinematics. On the other hand, bevel gears produced via face milling processes have circular curved teeth. As mentioned in 3.2.3, this circular geometry combined with the conical shape of the gears results in an uneven distribution of the tooth thickness and the space width and also an extreme tapered tooth along the face width. Due to the constant space width and the extreme taper in tooth thickness, if both pinion and ring gear are manufactured with this process, they will not be compatible with one another in a gear pair. To overcome this compatibility issue, the root can be lifted towards the toe so that the root width remains constant but the space width is reduced proportionally from heel to toe. This way, the tooth thickness also increases proportionally from heel to toe and the two meshing gears can fit each other. The tapered tooth depth can be achieved with the use of a dedendum angle and the corresponding addendum angle. This configuration can be realized with the non-exact generating Method F. [10]

Method F

One of the methods described by Stadtfeld [10], shown in [Figure 4.6](#), is used when the root line of the tooth is tilted, thus a tapered tooth depth is produced. The generating gear axes for both pinion and ring gear are co-linear. The generating plane coincides with the root plane of the work gear. The cutters for both pinion and ring are tilted at an angle equal to (k_1+k_2) . The cutter blades follow the root plane of the work gear. Small flank form deviations are produced as a result of the cutter head tilt. Apparently, the geometry of the gears produced with method F conforms to the geometry described in the second gear presented in [Figure 2.18](#).

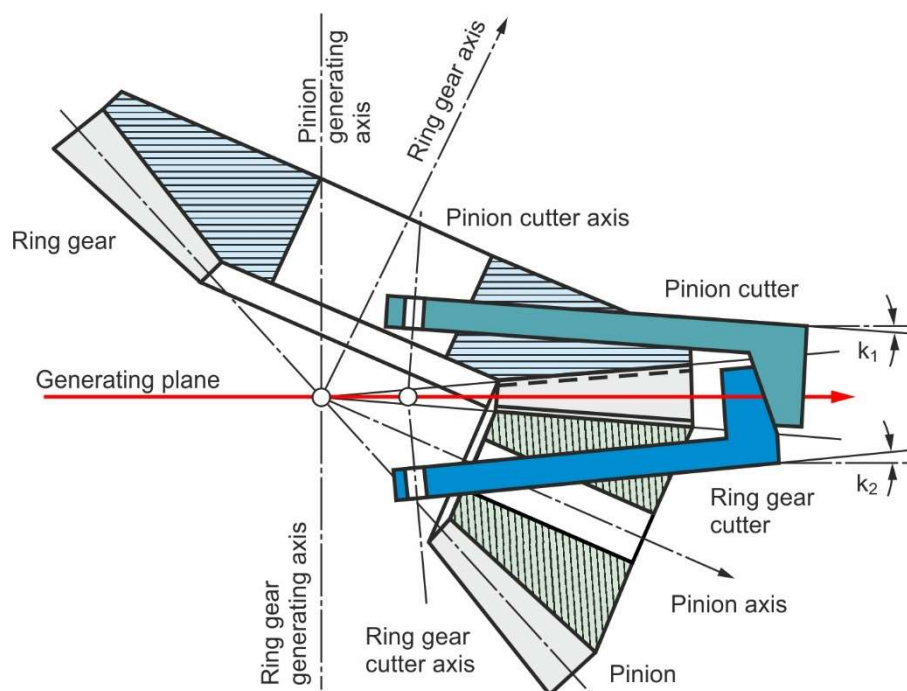


Figure 4.6: Generating Method F. [10]

4.1.1.4 Machining simulation parameters

Apart from the geometrical input data defining the work gear and cutting tool geometries, there are a few more process-related parameters which are essential for simulating the process. These parameters are also provided by the user and include, among others, the type of machining process, the type of calculation process and also the two parameters which define

the simulation resolution. [Table 4.3](#) shows all the process-related parameters that must be provided by the user prior to the simulation process being initiated.

Parameter	Value	Units
Machining method	Face milling / Face hobbing	-
Number of stages	Single stage finish / Two stage rough & finish	-
Calculation method	Method 0 / 2	-
Generation method	Method A / F	-
Plunge feed rate	f_p	mm/rev
Generation feedrate	f_g	°/rev
Revolution discretisation	φ	°
Finishing depth (stock)	t_f	mm

Table 4.3: Process-related input data.

4.1.2 Simulation process algorithm

Ithaca BevelSim3D is a simulation algorithm that integrates the two main processes for spiral bevel gear manufacturing. The model simulates the process kinematics so that the undeformed chip and tooth flank solid geometries are produced as an output. The simulation approach allows the investigation of optimal cutting parameters depending on the generated tooth flank surface as well as the calculation of the cutting forces using the simulated undeformed chip geometries. Modelling and simulation procedures are implemented in the six steps listed below.

- Step 1: Calculation / Modelling of blank gear geometry.
- Step 2: Tool profile and cutter head geometry calculation.
- Step 3: Kinematics simulation & tool trajectory generation.
- Step 4: Calculation of the undeformed chip geometry.
- Step 5: Calculation of the pinion and wheel tooth flank geometry.

Step 1. Calculation / Modelling of blank gear geometry

The process begins with the calculation of crucial bevel gear parameters according to ISO 23509:2016 [9] and the automatic modelling of blank gear geometry based on the input data provided by the user.

Step 2. Tool profile and cutter head geometry calculation

The blade profile geometry is then calculated and modelled according to established specifications of DIN 3972 [60]. Critical cutter head parameters such as the cutter radius and the number of blades or blade groups are considered.

Step 3. Kinematics simulation & tool trajectory generation

Then the user selects the desired method to apply, from the available face milling and face hobbing variants, and whether the work gear will be plunge cut or generated. In addition, the user specifies the required cutting parameters such as plunge and roll feed rates, finishing stock allowance, etc. The simulation resolution can also be altered according to the requirements for accuracy and simulation speed. When all necessary work gear, cutting tool, and process parameters are set, the simulation algorithm is executed and all the related motions of the tool, the work gear, and the imaginary generating gear (cradle of the machine) are automatically performed with the use of geometrical transformations. As mentioned above, the simulation is run in steps, whose resolution has already been defined by the user. Machining of one gear slot, can either be completed in one or two stages. In the first case, which is the single-stage completion, the tool executes two combined motions of plunging and

generation rolling. In the second case, the two-stage completion, the tool first plunges into the work gear to a certain depth, without rolling, leaving a predefined amount of stock for the following finishing operation. Afterwards, the cutter begins the generating roll motion to the final slot depth until both slot flanks have been generated from heel to toe.

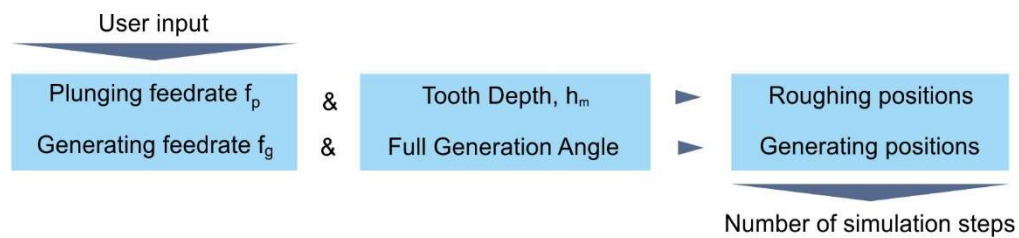


Figure 4.7: Calculation of Simulation steps.

Machining simulation steps: Each simulation step corresponds to one plunge or generation position. [Figure 4.7](#) shows the discretization of simulation in steps and [Figure 4.8](#) shows the subdivision of the total generating roll motion into discrete plunge or generation positions.

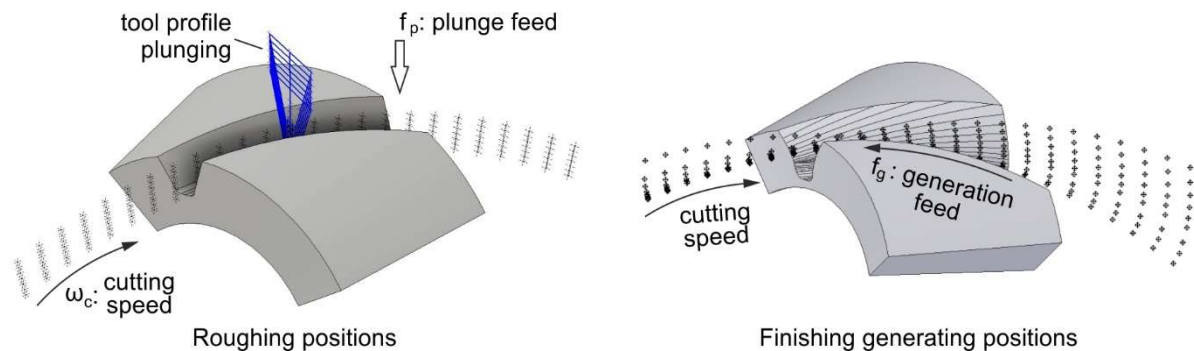


Figure 4.8: Roughing and finishing generation positions.

3D-tool geometry is calculated as a combination of the 2D-profile and the kinematic tool trajectory which is altered at each step. The produced simulated work gear geometry from the previous simulation step is used as a blank gear geometry in the following step. [Figure 4.9](#) presents the process of cutting tool generation for every simulation step. The final 3D tool geometry modelled at each **plunge** or **generation step** is basically a solid feature created by the several tool profiles at every revolving position, therefore it is a combination of the basic tool profile and the tool trajectory, which is formed by the relative tool rotations and revolutions. [Figure 4.9](#) shows an example of 3D-cutting tool geometry, as well as the participating revolved profiles, cutting planes and coordinate systems.

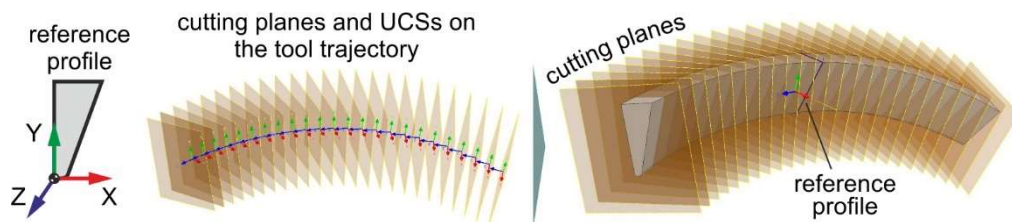


Figure 4.9: Cutting tool 3D geometry creation. [59]

Step 4 & Step 5. Calculation of the undeformed chip geometry and the tooth flank geometry

In each simulation step, the algorithm creates the machining assembly which consists of the work gear and tool solid geometries. The machining assembly is created so that the two solid

geometries of the simulated tooth flank and the 3D undeformed chip, can be calculated through the Boolean operations of subtraction and intersection respectively. [Figure 4.10](#) presents this process which is the core of the simulation algorithm.

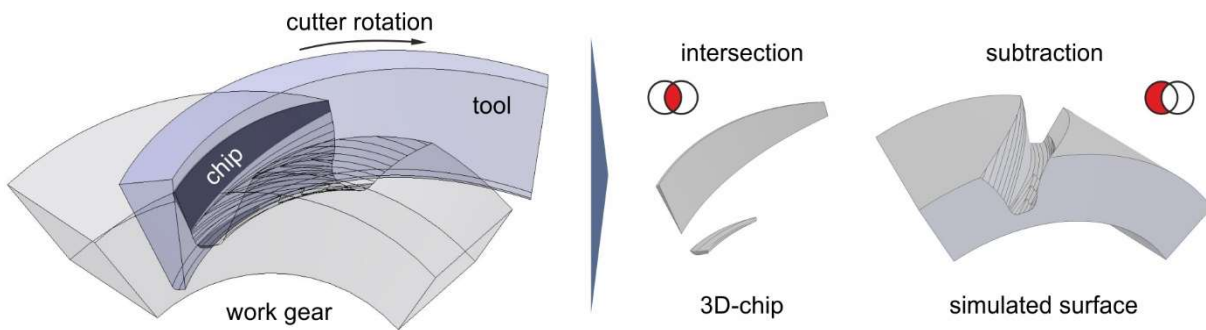


Figure 4.10: Boolean operations in machining simulation. [55, 59]

4.2 Kinematic Analysis

Analysing and simulating process kinematics can prove very challenging when it comes to spiral bevel gear cutting. The following paragraphs will attempt to provide an analysis of the process kinematics in a comprehensible and figurative way.

4.2.1 Revolving Positions

As described in sections 3.2.2 and 3.3.2, kinematics of face milling and face hobbing processes is a combination of the rotations of the cutting tool, the work gear and the generating gear around their axes. The algorithm carries out the kinematic simulation of the processes by incorporating all the related rotations included in the process kinematics. In order to achieve this, the algorithm automatically creates multiple User Coordinate Systems that define the position and orientation of the tool profile in every revolving position. This iterative process begins with the creation of the first coordinate system, which is used as a reference for all the succeeding revolving positions. The algorithm then creates the second UCS by rotating the reference UCS by means of consecutive transformation matrices, each of one representing a rotation of the tool around its axis or a revolution relative to the work gear or the cradle. This way, all the rotations implemented by the tool, the work gear and the cradle are transformed into revolutions of the tool so the correct tool trajectory can be built. [Figure 4.11](#) In both face milling and face hobbing, the tool performs a total of five relative-to-work-gear rotations and revolutions in each revolving position. These revolutions are performed in a specific order so that they can mimic the actual machine tool motions in the most accurate possible way. The five relative revolutions are the following:

- Rotation of the cutter (cutting blade UCS) around its axis.
- Revolution of the cutter (cutting blade UCS) around the cradle's (generating gear) axis.
- Revolution of the cutter (cutting blade UCS) around the work gear's axis.
- Revolution of the cutter axis around the cradle's axis.
- Revolution of the cutter axis around the work gear axis.

[Figure 4.11](#) shows the successive transformations applied to the coordinate system of the blade tip to revolve around an axis/vector R other than the X , Y , and Z axes of the global coordinate system G . In formate face milling, vector R may represent either the cutter's or the cradle's axis while in face hobbing or generating face milling, vector R may also represent the work gear's axis. The blade tip coordinate system is revolved around the above-mentioned

axes, while the cutter's axis is revolved around the cradle axis. These transformations are applied for each revolving position included in every generation position.

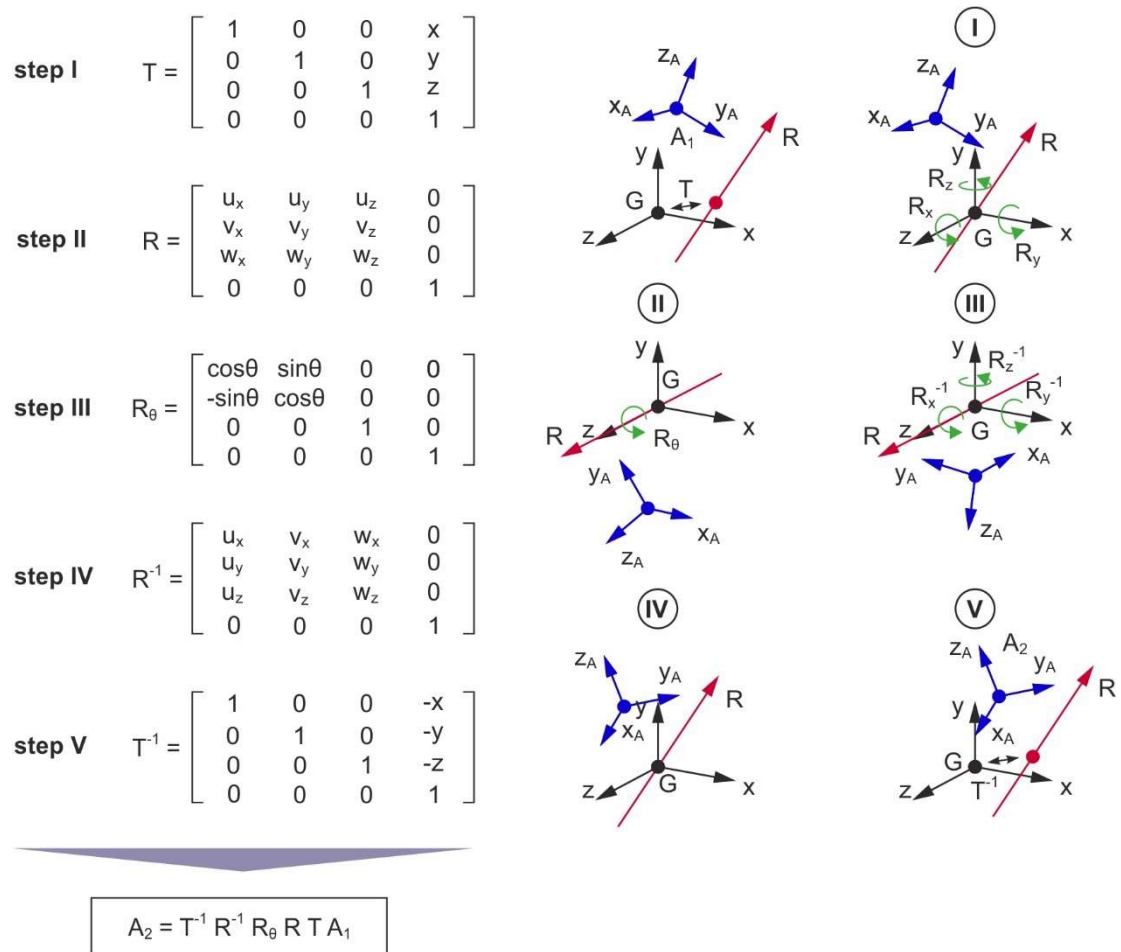


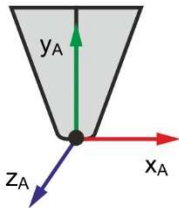
Figure 4.11: Cutting tool to work gear relative revolutions. [55]

The results of these motions for both processes are shown in [Figure 4.12](#), where five intermediate generation positions (g.p.) of the tool are presented relative to the work gear. As illustrated in the figure, in face milling, the coordinate systems of the revolving positions, included in each generation position, form an approximate circle. This is the result of the heavier impact of the cutter's rotation around its axis on the position of the blade tip compared to the impact of the generating speed. In face hobbing though, the resulting tool trajectory in each generation position is more complex, due to the synchronized rotation of the work gear and the cutter. As it can be observed in the figure, the series of revolving positions is denser within the tool width calculation area and sparse for the rest of the revolutions in a generation position. This variation in the density of the revolving positions was included in the calculation algorithm to improve the resolution of the results without reducing the speed of the simulation.

Face milling simulation major revolutions

1. Rotation of the cutter around its axis $A_1 \rightarrow A_2$
2. Revolution of the cutter around the cradle axis $A_2 \rightarrow A_3$
3. Revolution of the cutter axis around the cradle $R_1 \rightarrow R_2$

FACE MILLING



FACE HOBBING

Face hobbing simulation major revolutions

1. Rotation of the cutter around its axis $A_1 \rightarrow A_2$
2. Revolution of the cutter around the cradle axis $A_2 \rightarrow A_3$
3. Revolution of the cutter around the work gear axis $A_3 \rightarrow A_4$
4. Revolution of the cutter axis around the cradle $R_1 \rightarrow R_2$
5. Revolution of the cutter axis around the work gear axis $R_2 \rightarrow R_3$

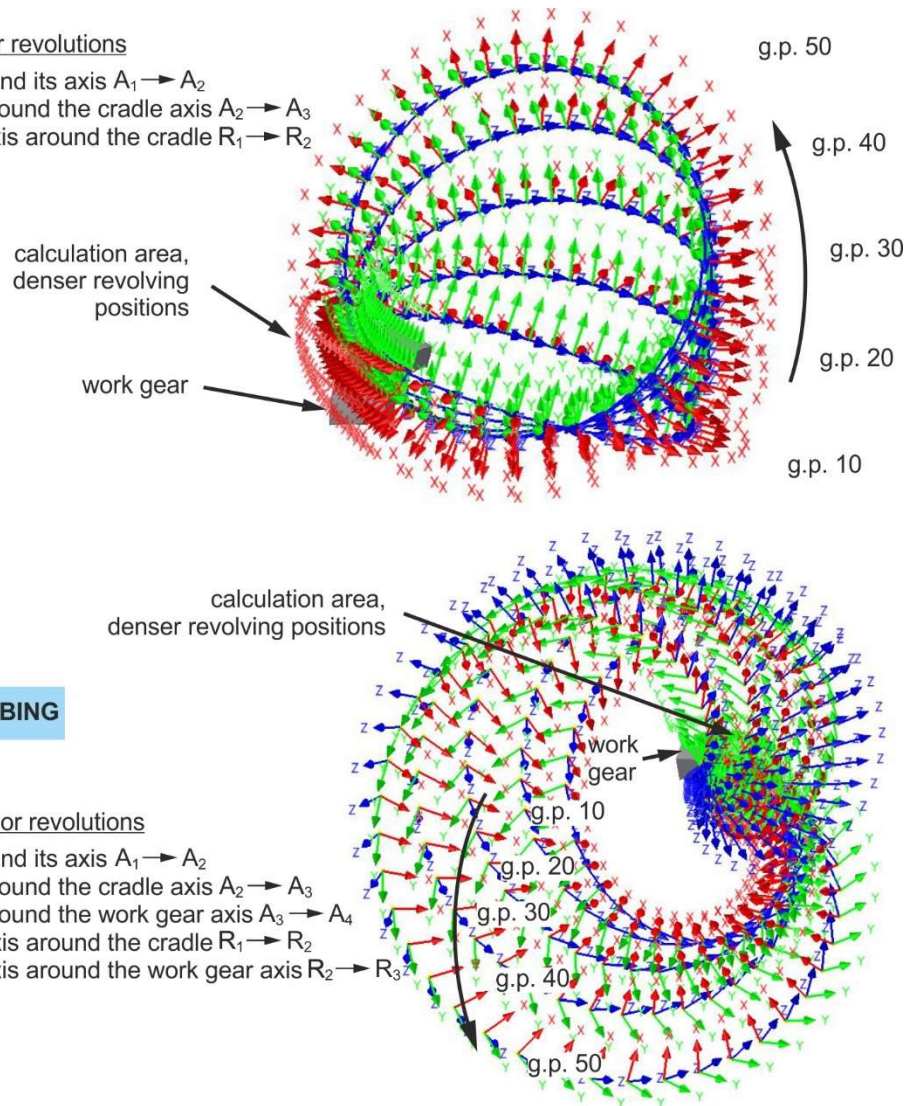


Figure 4.12: Face milling and face hobbing UCS revolutions. [55, 59]

4.2.2 Generation Positions

The generating roll motion is simulated as an iterative process which is performed as many times as necessary so that the tool can generate both convex, root and concave flank surface geometries. The first position of the tool profile is defined by the reference user coordinate system. This position initiates the simulation process since it is the 1st revolving position of the 1st **generation position**. The iterative process of revolving starts at the first revolving position and terminates at the last revolving position of each generation position. Apart from the first generation position, which initiates with the reference UCS, all the succeeding generating iterations (m) begin with a (n) UCS which is created as a result of the revolution of the previous (n-1) UCS which is the last UCS of the previous generation position (m-1).

Each revolving position is superimposed on the previous one in such a way that a series of revolving positions results in a completed generation position. The number of revolving positions included in each generating step results from the revolving discretization selected by the user. When simulating face milling and face hobbing, each generation position corresponds to a full rotation of the cutter around its axis and also includes the relative rotation of the cradle (generating gear) and the work gear around their axes, depending on the generating ratio of roll and the indexing ratio respectively.

This 360° rotation of the cutter (master rotation) is translated to a respective rotation of the work gear (1st slave rotation) and a respective rotation of the cradle (2nd slave rotation), both calculated according to [equations 4.1](#) to [4.3](#). Work gear rotation angle θ_w , cutter rotation angle θ_c , and cradle rotation angle θ_g are combined so that both cutting and generating motions of the tool and the workpiece can be simulated.

$$\theta_c = v \text{ }^\circ \quad (4.1)$$

$$\theta_w = R_i \cdot \theta_c \text{ }^\circ \quad (4.2)$$

$$\theta_g = R_g \cdot \theta_w \text{ }^\circ \quad (4.3)$$

When all angles are calculated, the number of the revolving steps is calculated based on the revolving resolution. As can be seen in [Figure 4.12](#), the revolving positions are not equally distributed on the tool trajectory. On the contrary, the series of revolving positions is denser within the tool width and sparse for the rest of the revolution in a generation position. This difference in the revolving precision within a step is also controlled by the user in such a way that the precision in the area of interest remains high while at the same time, the simulation time does not increase dramatically. In case that the simulated process is a non-generating process, the same principles apply to describe a **plunge position**, excluding the generating revolution from the five relative revolutions presented in [section 4.2](#) and [Figure 4.12](#). In order to fully describe the process kinematics, it is necessary to include as many generation positions as possible, so that the tool accurately forms the whole gear slot surface topography. Similar to the revolving positions, the number of generation positions is calculated by the total generating angle (θ_g) and the generation resolution factor (p_g). [Figure 4.13](#) and [Figure 4.14](#) show the generating motion of the inner and outer blades of the cutter in a face milling simulation. The rotational motion of the cutter is implemented from toe to heel as described above. The generating roll motion between the work gear and the cutter is implemented starting from the tip of the tooth on the outside diameter of the gear (heel), passing through the root area at the middle of the tooth and gradually moving towards the inside diameter (toe), exiting the work gear from the tip of the toe.

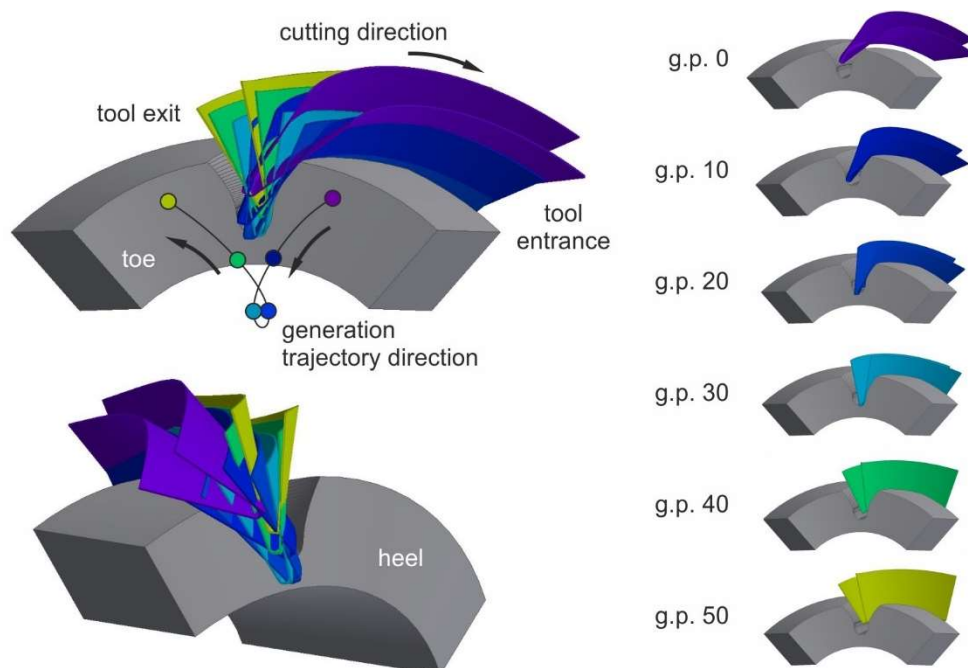


Figure 4.13: Generation trajectory – Inner blade. [59]

Therefore, the generation develops exactly as expected from the tip of the tooth to the root area and to the opposite flank tip, but also from heel to toe. Six characteristic intermediate generation positions, extracted from the simulation results, are shown for both blades, allowing a rough visual evaluation of the resulting motion which reveals that the simulated face milling kinematics agree with literature data. The abbreviation g.p. refers to a specific generation position. It must be mentioned that during a face milling process each blade, for example the inner, is positioned very close to the opposite tooth flank, which is machined by the outer blade. Therefore, any inaccuracy in the tool trajectory would result in the wrong positioning of the two blades with respect to each other and would consequently cause undesired collisions of each blade with the opposite tooth flank.

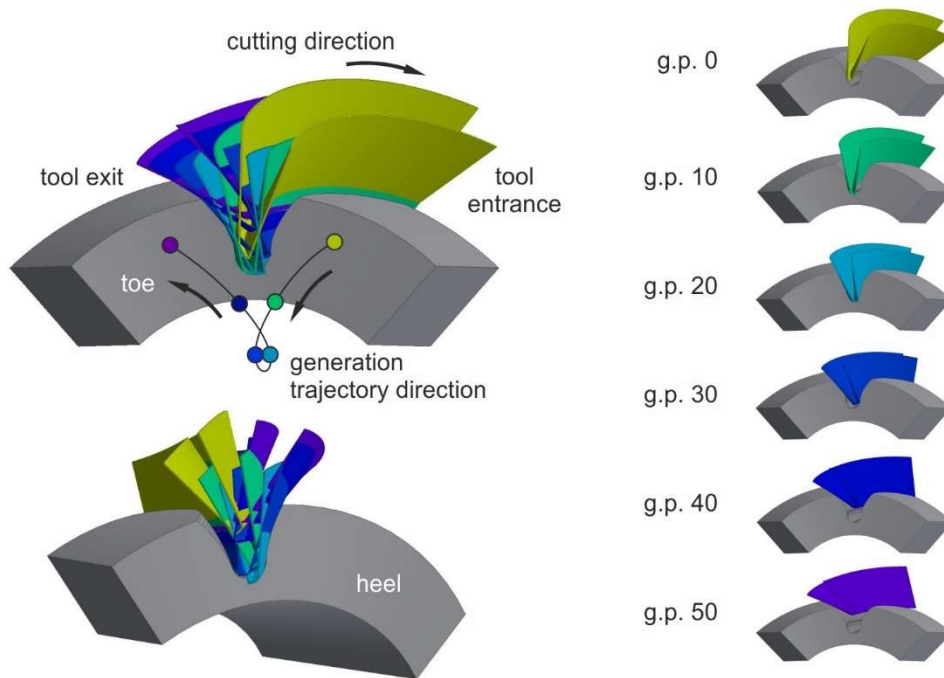


Figure 4.14: Generation trajectory – Outer blade. [59]

4.3 Simulation Results: Simulated work gear geometry and simulated undeformed chip geometry

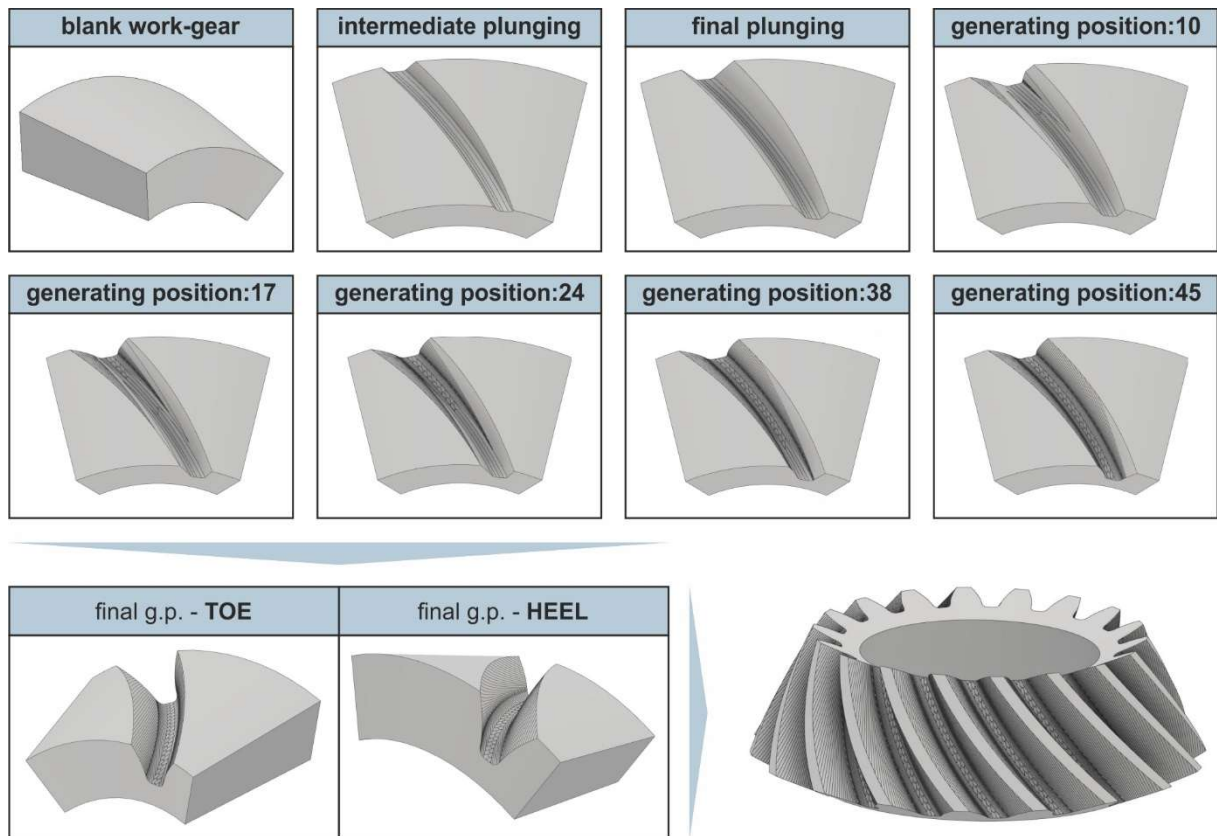
Once the machining assembly is created, the simulated gear geometry and surface topography as well as the undeformed chips are calculated for each plunge and generation position. Both geometries are produced by simple Boolean operations performed between the two solid geometries of the work gear and the cutting tool. The simulated gear geometry is the result of a Boolean subtraction of the cutting tool from the work gear, while the undeformed chip geometry is generated as the intersection of the tool with the work gear. Each simulated work gear and chip solid is a unique solid geometry, stored in a separate solid file. The chip solids are then used to calculate the cutting forces through an analysis of the chip geometry. It should be noted that the inner and outer blades create different chip and work gear geometries considering that the inner blade interacts with the convex tooth flank while the outer blade interacts with the concave tooth flank.

4.3.1 Simulated work gear geometry

4.3.1.1 Face milling results

First, the resulting pinion and ring gear geometries from a face milling simulation will be presented. A case study, in which a spiral bevel gear pair is machined with a two-stage roughing by plunging and finishing by generating operation, was selected for presentation.

Figure 4.15 and Figure 4.16 show a simulated gear slot including the convex, the concave flank and also the root area from a pinion and a ring gear face milling simulation respectively.



Gear geometry input data:

gear type: pinion, $z_1=18$, spiral direction: left, $\beta_m=35^\circ$, $b=25.4\text{mm}$, $d_{e2}=176.893\text{mm}$, $\theta_{a2}=2.6186^\circ$, $\theta_{f2}=2.6186^\circ$

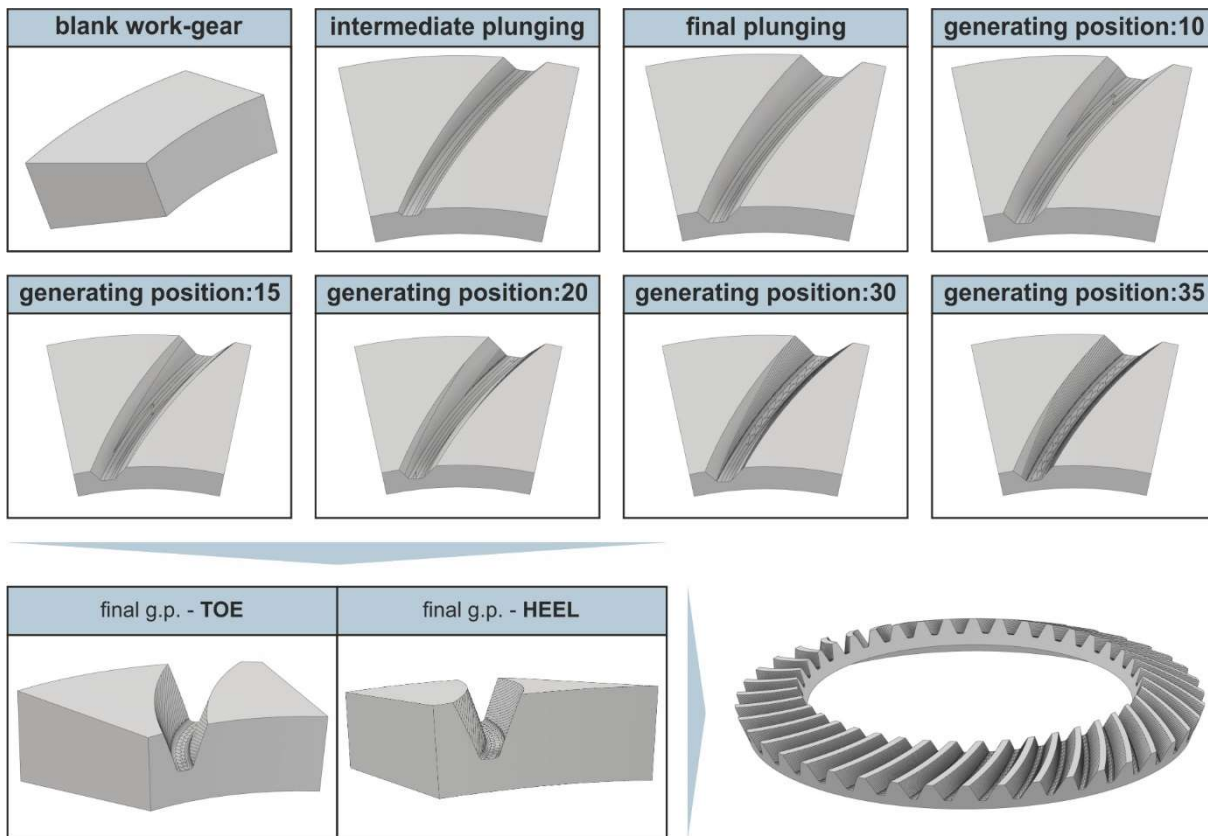
Process input data:

manufacturing: face milling, profile: DIN 3972 Profile II, $a_n=20^\circ$, $r_{c0}=82\text{mm}$, $t_f=0.4\text{mm}$, $f_p=0.5\text{mm/rev}$, $f_g=0.58^\circ/\text{rev}$

Figure 4.15: Simulated tooth flank surfaces of a face-milled pinion gear. [59]

The subtraction of the two opposite chip geometries from the previously produced work gear geometry in every simulation step results in the plunge cut or generated gear slot consisting of a convex and a concave tooth flank. Both figures 4.15 and 4.16 show some examples of tooth flank geometries produced in various plunge-cut and generation steps. For brevity purposes, a limited set of representative intermediate plunge and generation positions is included in the figures in order to show the development of the process. More specifically, the plunging stage is presented with one intermediate and the final plunge position in which the depth of the slot equals the final slot depth of the gear minus the finishing stock allowance for the generating stage of the process. The number of the simulated roughing geometries results from the final slot depth, the depth of cut of every plunging pass (plunge feedrate) and the finishing stock allowance. The final geometry of this stage (final plunging) is the output of the roughing-plunging stage and the input for the following generating process. As it can be observed even in these first roughing steps, the tooth depth is tapered as a result of the root line tilting so that a proportional split of tooth thickness and space width can be achieved as described in previous sections. The generation of the tooth flanks and finishing of the root area can be realized in one or more finishing stages. In this example, the final finishing stage is presented for both pinion and ring gear. The slot geometry in both gears is built from heel to toe. All simulated geometries are extracted and stored for each simulation step so that the changes in the tooth flank topography, caused by the consecutive cutting tool traces as the

process progresses, can be revealed. Each discrete chip is also stored as a solid geometry so it can be subsequently used for the calculation of the cutting forces. [59]



Gear geometry data:

gear type: gear, $z_2=41$, spiral direction: right, $\beta_m=35^\circ$, $b=25.4$ mm, $d_{e2}=176.893$ mm, $\theta_{a2}=2.6186^\circ$, $\theta_{f2}=2.6186^\circ$
 $m_{mn}=3.0695$ mm

Process data:

manuf/ring: face milling, profile: DIN 3972 Profile II, $a_n=20^\circ$, $r_{c0}=82$ mm, $t_f=0.4$ mm, $f_p=0.5$ mm/rev, $f_g=1.26$ °/rev

Figure 4.16: Simulated tooth flank surfaces of a face-milled ring gear. [59]

As described in a previous section, face-milled tooth geometry is characterized by an arc-shaped lengthwise curve, a tapered tooth depth, and a tapered tooth thickness along the width of the tooth. Both flanks of the gear slot, convex and concave, are cut at each simulation step by the inner and outer cutting blade respectively. The outside blade proceeds and the inside blade follows. The machining action is initiated at the toe and is directed towards the heel for better burr formation on the outside diameter of the gear and the direction of cutting forces towards the fixture. The tooth cutting traces are almost parallel to the contact lines which is a typical characteristic of the face milling method. A total of five intermediate generation positions are presented in both Figure 4.15 and Figure 4.16 in the top view, while the final finished geometries are demonstrated from toe and heel sides. Finally, the full gear geometry is presented at the right bottom part of the figures showing all finished slots. The gear pair selected for the presentation of simulation results consists of a generated pinion and generated wheel. The calculation algorithm is also capable of producing non-generated ring gears in case this option is selected by the user. The pair has a shaft angle of $\Sigma=90^\circ$ and consists of a pinion with $z_1=18$ teeth, left spiral and a ring gear (wheel) with $z_2=41$ teeth and a right spiral. The outside diameter of the wheel is $d_{e2}=176.893$ mm with a $m_{mn}=3.0695$ mm mean normal module. The face width of the tooth for both members of the pair equals $b=25.4$ mm with a $a_n=20^\circ$ normal pressure angle. The addendum and dedendum angles are equal and set to $\theta_{a2}=\theta_{f2}=2.6186^\circ$. The radius of the cutter $r_{c0}=82$ mm is selected to be slightly smaller than

the mean cone distance R_m which is a good choice for these processes, according to Stadtfeld [10]. The profile of the cutter blades, hence the reference geometry of the gears, is designed according to DIN 3972 Profile II specification. All cutting parameters such as the plunge feed per cutter revolution f_p (mm/rev), the finishing stock allowance t_f (mm), as well as the feedrate of the generating stage f_g ($^\circ$ /rev) are provided at the bottom part of the figures. [59]

Figure 4.17 presents the assembled gear pair after the completion of the manufacturing simulation, where the produced surface topography in both members can be seen. A cross-section of the gear pair close to the meshing position is also shown in the figure. Magnified views of the pinion and ring gear produced topographies are also presented in Figure 4.17, allowing a visual examination of the simulated cutting lines which appear to be perfectly symmetrical, uniformly distributed along the tooth profile and parallel with respect to the contact lines, exactly as expected.

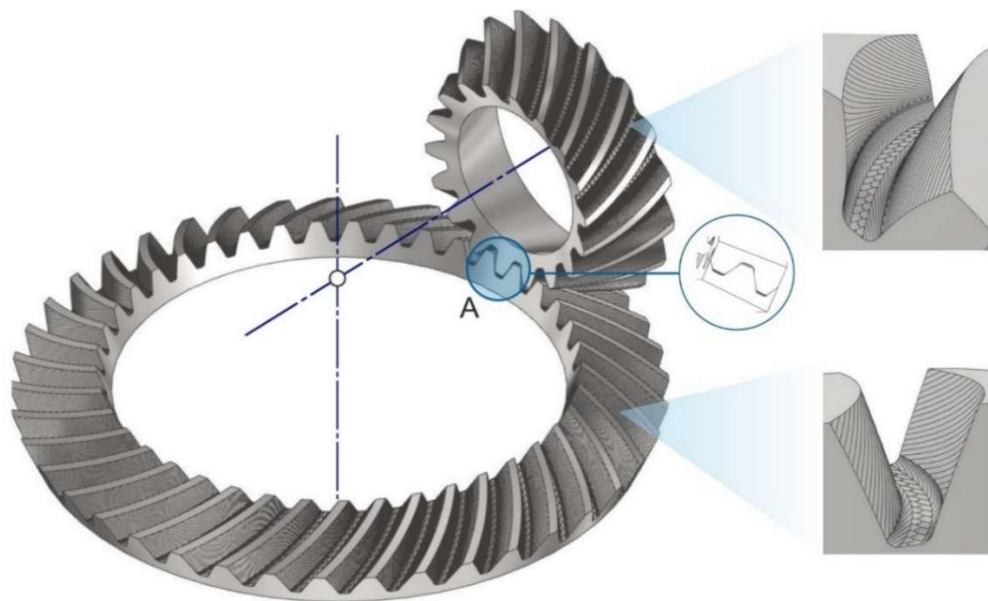
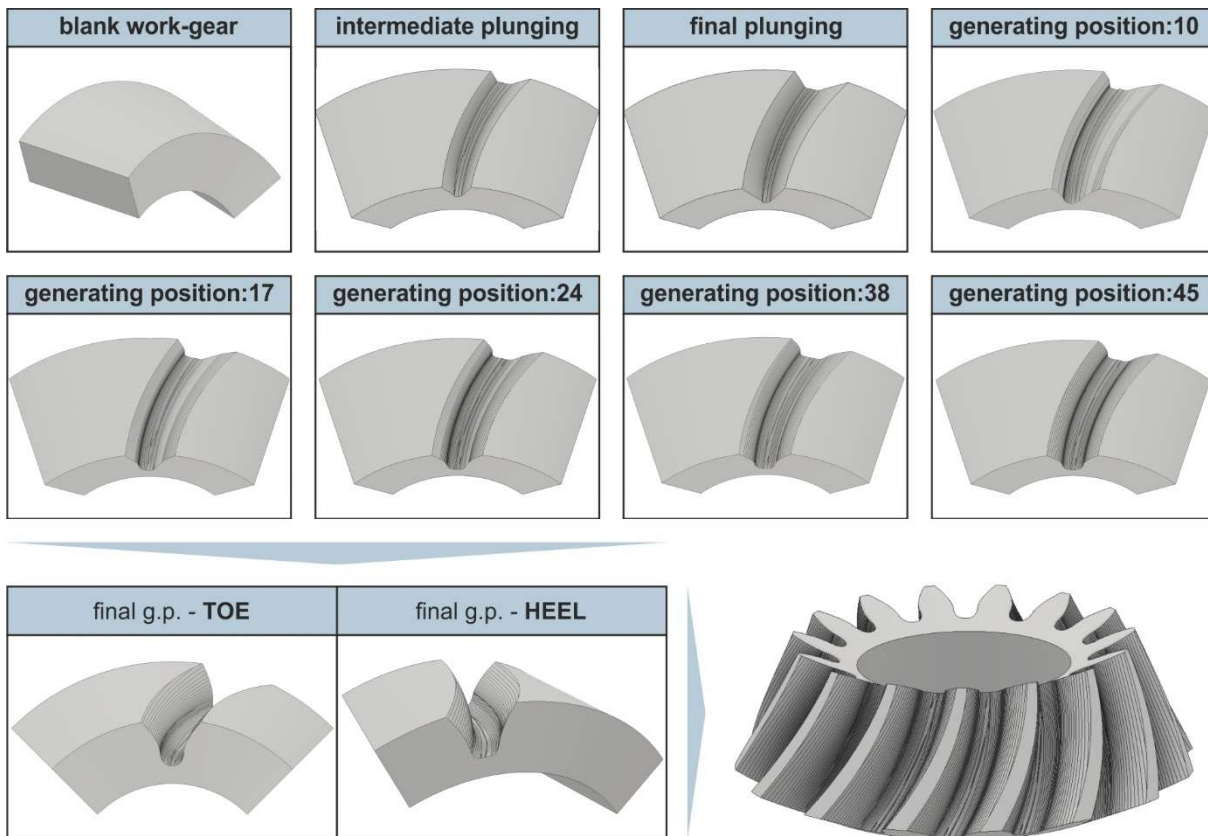


Figure 4.17: Assembly of a simulated face-milled gear pair. [59]

4.3.1.2 Face hobbing results

The simulated face-hobbed pinion and ring gear geometries are presented in this section with the use of actual solid geometries, produced in a sample simulation case study. The face-hobbed gear geometry is characterized by an extended epicycloid lengthwise tooth curve, a constant tooth depth, and a uniformly distributed tapered tooth thickness along the face width of the tooth. The outer and inner blades of the cutter, machine the concave and the convex flanks of the tooth respectively, with the outer blade preceding, followed by the inner blade. [55] Figure 4.18 and Figure 4.19 present two sample simulated gear slots from a face-hobbed pinion and a ring gear respectively. The slots consist of the convex and concave flanks of two consecutive teeth and also the slot root area. The two gears are part of the same pair and are both machined with a two-stage roughing by plunging (forming) followed by a generating finishing operation. Two intermediate plunge and generation positions are shown in the figures for both gears, and the final geometries are also presented. All geometrical and process-related data are provided in the bottom part of the figures. In both figures, the uniform slot depth and the tapered slot width can be observed in all simulation stages. The cutting action is taking place from toe to heel while the slot geometry is built from heel to toe as a result of the down milling strategy selection for the finishing generation stage.

**Gear geometry input data:**

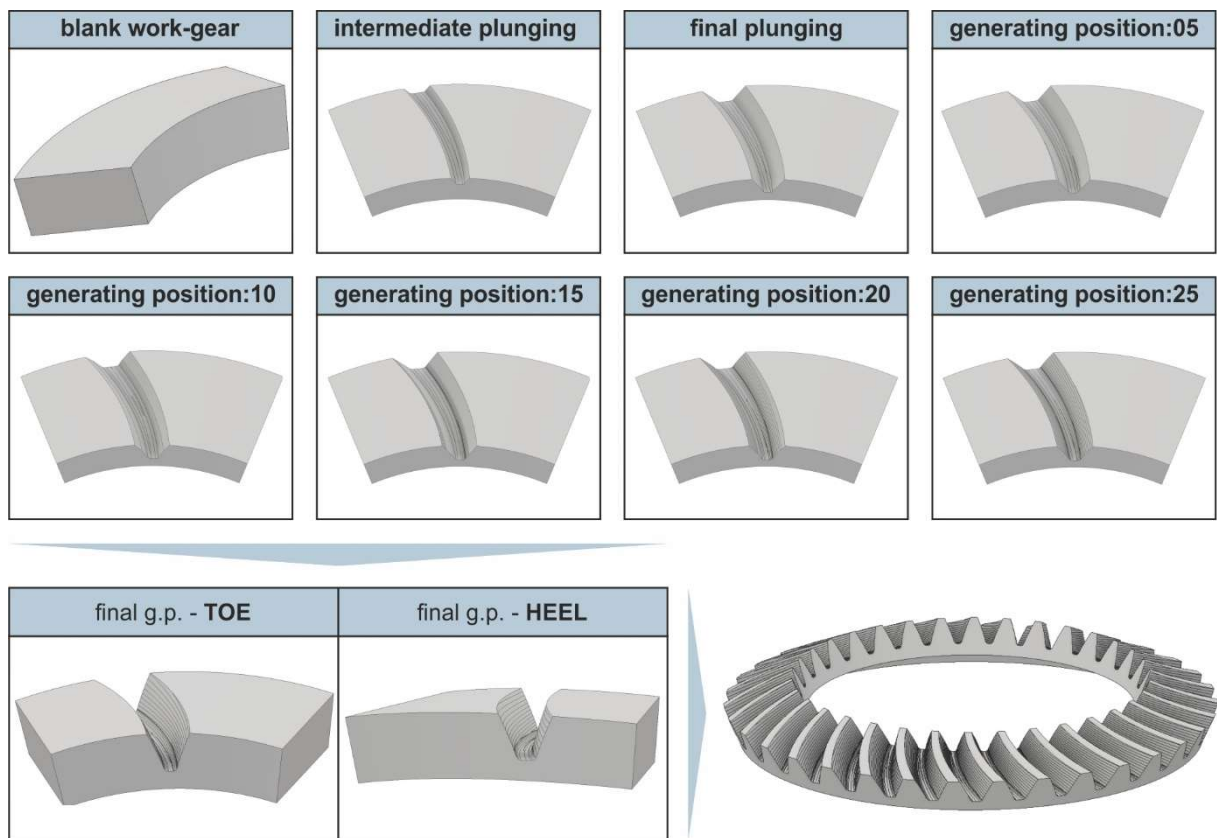
gear type: pinion, $z_1=15$, spiral direction: right, $\beta_m=21^\circ$, $b=26$ mm, $d_{m2}=146.7$ mm, $\theta_{a2}=0^\circ$, $\theta_{f2}=0^\circ$

Process input data:

manufacturing: face hobbing, profile: DIN 3972 Profile II, $a_n=20^\circ$, $r_{c0}=75$ mm, $z_0=15$, $t_f=0.5$ mm, $f_p=0.5$ mm/rev, $f_g=0.022^\circ$ /rev

Figure 4.18: Simulated tooth flank surfaces of a face-hobbed pinion gear. [55]

As it can be seen in both figures the tool cutting traces are inclined relative to the contact lines which is typical for the face hobbing method. The depth of the tooth in both cases remains constant along the face width, while the kinematics of face hobbing form an extended epicyclic flank line which produces a balanced taper between the gear tooth and the gear slot. Both tooth thickness and space width decrease from heel to toe. As both members of a gear pair are machined in the same way, the tapered teeth of the pinion fit in the tapered slots of the ring gear and vice versa. At the bottom of the figure, two views of the finished gear slot captured from toe and heel positions are presented, where the variance in the width of the slot is obvious. The simulated pair has a shaft angle of $\Sigma=90^\circ$ and consists of a pinion with $z_1=15$ teeth, a right spiral and a ring gear (wheel) with $z_2=34$ teeth and a left spiral. The mean pitch diameter of the wheel is $d_{m2}=146.7$ mm with a $m_{mn}=4.0281$ mm mean normal module. The face width of the tooth for both members of the pair equals $b=26$ mm with an $a_n=20^\circ$ normal pressure angle and a $\beta_m=21^\circ$ helix angle. The addendum and dedendum angles are equal and set to $\theta_{a2}=\theta_{f2}=0^\circ$. The radius of the cutter $r_{c0}=78$ mm is selected to be close to the mean cone distance R_m . [Figure 4.19](#) shows the simulated ring gear geometry with the respective intermediate plunge and generation positions. [55]

**Gear geometry input data:**

gear type: ring, $z_2=34$, spiral direction: left, $\beta_m=21^\circ$, $b=26$ mm, $d_{m2}=146.7$ mm, $\theta_{a2}=0^\circ$, $\theta_{r2}=0^\circ$, $m_{mn}=4.0281$ mm

Process input data:

manufacturing: face hobbing, profile: DIN 3972 Profile II, $a_n=20^\circ$, $r_{c0}=78$ mm, $z_0=16$, $f_g=0.044^\circ/\text{rev}$, $t_f=0.5$ mm, $f_p=1$ mm/rev

Figure 4.19: Simulated tooth flank surfaces of a face-hobbed ring gear. [55]

The cutting blade profiles are designed according to DIN 3972 Profile II specification [60], so the reference geometry of the gears corresponds to this specification. The rest of the cutting parameters such as the number of blade groups, the finishing stock allowance as well as the plunge and generation feedrates are shown in the bottom part of both figures. The generation feedrate is chosen for both gears so that an acceptable topography can be produced with multiple cutting lines formed at each tooth flank. In the case of the face-hobbed pinion, the distance between the consecutive cutting lines ranges from 0.4 mm to 0.8 mm, while for the face hobbed ring gear the cutting lines are at about 0.7 mm up to 1.2 mm distance from each other. The simulation algorithm can produce a full gear pair as the one presented in [Figure 4.18](#) and [Figure 4.19](#). [Figure 4.20](#) shows the two members of the gear pair as they would be assembled in a gearbox. The cut lines are visible for both gears and a magnified view close to the meshing position is also presented in the figure. [55, 60]

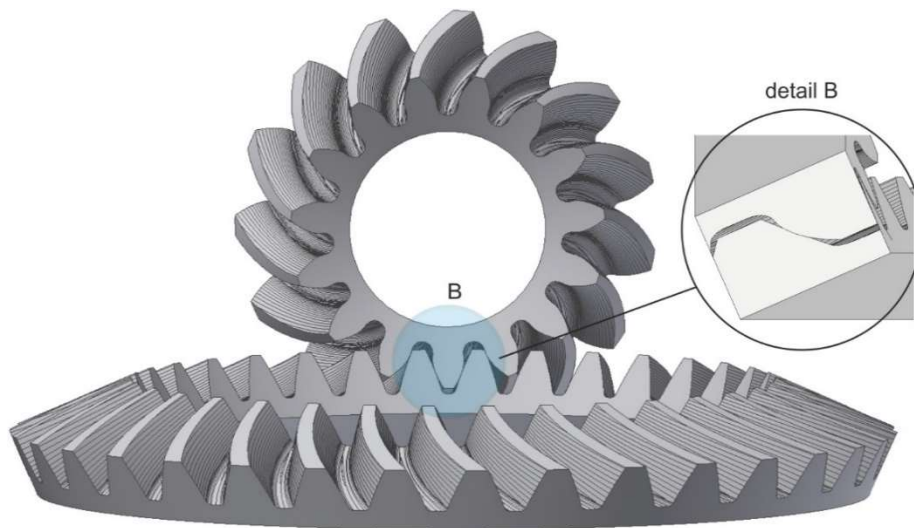


Figure 4.20: Assembly of a simulated face-hobbed gear pair. [55]

4.3.2 Simulated undeformed chip geometry

Apart from the solid tooth flank geometry, the undeformed chip 3D geometry is also automatically calculated in each simulation step. Each plunge or generation position includes two individual solid chip geometries resulting from the interaction of the inner and outer blades with the gear slot surfaces. All chip geometries are stored so they can be used for the calculation of cutting forces. A first insight into the chip formation process can be obtained by a geometric analysis of the produced chips, prior to the cutting forces calculation.

4.3.2.1 Face milling results

The following figures show some samples of undeformed chip geometries produced for a specific gear slot by the outer and inner blades of the cutter in face milling simulation. For the sake of concision and clarity, not all intermediate generation positions are included in the figures. [Figure 4.21](#) and [Figure 4.22](#) show the chip geometries produced in face milling of a pinion gear and a ring gear respectively. The chips produced in certain positions during plunge cutting and generating roll are indicated in all figures by the abbreviations p.p. for plunge position and g.p. for generation position. On the left part of the figures, some intermediate chips produced during the plunging stage are shown. While performing the plunging, the cutter is fed towards the final slot depth leaving a finishing stock allowance for the following generating stage. The two motions that take place during this stage are the rotation of the cutter, which provides the cutting motion, and the feed of the cutter in the work gear. The two blades cut with both cutting edges (flank and tip) and the edge radius, therefore the chips include both parts of the roughed flank and root area. On the right side of the figures, the chips produced in the generation stage are shown. As can be easily observed, there are certain stages in the generation process in which the blades cut only parts of the flank and others in which part of the root area is also machined. It should be noted that the outer and inner blade chips, illustrated in pairs in the figure, represent certain instances in the process. [55, 59]

As described above, when using a face milling cutter, the outer blade precedes and the inner blade follows. Depending on the number of cutting blades the distance from the outer to the inner blade produces a phase difference in the generating process between the two blades. This phase difference is taken into account in the algorithm, thus the chips produced by the outer blade at a certain point in the process are more advanced in terms of generation than the respective chips of the inner blade.

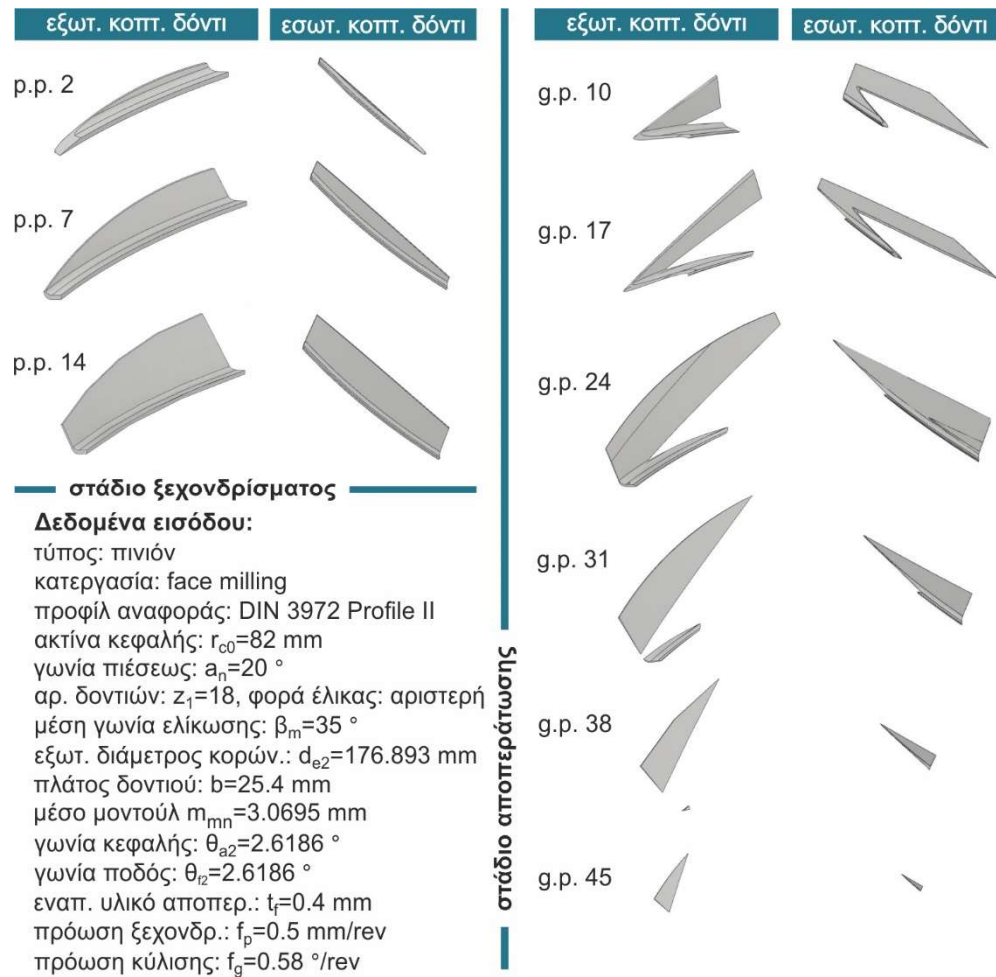


Figure 4.21: Undeformed solid chip geometries of a pinion gear for various simulation steps of face milling method. [59]

Regarding the chip thickness values for the pinion as the process progresses, the maximum chip thickness during plunge cutting is 500 μm at the root area for both inner and outer blades, a value that is provided as an input for the process, indicated as the plunge feed rate f_p and set by the user, while the maximum thickness on the flank is 250 μm and 200 μm for the outer and inner blade respectively. In the finishing generation stage, the chips produced by the outer and inner blades presented in Figure 4.21 have maximum thickness values shown in [Table 4.4](#).

PINION	Chip thickness (μm)						
	Outer blade	g.p. 10	g.p. 17	g.p. 24	g.p. 31	g.p. 38	g.p. 45
Flank		75	60	80	105	85	50
Root		186	151	200	98	12	-
Inner blade	g.p. 10	g.p. 17	g.p. 24	g.p. 31	g.p. 38	g.p. 45	
Flank		147	102	88	50	40	17
Root		73	22	189	89	20	-

Table 4.4: Maximum chip thickness values in the finishing generation stage of the face-milled pinion gear.

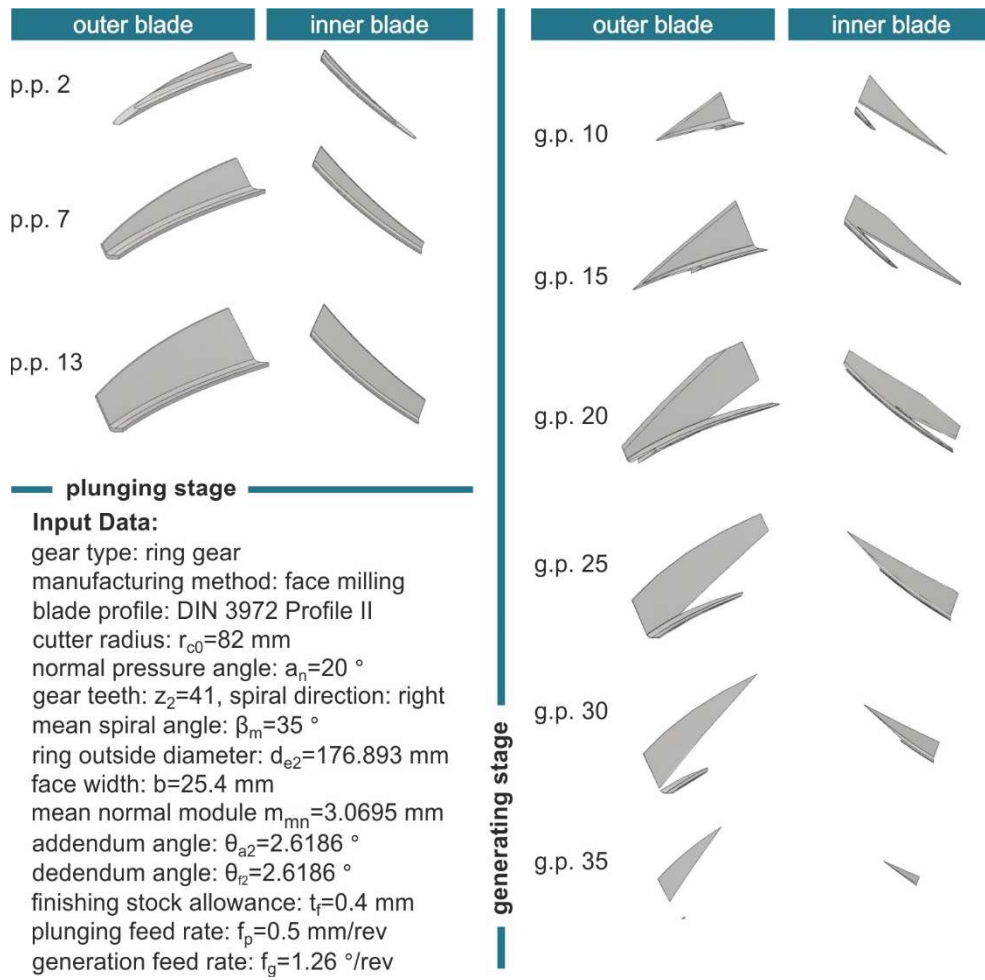


Figure 4.22: Undeformed solid chip geometries of a ring gear for various simulation steps of face milling method. [59]

Concerning the ring gear chip thickness values, the maximum chip thickness on the root area during plunge cutting is 500 μm , as defined by the user and 230 μm on the flank for both inner and outer blades. In the finishing generation stage, the chips produced by both blades, presented from top to bottom in Figure 4.22, have maximum thickness values shown in Table 4.5 below.

RING GEAR	Chip thickness (μm)						
	Outer blade	g.p. 10	g.p. 15	g.p. 20	g.p. 25	g.p. 30	g.p. 35
Flank		40	40	20	50	37	25
Root		90	60	70	50	30	-
Inner blade	g.p. 10	g.p. 15	g.p. 20	g.p. 25	g.p. 30	g.p. 35	
Flank		50	40	35	40	25	12
Root		90	40	31	60	30	-

Table 4.5: Maximum chip thickness values in the finishing generation stage of the face-milled ring gear.

4.3.2.2 Face hobbing results

Figure 4.23 and Figure 4.24 show the undeformed chip geometries produced in a two-stage face hobbing process of a pinion and a ring gear respectively. On the left part of Figure 4.23 and Figure 4.24, a series of intermediate chip geometries produced in the roughing plunge cut (forming) are presented. At this stage, the cutter head is fed to the final slot depth leaving the

desired stock allowance for the finishing generating phase. The motions that take place in the plunging phase are the feed of the cutter in the work gear as well as the timed rotation of the cutter head and the workpiece which provides both the cutting action and the engagement of the cutter with the work gear, so all slots can be machined at once. The solid chip geometries result from the interaction of both cutting edges of each blade with the respective flank and root area of the slot. The chips produced during the generation stage of the process consist of either both flank and root area chip portions or only flank area portions, depending on the relative position of the tool and work gear at each generating step. When machining with a face hobbing process, the outside blade of each blade group precedes, followed by the inside blade. The angular distance between the two blades introduces a phase difference in the convex and concave flank generation process. This phase difference is considered in the algorithm, therefore the cutting chips produced by the outer blade are more advanced than the ones produced by the inner blade. [55, 59]

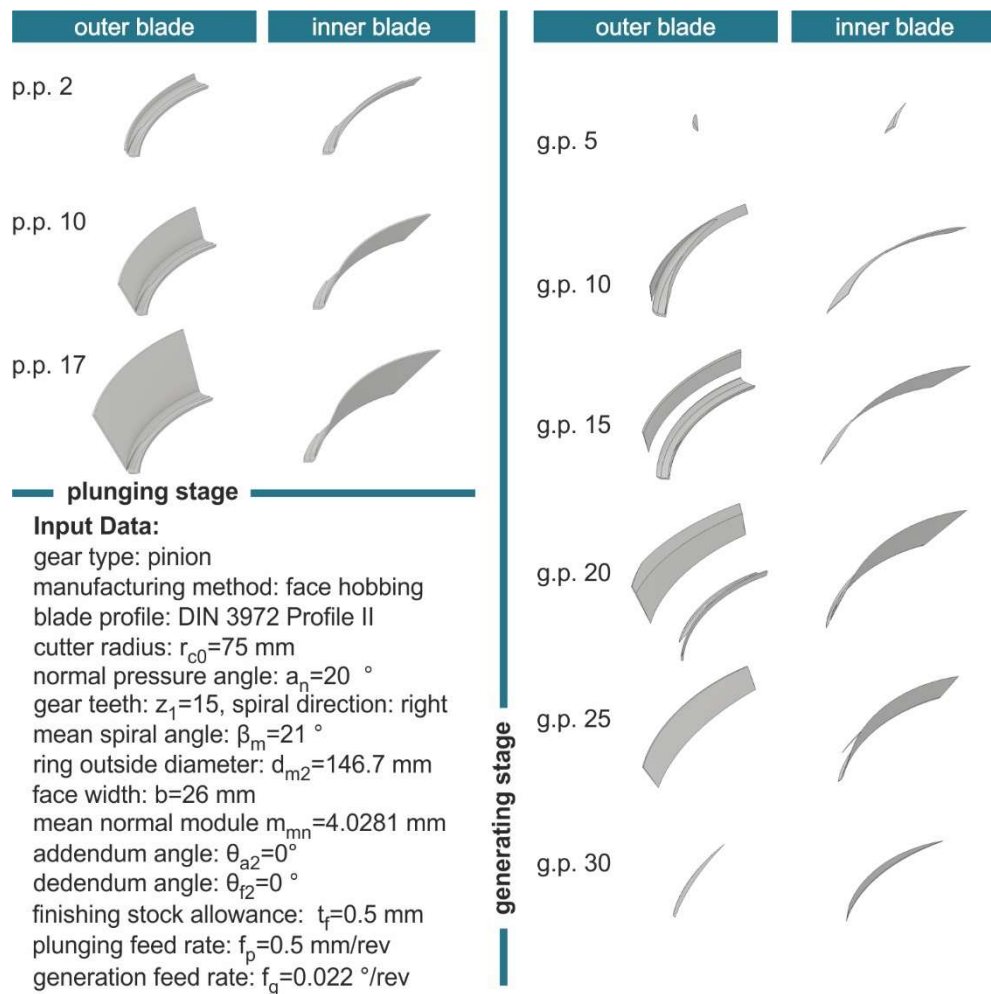


Figure 4.23: Undeformed chip geometries of a pinion gear for various simulation steps in face hobbing method. [55]

The ring gear of the pair was roughed with the cutting depth set to 1mm/rev. As a result, the roughing chips presented in Figure 4.24 are much thicker in this case. As can be seen in the right part of the figure, the generating chips are narrower than those produced in the pinion generation and this is due to the “lighter” conical shape of the wheel. Table 4.6 provides the maximum chip thickness values for both inner and outer blades in roughing and finishing of the pinion and ring gear. Regarding the maximum chip thickness values of the pinion and the evolution of the chip thickness as the process progresses, the maximum chip thickness during

plunge cutting is 500 μm on the root area for both inner and outer blades, which corresponds to the desired plunge feedrate f_p provided as an input to the model.

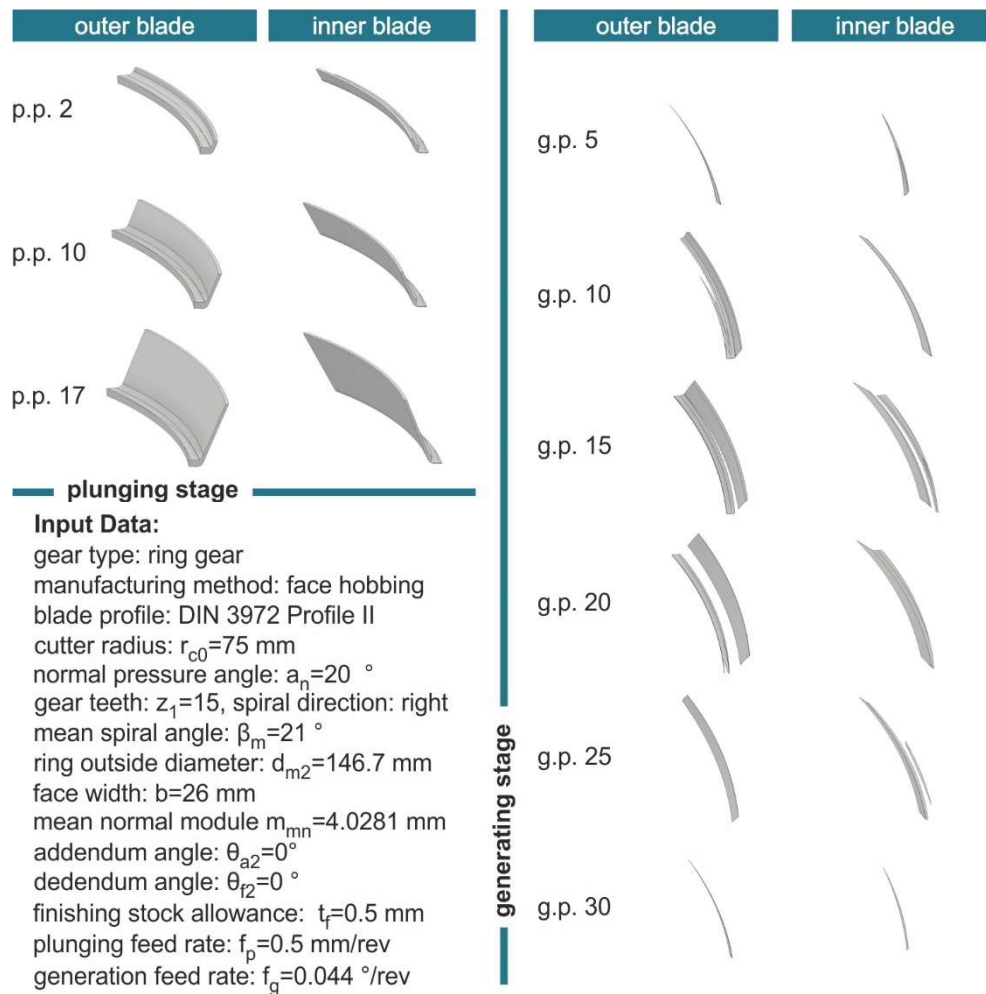


Figure 4.24: Undeformed solid chip geometries of a ring gear for various simulation steps of face hobbing method.

The maximum chip thickness on the flank is 260 μm and 360 μm for the outer and inner blades respectively. Although the chip thickness remains almost constant during the roughing stage, the shape and thickness of the chips show great variability during the generating process. For the outer blade, the maximum chip thickness is located at the root area in the first finishing positions, while the chip becomes gradually thicker at the flank area as the finishing process progresses. This indicates that the cutting action for the outer blade begins at the root of the slot and ends at the tip of the tooth. Another point worth mentioning is that all the chips are thicker closer to the toe of the gear and become thinner towards the heel. Given that the cutter rotates from toe to heel and the generation is performed heel to toe, this variation in tooth thickness is explained by the climb cutting strategy of the outer blade. Contrary to the outer blade, the generating action of the inner blade begins at the convex tooth flank and gradually moves towards the slot root area, so maximum chip thickness is measured at the flank area in the first finishing positions and in the root area at the end of the process. Opposite to the outer blade, the convex chips produced by the inner blade are thinner at the toe area of the gear and become gradually thicker towards the heel. This is because the inner blade performs a conventional cutting process. As to the plunge cut of the ring gear, the maximum thickness of the chip on the root area is 1000 μm for both inner and outer blades, which is a value set by the user. The maximum value of chip thickness on the flank is 350 μm for the outer and 370 μm for the inner blade. In the finishing generation stage of the ring gear, the maximum chip

thickness at the root area is 190 μm and 120 μm for the outer and inner blades respectively, while the respective values on the flank are 75 μm and 88 μm . Similar to the pinion generation, the cutting action of the outer blade begins in the root area of the slot and progresses towards the concave flank, while the inner blade starts cutting on the convex flank and moves towards the root area. The same variation in the thickness of the chip from toe to heel observed on the pinion, applies to the ring gear as well, since the outer blade follows a climb cut strategy and the inner blade performs a conventional cut. [55]

PINION	Outer blade		Inner blade	
	Root area	Flank area	Root area	Flank area
Roughing (μm)	500	260	500	360
Finishing (μm)	330	140	190	120
RING GEAR	Outer blade		Inner blade	
	Root area	Flank area	Root area	Flank area
Roughing (μm)	1000	350	1000	370
Finishing (μm)	190	75	120	88

Table 4.6: Maximum chip thickness values in the finishing generation stage of the face-hobbed pinion and ring gears.

4.4 Ithaca Bevel Gear Suite - Graphical User Interface

The *Ithaca Bevel Gear Suite* is a novel platform developed as part of the current research, dedicated to the integrated study of spiral bevel gear cutting.



Figure 4.25: *Ithaca Bevel Gear Suite* GUI.

The platform allows the kinematic simulation of the process via the *BevelSim3D* algorithm, the calculation of the cutting forces generated during the process via the *BevelForce3D* algorithm and also the validation of the simulation results via the *BevelCurve3D* application. The Bevel Gear Suite platform is developed in Visual Studio. [Figure 4.25](#) shows the graphical user interface that provides access to all the aforementioned applications.

4.4.1 Ithaca BevelSim3D – Graphical User Interface

BevelSim3D is a novel application for the kinematic simulation of spiral bevel gear cutting developed using the API of a leading CAD system. The following paragraphs present the graphical user interface of the software as it appears on the screen when the user sets and executes a simulation case. The simulation model was developed within the Application Programming Interface of Autodesk Inventor using VBA. Autodesk Inventor's API enables the creation of custom applications which automate the design process and provide control on the design parameters. The application exploits the benefits of object-oriented programming in combination with the extended parametric design capabilities of Autodesk Inventor. In order to start a new simulation project, the user provides the algorithm with the input parameters values in the form of a text file. The input data file contains a total of 28 parameter values that are being used throughout the simulation. The user might also interactively alter these parametric values directly on the program form after loading them from the input file and may also save them to a new or existing data file inside the project folder. [Figure 4.26](#) shows the *Configuration* tab of the program.

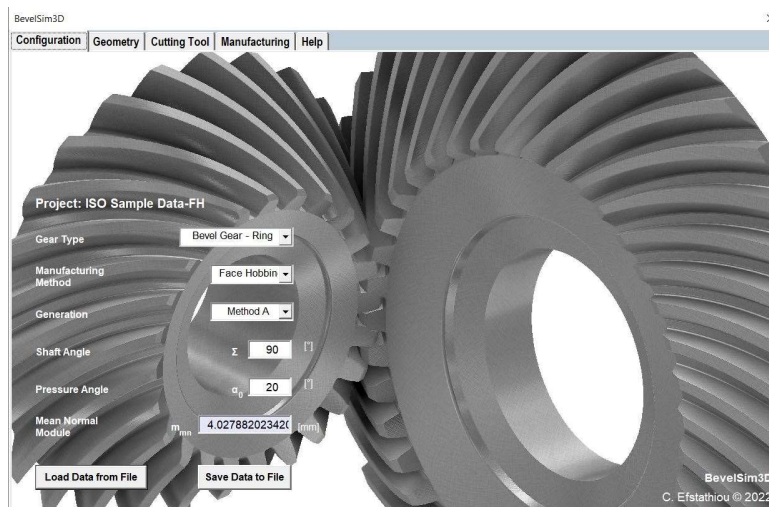


Figure 4.26: Configuration tab.

When all necessary data have been imported to the calculation algorithm, the set-up process continues with the creation of the 3D model of the work gear. [Figure 4.27](#) shows the workpiece setup tab (*Geometry*) of the software. Some of the most significant geometric parameters of the tooth geometry are listed on the tab so that the user can revise and alter them, if necessary, before modelling the 3D geometry.

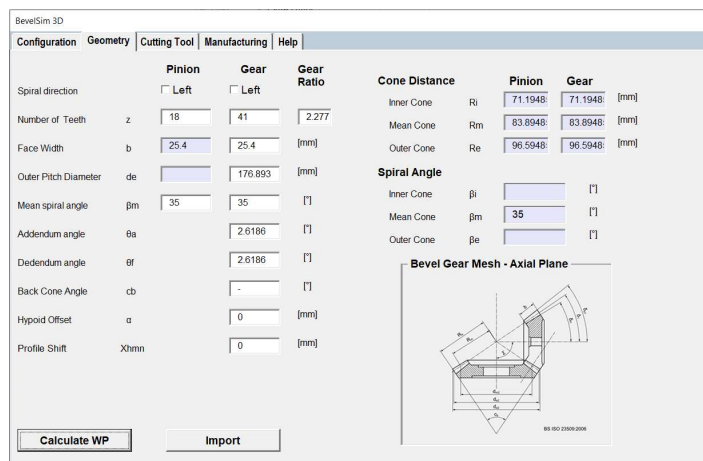


Figure 4.27: Geometry setup tab.

The tab also shows the basic bevel gear geometry as specified in ISO 23509:2016. Following the 3D work gear generation, the user clicks on the *Cutting Tool* tab that contains all the basic tool-related features which are also filled automatically during the data input process. The user fills in a series of values that are missing and can also modify all the values before running the simulation. On the right part of the tab, there are some informative figures about the cutting tool and blade geometry. After all the values are filled, the user activates the “set tool parameters” command so that the values can be stored and used by the algorithm during the simulation. [Figure 4.28](#) shows the *Cutting Tool* setup tab.

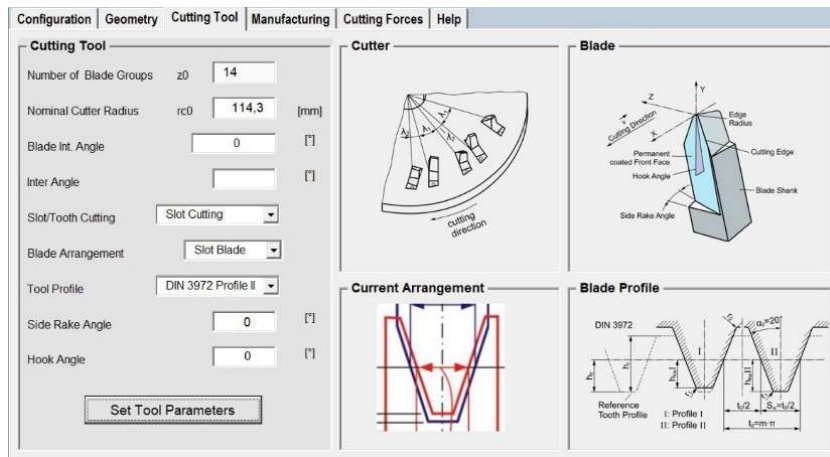


Figure 4.28: Cutting tool setup tab.

The final tab before the beginning of the simulation is the *Manufacturing* tab which is used for the configuration of all process-related parameters such as the accuracy of the simulation, the depths of cuts, the indexing and generating ratios etc. These parameters are automatically populated during the data import process, but the user may alter them as per the requirements of the manufacturing process. [Figure 4.29](#) shows the manufacturing setup tab.

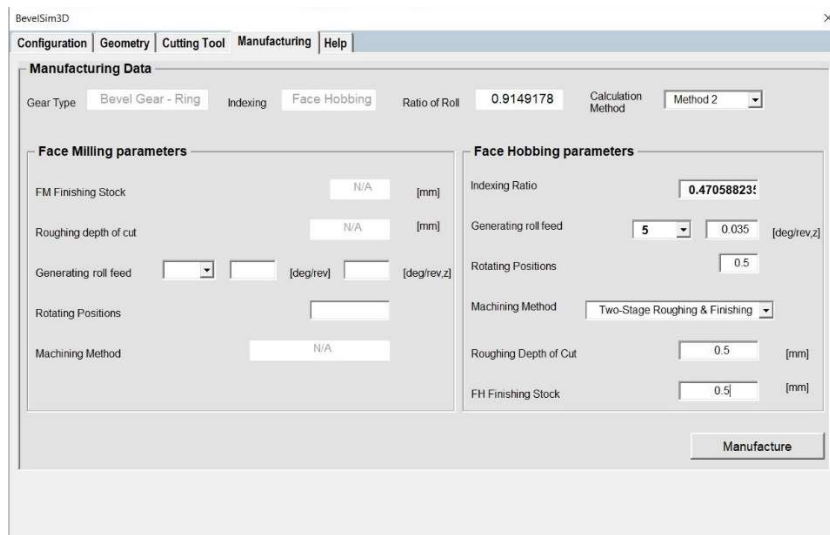


Figure 4.29: Manufacturing setup tab.

[This page intentionally left blank]

5. VALIDATION OF THE SIMULATION MODEL

The simulated tooth flank geometry is a result of the process kinematics that define the motion of the cutter and the workpiece. Therefore, the simulated tooth surface has an octoid form, like the surfaces produced by most face milling and face hobbing processes. However, the exact theoretical spiral bevel gear geometry is based on the spherical involute function. Due to the fact that the solid flank geometry is not determined by the theoretic definition of bevel gear geometry, it is not governed by the mathematical expression of the spherical involute curve. The octoid form resembles the spherical involute form but also deviates from the accurate spherical involute in the range of tolerance for common spiral bevel gear applications [61]. While this simulation model attempts to reproduce the kinematics of the machine, it is still necessary to compare the simulated geometry with the theoretical one to validate the model. [55, 59]

A validation application named *Hermes BevelCurve3D* was developed in order to validate the simulation results and specifically the 3D tooth flank geometry. Similar to the two previously discussed applications, *BevelCurve3D* can be launched via the Bevel Gear Suite platform. A key objective of this application is to enable quick and easy validation of the simulation results against the theoretic solid geometry. *Hermes BevelCurve3D* application is introduced in the following sections and the validation procedure along with some validation results are presented and thoroughly discussed.

5.1 Hermes BevelCurve3D validation software

5.1.1 Application GUI

BevelCurve3D is an application developed for the validation of *BevelSim3D* simulation results and can be accessed via the Bevel Gear Suite platform. [Figure 5.1](#) shows the main window of the application GUI. The user has the following options: 1. Run a new validation case, 2. Import the current or previous validation results into the form and 3. Show the results in the form of 3D-graphs. In case the user chooses to run a new validation example, the program automatically opens the validation form, shown on the right part of [Figure 5.1](#), where all input data referring to the specific simulation case must be entered. Instead of manually entering the necessary data, the user can import the data from the input text file produced when the simulation is executed. Additionally, before running the validation the user must make sure that the theoretic solid geometry file is named properly and placed in the correct validation results folder. Upon completion of the validation, the user can import the results into the *BevelCurve3D* form and view them in three graphs.

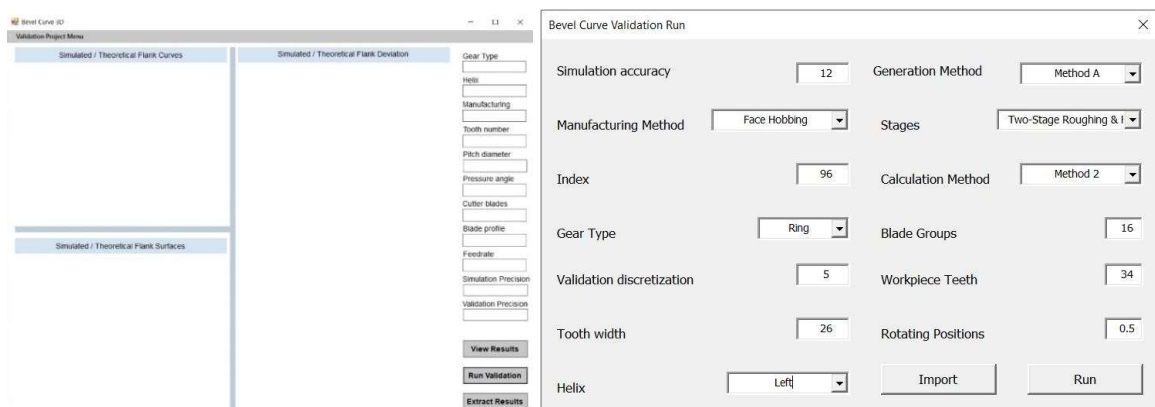


Figure 5.1: *BevelCurve3D* graphical user interface.

5.1.2 Validation procedure

The final tooth flank geometry produced by the simulation algorithm is a result of the interaction between the tool and the work gear based on the process kinematics. Since the simulated flank profile is not modelled analytically according to the spherical involute function, the results must be compared to the theoretical geometry and validated. *Hermes BevelCurve3D* is a novel algorithm for the validation of the simulation results and specifically the convex and concave tooth flank surfaces as well as the root area surface. The inputs provided automatically to the validation algorithm, when a certain simulation case is selected for validation, are the simulated and the theoretical gear flank geometry, the last is derived by *Kisssoft*, a commercial and well-established gear design and calculation software. In this regard, it is important to clarify that *BevelCurve3D* does not produce or calculate the theoretical (target) gear geometry, but rather receives this geometry as input from *Kisssoft* as a solid model. After the theoretical model is extracted from the software, no modifications or alterations are applied to the geometry that is directly used to validate the simulated gear geometry. [55, 59]

The validation algorithm is executed in three stages. First, the user selects the specific simulation case to be validated and all necessary simulation data are loaded into the program. At this point, the user can alter the validation resolution and run the validation. The second stage involves the execution of the validation procedure by comparing the two geometries - theoretical and simulated - as to the form of the flank surfaces along the tooth width. For this reason, the algorithm automatically creates a series of concentric spheres, the centre of which lies on the apex of the pitch cone of the gear. Depending on the validation resolution, the algorithm creates the necessary number of intersection spheres to cover the entire facewidth of the tooth. When a sphere is created, the algorithm draws the intersection curve between the sphere and the gear geometry. Finally, all simulated curves are automatically discretized in points, the coordinates of which are exported as output from the program. This procedure is followed for both the simulated and the theoretical tooth flank geometry, except for the 3D point discretization which is applied only for the simulated geometry. [Figure 5.2](#) presents the validation process with the creation of the spherical intersection surfaces, the flank profile curves and finally, the 3D profile points for a simulated pinion. [Figure 5.3](#) shows the respective procedure followed for the theoretical geometry. Apart from the profile point coordinates, the deviation between the simulated and theoretical profile geometry is also calculated as the minimum distance of each simulated profile point from the theoretical profile curve. All the above-mentioned validation output data, that is the simulated and theoretical profile point coordinates and also the deviation values, are stored in separate text files in every validation step. The third and final stage of the validation procedure involves the presentation of all the results indicated above in useful graphs that allow the user to evaluate the results and examine whether the deviation between the theoretical and the simulated geometry is acceptable or not. The three figures shown automatically on the program form are the flank/root area curves of the simulated and theoretical curves, the simulated and theoretical surfaces and also the deviation on the surface along the face width. [55, 59]

Section 5.1.1 provided a brief introduction to the validation software interface. The following paragraphs present the validation procedure which results in the validation figures. The validation procedure is implemented in three steps which are executed automatically after the user starts running a specific validation case:

1. Firstly, the simulated solid geometry of the produced gear slot is discretized along the face width of the tooth but also along the profile of the tooth flanks. The discretization along the face width of the tooth is controlled by the user and can be altered in the main form of the program, presented in [Figure 5.1](#). The discretization of the profile curve is predefined in the algorithm. [Figure 5.2](#) shows an example of this geometric discretization. The top left part of the figure shows the complete solid geometry as it is extracted from the simulation algorithm *BevelSim3D*.

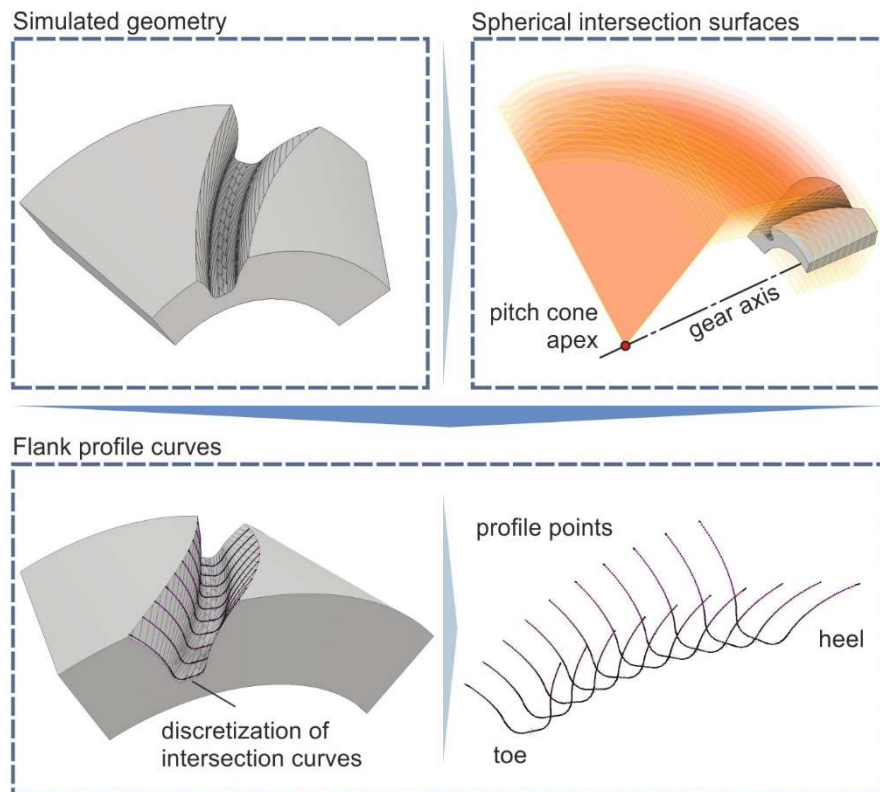


Figure 5.2: Calculation of the simulated flank profile curves and extraction of points in *BevelCurve3D*. [59]

The upper right part of the figure shows the multiple spheres used to create the profile curves. All intersection spheres are concentric, and their centre is located at the apex of the gear. The radius of the spheres depends on the mean cone distance R_m , the tooth width b and each sphere are smaller than the next one by an offset value which is implicitly defined by the user with the validation resolution. The bottom part shows the validation profile curves. After the profile curves are drawn, they are discretized into 3D points, whose XYZ coordinates are then exported to text files as output of the validation process.

2. The second step of the validation process deals with the discretization of the theoretical gear geometry and follows the same pattern described in the previous step. The slot geometry is discretized along the face width and validation profile curves are created at the same distance from the gear apex as the simulated ones so that the respective curves of the theoretical and the simulated geometry are comparable with each other. Figure 5.3 shows an example of this process where the simulated geometry corresponds to the theoretical presented in Figure 5.2.
3. In the final step of the validation process, the calculation of the theoretical and simulated geometries deviation is carried out. The deviation is calculated as the distance of each simulated profile curve point from the theoretical profile curve. These values are then exported to text files and plotted in deviation figures so they can be evaluated by the user.

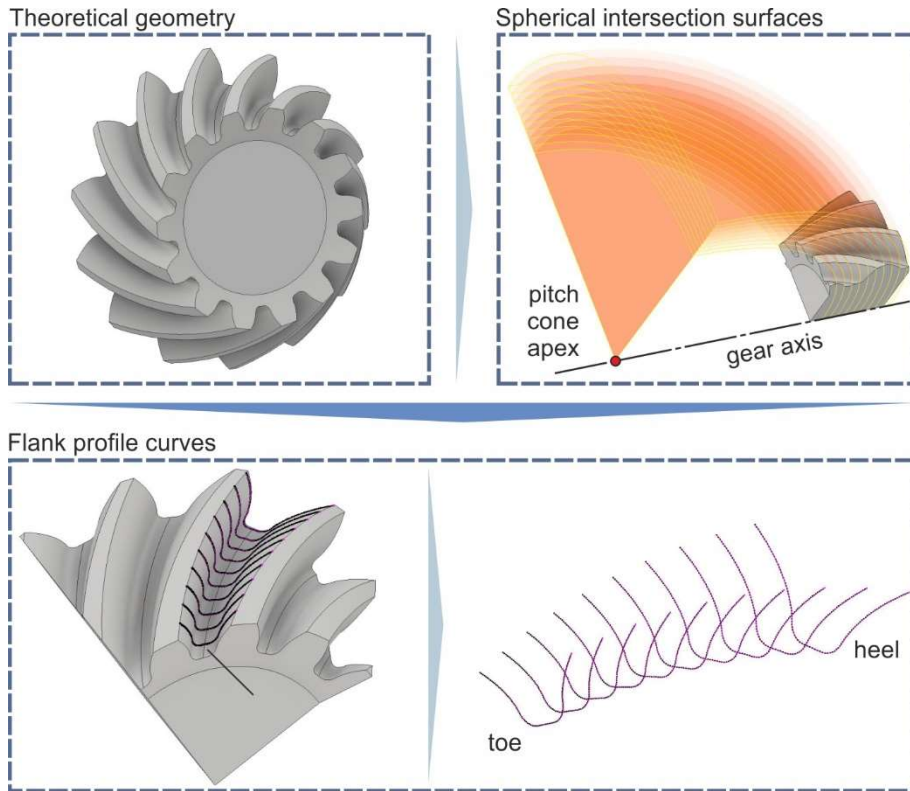


Figure 5.3: Calculation of the theoretical flank profile curves in *BevelCurve3D*.

Figure 5.4 shows an example of the validation graphs as they are presented for each validation case. The first figure on the top left of the form shows the consecutive profile curves for both simulated and theoretical geometries. The graph on the bottom left part of the form illustrates the simulated and theoretical tooth flanks. The top right figure shows the deviation of the simulated flank with respect to the theoretical one. The figure also includes a colour scale which relates the several colours on the flank with specific deviation values. Important process and geometric parameters of each validation case are also included in the form.

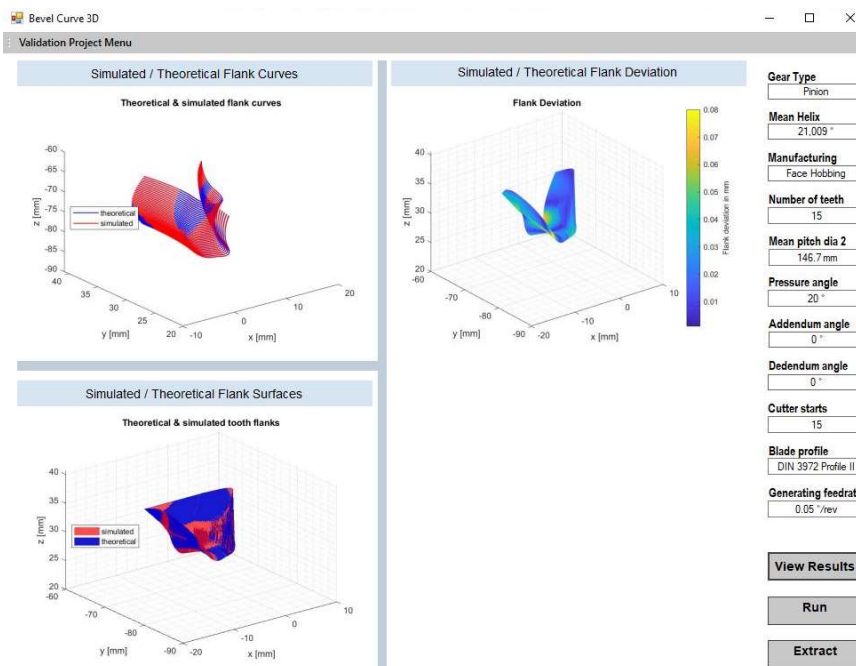


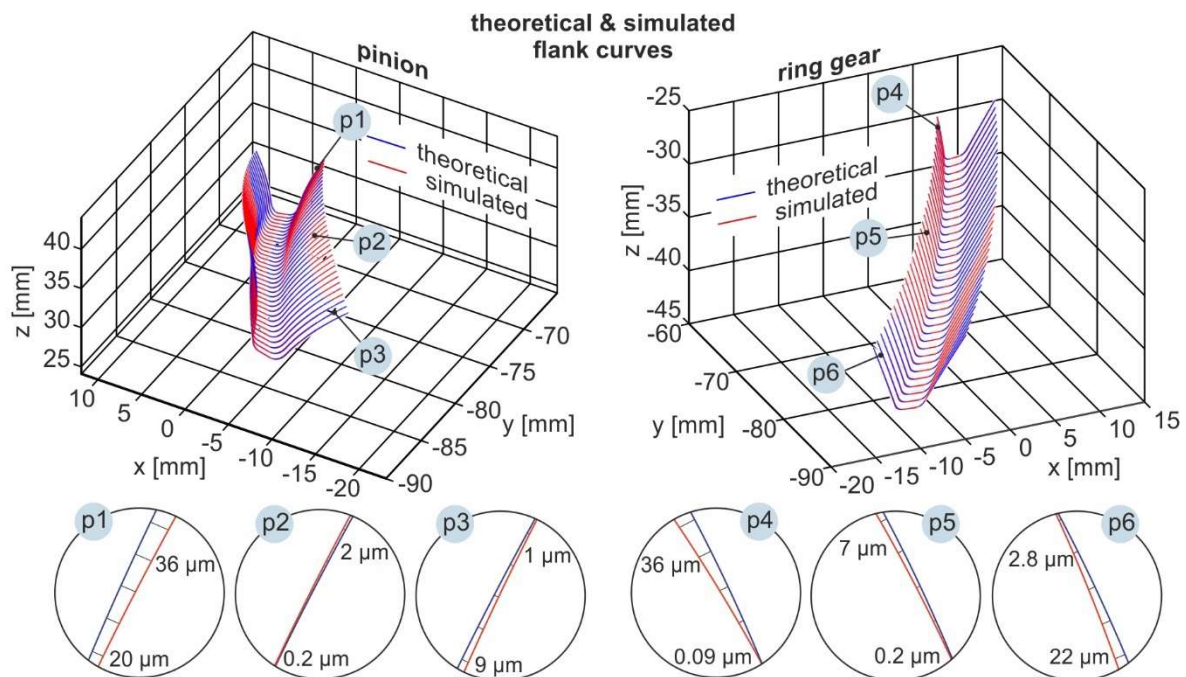
Figure 5.4: Validation graphs in *BevelCurve3D* interface.

5.2 Simulation Model Validation

The exact theoretical bevel gear profile geometry is based on the spherical involute function which is the equivalent of the involute function in cylindrical gears. Ithaca *BevelSim3D* algorithm simulates the kinematics of the actual gear machining process, therefore the resulting 3D geometry is expected to approximate the form of the octoid curve. Solid bevel gears modelled via a commercial gear calculation and design software were used as a medium for the validation. Following, two validation case studies for face milling and face hobbing are presented.

5.2.1 Face milling validation case study

Figure 5.5 presents the graphs of flank and root area curves of a face-milled pinion and ring gear. As can be seen, the simulated curves in red show very good agreement with the theoretical ones in blue. The deviation between the flanks, which will be analysed further in the following paragraph, is low and the two curves look almost identical. However, the validation algorithm not only exports an image of these graphs, but the source figure file, allowing the user to zoom in/out and rotate the graph to identify any areas of specific interest, for instance, the areas where the deviation is maximized. Another clarification concerning the curve figures is that the profile curves only appear in one of the two colours in certain areas, and this is because the two curves are very close to each other and hide one behind the other depending on the view angle selected for presentation. Some examples of deviation values are also indicated below the two figures and correspond to six characteristic positions in the two gear slots. [59]



gear type: pinion-ring, blade profile: DIN 3972 II, face milling, $r_{c0}=82$ mm, $z_1=18$, $z_2=41$, $d_{e2}=176.893$ mm, $\beta_m=35^\circ$, $b=25.4$ mm, $a_n=20^\circ$, $\theta_{a2}=2.6186^\circ$, $\theta_{t2}=2.6186^\circ$, $t_f=0.4$ mm, $f_p=0.5$ mm/rev, $f_{g1}=0.58^\circ/\text{rev}$, $f_{g2}=1.26^\circ/\text{rev}$

Figure 5.5: Simulated and theoretical profile curves for pinion (left) and ring gear (right). [59]

As indicated in the six circles, deviation at p1 position which is located at the toe area of the convex flank of the pinion has a minimum value of 20 μm and a maximum of 36 μm . Deviation decreases to minimum values near the middle of the convex flank, where it varies from 0.2 μm up to 2 μm , to increase again at p3 towards the heel of the tooth, where the values vary between 1 μm to 9 μm . Regarding the respective values on the ring gear, deviation on p4 position ranges between 0.09 μm and 36 μm , it then decreases dramatically near the middle

of the tooth to $0.2 \mu\text{m} - 7 \mu\text{m}$ and finally increases to reach higher values of $2.8 \mu\text{m} - 22 \mu\text{m}$ on p6, close to the heel of the tooth. It must be clarified that deviation curves on p1, p2, ..., p6 are only used for illustration/visualization purposes of the above-mentioned deviation values and do not represent the actual form and tilt of the flank curves. Simply put, deviation and tilt between the theoretical and simulated flank curves are magnified in p1, p2, ..., p6 so that all deviation values can be clearly visualized in the same figure. The actual deviation of the surfaces and the tilt of the profile curves is as shown in the two slot figures at the top of Figure 5.5. [59]

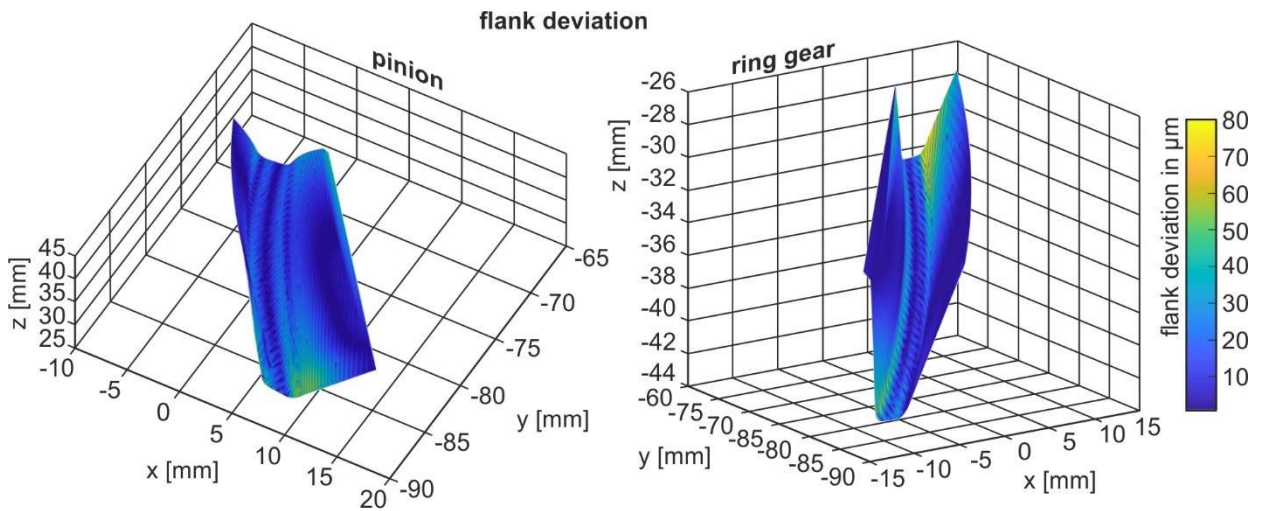
One of the most important outputs from the validation process is presented in [Figure 5.6](#). Upon completion of the validation process, the user has access to these surface deviation source figures from which crucial conclusions about the process can be drawn. Since all deviation values are stored in text files, they can be used for further, more analytical investigation. The results shown as an example for the presentation of the validation algorithm, correspond to the same face milled pinion and ring gear geometries presented throughout the paper. Regarding the actual numerical deviation figures, the main values and observations are outlined below. [Table 5.1](#) provides some characteristic surface deviation values measured in three key areas for both pinion and ring gear. These areas are 1. the heel, close to the outside diameter of the gear, 2. the toe, close to the inside diameter of the gear and 3. the area at the middle of the face-width of the tooth. Each of these areas is subdivided into three zones along the flank of the tooth: a. The concave side of the tooth, b. the root area of the gear slot and c. the convex side of the tooth. In reference to both pinion and ring gear geometries, it can be deduced that the deviation remains low on the concave and convex flanks of the tooth, while it rises in the area closer to the root. This difference in the deviation between the two flanks and the root area can be explained by the fact that the cutting action close to the root area is unstable because it is the cutting blade tip rather than the side cutting edge that mostly participates in the cutting action. [59]

SURFACE DEVIATION (μm)			
Pinion Gear	Convex Flank	Root Area	Concave Flank
Heel	1-9	30-55	2-25
Middle of face-width	0.02-2	15-28	3-7
Toe	20-36	29-66	8.5-20
Ring Gear	Convex Flank	Root Area	Concave Flank
Heel	2.8-22	40-68	3.7-34
Middle of face-width	0.2-7	2-27	0.05-9
Toe	0.09-36	25-73	20-30

Table 5.1: Minimum and maximum values of tooth surface deviation between theoretical and simulated geometries.

Regarding the tooth geometry along the face-width, it can be observed that the deviation values remain average closer to the heel and toe sides of the tooth, but drop to low levels in the middle of the tooth (middle of the face-width) and especially on the flanks. The flank surface is almost identical to the theoretical one at the middle of the face width, in the range of a few microns $<10 \mu\text{m}$, while the deviation for most of the flank surface remains less than $10-20 \mu\text{m}$ and gradually increases to reach slightly higher values of a few tenths of microns right on the edges of the heel and toe. [59] A common conclusion after the evaluation of the validation results for the two members of this gear pair is that the simulated geometry matches the theoretical one at a satisfactory level for the biggest part of the flank surface close to the middle

of the tooth, which is the area of great interest since it is the main contact area of the two gears when they are in mesh. The deviation exceeds the desired values for most of the gear slot root area, for the reasons explained above, but this area is not critical for the smooth function of the gear pair as it is always outside the contact area due to the clearances applied. [59]



gear type: pinion-ring, blade profile: DIN 3972 II, face milling, $r_{c0}=82\text{mm}$, $z_1=18$, $z_2=41$, $d_{e2}=176.893\text{mm}$, $\beta_m=35^\circ$, $b=25.4\text{mm}$, $a_n=20^\circ$, $\theta_{a2}=2.6186^\circ$, $\theta_{f2}=2.6186^\circ$, $t_f=0.4\text{mm}$, $f_p=0.5\text{mm/rev}$, $f_{g1}=0.58^\circ/\text{rev}$, $f_{g2}=1.26^\circ/\text{rev}$

Figure 5.6: Simulated surface deviation for face-milled pinion (left) and ring gear (right).

5.2.2 Face hobbing validation case study

The face hobbing simulation case presented in section 4.3 will be used to showcase the face hobbing validation algorithm. Both members of the face-hobbed simulated bevel gear set were validated with the *BevelCurve3D* application and the validation results are presented below. Figure 5.7 shows the graphs of the simulated and theoretical profile curves of the face-hobbed pinion (left) and ring gear (right). This validation example uses the same simulation case study presented above for the pinion, but the generation feedrate of the ring gear equals $0.025^\circ/\text{rev}$. All the simulation-related data remain the same and are included at the bottom of Figure 5.7. As it can be observed, the blue curves which correspond to the theoretical profile curves, and the red curves for the simulated profile curves, are almost identical to the point that, depending on the viewpoint, only one of the two curves is visible. The source figure files of the profile curve graphs are available to the user so they can study the curves in more detail. Below the two profile curve graphs, six profile positions, three for the concave and another three for the convex flank, are included. The p1, p2 and p3 circles show the numerical values of profile deviation on the convex flank of the ring gear starting from heel to toe. As can be seen, the deviation values range is quite low at the heel of the tooth (-2 to $7.5\ \mu\text{m}$), increases slightly at the middle of the face width (3.5 to $10\ \mu\text{m}$), and rises more towards the toe of the gear tooth (9 to $13.5\ \mu\text{m}$). Positions p4, p5 and p6 refer to the concave flank, heel to toe, where the deviation values start from (-5.5 to $6.5\ \mu\text{m}$) at the heel of the tooth, dropping drastically in the middle area of the tooth (0.01 to $3.5\ \mu\text{m}$) and increase closer to the toe area (-3.5 to $8\ \mu\text{m}$). A general conclusion that is indicative of all the simulation case studies carried out as part of the present research, is that the deviation on the flank surfaces of the pinion gear is always higher than the corresponding values on the ring gear, and this is explained by the fact that the curvature of the pinion tooth surface is significantly higher than the curvature of the ring gear. This makes the process kinematics and machine settings much more difficult to approach, therefore it is more challenging to reproduce the theoretical surface of the tooth. [55]

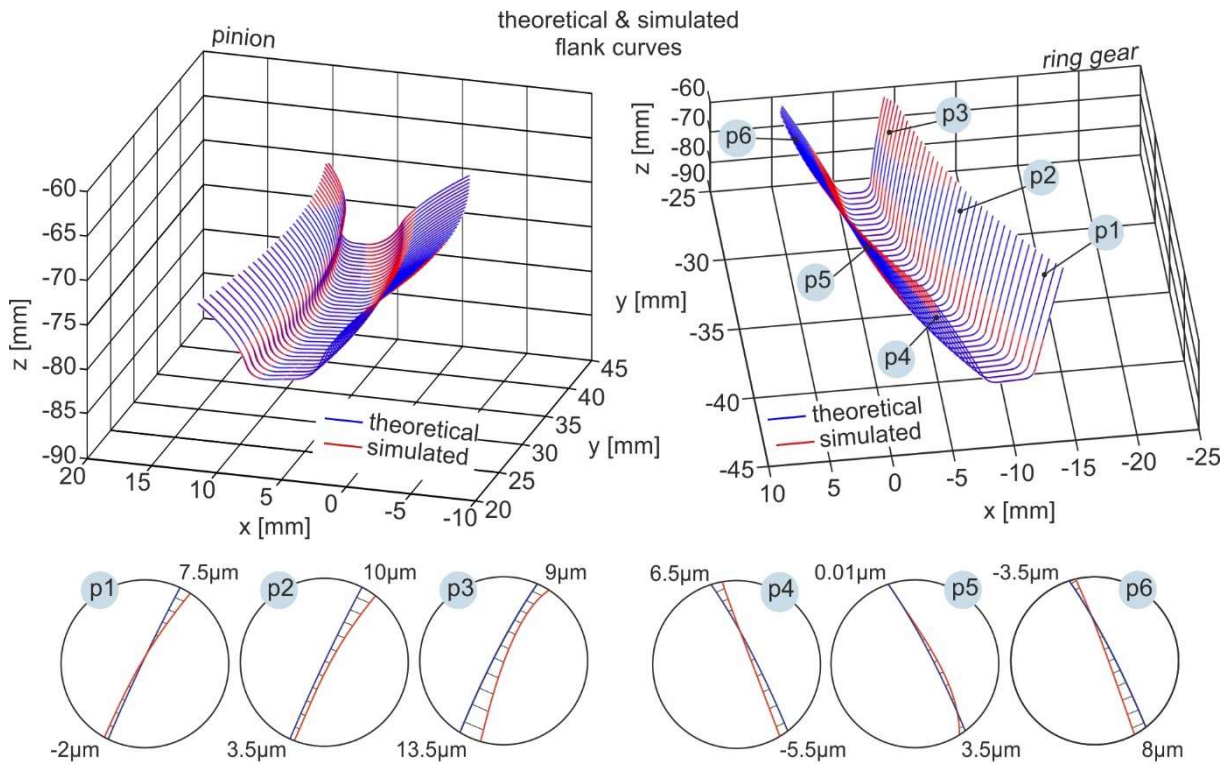


Figure 5.7: Simulated and theoretical profile curves for pinion (left) and ring gear (right). [55]

Another general and quite crucial conclusion concerning the validity of the face hobbing simulation results is the fact that for all executed simulation case studies, the deviation between the simulated and theoretical surface remains significantly low for most of the area not far from the middle of the tooth, while it is higher at the toe and heel areas of the tooth. The area close to the middle of the tooth is the area of interest in spiral bevel gears since most of the contact action, when two spiral bevel gears are in mesh, happens closer to the middle of the tooth.

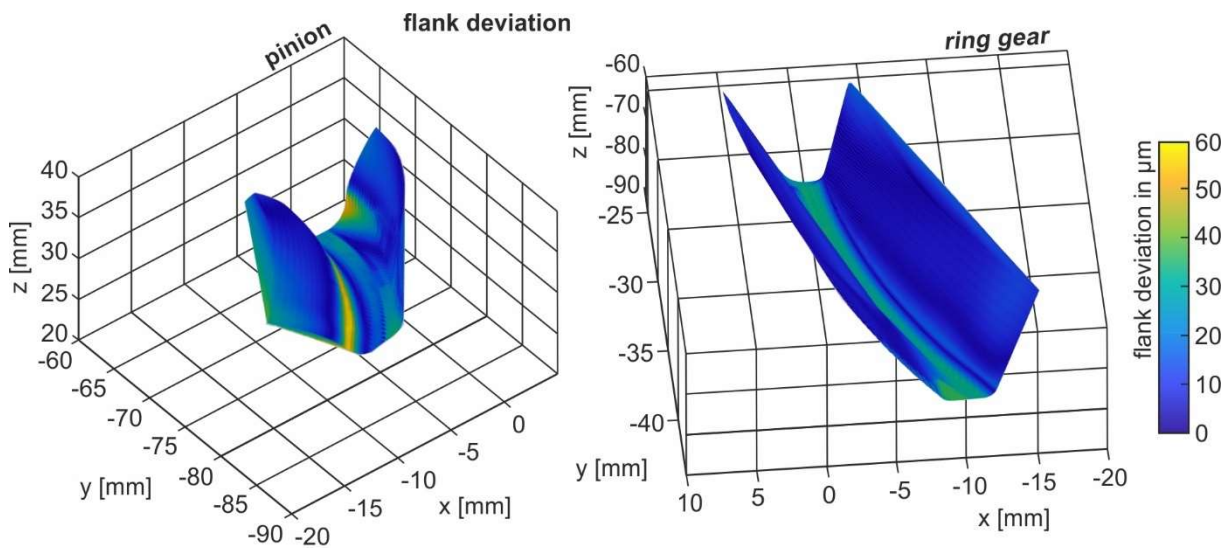


Figure 5.8: Simulated surface deviation for face-hobbed pinion (left) and ring gear (right). [55]

Valuable results of the validation process are also the surface deviation graphs such as the ones shown in Figure 5.8. As soon as the validation procedure is completed, the source surface deviation graphs are available for a more analytical investigation from which important conclusions can be drawn. The two deviation graphs presented in Figure 5.8 correspond to the same simulation case study presented in Figure 5.7. Concerning the deviation development along the flank of the tooth, deviation values remain relatively low on the tooth flanks, especially closer to the middle of the face-width but reach much higher values at the root area of the gear slot. This significant difference in the deviation between the tooth flank and tooth-root areas is justified by the fact that the cutting action close to the root area is quite unstable as it is the cutting blade tip rather than the side cutting edge that mostly participates in the cutting action. However, the root area of the gear slot is not a region of interest because in most cases a clearance between the tip and the root area of two meshing gears is applied. This way the root area is excluded from the contact path of the gears in mesh. It can be therefore concluded that the simulated tooth surface matches the theoretical geometry to a great extent for most of the flank surface. [55]

5.3 Tool trajectory validation

In a purely kinematical simulation like the one presented in the present thesis, where no physical or thermal phenomena are considered, the only factors influencing the result of the simulation are the geometry of the cutting tool and the kinematic chain of the process. As discussed above, the blank gear geometry is modelled automatically in the simulation algorithm with the implementation of accurate and established ISO 23509 equations. Likewise, the cutting blade profile is modelled according to DIN3972 standard geometry. Therefore, the only factor left that could affect the accuracy of the results is the process kinematics, which can be validated by confirming both the tool trajectory and the produced gear tooth surface. The accuracy of the produced trajectory was examined as part of the development of the model.

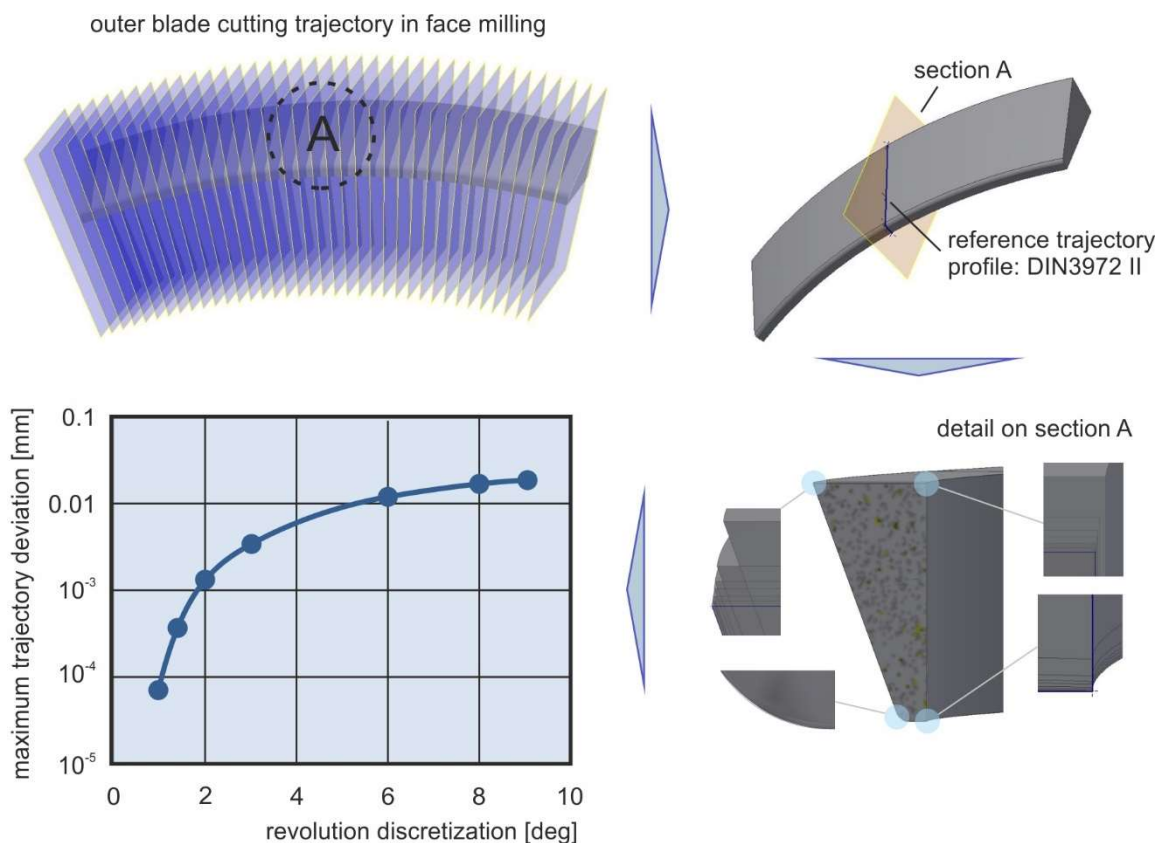


Figure 5.9: Tool trajectory deviation. [59]

Figure 5.9 shows an investigation of the tool trajectory deviation with respect to the DIN 3972 II reference geometry, as the discretization of the revolving positions changes. The investigation is carried out by examining the section of the different trajectories on a reference plane where the DIN 3972 profile II is modelled. As shown in Figure 5.9, the tool trajectory accuracy improves with the decrease of the discretisation revolving angle. Based on the figure, using a revolution angle of 1° produces an acceptable blade surface with $0.086 \mu\text{m}$ deviation with respect to the theoretical blade profile as defined in DIN 3972 II. In the present study, a discretisation of $1^\circ \sim 1.5^\circ$ is used for all simulation case studies. [59]

6. CUTTING FORCES CALCULATION

The goal of the present study is the calculation of surface topography and cutting forces, both in face milling and face hobbing operations. Cutting forces calculation can significantly contribute to the reduction of tool wear and the increase in productivity. Excessive tool wear caused by the developed cutting forces may lead to unplanned production stoppages for cutting tool replacements, increasing the manufacturing cost by a considerable amount. Additionally, there are several issues that must be considered and make cutting forces particularly important, such as deflection of the work gear and the residual stresses on the workpiece after the process has been completed, as well as the type of fixture and clamping force that has to be applied on the work gear prior to machining. [55] The following sections provide a brief introduction to the theoretical aspect of cutting forces as well as a presentation of the cutting forces calculation algorithm integrated in the *BevelForce3D* application.

6.1 Forces in machining operations

The most common metal removal processes involve complex kinematics and geometric characteristics. However, in metal cutting literature, the simple model of two-dimensional orthogonal cutting is used to describe the general characteristics and mechanics of metal cutting. Orthogonal cutting resembles a planing process in which a cutting tool performs a linear movement relative to a workpiece with the cutting edge being perpendicular to this movement. Regarding the cutting forces in this case, two components are examined, namely the tangential (F_t) and feed (F_f) force. The machined chip which is sheared off from the workpiece has a width b and a height h . Oblique cutting on the other hand, is a three-dimensional process the mechanics of which are used to describe the mechanics of complex three-dimensional cutting processes such as turning, drilling, and milling, through geometric and kinematic transformations applied to orthogonal cutting. Cutting forces in the case of oblique cutting can be calculated by transforming and adjusting the respective orthogonal cutting parameters. In oblique cutting, the edge of the cutting tool is inclined relative to the cutting motion. This causes a third force component (F_r) to act on the tool in the radial direction. [62, 63]

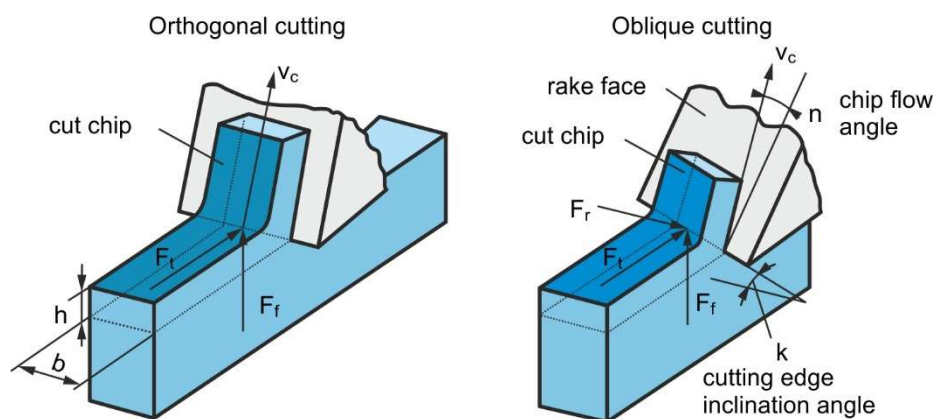


Figure 6.1: Cutting force components in orthogonal and oblique cutting. [62]

Figure 6.1 shows the orthogonal vs. oblique cutting geometry and kinematics, as well as the force components acting on the tool in both cases.

In the present study, Kienzle-Victor [64] exponential model for cutting force analysis is used. The Kienzle-Victor model is commonly used in cutting forces calculation and is based on a purely empirical method. The Kienzle-Victor model is based on the following assumptions [65]:

- The cutting speed v_c has no significant influence on cutting force (when selected so there is no built-up edge).
- The increase in depth of cut leads to an increase in cutting forces.
- The relation between feed rate and cutting force is exponential. Higher feed rate results in a much higher cutting force.
- The influence of the workpiece material is expressed by the specific cutting force K . This is equivalent to the cutting force that would be measured if this material were machined with 1 mm depth of cut and 1 mm/rev feed rate.

Figure 6.2 shows the cutting force analysis which considers all the relative force and velocity components in the three-dimensional metal cutting.

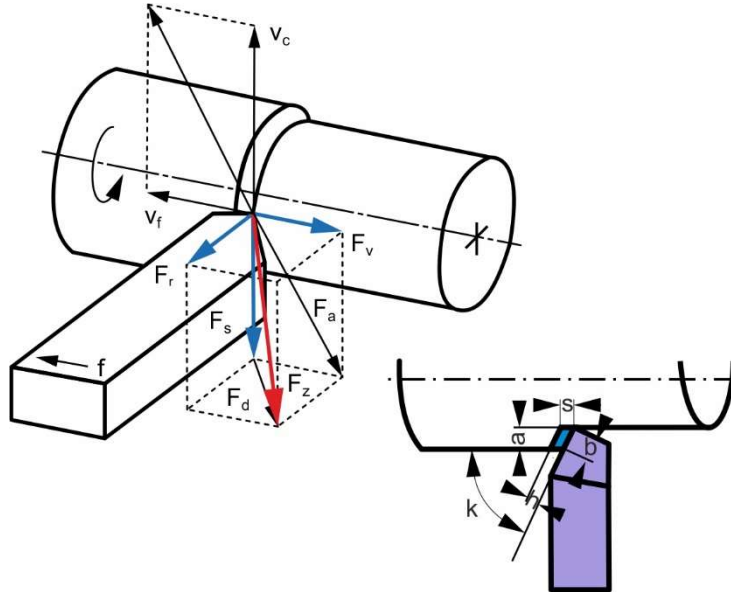


Figure 6.2: Cutting force analysis. [55]

The main force components F_s , F_r , F_v are calculated based on the following equations, 6.1 to 6.3.

$$F_s = b_{eq} \cdot K_s \cdot h_{eq}^{1-s} \quad (6.1)$$

$$F_r = b_{eq} \cdot K_r \cdot h_{eq}^{1-r} \quad (6.2)$$

$$F_v = b_{eq} \cdot K_v \cdot h_{eq}^{1-v} \quad (6.3)$$

where:

F_s	tangential cutting force	(N)
F_r	passive (or radial) force	(N)
F_v	feed force	(N)
F_a	active force	(N)
F_d	thrust force	(N)
F_z	resultant force	(N)
v_c	cutting speed	(m/min)
v_f	feed rate	(mm/min)
b_{eq}	equivalent chip width	(mm)

h_{eq}	equivalent chip thickness	(mm)
K_s, K_r, K_v	material specific cutting force	(N/mm ²)
s, r, v	material specific constant value	(-)

6.2 Cutting forces calculation algorithm

BevelForce3D is an algorithm developed to enable the accurate calculation of forces in spiral bevel gear cutting with face milling and face hobbing processes. The undeformed chip geometries generated by *BevelSim3D* are the main input data for the cutting force analysis performed by *BevelForce3D* algorithm. As shown in [Figure 6.3](#), *BevelForce3D* receives the undeformed chip geometry at each plunging/generating simulation step and analyses this geometry by sectioning the chip in each revolving position. For this purpose, cutting planes in all revolving positions are created. This iterative process discretizes the chip geometry in elementary chip entities which are then used for the calculation of the elementary force components. To achieve this, the chip is sectioned at the corresponding revolving position using a plane perpendicular to the cutting direction, and then segmented into 2D sections (elementary chips) which are automatically drawn on the current cutting plane. Depending on the chip geometry, each chip segment can be either a normal trapezium (chip zone a) or a curved trapezoid (chip zone c). [55]

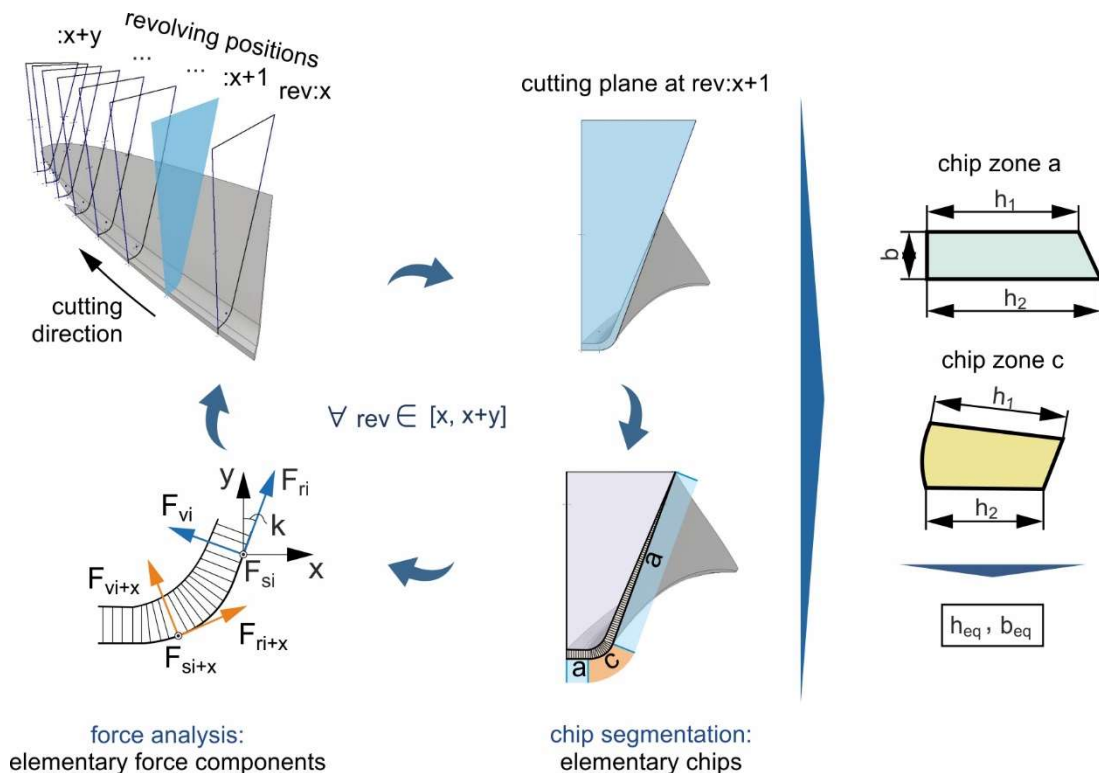


Figure 6.3: Calculation of the cutting force components on each cutting plane, for every generation position. [55]

Chip segmentation and geometry analysis

[Equation 6.4](#) provides the formulas employed to analyze the chip geometry in zone a and calculate the respective equivalent values of chip thickness and width so that they can be used in the calculation of forces. [55]

$$h_{eq} = \frac{h_1 + h_2}{2}, \quad b_{eq} = b \quad (6.4)$$

where:

- h_1, h_2 the chip thickness on the two sides of the elementary chip (mm)
 b the width of the elementary segment of the chip (mm)

Equations 6.5-6.10 provide the respective formulas for the chip thickness and width calculation, in the case of a curved trapezoid chip segment in zone c. [66]

$$h_{av1} = \frac{h_1 + h_2}{2} \quad (6.5)$$

$$b_{av1} = \frac{(b_1 + b_2) \cdot \cos \frac{\varphi}{2}}{2} \quad (6.6)$$

$$h_{av2} = 0.1 \cdot m_{mn} \cdot (1 - \cos(\frac{\varphi}{2})) \quad (6.7)$$

$$b_{av2} = \frac{(0.2 \cdot m_{mn})^2 \cdot (\frac{\varphi}{2} - (\cos \frac{\varphi}{2} \cdot \sin \frac{\varphi}{2}))}{2} \quad (6.8)$$

$$h_{eq} = \frac{(b_{av1} \cdot h_{av1}^2) + (b_{av2} \cdot h_{av2}^2)}{(b_{av1} \cdot h_{av1}) + (b_{av2} \cdot h_{av2})} \quad (6.9)$$

$$b_{eq} = \frac{(b_{av1}^2 \cdot h_{av1}) + (b_{av2}^2 \cdot h_{av2})}{(b_{av1} \cdot h_{av1}) + (b_{av2} \cdot h_{av2})} \quad (6.10)$$

where:

- h_{av1}, h_{av2} chip thickness on the upper and lower part of the elementary segment (mm)
 b_{av1}, b_{av2} chip width on the upper and lower part of the elementary segment (mm)
 φ angle included between the two sides of the elementary segment ($^{\circ}$)

Cutting forces calculation

The force components F_s, F_r, F_v are then calculated according to equations 6.1-6.3 and this procedure is followed iteratively on each elementary chip, in each revolving position for all the generation positions. After the force components are calculated, they are analyzed and transformed in the x, y, and z directions relative to the local XYZ-CSYS of each cutting plane, as presented in [Figure 6.4](#). This transformation leads to the calculation of the $F_{x,loc}, F_{y,loc}, F_{z,loc}$ force components, relative to the local XYZ-CSYS. The $F_{x,loc}, F_{y,loc}, F_{z,loc}$ components are calculated as follows:

$$F_{x,loc} = [\cos(k) \cdot F_v] - [\sin(k) \cdot F_r] \quad (6.11)$$

$$F_{y,loc} = [\sin(k) \cdot F_v] + [\sin(k) \cdot F_r] \quad (6.12)$$

$$F_{z,loc} = F_s \quad (6.13)$$

where:

- k the angle between the cutting edge on the specific elementary chip and the y-axis (or the tool axis) (°)

The local force components ($\Sigma F_{x,loc}$, $\Sigma F_{y,loc}$, $\Sigma F_{z,loc}$ in Figure 6.4) on the tip of each cutting blade correspond to the force values measured during the cutting process, provided that the dynamometer is mounted on the cutting tool and follows all the revolutions performed by the cutting blades. These local force components are then transformed according to the global coordinate system which lies on the pitch cone apex of the work gear. The x-, y-, and z- forces of all generation positions for both inner and outer blades are summed in three total $\Sigma F_{x,glob}$, $\Sigma F_{y,glob}$, and $\Sigma F_{z,glob}$ components according to the global coordinate system. [55]

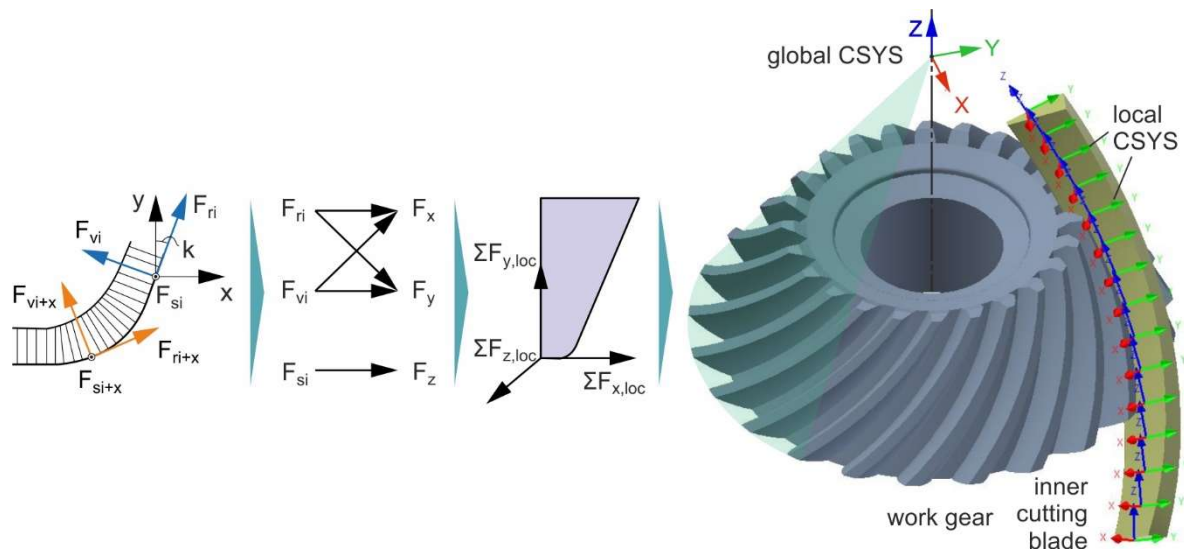


Figure 6.4: Transformation of cutting force components to XYZ CSYS of each cutting plane. [55]

The correct calculation of cutting forces was verified by comparing the automatically measured h_{eq} , b_{eq} , k , F_s , F_r , F_v , $F_{x,loc}$, $F_{y,loc}$, $F_{z,loc}$ values with the ones measured manually, utilizing the user interface tools of the 3D modelling software. All automatically calculated values were found to match the manually measured widths, thicknesses, and angles as well as the manually calculated force component values. This verification procedure was carried out for several elementary chips in various simulations. Also, as presented in Chapter 5, the simulated surface agrees with the theoretical one, showing that the process kinematics are simulated correctly. Therefore, the tool trajectory is accurate to a satisfactory level, so the cutting chip geometry and the calculated force components should close-approximate the respective forces of the actual machining process. [55]

6.3 Ithaca BevelForce3D - Cutting forces calculation software

The *BevelForce3D* application can be launched by the user through the *Bevel Gear Suite* interface after the kinematic simulation results are obtained from the *BevelSim3D* algorithm.

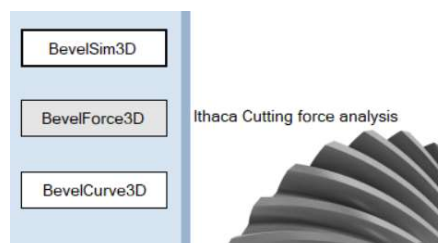


Figure 6.5: Initiation of the Bevel Force 3D application.

The cutting forces calculation can be applied to all completed cutting simulation cases. [Figure 6.5](#) shows the control that is used to launch the application. When the application is initiated, the user can choose to either start a new calculation or present the results of an already completed one. [Figure 6.6](#) shows the main window of *BevelForce3D* which provides access to both procedures. If forces calculation is selected, the respective window shown in [Figure 6.7](#) appears and the user can then select among all available simulation cases to run the forces calculation algorithm.

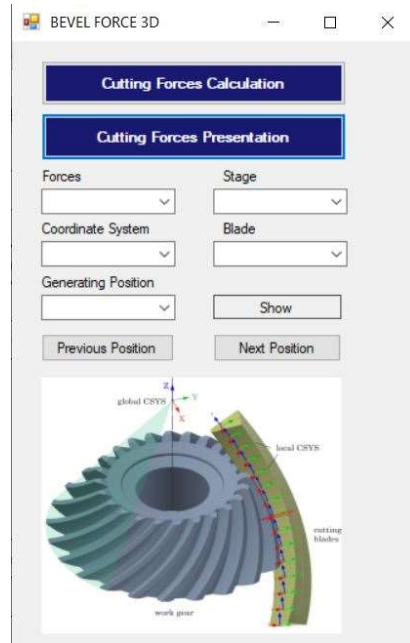


Figure 6.6: *BevelForce3D*.

After the selection of the specific simulation case, all the controls on the window are filled with the calculation-specific data such as the workpiece material properties and the desired calculation resolution. All data is provided via a text data file created as a result of the previous cutting simulation and is stored in the respective simulation output folder. The simulation-related data can also be altered by the user before the force calculation procedure starts.

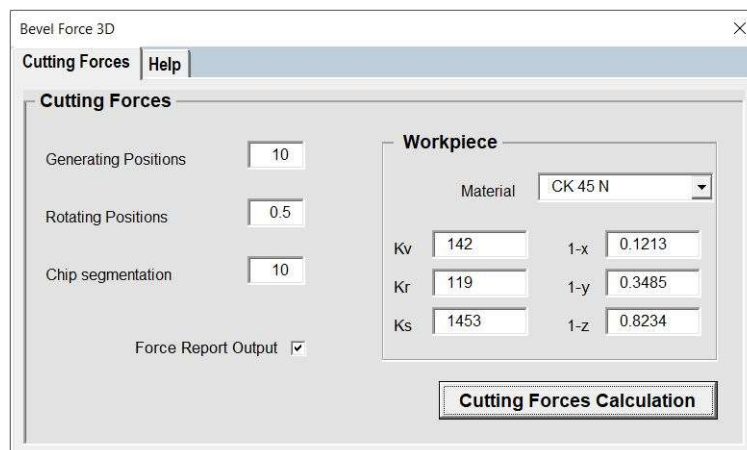


Figure 6.7: Main window of *BevelForce3D* application for the calculation of the cutting forces.

The calculation of cutting forces is then initiated and all output results are stored in the same simulation case folder. Such output results include:

1. The force solid files created for each generation position for both inner and outer blades. Each force file is created based on the 3D undeformed chip output files from the kinematic simulation, which is analysed so that all essential data for the calculation of cutting forces is obtained. Figure 6.8 shows an example of how the chip is analysed.

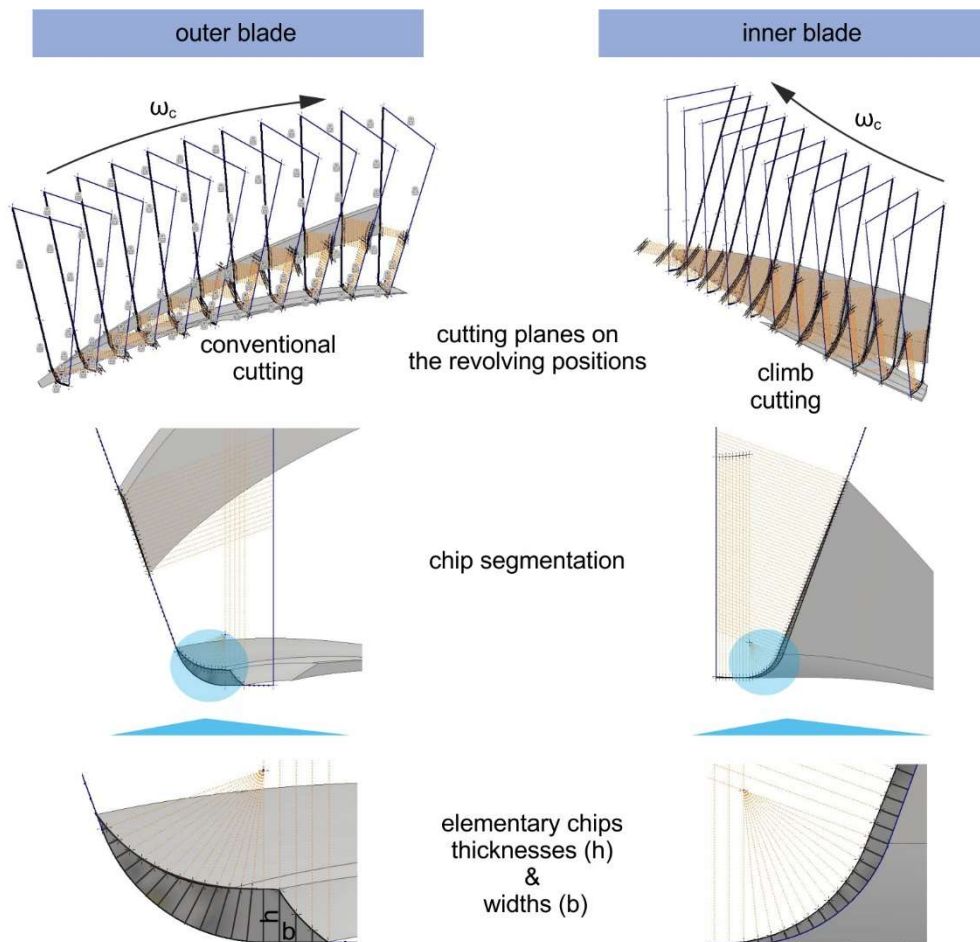


Figure 6.8: Inner and outer blade 3D chip analysis sample.

As described above, several sections matching the revolving positions are created on the chip. Each section is then discretized in elementary chips so that a more accurate calculation of the cutting forces can be achieved. Cutting forces are calculated for each elementary chip by analysing the geometry by means of the equations 6.4-6.10. To this end, all thickness and width values are obtained, and cutting forces are then calculated via equations 6.1-6.3 which are subsequently transformed to F_x , F_y and F_z components relative to the local XYZ coordinate system according to equations 6.11-6.13.

2. The force text files include all widths, thicknesses, cutting edge angles and elementary force components on the cutting plane on each revolving position of every generation position. Table 6.1 contains all data included in a sample text force file. For presentation reasons, only sample data lines of a certain text file are included in the table. There are three discrete areas that can be distinguished on the table. The first area includes the elementary chips on the inclined cutting edge of the blade, the second area refers to the circular arc of the cutting edge and the third area includes the linear edge on the tip of the blade. **Chip widths:** The first three columns include the widths of the elementary chips. As can be seen on both linear areas all widths are equal so the discretization of the chip into elementary parts is achieved in a more

uniform way. Elementary chip widths on the second area vary due to the circular shape of the cutting edge. **Chip thicknesses:** On the contrary, thickness values may vary along the cutting edge as a result of the non-uniform shape of the chip. **Cutting forces:** Cutting forces F_v , F_r , F_s are calculated for each elementary chip and also exported to the force text file. **Cutting edge angles:** The varying cutting edge angle plays an important role in the final calculation of F_x , F_y , F_z components, so these values are also included in the exported results. As can be easily observed, the k angle values are constant along the linear cutting edges (20° on the inclined and 90° on the horizontal) but range between these two values on the circular area. **XYZ force components:** Finally, the force components F_x , F_y , F_z are calculated and exported to the force file.

chip widths			chip depths			cutting forces			edge angle	XYZ force components		
b_1	b_2	b_{eq}	h_1	h_2	h_{eq}	F_v	F_r	F_s	k	F_x	F_y	F_z
[mm]	[mm]	[mm]	[mm]	[mm]	[mm]	[N]	[N]	[N]	$^\circ$	[N]	[N]	[N]
0,082	0,082	0,082	0,093	0,092	0,092	9,213	4,967	19,644	90,0	4,967	9,213	-19,644
0,082	0,082	0,082	0,092	0,091	0,091	9,183	4,941	19,497	90,0	4,941	9,183	-19,497
0,082	0,082	0,082	0,091	0,090	0,091	9,152	4,914	19,351	90,0	4,914	9,152	-19,351
0,082	0,082	0,082	0,090	0,089	0,090	9,121	4,887	19,203	90,0	4,887	9,121	-19,203
0,082	0,082	0,082	0,089	0,088	0,089	9,090	4,860	19,056	90,0	4,860	9,090	-19,056
0,082	0,082	0,082	0,088	0,087	0,088	9,059	4,833	18,908	90,0	4,833	9,059	-18,908
0,082	0,073	0,077	0,093	0,090	0,091	8,683	4,671	18,434	87,1	4,224	8,909	-18,434
0,082	0,073	0,078	0,090	0,085	0,087	8,581	4,572	17,866	81,2	3,213	9,176	-17,866
0,082	0,074	0,078	0,085	0,079	0,082	8,418	4,419	17,015	75,4	2,157	9,259	-17,015
0,082	0,075	0,078	0,079	0,072	0,075	8,218	4,237	16,020	69,6	1,104	9,180	-16,020
0,082	0,075	0,079	0,072	0,064	0,068	7,977	4,022	14,873	63,7	0,079	8,933	-14,873
0,082	0,076	0,079	0,064	0,055	0,060	7,684	3,770	13,568	57,9	-0,887	8,513	-13,568
0,082	0,077	0,080	0,055	0,047	0,051	7,328	3,476	12,093	52,1	-1,761	7,917	-12,093
0,082	0,078	0,080	0,047	0,037	0,042	6,889	3,131	10,434	46,2	-2,503	7,142	-10,434
0,082	0,079	0,081	0,037	0,027	0,032	6,338	2,721	8,567	40,4	-3,061	6,181	-8,567
0,082	0,080	0,081	0,027	0,017	0,022	5,612	2,222	6,448	34,6	-3,359	5,014	-6,448
0,082	0,082	0,082	0,083	0,082	0,082	8,851	4,653	17,938	20,0	-6,726	7,399	-17,938
0,082	0,082	0,082	0,082	0,081	0,081	8,819	4,625	17,790	20,0	-6,705	7,362	-17,790
0,082	0,082	0,082	0,081	0,080	0,080	8,786	4,597	17,640	20,0	-6,684	7,325	-17,640
0,082	0,082	0,082	0,080	0,079	0,079	8,753	4,569	17,491	20,0	-6,662	7,287	-17,491
0,082	0,082	0,082	0,079	0,078	0,079	8,720	4,541	17,341	20,0	-6,641	7,249	-17,341
0,082	0,082	0,082	0,078	0,077	0,078	8,686	4,512	17,190	20,0	-6,619	7,211	-17,190
0,082	0,082	0,082	0,077	0,076	0,077	8,653	4,484	17,039	20,0	-6,597	7,173	-17,039
0,082	0,082	0,082	0,076	0,075	0,076	8,619	4,455	16,888	20,0	-6,575	7,134	-16,888
0,082	0,082	0,082	0,075	0,075	0,075	8,584	4,426	16,737	20,0	-6,553	7,095	-16,737
0,082	0,082	0,082	0,075	0,074	0,074	8,550	4,397	16,585	20,0	-6,530	7,056	-16,585
0,082	0,082	0,082	0,074	0,073	0,073	8,515	4,368	16,432	20,0	-6,508	7,017	-16,432
0,082	0,082	0,082	0,073	0,072	0,072	8,480	4,339	16,279	20,0	-6,485	6,977	-16,279

Table 6.1: Forces calculation text output sample file.

- The summarizing global force text files contain the sum global forces for every generation position. The XYZ force components are transformed into the global coordinate system and the summarized global forces are calculated and stored in separate text files.

6.4 Cutting Forces presentation

6.4.1 Introduction

Following the calculation of cutting forces, the user can proceed to the presentation and assessment of the results using the *BevelForce3D* platform. [Figure 6.9](#) illustrates the main window of the platform as the user loads the calculation data.

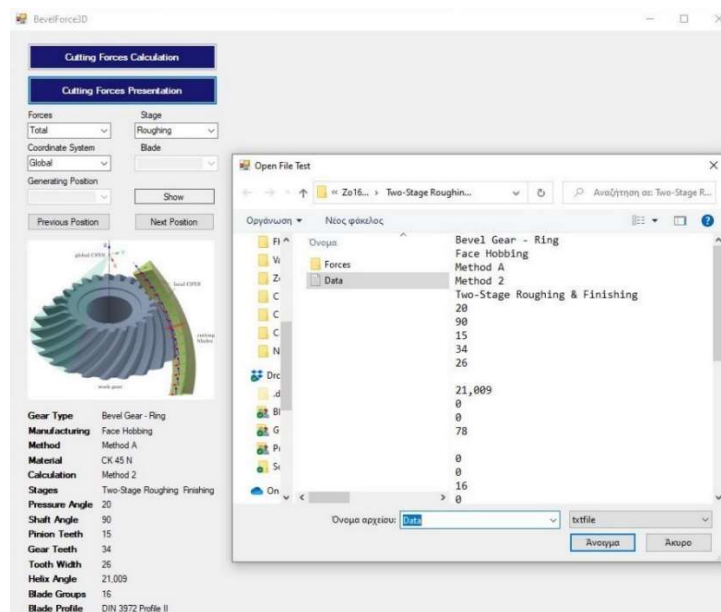


Figure 6.9: Cutting forces presentation and data input GUI.

All calculated force components and sums can be presented on the platform in the form of cutting force graphs. More specifically, the sets of forces presented are the following:

- Discretized Forces:** The summarized forces of all cutting planes on each generation position.
- Total Forces:** The total forces acting on the cutter by both inner and outer blades on all generation positions.
- Local Forces:** Discretized forces can be presented with respect to the local coordinate systems of the revolving positions of each generation position.

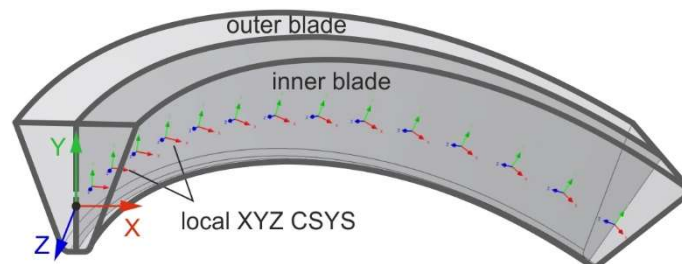


Figure 6.10: Local XYZ CSYS for both inner and outer blades.

- **Global Forces:** Both discretized and total forces can be presented relative to the global coordinate system of the work gear (pinion or ring). The position of the global CSYS, as illustrated in [Figure 6.11](#), matches the pitch cone apex of the work gear.

Figure 6.11 shows the local coordinate systems on the inner and outer blades. As shown in the figure, Y-axis of the CSYS is set on the axis of the blade profile, while Z-axis is perpendicular to the plane facing opposite the cutting direction, thus facing towards the cutting blade. This setup of the CSYS is common for both blades and is repeated on every cutting (revolving) plane of each generation position. Therefore, when F_x force component is calculated with respect to the local CSYS of the inner blade, the force has a negative sign, in contrast to the outer blade where the calculated F_x force is calculated with the actual positive value. The respective F_z force component of the outer blade is calculated with the opposite negative value based on the local coordinate system of the blade tip.

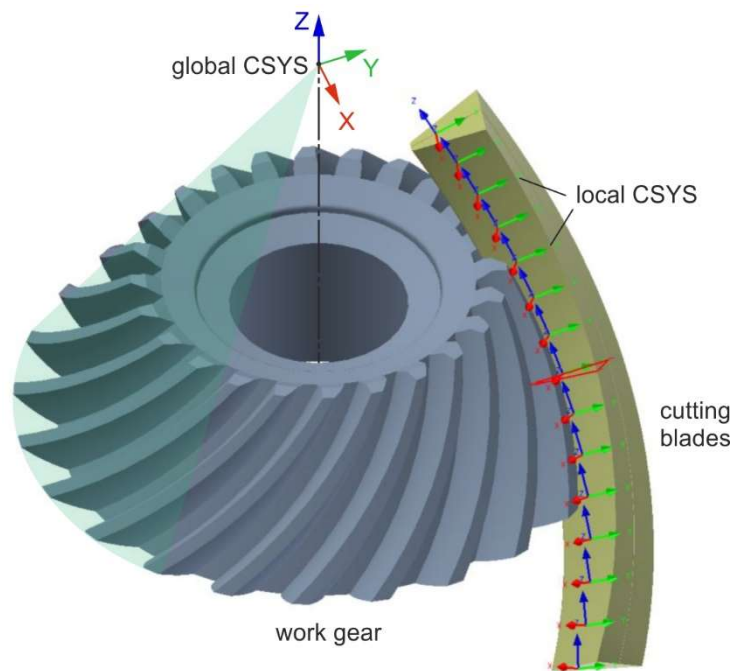


Figure 6.11: Local and Global Coordinate Systems.

6.4.2 Cutting forces graphs

Since all forces-related data are loaded to the platform and the user has selected the discretized or summarized forces, the desired coordinate system as described above, and the generation position in case of discretized forces, the following graphs appear, and the results can be qualitatively and quantitatively assessed.

Discretized forces on the local XYZ CSYS as a means to predict tool wear

Discretized forces can be displayed for every single generation position, these are the values of F_x , F_y , and F_z components on each cutting plane (revolving position). In the case of the local forces, the cutting force is analysed in three components relative to the local CSYS of each cutting plane and these values are then displayed in a graph that represents the specific generation position and includes all revolving positions of it. The local discretized forces are essentially the cutting forces developed at the tool tip. Unlike global total forces, local forces are measured on the local coordinate systems of both inner and outer blade tips that follow the exact motion of the cutter. The local cutting forces can greatly contribute to the prediction of tool wear. [Figure 6.12](#) shows some sample graphs of the local forces developed for a given pass of the tool in a plunging (forming) ring gear simulation case. The plunge feedrate is set

to $f_p=0.1$ mm/rev. The three graphs on the left of the figure refer to local discretised cutting forces developed as a result of the material removed by the outer blades of the cutter while the graphs on the right of the figure present the forces on the inner blade. The phase difference between the inner and outer blade cutting is visible in the graphs, with the inner blade curve shifted towards the right side on the x-axis. It must be mentioned that F_z local forces are negative on the outer blade and positive on the inner blade, which is explained by the opposite direction of Z-axis on the local coordinate system of each blade.

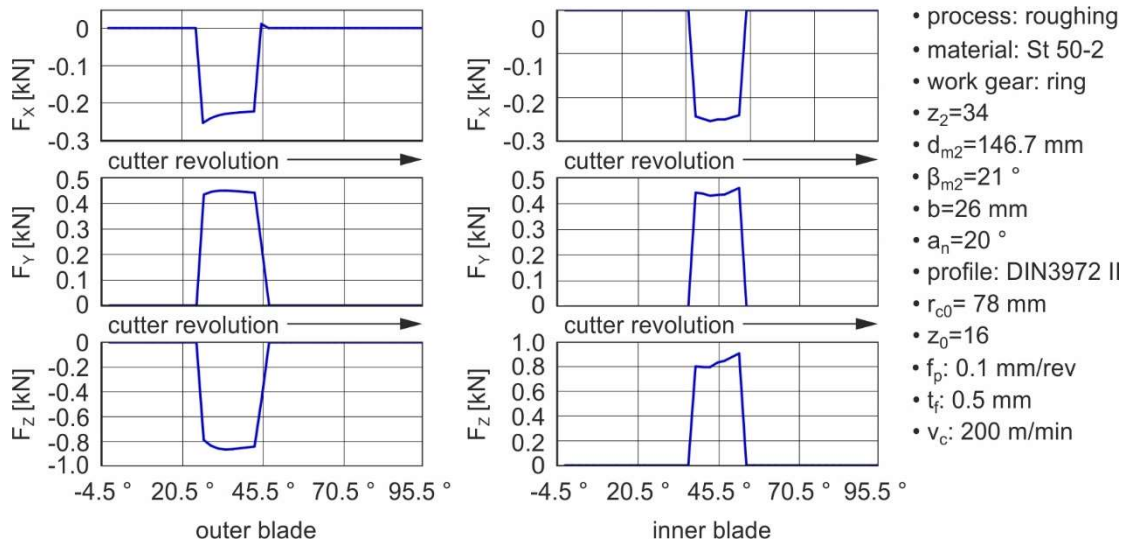


Figure 6.12: Discretized forces on inner and outer blades relative to the local blade coordinate system. [55]

Total forces on the global XYZ CSYS

Local discretized forces are transformed into the global coordinate system of the work gear and they are subsequently summed for all generation positions. A sample graph for the same plunging simulation case presented in Figure 6.12 is displayed in Figure 6.13.

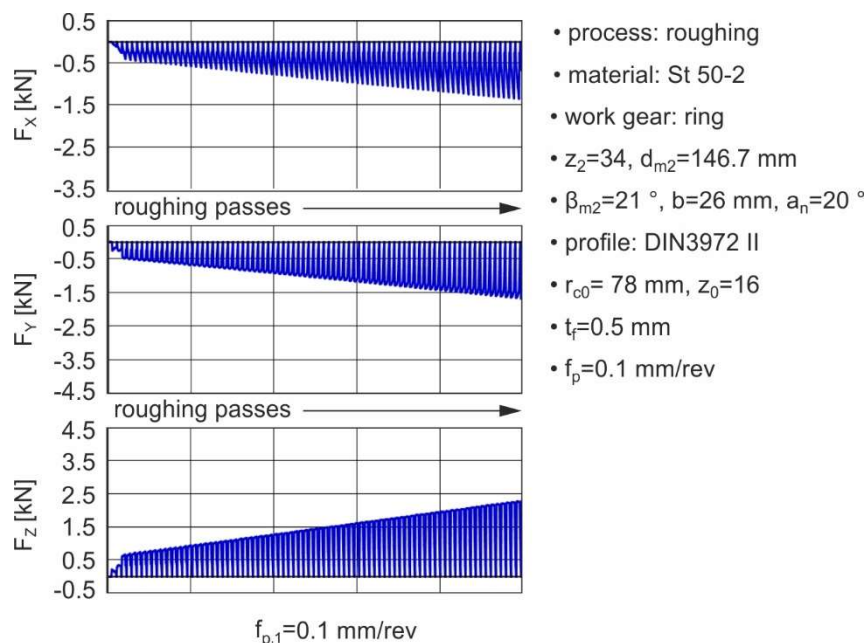


Figure 6.13: Total forces from inner and outer blades for all generation positions relative to the global gear coordinate system. [55]

All the results presented in section 7.3, which deal with the total global forces that act on a fixed point of the work gear, provide a valuable tool for the prediction of the deformation of the work gear due to the residual stresses introduced into the workpiece, as well as the type of fixture and the clamping force which must be applied to the work gear prior to machining.

7. SIMULATION RESULTS ANALYSIS AND PROCESS PARAMETERS INVESTIGATION

7.1 Chip thickness and cross-sectional area analysis

Calculation of the undeformed solid chips enables the detailed analysis of the chip geometry that provides further insight into the spiral bevel gear cutting process. Useful conclusions can be drawn, by analysing the produced chip geometries, with an examination of the chip area and thickness evolution along several generation positions. [59]

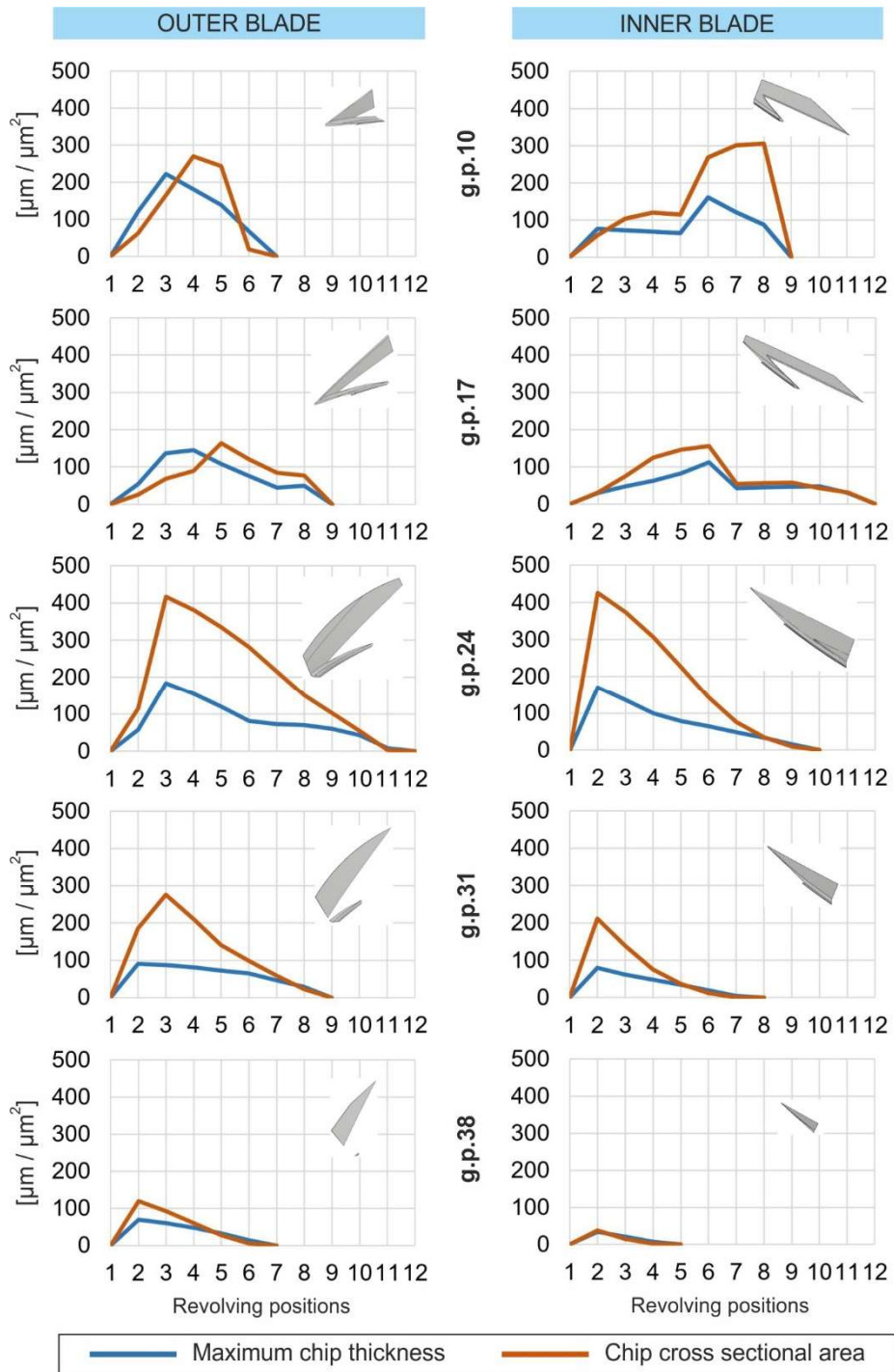


Figure 7.1: Maximum chip thickness and cross-sectional area analysis. [59]

Maximum chip thickness and chip cross-sectional area values, measured on the cutting planes perpendicular to cutting speed for the consecutive revolving positions, can provide a good

indication of the developed cutting forces. [Figure 7.1](#) shows an example with some sample calculations based on the case of a pinion gear face milling operation. The graphs shown in the figure reveal the evolution of both maximum chip thickness and cross-sectional area in five sample generation positions which correspond to the first five pinion chip geometries (g.p.10 → g.p.38) presented in [Figure 4.21](#). [59] As it can be observed, the development of the cross-section area follows the evolution of maximum chip thickness along the several revolving positions in all generation positions. Starting from g.p.10 which is closer to the initial generation positions when the tool enters the slot from the heel to start the generating motion, the maximum chip thickness values are on the tooth flank for the inner blade which generates the convex flank and on the root area for the outer blade which generates the concave flank of the tooth. Normally, this difference between the two blades is to be expected since the inner blade starts the generating cut from the flank while the outer blade starts the generation closer to the root area of the slot. For both blades, the maximum chip thickness increases towards the last revolving position, after the middle of the chip, and then drops towards the end of the chip, where it becomes zero. At this stage, the maximum values are located closer to the end of the chip because this part of the chip is closer to the center of the slot. The maximum chip thickness values are approximately 200 μm and cross-sectional areas are approximately 300 μm^2 for both blades. A similar chip shape is observed in g.p.17, although the maximum chip thickness and cross-sectional area values are smaller. This is explained by the fact that as the tool moves towards the middle of the slot by mainly cutting the flanks of the tooth, the chip becomes both thinner and longer, as also indicated in the graphs with the additional revolving positions in g.p.17 compared to g.p.10. The maximum chip thickness and cross-sectional area values in g.p.17 are approximately 100 μm and 20 μm^2 respectively for both blades. In the next generation position (g.p.24), the measured values are almost doubled, where the maximum chip thickness is in the root area for both blades in most revolving positions. This also explains the increase in thickness, since there is much more material left in the root area from the roughing operation than the remaining stock on the flanks. The cross-sectional area and maximum chip thickness are about 400 μm^2 and 200 μm respectively for both blades. At this point in the process, the maximum chip thickness values are found at the initial revolving positions which are the ones closer to the middle of the slot. The form of the chip remains approximately the same until the final generation position, while the thickness and cross-sectional area in g.p.31 and g.p.38 gradually decrease. [59]

Chip thickness provides a measure of the loading of the tool which, through further analysis and calculation, can lead to the estimate of in-process cutting forces and tool wear in various cutting tool areas. The above measurements and observations are useful for a first rough qualitative estimate of the areas of maximum force on each blade as the cutting action develops. For example, at the start of the generating action, the inner blade's side cutting edge (flank) is more heavily loaded than the tip of the cutter, because the generating motion is initiated on the flank of the gear tooth. As the cutting motion progresses, the chip thickness in the root area increases and therefore the blade tip is subjected to higher load. Towards the end of the generating action, the inner blade is loaded more on the side cutting edge as the blade moves away from the root area of the gear slot and only the flank is engaged with the workpiece. In general, the greatest chip thicknesses are observed at the blade tip due to the greater engagement in that area, where there is more stock material left from the roughing operation than the material left on the tooth flanks. Therefore, the blade tips are subjected to the greatest stresses. [59]

7.2 Investigation of the effect of process parameters on simulated gear topography

7.2.1 Investigation of process parameters in face hobbing

After the validation of the face hobbing simulation methodology, the model can be used to study the influence of process parameters on the gear tooth flank geometry. The fundamental purpose of this simulation model is to provide valuable process data and also to enable analytical study of the spiral bevel gear cutting process without the need for time-consuming and costly machining trials. A total of five simulations were performed using the *BevelSim3D* algorithm, to reveal the effect of generation feedrate f_g on the generated geometry. This particular process parameter was chosen because it does not affect the target – theoretical geometry, which remains the same for all five case studies. The work gear topographies generated from the five simulation cases were compared to the theoretical gear geometry of the ring gear investigated using the *BevelCurve3D* algorithm. For this purpose, five intersection curves covering the tooth area from heel to toe were plotted using the method described in Chapter 5. For all simulation cases, the deviation values were extracted revealing the difference between the simulated and theoretical gear geometries. [Figure 7.2](#) and [Figure 7.3](#) show five graphs, each corresponding to the respective intersection curve along the width of the tooth, for the concave and convex flanks cut by the outer and inner blades respectively. Each graph shows the deviation curves for the five simulations, performed with a variable generation feedrate, on the specific intersection surface. [55]

The goal of this investigation is to reveal the effect of the generation feed rate on the simulated surface quality, as this is one of the primary parameters which greatly impacts the actual cutting process. As shown in both figures (7.2 & 7.3) the higher the generation feedrate, the lower the quality of the flank surfaces to the point that the surface deviation is doubled in $f_g=0.055$ °/rev compared to $f_g=0.015$ °/rev. What is more, increasing the generation feedrate results in an escalation of the surface deviation in the examined intersection surfaces from the heel to the toe of the tooth. Regarding the concave flank shown in [Figure 7.2](#), the 3rd and 4th surface intersections are those closest to the middle of the gear slot and are distinguished by very low surface deviation values, less than 5 μm for most of the flank surface. All deviation values remain below ± 5 μm in the areas near the centre of the tooth shown in the intermediate sub-figures of [Figure 7.2](#) and below ± 10 μm in the areas closest to the heel and the toe of the gear tooth. Another point worth mentioning is that in the case of the concave flank as shown in [Figure 7.2](#), positive deviation values indicate that excess material is left on the work gear, while negative deviation values indicate that the outer blade has removed more material than expected.

As regards the deviation of the simulated convex flank from the theoretical one, shown in [Figure 7.3](#), it can be noted that the areas close to the middle of the tooth, shown in the three intermediate sub-figures, display deviation values in the range of $[0,+10]$ μm , while closer to the heel and the toe of the tooth the deviation range increases to $[-5,+10]$ μm and $[0,+20]$ μm , respectively. As in the concave flank, negative values of the convex surface deviation indicate that more material has been removed from the surface, while positive deviation values show that less material has been removed, compared to the theoretical values. [55]

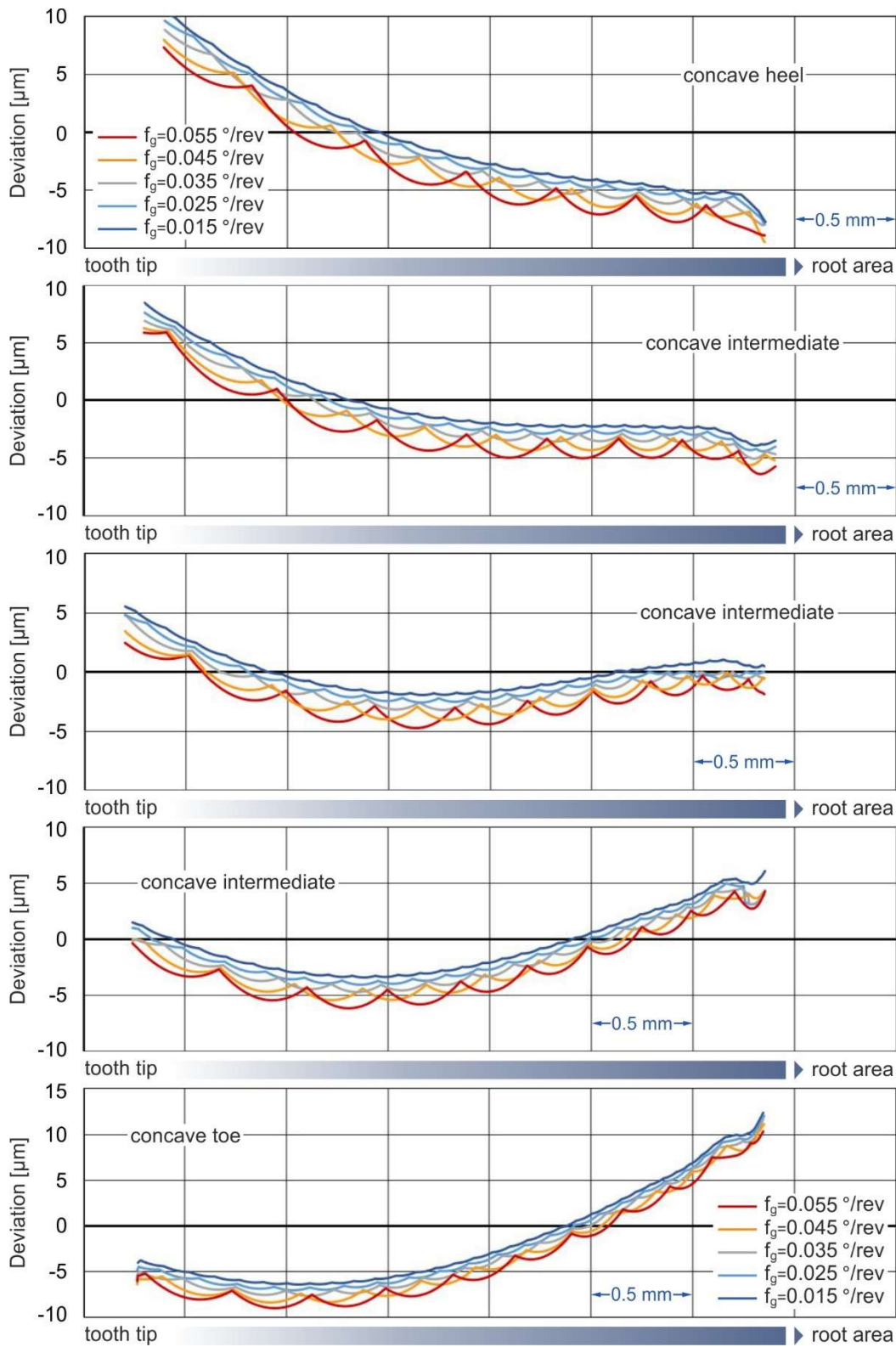


Figure 7.2: Effect of generation feedrate on the quality of the produced concave surface. [55]

The causes behind the deviation between the simulated and theoretical surface are as follows: First, the simulated octoid surface is compared with the theoretical spherical involute surface. Secondly, there are some machine and tool-related input data that have not been considered in the model.

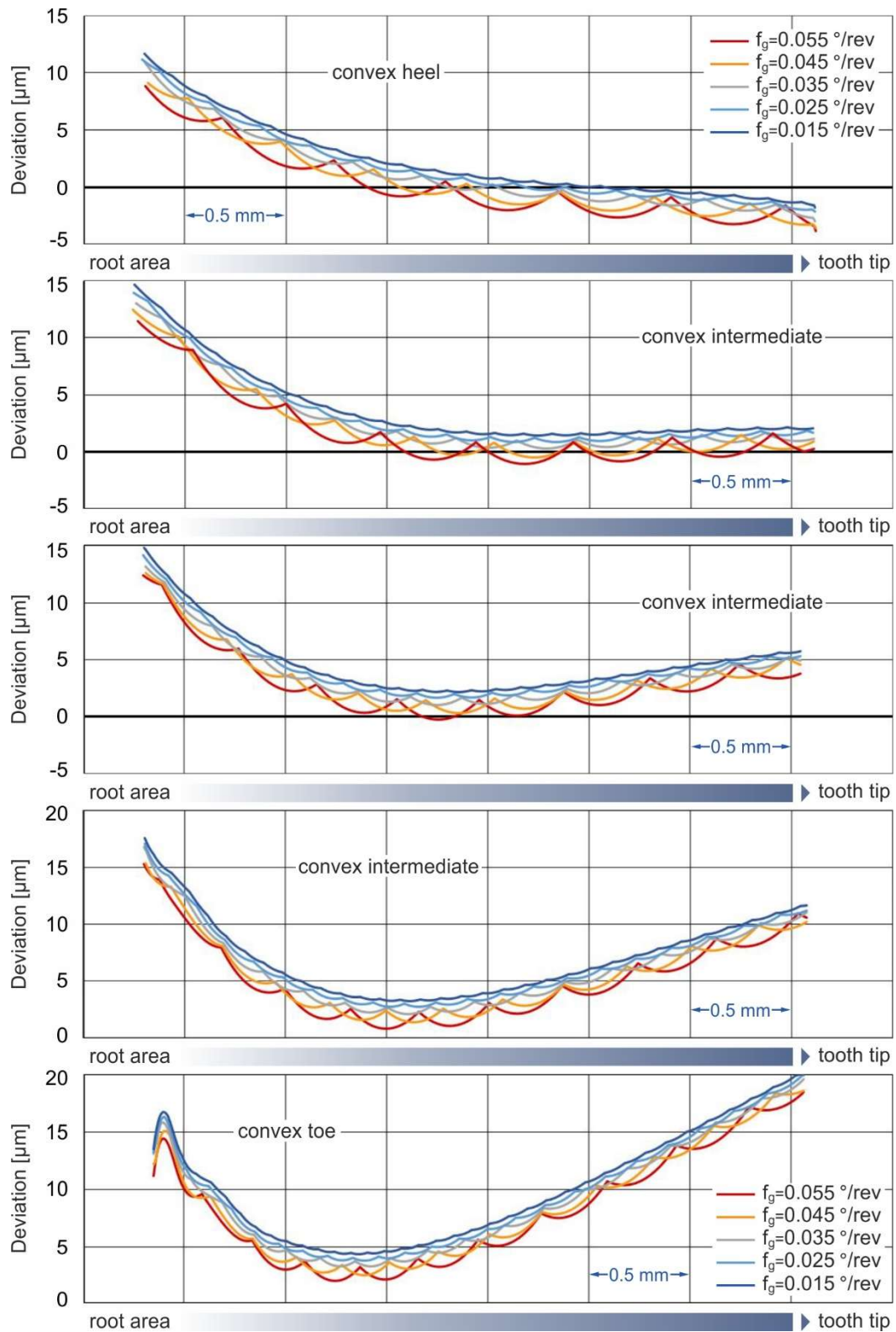


Figure 7.3: Effect of generation feedrate on the quality of the produced convex surface. [55]

Ideally, the deviation values would be close to zero and the deviation curves would be tangent to the zero-plane (x-axis on Figure 7.2 and Figure 7.3). Regarding the variation in surface deviation with the variation of feedrate in most of the graphs of Figure 7.2 and Figure 7.3, the reasons lie mainly in process kinematics and secondly in simulation resolution. In spiral bevel gears generation, the generation feedrate is a vector always parallel to the tool trajectory which is a freeform 3D curve. Increasing and decreasing the feedrate affects the form of the tool trajectory curve and therefore the form of the machined surface. On the process modelling

side, there are considerably more revolving and generation positions produced when a simulation is executed with a lower feedrate than at higher feedrate. [55]

Another useful conclusion that can be drawn from the above study on the effect of generation feedrate on the quality of the tooth flank surfaces is the progression of the mean total height R_t of the surface roughness profiles shown in Figure 7.2 and Figure 7.3. Figure 7.4 shows the evolution of the mean total height R_t as the generation feedrate increases. The two curves shown in the figure represent the concave and convex flank surfaces. The mean total height R_t is the average of the total height values for all five intersecting surfaces shown in the figures above. As illustrated, the total height R_t increases as the generation feedrate f_g increases both on the concave and on the convex flanks. In addition, the gradient of the curve increases with increasing f_g , indicating a more dramatic decrease in the simulated surface quality at higher f_g values. [55]

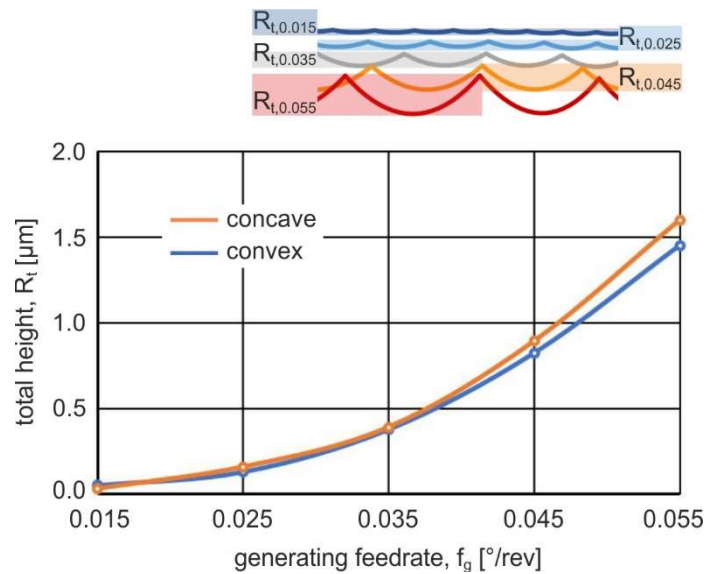


Figure 7.4: Effect of the generation feedrate on the quality of the produced work gear surface – face-hobbed ring gear. [55]

7.2.2 Investigation of process parameters in face milling

Following the same procedure to investigate the influence of process parameters in face milling, a series of five simulations of face-milled pinion gears were performed using the *BevelSim3D* algorithm. Simulated and theoretical geometries were compared on five intersection surfaces starting from heel to toe. The effect of generation feedrate on the simulated surface quality is shown in Figure 7.5. The two curves included in the figure reveal the progression of the mean total height R_t of the surface roughness profiles with the increase of the generation feedrate. Similar to face hobbing results described above, the mean total height R_t value equals the average height of the five heel-to-toe deviation curves. The total height R_t increases as expected with the increasing generation feedrate. The gradient of the two curves remains almost constant, which means that the simulated surface quality steadily decreases as feedrate f_g increases. [55]

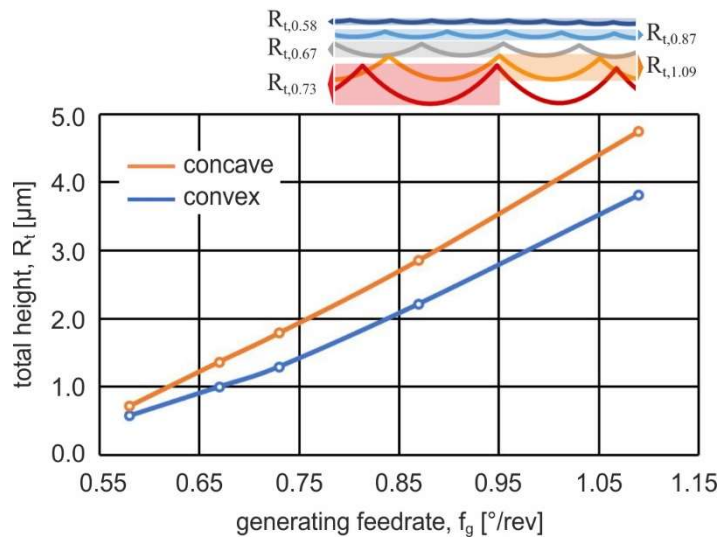


Figure 7.5: Effect of generation feedrate on the quality of the produced work gear surface – face-milled pinion. [55]

7.3 Investigation of the effect of process parameters on the developed cutting forces

Following the numerical verification of the calculated force components, several studies were performed on the effect of cutting parameters on the cutting forces, the most significant results of which are presented in the following sections. Since the cutting forces developed during the process are largely influenced by the volume and shape of the produced chips, the parameters selected for the investigation are those that have the greatest influence on the cutting chips. These are the plunge feedrate (f_p), the generation feedrate (f_g) as well as the finishing stock allowance (t_f). The material of the work gear, in all simulation results shown below, is St 50-2 carbon steel and the material-dependent parameters, i.e., the material cutting resistance, and material-specific constant are experimentally determined in [67]. All simulations presented in the following sections were conducted for the face-hobbed ring gear examined in Chapter 4, the main geometric and machining parameters of which, are included in [Table 7.1](#).

Geometric parameters		Cutter & machining parameters	
Gear	Ring gear	Blade edge radius, r_1	0.8055 mm
Number of teeth, z_2	34	Number of blade groups, z_0	16
Wheel face width, b_2	26 mm	Cutter radius, r_{c0}	78 mm
Mean pitch diameter, d_{m2}	146.7 mm	Normal pressure angle, α_0	20 °
Mean spiral angle, β_{m2}	21 °	Machining method	Face hobbing
Addend./dedendum angle, θ_{a2}/θ_{f2}	0 ° / 0 °	Rake angle	0 °
Mean normal module, m_{mn}	4.027882 mm	Cutting speed, v_c	200 m/min

Table 7.1: Geometric and cutting parameters in the investigation of the effect of process parameters on cutting forces. [55]

7.3.1 The effect of finishing stock allowance on cutting forces

Aiming to examine the effect of finishing stock allowance on the cutting forces developed in a two-stage face hobbing process, including a roughing (forming) and a finishing (generating) stage, three simulations were carried out. All simulation runs deal with the face-hobbed ring gear presented in the previous section, therefore all geometric and process-related parameters, except for the finishing stock allowance, remain the same and are shown in [Table 4.2](#) and [Figure 7.6](#). The finishing stock allowance, i.e., the material left at the root surface of

the slot after the roughing stage is completed, is set to 0.5 mm, 0.75 mm, and 1 mm. Figure 7.6 shows the summarized global ΣF_x , ΣF_y and ΣF_z force components according to the fixed coordinate system on the pitch cone apex. As can be seen, the increase in the finishing stock allowance has a great impact on the developed cutting forces, which is clearly explained by the increase in the undeformed chip volumes shown at the bottom right part of the figure. [55]

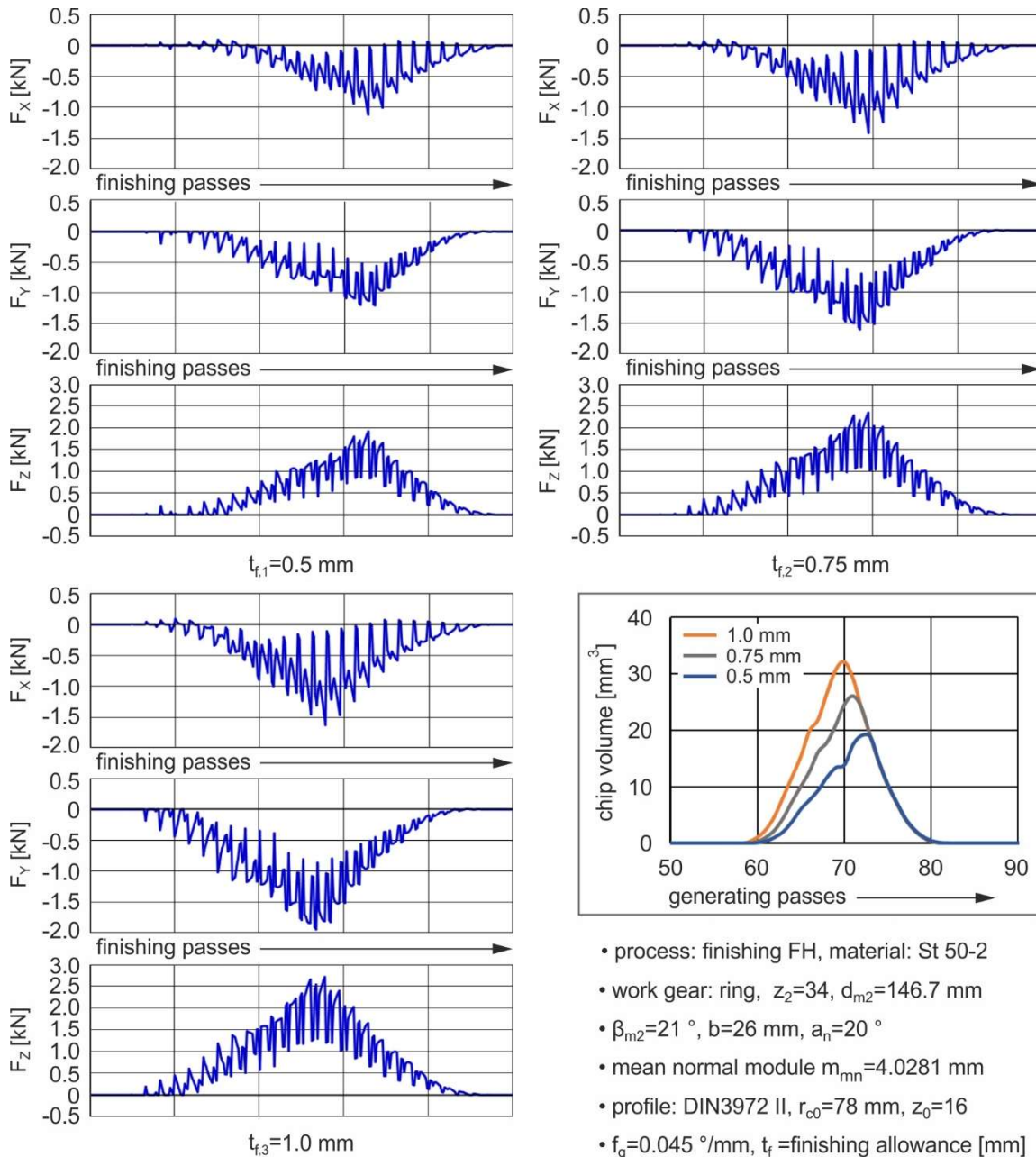


Figure 7.6: Effect of finishing allowance on the developed cutting forces. [55]

As the finishing stock on the root of the slot increases, the material left on the flanks of the tooth also grows, and with all the other strategy parameters, such as feedrate, remaining unchanged, the volumes of the undeformed chips increase causing an increase in the cutting forces. As can be seen in the chip volume graph of Figure 7.6, the chips are smaller in size at the start of the finishing process and increase as the process progresses as engagement with the work gear is increased and the tool advances at a larger depth into the work gear. Furthermore, the cutting process begins earlier with a higher stock allowance, than in the cases of smaller stock, and this is indicated in Figure 7.6 by both the cutting forces graphs and the chip volume curves. Another interesting conclusion can be drawn from the form of all three

chip volume curves after the middle of the cutting action. The three curves coincide for the last part of the process which can be explained by the fact that the tool has already made one pass on both flank surfaces at that point. Therefore, the remaining stock for the last pass is the same. [55]

7.3.2 The effect of plunge feedrate in the roughing stage of the process

To investigate the plunge feedrate during the roughing (forming) stage of the process, three simulations of a two-stage, face-hobbed ring gear were performed. All geometric and process-related parameters, except the depth of the roughing pass (f_p), are the same as in previously presented simulations. The simulations were carried out for a plunge feedrate of 0.1 mm/rev, 0.2 mm/rev and 0.3 mm/rev. The results presented in Figure 7.7 show a significant increase in the developed cutting forces with increasing depth of the plunging passes.

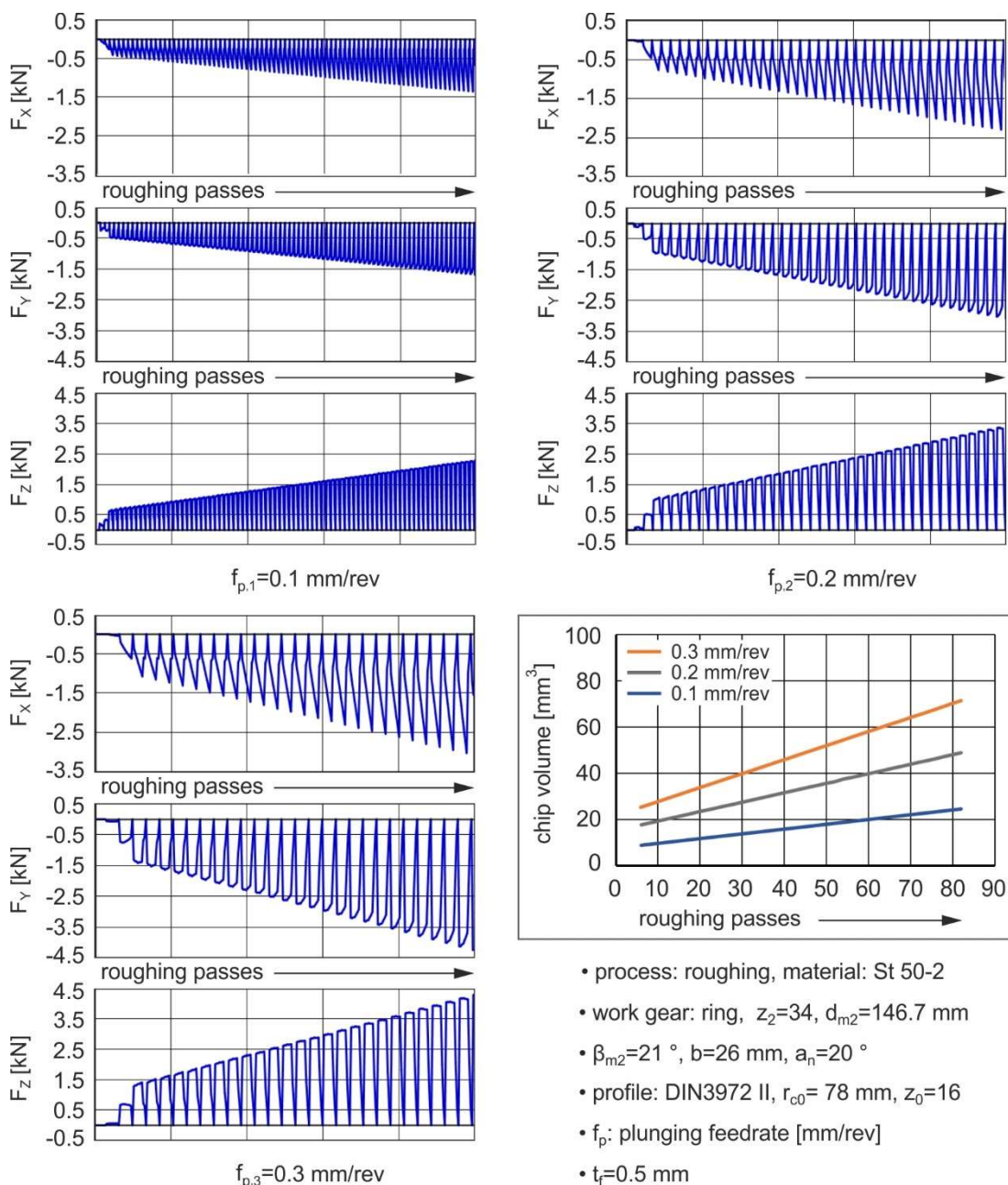


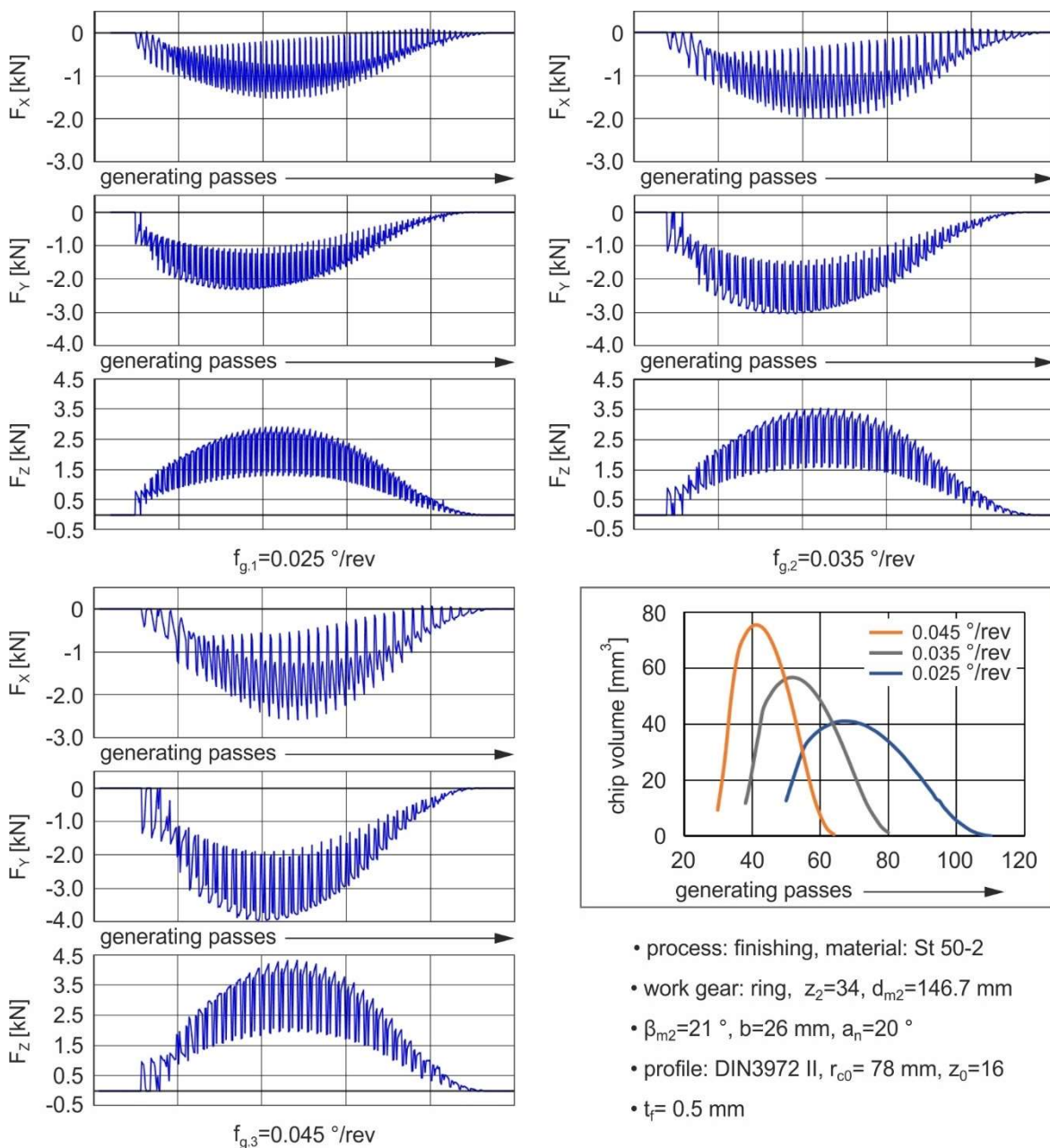
Figure 7.7: Effect of plunge (forming) feedrate on the developed cutting forces. [55]

The figure shows the summarized global ΣF_x , ΣF_y and ΣF_z force components according to the fixed coordinate system at the pitch cone apex. As the forming feedrate increases, the material

removed in each pass increases, increasing the volumes of the undeformed chips, causing a significant rise in the cutting forces. This increase in chip volumes as the plunge feedrate increases is illustrated in the bottom right graph of Figure 7.7. The cutting force graphs in all simulations display a change in the first roughing pass caused by the different shape of the chip as the tool penetrates the workpiece. Another interesting point revealed in Figure 7.7, is that as the roughing process progresses, the cutting forces increase, which is caused by the increasing volume of the chip as the tool plunges deeper into the work gear due to the DIN 3972 II profile of the cutting blades. It should be noted that this study of the effect of plunge feedrate on the developed cutting forces is equivalent to the respective investigation of the face hobbing forming process. [55]

7.3.3 The effect of generation feedrate in a single stage finishing process

The effect of generation feedrate was examined in both a two-stage and a single-stage face hobbing process.



- process: finishing, material: St 50-2
- work gear: ring, $z_2=34$, $d_{m2}=146.7$ mm
- $\beta_{m2}=21^\circ$, $b=26$ mm, $a_n=20^\circ$
- profile: DIN3972 II, $r_{c0}=78$ mm, $z_0=16$
- $t_f=0.5$ mm

Figure 7.8: Effect of generation feedrate on the developed cutting forces in a single stage process. [55]

Regarding the two-stage process, where generation takes place as a finishing operation with relatively low chip volumes, the investigation revealed a rather low sensitivity of the cutting forces to the increase or decrease of generation feedrate. The cutting forces followed the expected upward trend with the increase of feedrate, but the variance was small. On the contrary, in a single-stage face hobbing process, where generation is performed throughout the roughing/finishing phase, the generation feedrate has a remarkable effect on cutting forces, as shown in [Figure 7.8](#). The above figure shows the summarized global ΣF_x , ΣF_y and ΣF_z force components in three simulations with $f_g=0.025$ °/rev, $f_g=0.035$ °/rev, and $f_g=0.045$ °/rev. Increasing the feedrate produces notably larger chips which consequently raises the cutting forces developed at the tool tip. As can be seen in the chip volume graph at the bottom right part of Figure 7.8, in all three cases the chip volume is relatively low at the beginning of the process, it becomes larger towards the middle of the process and then gradually decreases towards the end of the process, as expected from the initial evaluation of the chip form in Figure 4.24. [55]

[This page intentionally left blank]

8. CONCLUSIONS

In this study, a novel 3D CAD-based model aimed at simulating the spiral bevel gear manufacturing processes was introduced. Three algorithms have been developed for the integrated analysis of the cutting process. First, the *BevelSim3D* algorithm developed for the kinematic simulation of spiral bevel gear *face milling* and *face hobbing*. The algorithm allows the automated creation of gear tooth and undeformed chip solid geometries. Second, the *BevelCurve3D* algorithm was developed for the validation of kinematic simulation results. The algorithm compares the simulated gear flank geometry with the theoretical geometry, which is obtained from a well-established gear design and calculation software. Finally, the *BevelForce3D* algorithm was developed for the calculation of cutting forces through the analysis of the undeformed chip geometry. The algorithm was also utilised for the investigation of the effect of a series of cutting parameters on the developed cutting forces. Several simulations were executed for the validation of the *BevelSim3D* model and the investigation of the effect of cutting parameters on the produced tooth surface and the developed forces. *BevelCurve3D* revealed good agreement between the simulated surface geometry and the theoretical surface, especially in the case of ring gear simulations. The surface deviation for the pinion was found to be higher than the corresponding values for the ring gear and this is explained by the fact that the curvature of the pinion tooth surface is remarkably higher than the curvature of the ring gear. The cutting process is more difficult to analyse and simulate, therefore the simulation results show lower accuracy. After the validation of the model, a study was conducted to investigate the effect of generation feedrate on the produced tooth surface, which showed that feedrate greatly affects the surface roughness and the simulated surface deviation. In particular, increasing the feedrate increases both the deviation of the simulated surface from the theoretical one, and the total height R_t of the surface roughness profile.

The results of the cutting force calculation algorithm, *BevelForce3D*, were verified by comparing the values measured automatically by the algorithm, with the values measured manually via the user interface tools of the 3D modelling software. All automatically calculated force component values were found to be consistent with the manually calculated forces. This verification procedure was followed for several elementary chips in various simulations. Provided that the tool trajectory is simulated correctly, as proven by the *BevelCurve3D* algorithm, the cutting chip geometry and the calculated force components should closely approximate the respective forces of the actual machining process. After the verification of the model, the influence of finishing stock allowance, plunge feedrate and generation feedrate on the developed cutting forces was examined. The results revealed a significant influence of these cutting parameters on the volume of the undeformed chip and therefore on the cutting forces developed. The *BevelForce3D* algorithm calculates both the cutting forces developed at the tool tip, as they would be measured if a dynamometer was adjusted on the tool following the machine kinematics, but also the global forces calculated on a coordinate system placed on the pitch cone apex as if the dynamometer was placed steadily on the work gear. Local forces can be used to predict tool wear and help optimize process productivity, while global forces can be used as a guide to predict the deformation of the work gear due to the residual stresses introduced into the workpiece, as well as the type of fixture and the clamping force that must be applied to the work gear before machining.

The author is working actively on developing and extending the simulation model and introducing more cutting tool parameters, machine settings, and cutting blade profiles to improve the simulation results and enhance the universality of the proposed approach. Research also focuses on improving the simulated pinion flank geometry. The next steps to extend the simulation algorithm include the variability of the surface quality depending on the selected tool geometry and the influence of the rake angle on the developed cutting forces.

[This page intentionally left blank]

REFERENCES

- [1] Klingelberg J. *Bevel Gear – Fundamentals and Applications*. Berlin Heidelberg, 2016.
- [2] Osakue E, Anetor L, Harris K. Contact Stress In Helical Bevel Gears. *FME Transactions* 2021; 49: 519–513.
- [3] www.mathworks.com.
- [4] Rolls Royce plc. *The Jet Engine*. 5th ed. 2015.
- [5] Stergiou I, Stergiou K. *Machine Elements II - Motion Transmission - Gears, Belts, Chains*. Athens, 2002.
- [6] J.R. Davis. *Gear materials, properties, and manufacture*. ASM International, 2005.
- [7] KHK Gears, Stock gear manufacturer.
- [8] ANSI/AGMA 2005-D03. Design manual for bevel gears. .
- [9] ISO 23509:2016. Bevel and hypoid gear geometry.
- [10] Stadtfeld H. *Gleason Bevel Gear Technology*. Rochester, New York: The Gleason Works, 2014.
- [11] Fuentes-Aznar A, Gonzalez-Perez I. Mathematical definition and computerized modeling of spherical involute and octoidal bevel gears generated by crown gear. *Mech Mach Theory* 2016; 106: 94–114.
- [12] Tokugawa Trading Shenzhen - Gear cutting solutions.
- [13] Klein A. *Spiral bevel and hypoid gear tooth cutting with coated carbide tools*. RWTH Aachen University, 2007.
- [14] Zhang C, Yang J. *A history of mechanical engineering*. Springer Singapore, 2020.
- [15] Kisssoft user manual. *Kisssoft AG*.
- [16] Fan Q. Computerized Modeling and Simulation of Spiral Bevel and Hypoid Gears Manufactured by Gleason Face Hobbing Process. *Journal of Mechanical Design* 2006; 128: 1315.
- [17] Fan Q, DaFoe RS, Swanger JW. Higher-Order Tooth Flank Form Error Correction for Face-Milled Spiral Bevel and Hypoid Gears. *Journal of Mechanical Design* 2008; 130: 072601.
- [18] Maiuri TJ. Spiral bevel and hypoid gear cutting technology update. *Gear Technology* 2007; 28–39.
- [19] Klocke F, Klein A. Tool Life and Productivity Improvement. *Gear Technology*; 41.
- [20] Zheng F, Hua L, Chen D, et al. Generation of Noncircular Spiral Bevel Gears by Face-Milling Method. *J Manuf Sci Eng* 2016; 138: 081013.
- [21] Zhang Y, Yan H zhi, Zeng T, et al. Tooth surface geometry optimization of spiral bevel and hypoid gears generated by duplex helical method with circular profile blade. *J Cent South Univ* 2016; 23: 544–554.
- [22] Wang PY, Fong ZH. Adjustability improvement of face-milling spiral bevel gears by modified radial motion (MRM) method. *Mech Mach Theory* 2005; 40: 69–89.
- [23] Xie S. *An accurate approach to modeling the genuine tooth surfaces of the face-milled spiral bevel and hypoid gears*. Concordia University, 2012.
- [24] Usubamatov R, Yahaya NZ. Double Cutter Face Milling of Spiral Bevel Gears. *International Journal of Engineering Research & Technology*; 03.
- [25] Zheng F, Zhang M, Zhang W, et al. The fundamental roughness model for face-milling spiral bevel gears considering run-outs. *Int J Mech Sci* 2019; 156: 272–282.
- [26] Zhou Y, Peng S, Liu X, et al. A novel method to generate the tooth surface model of face-milled generated spiral bevel gears. *The International Journal of Advanced Manufacturing Technology* 2019; 102: 1205–1214.
- [27] Mu Y, Li W, Fang Z. Tooth surface modification method of face-milling spiral bevel gears with high contact ratio based on cutter blade profile correction. *The International Journal of Advanced Manufacturing Technology* 2020; 106: 1–9.

- [28] Zheng F, Han X, Lin H, et al. Research on the cutting dynamics for face-milling of spiral bevel gears. *Mech Syst Signal Process* 2021; 153: 107488.
- [29] Mazak J, Klocke F, Bergs T, et al. Simulation-based process analysis for discontinuous cutting of generated bevel gears. *Proc Inst Mech Eng C J Mech Eng Sci* 2019; 233: 095440621984540.
- [30] Litvin F, Tsung W-J, Coy J, et al. New Generation Methods for Spur, Helical, and Spiral-Bevel Gears.
- [31] Vimercati M. Computerized Design of Face Hobbed Hypoid Gears : Tooth Surfaces Generation , Contact Analysis and Stress Calculation. *Agma 05Ftm05*.
- [32] Fan Q. Kinematical Simulation of Face Hobbing Indexing and Tooth Surface of Spiral Bevel and Hypoid Gears. *Gear Technology* 2006; 30–38.
- [33] Shih Y-P, Fong Z-H, Lin GCY. Mathematical Model for a Universal Face Hobbing Hypoid Gear Generator. *Journal of Mechanical Design* 2006; 129: 38.
- [34] Simon V v. Optimal Machine-Tool Settings for the Manufacture of Face-Hobbed Spiral Bevel Gears. *Journal of Mechanical Design* 2014; 136: 081004.
- [35] Habibi M, Chen ZC. A New Approach to Blade Design With Constant Rake and Relief Angles for Face-Hobbing of Bevel Gears. *J Manuf Sci Eng* 2015; 138: 031005.
- [36] Habibi M, Chen ZC. A semi-analytical approach to un-deformed chip boundary theory and cutting force prediction in face-hobbing of bevel gears. *CAD Computer Aided Design* 2016; 73: 53–65.
- [37] Gonzalez-Perez I, Fuentes Aznar A. *Comparison of Cyclo-Palloid and Cyclo-Cut Cutting Methods for Generation of Spiral Bevel Gears*. 2017. Epub ahead of print 6 August 2017. DOI: 10.1115/DETC2017-67793.
- [38] Gonzalez-Perez I, Fuentes-Aznar A. Conjugated action and methods for crowning in face-hobbed spiral bevel and hypoid gear drives through the spirac system. *Mech Mach Theory* 2019; 139: 109–130.
- [39] Liu S, Song C, Zhu C, et al. Investigation on the influence of work holding equipment errors on contact characteristics of face-hobbed hypoid gear. *Mech Mach Theory* 2019; 138: 95–111.
- [40] Zhang W, Guo X, Wang Y, et al. A CNC tooth grinding method for formate face hobbed hypoid gears. *Mech Mach Theory* 2020; 144: 103628.
- [41] Guo W, Mao S, Yang Y. Tool path active design for tooth modification of face-hobbed spiral bevel gears. *J Phys Conf Ser* 2020; 1633: 012053.
- [42] Habibi M, Chen Z. Machining Setting Optimization for Formate ® Face-Hobbing of Bevel Gears With the Cutting Force and Tool Wear Constraints. *Journal of Mechanical Design*; 138. Epub ahead of print 27 June 2016. DOI: 10.1115/1.4033992.
- [43] Álvarez A, Lacalle LNL de, Olaiz A, et al. Large Spiral Bevel Gears on Universal 5-axis Milling Machines: A Complete Process. *Procedia Eng* 2015; 132: 397–404.
- [44] Zhou Y, Chen Z, Tang J. A New Method of Designing the Tooth Surfaces of Spiral Bevel Gears With Ruled Surface for Their Accurate Five-Axis Flank Milling. *J Manuf Sci Eng* 2017; 139: 061004.
- [45] Shih YP, Sun ZH, Wu FC. A disk tool cutting method for bevel gear manufacture on a five-axis machine. *International Journal of Advanced Manufacturing Technology* 2018; 94: 855–865.
- [46] Klocke F, Brumm M, Herzhoff S. Influence of gear design on tool load in bevel gear cutting. *Procedia CIRP* 2012; 1: 66–71.
- [47] Brecher C, Klocke F, Brumm M, et al. Analysis and Optimization of Bevel Gear Cutting Processes by Means of Manufacturing Simulation. In: Pina N, Kacprzyk J, Filipe J (eds) *Simulation and Modeling Methodologies, Technologies and Applications: International Conference, SIMULTECH 2011 Noordwijkerhout, The Netherlands, July 29-31, 2011 Revised Selected Papers*. Berlin, Heidelberg: Springer Berlin Heidelberg, pp. 271–284.

- [48] Jiang C, Deng X, Zhang H, et al. Prediction and simulation of cutting force in hypoid gear machining using forming method. *The International Journal of Advanced Manufacturing Technology* 2017; 93: 2471–2483.
- [49] Brecher C, Löpenhaus C, Knecht P. Design of Acoustical Optimized Bevel Gears Using Manufacturing Simulation. *Procedia CIRP* 2016; 41: 902–907.
- [50] Litvin FL, Fuentes A. *Gear Geometry and Applied Theory*. 2nd ed. Cambridge: Cambridge University Press. Epub ahead of print 2004. DOI: DOI: 10.1017/CBO9780511547126.
- [51] Figliolini G, Angeles J. Algorithms for Involute and Octoidal Bevel-Gear Generation. *Journal of Mechanical Design* 2004; 127: 664–672.
- [52] Bijonowski B. A Practical Approach for Modeling a Bevel Gear. *Gear Technology*, 2015.
- [53] American Gear Manufacturers Association. *AGMA 929-A06 Calculation of Bevel Gear Top Land and Guidance on Cutter Edge Radius*. August 2006.
- [54] Shiraishi S, Kusaka T, Matsumura T. Cutting force prediction in hypoid gear machining. *Journal of Advanced Mechanical Design Systems and Manufacturing*; 10.
- [55] Efstathiou C, Tapoglou N. Simulation of spiral bevel gear manufacturing by face hobbing and prediction of the cutting forces using a novel CAD-based model (Reproduced with permission from Springer Nature). *The International Journal of Advanced Manufacturing Technology* 2022; 122: 3789–3813.
- [56] Radzevich SP. *Gear Cutting Tools: Science and Engineering*. CRC Press, 2018.
- [57] Colbourne JR. Conjugate Action. In: Wang QJ, Chung Y-W (eds) *Encyclopedia of Tribology*. Boston, MA: Springer US, pp. 440–446.
- [58] Fan Q. Enhanced Algorithms of Contact Simulation for Hypoid Gear Drives Produced by Face-Milling and Face-Hobbing Processes. *Journal of Mechanical Design* 2006; 129: 31–37.
- [59] Efstathiou C, Tapoglou N. A novel CAD-based simulation model for manufacturing of spiral bevel gears by face milling. *CIRP J Manuf Sci Technol* 2021; 33: 277–292.
- [60] DIN3972: Bezugsprofile von Verzahnwerkzeugen für Evolventenverzahnung nach DIN 867.
- [61] Bae I, Schirru V. *An Approach to Find Optimal Topological Modification to Duplicate Tooth Flank Form of the Existing Gear*. 2014.
- [62] Altintas Y. *Manufacturing Automation: Metal Cutting Mechanics, Machine Tool Vibrations, and CNC Design*. 2nd ed. Cambridge: Cambridge University Press. Epub ahead of print 2012. DOI: DOI: 10.1017/CBO9780511843723.
- [63] Shaw MC. *Metal cutting principles*. 2nd ed. Oxford University Press, 2005.
- [64] Kienzle O, Victor H. Die bestimmung von kräften und leistungen anspannenden werkzeugmaschinen. *VDI-Z* 1952; 94: 299–305.
- [65] de Vos P, Stahl J-E. *Applied Metal Cutting Physics: Best Practices*. Fagersta, Sweden: Seco Tools AB, 2016.
- [66] Tapoglou N. *Gear hobbing simulation and investigation of the technological parameters involved*. Technical University of Crete, 2012.
- [67] König W, Essel K. Spezifische Schnittkraftwerte für die Zerspanung metallischer Werkstoffe.